UNIVERSITA' DEGLI STUDI DI NAPOLI

"FEDERICO II"

Facoltà' di Scienze Matematiche, Fisiche e Naturali

"Eventi a Foraminiferi planctonici e variazioni climatiche registrate in sedimenti del Tirreno Meridionale durante gli ultimi 80 ka."

"Planktonic foraminiferal events and climatic variability in sediment of Southern Tyrrhenian Sea during the last 80 Kyr "

XXI° Ciclo Dottorato di Ricerca in

Scienze della Terra

by

Mattia Vallefuoco

Tutors

Prof. Bruno D'Argenio[1,2]
Prof.ssa Vittoria Ferreri[1,2]

Co-Tutors

Dr. Fabrizio Lirer[2]
Dr.ssa Luciana Ferraro[2]

[1] **Uni**versità Degli Studi di **Na**poli Federico II (*Dipartimento di Scienze della Terra*)
[2] **I**stituto per l'**A**mbiente **M**arino **C**ostiero-CNR Napoli, Italia

Università di Napoli Federico II

Prof. Stefano Mazzoli
Dipartimento di Scienze della Terra
Largo San Marcellino 10
80138 Napoli, Italy
Tel. (+39) 0812538121
Fax. (+39) 0815525611
E-mail: stefano.mazzoli@unina.it

24 Novembre 2008

Valutazione attività dottorando Mattia Vallefuoco

Il Collegio dei Docenti del Dottorato in Scienze della Terra, XXI Ciclo, riunito in data 20/11/2008, in considerazione dell'esame della tesi di dottorato, della relazione prodotta dal dottorando sulle attività di ricerca e sulla didattica seguita, della relazione del tutor e della relazione del referee esterno ha formulato, con delibera presa all'unanimità, il giudizio sottostante:

VALLEFUOCO MATTIA

Titolo: *Eventi a Foraminiferi planctonici e variazioni climatiche registrate in sedimenti del Tirreno meridionale durante gli ultimi 80 ka.*

Tutor: Prof. Bruno D'Argenio.

Nella tesi il dottorando ha effettuato uno studio biostratigrafico di alta risoluzione su sedimenti marini del tardo Quaternario; ha ottenuto significativi contributi alle conoscenze delle variazioni paleo-oceanografiche e paleo-climatiche del Mediterraneo.

Il Consiglio, sentito il parere del tutor e del referee esterno dott.ssa Lucilla Capotondi dell'Istituto di Scienze Marine di Bologna, esprime un giudizio ampiamente positivo sulla tesi e ritiene all'unanimità di ammettere il dottorando all'esame finale.

Il coordinatore del Dottorato in Scienze della Terra

Prof. Stefano Mazzoli

CONTENTS

Contents

SYNOPSIS

SYNOPSIS

Drastic and/or gradual changes have occurred in the Mediterranean Area during the last 100 kyr and they resulted well detectable in shallow and deep marine paleoarchives. This study is mainly focused on the Tyrrhenian Sea which resulted the marina area less studied of the entire Mediterranean. It is important to remember that the Tyrrhenian Sea represents the key area where the Modified Atlantic Water (MAW), which coming from the Strait of Gibraltar (Bryden and Kinder, 1991), diverges from the part that enters the Eastern Mediterranean and flows through the Sardinia Channel into the Tyrrhenian Sea along the northern Sicilian coast (Millot, 1987), forming a secondary circulation gyre. For this, southern part of the Tyrrhenian Sea represent an interesting area for high resolution paleoceanographic investigations. So that to study marine records which have different sedimentation rate offers the unique opportunity to identify, through a multiproxy approach, the main events which experienced the Tyrrhenian Sea trying to find events regionally recognised.

The here proposed general PhD thesis includes detailed studies, by different methodological approach, of sediments referable to the last 80 kyr. With a particular detail, three different marine sites were been studied, corresponding to the last 500 years, the Holocene epoch and the last 80 kyr. Due to the different geographic position, these sites offer the possibility to recover continue and undisturbed sedimentary sequences, which allowed to acquire climate paleoarchives useful for high resolution Event Stratigraphy.

This study is based on the abundance fluctuations of planktonic foraminifera associated with calcareous nannofossils (for the Holocene) and benthic foraminifera (for the last 500 years).

Regarding this, it is important to specify that the chapters 4, 5, 6 of this PhD thesis are or will be published as separated papers in peer reviewed scientific journals. Moreover,

due to the interdisciplinary project, several expertises are involved during this thesis with the collaboration of several researchers of different Institutions.

In particular, the following Institution were involved:

- Istituto per l'Ambiente Marino Costiero **(IAMC) – CNR** of Napoli
- Istituto Nazionale di Geofisica e Vulcanologia **(INGV)** of Pisa
- Istituto Nazionale di Geofisica e Vulcanologia **(INGV)** of Roma
- Dipartimento di Scienze della Terra – **Università degli Studi "Federico II"** of Napoli
- Dipartimento di Scienze Ambientali, **Seconda Università** of Napoli
- Istituto Scienze Marine (Sezione di Geologia Marina), **ISMAR – CNR** of Bologna

This PhD thesis is financially supported by VULCOST project (Team leader Prof. Bruno D'Argenio). This project represents the Line2 of the Italian project VECTOR.

Chapter 4

In this paper I present high-resolution study of shallow water marine record (water depth ~100) from eastern part of Tyrrhenian Sea (Salerno Gulf) based on the a multidisciplinary approach (planktonic and benthic foraminifera and tefrostratigraphy). The investigation allowed to detect the most relevant climatic events of the last 520 years. The chronological framework based on ^{137}Cs and ^{210}Pb radionuclide suggest a sedimentation rate of 0.20 cm/y for the last 520 yr. During this time interval three eco-intervals have been detected and dated considering benthic and planktonic foraminifera distribution. The boundaries of these intervals resulted almost coincident suggesting a similar response to climate forcing.

In term of benthic foraminiferal ecosystem the studied record is relatively enriched in infaunal species that dominate under more eutrophic conditions. On the other hand the

planktonic foraminifera document a drastic turnover between carnivore and herbivore-opportunistic species consequently to the Maunder event, and a possible and progressive swallowing of the phytoplankton productivity as indicated by the increase of *Globigerina bulloides* in the last century. The change between carnivore and herbivore species may be associated to a possible change in the water column food availability successively to the Maunder event. Moreover, the strong increase in abundance of *Globigerinoides quadrilobatus* during the warm intervals reflect the present day Mediterranean oligotrophic conditions.

Finally, a clear human impact on the marine environmental ecosystem associated to the building dam on Sele River (Salerno Gulf) at 1934 AD, which possibly changed the amount of grain-size river transport and the nutrient budge in the sea water. This hypothesis seems to be of support to the strong and progressive increased in abundance in *G. bulloides* distribution pattern, to the sudden increase in benthic foraminifer *B. aculeata* and to the further prominent increase of benthic and planktonic foraminifera (as number of specimens per gram of dry sediment) after 1934 AD.

Chapter 5

The present study reports a high-resolution Event Stratigraphy for the Eastern Tyrrhenian region during the last 10 kyr, from continental shelf marine record. The detailed chronology, for the studied Tyrrhenian composite core, based on the integration of AMS ^{14}C radiocarbon data, ^{210}Pb and ^{137}Cs radionuclides and tephrostratigraphic studies, allowed us to date the four eco-biozones. From the base to the top, the eco-biozone 4F spans from 9.8 kyr to 5.8 kyr, the eco-biozone 3F spans from 5.8 kyr to 3.9 kyr, the eco-biozone 2F spans from 3.9 kyr to 2.7 kyr and finally the eco-biozone 1F spans from 2.7 kyr to present day. The eco-biozone 1F presents two sub eco-biozone 1Fa and 1Fb which boundary is placed at 1280 AD.

In terms of climate events, two distinct humid phases have been recorded during the early and middle part of the Holocene, as well as the Medieval Warm Period, the Little

Ice Age and the modern warm period in the latest part of the Holocene. In particular, from the base to the top of the studied record, the recorded climatic events are as following.

The well-known early Holocene humid phase, associated to the deposition in the Mediterranean Area of Sapropel S1, is recorded between 9.8 kyr BP to 6.3 kyr BP. In the Tyrrhenian Sea, the lithological signature (dark coloured, sometimes laminated beds enriched in organic carbon) of sapropel S1 is not present, so that the identification of this climatic event is associated to the calcareous plankton signatures.

In particular, two distinct peaks in *G. ruber* oscillations show the occurrence of S1a and S1b phases separated by an interval (S1i) of decreased abundances of *G. ruber* and drastic increase of *N. pachyderma* and *T. quinqueloba*. Moreover, the concurrence of a distinct peak in abundance of calcareous nannofossil species *Brarudosphaera bigelowii*, supports the recognisation of the sapropel interruption event (S1i). This calcareous plankton signature is clearly recorded in several part of the Mediterranean basin with minor differences for the position of *B. bigelowii* increased mainly in the Ionian Sea.

The successive important humid phase recorded between 3.625 kyr BP and 2.25 kyr BP is well detected through calcareous plankton signature. This humid phase presents the similar calcareous plankton signature of the previous humid phase associate to sapropel S1 equivalent deposition, with the only exception that during this time interval (3.625-2.25 kyr BP) *G. quadrilobatus*, a typical surface Mediterranean water dweller and prolific at the end of summer, has a distinct acme distribution (>30%). This framework could support the hypothesis that, during that time interval, the climate was similar to the early Holocene humid phase (Sapropel S1).

The calcareous plankton data for the subsequently last 2000 years represent the first high-resolution dataset available in the Mediterranean area. So that these data can not be correlated with others from other part of the Mediterranean basin.

During the last 2000 years, the two important climatic events, on which there are no universally accepted and precise definitions for the duration are the Medieval Warm Period (MWP) and Little Ice Age (LIA).

The MWP, which was generally characterized by temperatures that were slightly higher than present-day conditions, do not show a distinct planktonic foraminiferal features. Tentatively, this warm interval may coincide with time interval spanning from ~560 AD to ~1300 AD and is mainly characterised by warm carnivore planktonic species. Within this long interval, two distinct warm water taxa oscillations are present. The uppermost part can really associated to the historically warmest part of the MWP (~900-1300 AD) which corresponds, in the studied record, a strong abundance peak in *G. ruber* distribution pattern.

The subsequently MWP-LIA transition, which represents a global-scale rapid climate change (RCC) event, is strongly marked by a progressive turnover between carnivore species and herbivore-opportunistic ones and is dated at 1480 AD.

The onset of Little Ice Age event marked by a planktonic foraminiferal assemblages mainly controlled by a strong increase in abundance of *T. quinqueloba*. In the present study the LIA starts at 1500 AD and tentatively ends at 1905 AD. During this time interval, the Maunder event is here centred at ~1700 AD. This cold event is characterised by the definitive decrease in abundance of warm water taxa and by the further increase of herbivore-opportunistic species. At that time, in northern part of Italy, during 1708-09 AD is reported the occurrence of the coldest winter in Europe for the least half millennium. During this winter, the Venice Lagoon was freeze.

Finally, following ~1900 AD, the uppermost climatic event which experienced the Mediterranean area is represented by the onset of modern warm condition.

Planktonic foraminiferal data show very low values in *G. ruber* distribution and a further increased (from 1934 AD) in abundance of *G. bulloides* distribution pattern associated with a slightly increase in abundance (from 1934 AD) of *G. quadrilobatus*. Apparently, these data seem to not reflect the modern global warming. Contrarily, they

suggest a clear human impact on the marine environmental ecosystem associated to the building dam on Sele River (Salerno Gulf) at 1934 AD.

Chapter 6

A quantitative analysis of planktonic foraminifera, coupled with petrophysical and paleomagnetic measurements, was carried out on a deep core recovered in the Sentinelle Valley (Central Tyrrhenian Sea, 2370 mbsl) during CIESM Sub2 survey. Significant changes in the quantitative distribution of planktonic foraminifera allowed the identification of several bio-events useful to accurately define the boundaries of 10 eco-biozones widely recognised in the Western Mediterranean records and used for large scale correlations.

In addition, sixteen codified eco-bio-events well-matching with the Alborean Sea planktonic foraminiferal data, were recognised. Besides, the integrated oscillation of planktonic foraminiferal curves pointed out four climatic global events (S1, YD, GI-1, GS-2) occurred in the last 23 kyr. Furthermore, the comparison between the $\delta^{18}O$ NGRIP ice core record with *G. ruber* oscillation of core C08, suggests the presence in the studied record of the Heinrich events (H1 to H6) and of the Younger Dryas (YD).

The identified eco-bio-events together with two ^{14}C-AMS calibration and the strong similarity between high-resolution colour reflectance record compared with the astronomically tuned high-resolution colour reflectance records of the Ionian sea (ODP-Site 964 and of cores KC01 and KC01B), concurred to define an accurate age model, spanning between 83 and 4 kyr Cal BP with a mean sedimentation rate of 7 cm/kyr. Based on this age model, several turbiditic event beds were chronologically constrained within relative low stand and lowering phases of the MIS 4 and MIS 3; a discrete tephra occurring at the base of the core dates 75.5 kyr.

Chapter 1

INTRODUCTION

1 INTRODUTION

At present, the study of historical records, aimed towards a better understanding of the Earth's climatic system and a more accurate prediction of its future evolution, represents one of the most important priorities of the scientific community.

Climatic variability reflects complex interactions between external forcing, hydrosphere-atmosphere-biosphere-cryosphere dynamics and a range of environmental feedbacks. They also interfere with a wide range of internal climatic processes, that arise from feedbacks and system responses to external forcing.

Earth history is therefore characterized by time periods in which the climate was significantly cooler and significantly warmer than the present day. Moreover, is clear that climate variability exists on all time scales, from calendar to million years. Astronomical cycles modulate the long-term patterns of solar energy impinging on the Earth, thus providing a clock for the onset of major glacial episodes. On the other hand, changes in solar irradiance operate on decadal to millennial timescales.

In this context, the study of paleoclimate provide information about the climate variability and fluctuation (long and short-terms) of the climate system which can be used to improve the climate model for prediction of the future climate variability.

At the same time, information derived from paleoarchives (marine, continental and ice records) are the unique tools to extend the instrumental record and characterize how the climate system varies naturally in response to changing conditions and variable forcing. The information that we gain from paleorecords also provide the way to quantify how rapidly, climate will respond to variable forcing and what the impacts of climate change on ecosystems will be.

At moment, a large huge of studies on several natural archives (marine, continental and ice records) are available with different degree in accuracy, clearly related to the studied time window (e.g. IPCC, 2001). In particular, these studies were been performed on different natural paleo-proxies such as tree-rings chronologies, stable isotopic

thermometry, a large suite of geochemical and sedimentological indicators obtained from ice and sediment archives (both continental and marine), and on human scale, the historical documents (e.g. Thompson, et al., 1998; de Menocal, et al., 2000; Matrat e al., 2004; Moberg et al., 2005).

Within this large variability of climate proxies, this PhD thesis is focussed on marine records.

Marine sediments allow to have undisturbed records (continues and with high sedimentation rate) (Dansgaard et al., 1993, Bond et al., 1997, Shackleton et al., 2000, Mayewski et al., 2004), and contain a summary of all processes involved in sediment origin (e.g., Hayes et al., 2005, Robinson et al., 2006, Cacho et al., 2006). We can obtain information of the different processes that drive climate sub-system: lithosphere (sedimentary regime), biosphere (productivity, plankton and benthos response), oceans (circulation and water oxygenation, ocean ventilation) and atmosphere (eolian input fluctuations to marine basins).

In this context, a numerous group of researchers has focused their attention on the study of the climatic evolution in marine sedimentary records. In the last decade a significant number of long time series have become available that describe paleoclimatic variability with different time resolution (IPCC, 2007, and references therein). The database generated by climate proxies contains evidence of repeated (from million to calendar scale) large and regionally extensive change in atmospheric and oceanic temperatures throughout time (Ruddiman, 2001) (Fig. 1.1).

Given the wide range of the geological time scales and spatial sensitivity of different regions, it is clear that certain time periods and time scales provide more useful information for understanding patterns of current climate variability. At the same time, highly sensitive regions may provide more valuable paleoclimate information.

Taking this into consideration this research focused on the recognition, through a multiproxy approach (planktonic and benthic foraminifera, calcareous nannofossils, tephrostratigraphy), of climate variability of the late-Quaternary (last 100 kyr).

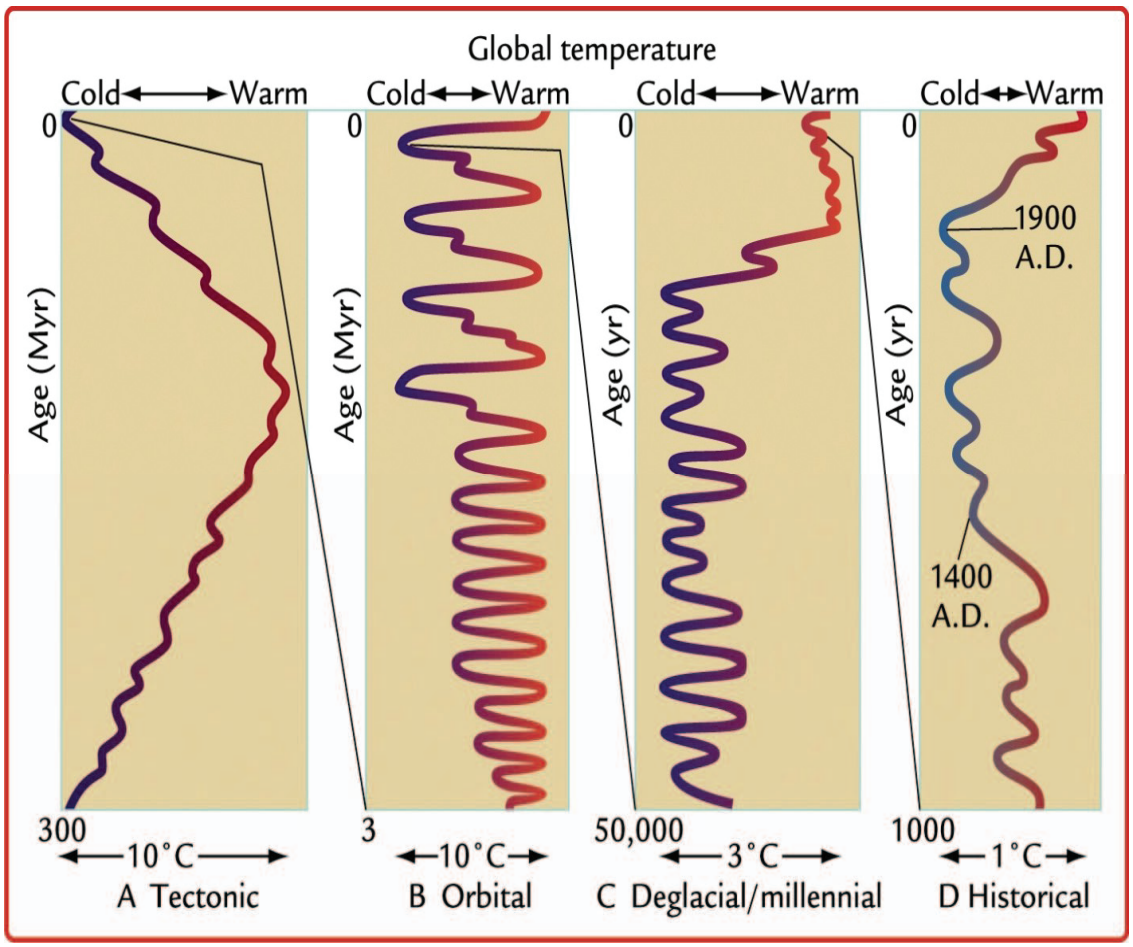

Fig. 1.1 Global temperature oscillations (warm-cold) at different time scales (from 300 million to 1000 years), with indication of data sources. The dates on the right diagram correspond to the top and bottom of the Little Ice Age (LIA) (by Ruddiman, 2001).

In particular, the last 100 kyr, represents an time interval where are recorded important climatic changes which are not completely full understood in term of planktonic foraminifera events.

The most significant events occurred at the different time scale, during the last 100 kyr are reported in the following scheme (Fig. 1.2):

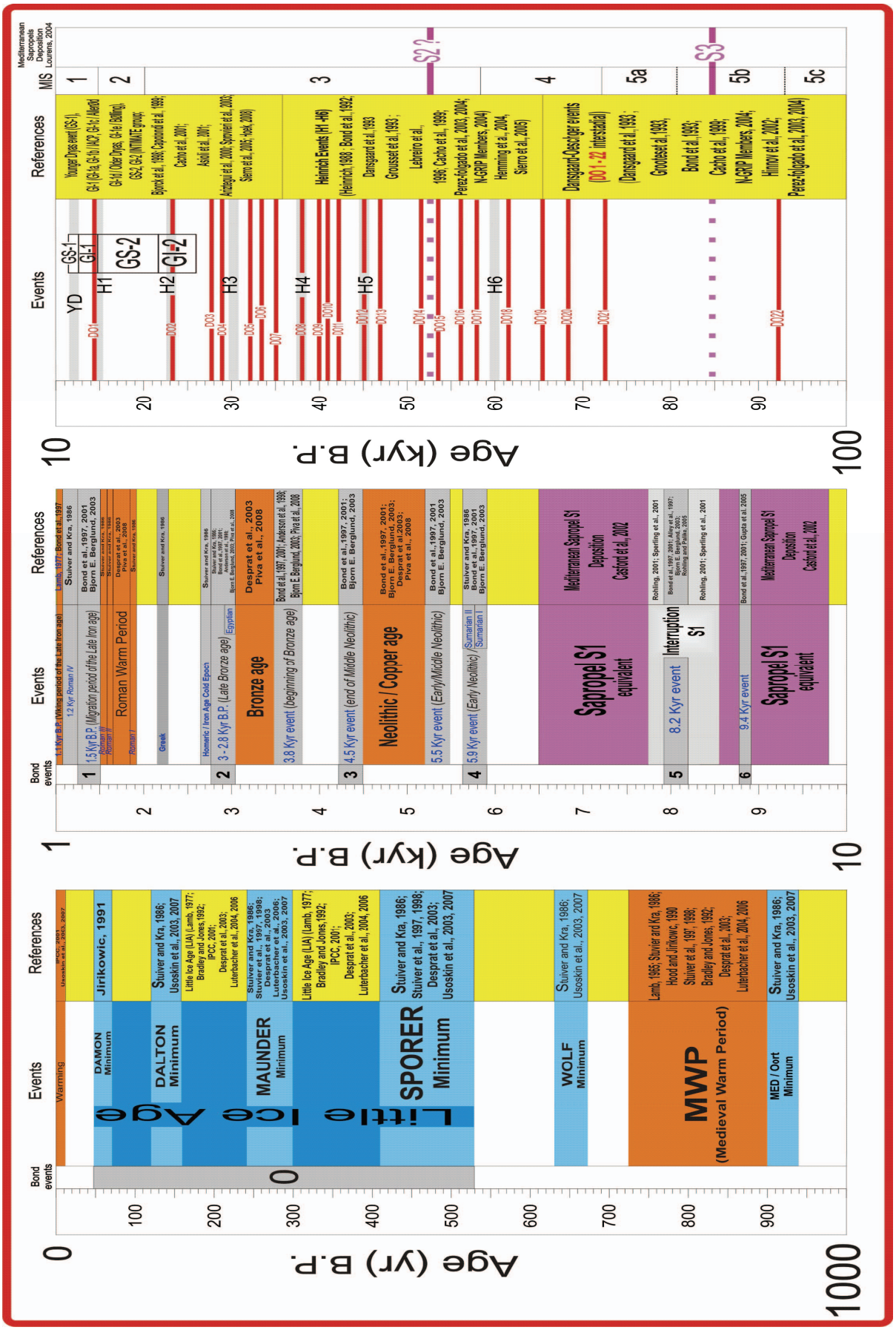
Age (yr) B.P.
Bond events
Events
References
Little Ice Age
DAMON Minimum
DALTON Minimum
MAUNDER Minimum
SPORER Minimum
WOLF Minimum
MWP (Medieval Warm Period)
MED / Oort Minimum
Warming
Jirikowic, 1991
Stuiver and Kra, 1986; Usoskin et al., 2003, 2007
Little Ice Age (LIA) (Lamb, 1977; Bradley and Jones,1992; IPCC, 200'; Desprat et al., 2003; Luterbacher et al., 2004, 2006
Stuiver and Kra, 1986; Stuiver et al., 1997, 1998; Desprat et al., 2003; Usoskin et al., 2003, 2007
Lamb, 1965; Stuiver and Kra, 1986; Hood and Jirikowic, 1990 Stuiver et al., 1997, 1998; Bradley and Jones, 1992; Desprat et al., 2003; Luterbacher et al., 2004, 2006
Age (kyr) B.P.
1.1 Kyr B.P. (Viking period of the Late Iron age)
1.2 Kyr Roman IV
1.5 Kyr B.P. (Migration period of the Late Iron age)
Roman III
Roman II
Roman I
Roman Warm Period
Greek
Homeric / Iron Age Cold Epoch
3 - 2.8 Kyr B.P. (Late Bronze age)
Egyptian
Bronze age
3.8 Kyr event (beginning of Bronze age)
4.5 Kyr event (end of Middle Neolithic)
Neolithic / Copper age
5.5 Kyr event (Early/Middle Neolithic)
5.9 Kyr event (Early Neolithic)
Sumarian III
Sumarian I
Sapropel S1 equivalent
8.2 Kyr event
Interruption S1
9.4 Kyr event
Lamb, 1977; Bond et al., 1997
Stuiver and Kra, 1986
Bond et al., 1997, 2001 Bjorn E. Berglund, 2003
Desprat et al., 2003 Piva et al., 2008
Bond et al., 1997, 2001; Anderson et al., 1992; Bond et al., 1997; Bjorn E. Berglund, 2003; Piva et al., 2008
Desprat et al., 2003 Piva et al., 2008
Bond et al., 1997, 2001; Bjorn E. Berglund, 2003
Bond et al., 1997, 2001; Bjorn E. Berglund, 2003; Desprat et al.2003; Piva et al., 2008
Bond et al., 1997, 2001 Bjorn E. Berglund, 2003
Stuiver and Kra, 1986 Bond et al., 1997, 2001 Bjorn E. Berglund, 2003
Mediterranean Sapropel S1 Deposition Castord et al., 2002
Rohling, 2001; Sperling et al., 2001
Bond et al.,1997, 2001; Alley et al., 1997; Bond et al., 2001; Rohling and Pälike, 2005
Rohling, 2001; Sperling et al., 2001
Bond et al., 1997, 2001; Gupta et al., 2005
Mediterranean Sapropel S1 Deposition Castord et al., 2002
Age (kyr) B.P.
Events
References
MIS
Mediterranean Sapropels Deposition Lourens, 2004
YD
GS-1
GI-1
GS-2
GI-2
H1
H2
H3
H4
H5
H6
S2
S3
Younger Dryas event (GS-1), GI-1 (GI-1a, GI-1b) (ACR) GI-1c Allerod
GI-1d (Older Dryas, GI-1e Bolling), GS-2, GI-2 (INTIMATE group)
Bjorch et al., 1998; Coppoind et al., 1999; Cacho et al., 2001; Asioli et al., 2001; Antonelli et al., 2008; Sprovieri et al., 2006; Sierro et al., 2005; Voelk, 2009)
Heinrich Events (H1 -H6) (Heinrich,1988; Bond et al., 1992; Dansgaard et al.,1993 ; Grousset et al.,1993 ; Lebreiro et al., 1996; Cacho et al., 1999; Perez-Folgado et al., 2003, 2004; N-GRIP Members, 2004) Hemming et a., 2004, Sierro et al., 2005)
Dansgaard-Oeschger events (DO 1 - 22 interstadial) (Dansgaard et al.,1993 ; Grootsset al.,1993, Bond et al.,1993; Cacho et al., 1999; N-GRIP Members, 2004; Himmov et al., 2002; Perez-Folgado et al., 2003, 2004)

Fig. 1.2 Climatic events chronology scheme for the last 100 kyr. The framework of the scheme show different time scales resolution. *Left*: climatic events recognised from 1 kyr to present (***Med/Oort Minimum*** (AD 1060-1090), the ***Medieval Warm Period*** (MWP) (AD 1100-1250), ***Wolf Minimum*** (AD 1280–1340), [***Sporer Minimum*** (AD 1420–1540), the ***Maunder Minimum*** (AD 1645–1710), ***Dalton Minimum*** (AD 1790-1830), ***Damon Minimum*** (AD 1880-1900)] that occur in the ***Little Ice Age*** (LIA, AD 1450–1900), ***modern warming*** **(**AD 1900-present)). *Center*: climatic events recognised from 10 kyr to 1 kyr BP (***Sapropel S1 deposition*** in the Eastern Mediterranean Sea (9.8-6.5 kyr BP), ***9.4 Kyr event (Bond event 6), 8.2 Kyr event (Bond event 5) 5.9 Kyr cold event/Early Neolithic (Bond event 4), 5.5 Kyr cold event/Early-Middle Neolithic, Neolithic/Copper age warm period (5.2 – 4.5 Kyr B.P.), 4.5 Kyr cold event/end of Middle Neolithic (Bond event 3), 3.8 Kyr cold event/beginning of Bronze age, Bronze age (3.5 – 3 Kyr B.P.), 3 – 2.8 Kyr cold event/Late of Bronze age (Bond event 2), Homeric/Iron Age cold Epoch (2.8 – 2.6 Kyr B.P.), Greek (2.3 – 2.1 Kyr B.P.), Roman warm Period (1.9 – 1.5 Kyr B.P.) with (RomanI, RomanII, Roman III), 1.5 Kyr cold event/Migration Period of the late Iron Age (Bond event 1), 1.2 Kyr event/Roman IV, 1.1 Kyr Viking period of the late Iron age***). *Right*: climatic events recognised from 100 kyr to 10 kyr BP (***The Dansgaard/Oeschger events*** (or Bond cycle, **22** interstadial events, or Dansgaard/Oeschger interstadial between 100 and 15 kyr B.P.), ***Sapropel*** "***S3"*** deposition in the Eastern Mediterranean Sea (84 kyr BP), ***Heinrich Events*** (labeled H6-H1 between 60 and 15 kyr B.P.), ***Sapropel "S2?"*** (whose existence is controversial) deposition in the Eastern Mediterranean (53 kyr BP), ***Younger Dryas*** (GS-1) 12,900 to 11,500 years B.P.). The references for all the climatic events chronology is also reported.

This research work focused on the Mediterranean Sea, considered a marginal sea that amplify responses to climate variation mostly because of its morphological constraints and the sharper gradients in the forcing. During the Late Pleistocene–Holocene, the Mediterranean Sea experienced global paleoclimatic changes and a paleoceanographic evolution which has been recorded by foraminifera assemblages (Cita et al., 1974, 1977; Raffi and Rio, 1979; Blanc-Vernet et al., 1984; Violanti et al., 1987; Verngnaud-Grazzini et al., 1988; Flores et al., 1997; Kallel et al., 1997; Capotondi et al., 1999;

Aritzegui et al., 2000; Cacho et al., 2001, Pèrez-Folgado et al., 2003, 2004; Sprovieri *et al.* 2003; Amore et al., 2004; Sierro et al., 2005). In this regard, high-resolution analysis of continuous and well-preserved sedimentary late-Quaternary records, collected from key areas of the Mediterranean Basin (e.g. Asioli et al., 2001; Rohling *et al*., 1999, 2002; Cacho *et a*l., 2000, 2001, 2002; Pèrez-Folgado et al., 2003, 2004; Sprovieri *et al.* 2003, 2006; Sbaffi et al., 2004, Geraga et al., 2005, Sierro et al. 2005) suggested that the principal climatic events and oscillations of the Northern Hemisphere, documented by multi-proxy records of the Greenland GRIP and GISP ice cores, were faithfully recorded in its sedimentary marine archives.

1.1 CLIMATIC VARIABILITY DURING THE LAST 100.000 YEARS: a brief review

During the last 100 kyr evidence from Greenland ice cores isotopic records (e.g., ice core GISP-2, GRIP, N-GRIP members, 2004; Johnsen et al., 1992; Dansgaard et al., 1993) Antarctic area (e.g. Bender et al., 1994; Mayewski et al., 1996; EPICA Community Members, 2006), and deep-sea sediments (e.g. Bond et al., 1992, 1997) indicate that the climate in the Northern Hemisphere was subject to rapid climate changes, globally distributed and dramatic in magnitude and timing. These climatic events have been labelled and globally exported.

In the last 10 years, high-resolution analysis of continuous and well-preserved sedimentary Holocene records from the Mediterranean Basin (e.g. Rohling *et al*., 2002; Cacho *et a*l., 1999, 2000, 2001; Sprovieri *et al.* 2003; Incarbona et al. 2008) clearly evidence that the principal climatic events documented and codified from Greenland GRIP and GISP ice cores, are faithfully recorded in its sedimentary archive.

The North Hemisphere codified climatic events occur at millennial scale as massive discharges of icebergs (Heinrich events from H1 to H6) (Fig. 1.2, 1.3) (Heinrich, 1988; Bond et al., 1992, 1993; Broecker et al., 1992, hemming, 2004) or as massive atmosphere-ocean reorganizations that occur with ~1,500-year frequency

(Dansgaard/Oeschger stadial/interstadial events) (Fig. 1.2, 1.3) (Dansgaard et al., 1993; Bond and Lotti, 1995).

In particular, during Heinrich Events (labeled H6-H1 between 60 and 15 kyr B.P.) (Fig. 1.2, 1.3) (see Heinrich, 1988 for a review), iceberg melting affected the hydrology of the North Atlantic Ocean, particularly the latitudes between 40°N and 55°N (Ruddiman, 1977) where the major ice-rafted debris (IRD) layers were deposited. Ice-rafted debris (IRD) sediments are lithic grains or mineral, rock fragments entrained in floating ice (icebergs or sea ice) and that settled to the seafloor when the enclosing ice melted (Heinrich, 1988). At times of Heinrich events, the influence of icebergs and melt-water have extended southward and eastward into the subtropics and offshore Portugal (Heinrich, 1988; Grousset et al., 1993; Cortijo et al., 1997; Elliot et al., 1998, 2001; Shackleton et al., 2000; Schønfeld and Zahn, 2000; Bard et al., 2000; Cacho et al., 2000; Schønfeld et al., 2003), with a strong effect also on Mediterranean surface salinity and thermohaline circulation (Sierro et al., 2005). Moreover, in Sierro et al (2005) the authors confirm that in the Western Mediterranean, planktonic and benthic foraminifera show pronounced decreases in $\delta^{18}O$ and in $\delta^{13}C$ signals, at times of Heinrich events (HE), indicating the presence of melt-water on a millennial time scale.

The Dansgaard/Oeschger events (Fig 1.2, 1.3) are characterised by a warming (Interstadial) in Greenland of 8°C to 16°C within a few decades (see Severinghaus and Brook, 1999; Masson-Delmotte et al., 2005a for a review) followed by much slower cooling (Stadial) over centuries (Bond et al., 1997). The isotopic temperature records show several (22) interstadial events, (or Dansgaard/Oeschger interstadial), between 100 and 15 kyr B.P., first recognized in the GRIP record (Greenland ice core) (Dansgaard et al., 1993) (Fig 1.2, 1.3).

Periodic episodes of instability of the Northern Hemisphere ice sheet, and intensified formation of North Atlantic Deep Water (NADW), has been invoked to explain some of these events (Dansgaard/Oeschger interstadial) (Bond et al. 1992).

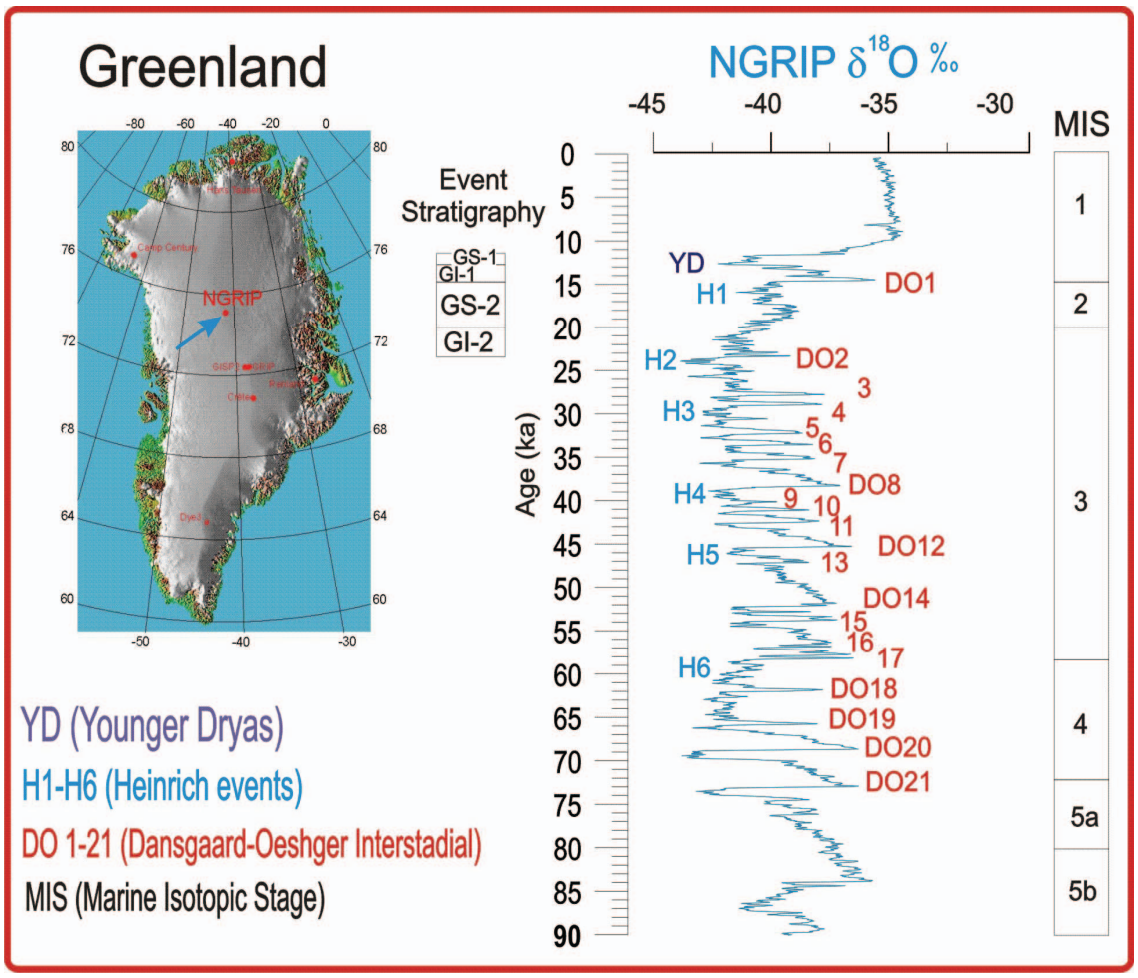

Fig. 1.3 Timing of Heinrich events and Dansgaard-Oeschger events (Interstadial) (Bond, 1992, 1993; NGRIP members, 2004; Hemming, 2004) inferred from geochemical records ($\delta^{18}O$ signal) of ice core NGRIP.

The process of North Atlantic Deep Water NADW formation is related to orbital factors, NADW forms when waters from the oceanic thermocline upwelling to the surface, cool, and sink in the seas around Greenland.

Meanwhile, the Mediterranean basin was characterized by the occurrence of organic rich, black sediment layers intercalated in the reddish brown pelagic sediments. These organic-rich layers are defined as S*apropel* (S3-S1) (Fig. 1.2) when their thickness

exceeds 1 cm and the total organic carbon (TOC) content exceeds 2% (see Kidd et al., 1978; Hilgen, 1991 for a review). Sapropels form during orbitally modulated intervals of Northern Hemisphere insolation maxima and consequent intensification of the African monsoon-fuelled river discharge into the southern margin of the basin (Rossignol-Strick et al., 1982; Rossignol-Strick, 1983, 1985; Hilgen, 1991; Rohling and Gieskes, 1989; Rohling, 1991; Corselli et al., 2002). The formation of *Sapropels* has attracted much attention over the years and for a deep knowledge see the following references (e.g., Olausson, 1961; Cita et al., 1977; Vergnaud-Grazzini et al., 1977; De Lange and ten Haven, 1983; Thunell and Williams, 1989; Rohling and Gieskes, 1989; Pedersen and Calvert, 1990; Rohling, 1991; Castradori, 1993; Rohling, 1994; Sancetta, 1994; Aksu et al., 1995; Emeis et al., 2000a,b; Warning and Brumsack, 2000; Corselli et al., 2002).

Moreover, the lithological signature (dark organic rich layer with TOC >2%) of sapropel deposition is not regionally recognised in the Mediterranean area, in fact in the Western Mediterranean marine sediments (from Gibraltar Strait to Sicily), the lithological signature is missing, meanwhile it is clearly present the calcareous plankton signatures (e.g. Sprovieri et al., 2003) throughtout these time intervals have been termed as sapropel equivalent.

For the Last Glacial-Interglacial Transition, often referred to as Weichselian Lateglacial or Last Termination, is important to specify that, the INTIMATE group proposed to relate the subdivision of the Last Termination in the North Atlantic record to an ‘event stratigraphy’ based on the GRIP Greenland ice-core record. The events, isotopically evaluated by the ‘counting from top’ procedure, include a sequence of cold (Stadial, GS) and warmer (Interstadial, GI) episodes, which can be subdivided into sub-stadial intervals with lower amplitude of the isotopic values and shorter duration (see Fig 1.2, Fig 1.4) (Sprovieri et al., 2003, Andersen et al., 2006).

Following the last glacial (14 kyr B.P.), as the climate warmed and ice sheets melted, climate went an abrupt cold phase, the so called the Younger Dryas (GS-1) (INTIMATE

group). The Younger Dryas (GS-1) stadial (Fig. 1.2, 1.4), was a brief cold climate period following the Bölling/Allerød interstadial (GI-1) (INTIMATE group, Hoek, 2008) at the end of the Pleistocene approximately between 12,900 to 11,500 years B.P. (Fig. 1.2). In Western Europe and Greenland, the Younger Dryas (GS-1) is a well-defined synchronous cool period. The prevailing theory holds that the Younger Dryas (GS-1) was caused by a significant reduction or shutdown of the North Atlantic thermohaline circulation (Broecker, 2006).

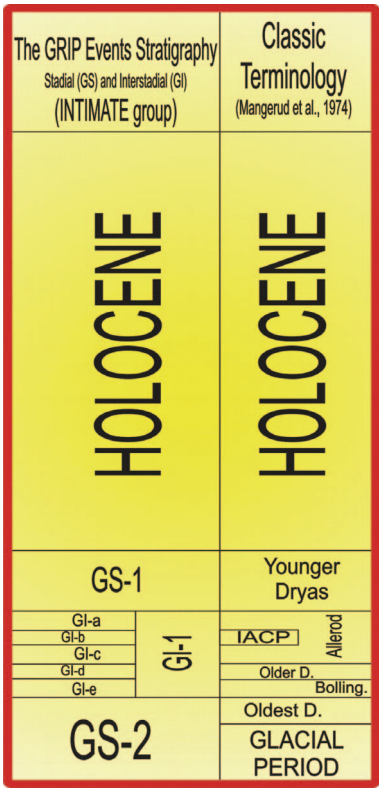

Fig. 1.4 Comparison between the GRIP event stratigraphy (Walker et al., 1999; INTIMATE group) for the Last Glacial-Interglacial Transition (*left side*) and the classic Lateglacial stratigraphy of NW Europe (Mangerud et al., 1974).

Finally, the Holocene represents a time interval intensely studied. This is partly motivated by the fact that this time interval may represents the paleoanalogous to the modern climatic conditions and mainly for the possibility to use independent age control (AMS ^{14}C radiocarbon data) to calibrate the studied records.

The significant changes in climate forcing during the Holocene induced significant and complex climate responses, including long-term and abrupt changes in temperature, precipitation, monsoon dynamics and the El Niño-Southern Oscillation (ENSO) (IPCC, 2001; Issar, 2003; Anderson et al., 2004; Luterbacher et al., 2006). Continuous paleoclimatic records from the GISP2 ice core demonstrate that Holocene climate is characterized by annual-to millennial-scale variability and that Holocene climate is significantly more complex than glacial age climate (Bond et al., 1997, 2001; Mayewski et al., 2004). (Fig. 1.2).

The early Holocene was generally warmer than the 20th century but the period of maximum warmth depends on the region considered. In general, the climate of southern west Greenland during the early- to mid-Holocene was more arid than today. The evidence for alternating wet-dry periods suggests that regional climate was quite dynamic in the early- to mid-Holocene (Steig, 1999).

During that time (early Holocene) the Eastern Mediterranean Sea, experienced the formation of *Sapropel* S1 (Fig. 1.2). Deposition of S1 occurred in two phases (S1a and S1b). The S1 interruption occurred concurrently with a short SST (Sea Surface Temperature) cooling about 8500 years BP (Rohling et al., 1997, 2001; De Rijk et al., 1999; Geraga et al., 2000; Cacho et al., 2002). This interruption is associated to an improvement of deep water ventilation conditions in the Eastern Mediterranean Sea (De Rijk et al., 1999; Myers and Rohling, 2000).

In terms of abrupt cooling, two events are identified in Greenland ice cores at 9.4 and 8.2 kyr B.P. (9.4 Kyr event / Bond event 6 and 8.2 Kyr event / Bond event 5) (Alley et al., 1997; Alley and Agustsdottir, 2005). In particular, the 9.4 Kyr event (Bond event 6) is correlated with the Erdalen event of glacier activity in Norway (Olaf et al,. 2002), as

well as with a cold event in China (Zhou Jing et al., 2007). The 8.2 Kyr event (Bond event 5) occurrence, is documented in Europe and North America by high-resolution continental proxy records (Klitgaard-Kristensen et al., 1998; von Grafenstein et al., 1998; Barber et al., 1999; Nesje et al., 2000; Rohling and Palike, 2005). Additionally, the Greenland ice core record proves that the 8.2 Kyr event (Bond event 5) is one of the coldest in the post-glacial period. A large decrease in atmospheric CH_4 concentrations (several tens of parts per billion; Spahni et al., 2003) reveals the widespread signature of the abrupt '8.2 Kyr event' associated with large-scale atmospheric circulation change recorded from the Arctic to the tropics with associated dry episodes (Hughen et al., 1996; Stager and Mayewski, 1997; Haug et al., 2001; Fleitmann et al., 2003; Rohling and Palike, 2005).

Finally, during the middle-late-Holocene (from 6 Kyr to Present), several warm-cold events have been recognized (Fig. 1.2). In particular:

5.9 Kyr cold event/Early Neolithic (Bond event 4) (Fig. 1.2). This is a well-dated period based on the regional and synchronous decline of naturally diffused trees in the Northwest Europe (Nilsson, 1964). Climatically, it was characterized by short-term wet/cool event with low solar intensity around 6 Kyr B.P. followed by ca. 300 years of dry/cold conditions with high solar intensity (Berglund, 2003). During these centuries, glacier activity increased, as also reflected in increased ice-rafting (IRD) in North Atlantic sediments during Bond's event 4 (Bond et al., 1997). The chronological precision for these climatic events is rather weak. It is generally accepted that climate had an important role behind the first agricultural expansion in Northwest Europe (Birks, 1986) and possibly also globally (Sandweiss et al., 1999).

5.5 Kyr cold event/Early-Middle Neolithic (Fig. 1.2). This is a rather well-dated event often named the regeneration phase, with the contraction of agricultural areas locally and regionally, e.g. in Scandinavia (Graslund, 1980; Berglund, 1986) and Ireland (Molloy and O'Connell, 1995). Climatically, a change to more wet/cool conditions is

demonstrated by raised lake levels, increased bog growth, and lowered tree line (Berglund, 2003).

Neolithic/Copper age warm period (5.2 – 4.5 Kyr B.P.) and 4.5 Kyr cold event/end of Middle Neolithic (Bond event 3) (Fig. 1.2)**.** A period with rather wet/cool conditions with raised lake levels in Southern Sweden and Central Europe, expanding bogs on Ireland, and glaciers in the Scandinavian mountains. Increased glacier activity is also reflected in the North Atlantic sediments by Bond's event 3 (4.5 Kyr event) (Bond et al., 1997). It is also important to note that dendroclimatic data from North Scandinavia reflects a changes from stable to more variable conditions around 5000–4500 B.P. (Eronen et al., 1999).

3.8 Kyr cold event/beginning of Bronze age (Fig 1.2)**.** In this period, dramatic change from more continental to oceanic climate was documented. The frequency of lake catchment erosion events increased distinctly from this time onwards. Peat humification data in northern Scotland indicate a main change from dry to wet conditions 3900–3500 B.P. (Anderson et al., 1998).

Bronze age (3.5 – 3 Kyr B.P.) (Fig. 1.2). During this phase the climate evidences for a generally warmer climate. During the Bronze Age in the Alps is reported the lowering of the tree line, glacier activity, proglacial lake level and traces of high-altitude mining activities (Leeman and Niessen, 1994). Expanding agriculture occurred in central settlement areas as well as in marginal land areas, particularly involving expanding pastures all over Northwest Europe (Berglund, 2003). This expansion led to one of the main prehistoric deforestation periods (Berglund, 2003).

3 – 2.8 Kyr cold event/Late of Bronze age (Bond event 2) and Homeric/Iron Age cold Epoch (2.8 – 2.6 Kyr B.P.) (Fig. 1.2). This period was complex, with cool/wet conditions just before 3000 B.P., followed by a warm/dry phase ca. 3000 B.P.; and then a change to cool/wet conditions again around 2800 B.P.. There is a general trend of raised lake levels and increased glacier activity around 3000 B.P.. The last phase around 2800 B.P. corresponds to Bond's event 2 (2.8 Kyr event) in the North Atlantic (Bond et

al., 1997). It corresponds with one of the most pronounced insolation drops during the Holocene, which has been much debated recently (van Geel et al., 1996, 1998).

Greek (2.3 – 2.1 Kyr B.P.) and Roman warm Period (1.9 – 1.5 Kyr B.P.) with (RomanI, RomanII, Roman III) (Fig. 1.2). This period present cool/wet conditions just before 2000 yr B.P., followed by a warm/dry phase. Expanding agriculture occurred in central settlement areas as well as in marginal land areas, particularly involving expanding pastures all over Europe (B.E. Berglund, 2003). This period include the time of the Roman Empire around 50 BC – 476 AD.

1.5 Kyr cold event/Migration Period of the late Iron Age (Bond event 1) and 1.2 Kyr event/Roman IV (Fig. 1.2). This phase corresponds to the interval following the Roman Empire collapse around AD 480 and the Justinian plague ca. AD 540 (Lamb, 1982; Ambrosiani, 1984). Data from tree ring and diatom assemblages suggest a rapid cooling (Eronen et al., 1999) that can be correlated with Bond's event 1 (1.5 Kyr event) documented in the North Atlantic sediments (Bond et al., 1997).

1.1 Kyr Viking period of the late Iron age (Fig. 1.2). The climatic proxies show the expansion of settlement and agriculture, with clearing of new areas for colonization, even involving remote areas such as Iceland and Greenland. This boom period covers several centuries from AD 700 to 1100. Climatically, it was a favourable period for agriculture in marginal areas of Northwest Europe.

The last millennium is of particular interest because, in addition to the available proxy data, it contains two important contrasted periods: the Medieval Warm Period (MWP) (Fig. 1.2), characterised by a warm climate under which, notably, Vikings were able to settle on Greenland (Brewer et al., 2007) and the Little Ice Age (LIA) (Fig. 1.2)., characterised by cold records in written historical sources (Lamb, 1977; Bradley and Jones, 1992)

Recently, the correlation between the GISP2 (Greenland Ice Sheet Project 2) $\delta^{18}O$ curve and the atmospheric $\Delta^{14}C$ record (Stuiver et al.,1997), suggest that solar activity constrains the climatic variability of the last millennium.

Moreover, based on direct reports of solar observations, old auroral records and notably $\Delta^{14}C$ analysis of tree rings, low/high sunspot activity events have been inferred in the beginning/middle of the last millenium.

These events are known as the ***Med/Oort Minimum*** (AD 1060-1090), the ***Medieval Warm Period*** (MWP), centred on the Grand Solar Maximum (AD 1100-1250), ***Wolf Minimum*** (AD 1280–1340) (Fig. 1.2). Moreover, Other historical sunspot minima have been detected either directly or by the analysis of $\Delta^{14}C$ in ice cores or tree rings for the last 550 years; these include the ***Sporer Minimum*** (AD 1420–1540), the ***Maunder Minimum*** (AD 1645–1710), ***Dalton Minimum*** (AD 1790-1830), ***Damon Minimum*** (AD 1880-1900) that occur in the ***Little Ice Age*** (LIA, AD 1450–1900) (Fig. 1.2).

The ***Little Ice Age*** (LIA) (Fig. 1.2), is the finest constrained chronologically and documented by several historical accounts, artistic production, economical and societal changes (Matthes, 1939; Lamb, 1977; Stuiver and Kra, 1986; Bradley and Jones, 1992; Bond et al. 1992; Camuffo, 1997; IPCC, 2001; Luterbacher et al., 2004, 2006).

In general, the LIA was a particularly humid period, which brought wetter conditions even in the sub-Saharan African region (Nicholson, 1978). In this regard, the LIA is characterized by a widespread cooling on the order of 0.5–1.0 °C and a lowering of the equilibrium line altitude of mountain glaciers around the world of about 100 m (ice extent was the greatest of any time since the Last Glacial Maximum) (e.g. Broecker 2001; Luterbacher et al., 2004, 2006).

At that time, in northern part of Italy, during 1708-09 AD is reported the occurrence of the coldest winter in Europe for the least half millennium during which the Venice Lagoon was freeze (Fig. 1.5) (Luterbacher et al., 2006).

Onwards, a general warming was experienced, particularly during the present century (Fig. 1.2). The instrumental temperature data that exist before 1850, although increasingly biased towards Europe in earlier periods, show that the warming observed after 1980 is unprecedented compared to the levels measured in the previous 280 years (IPCC, 2001).

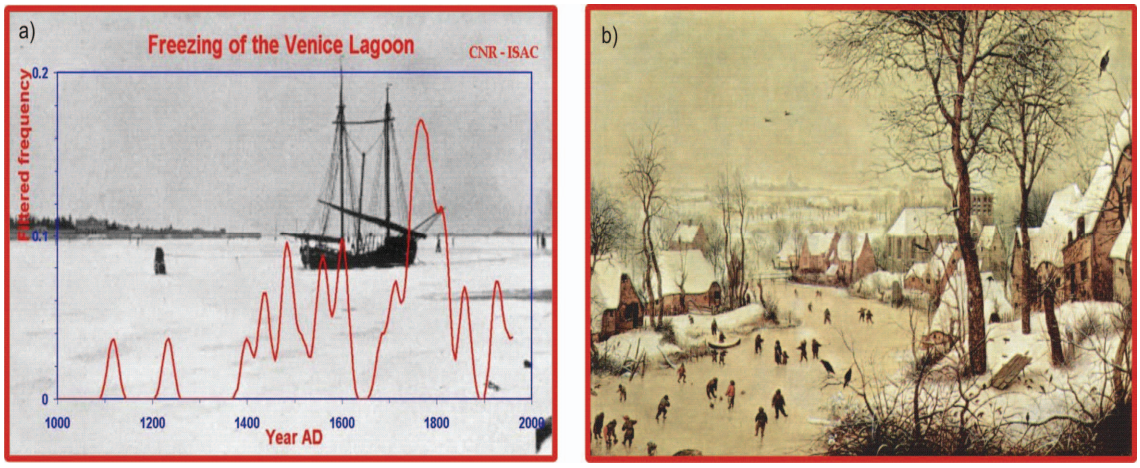

Fig. 1.5 a) Venice Lagoon freezing (Camuffo, 1997). b) Winter Landscape (Pieter Bruegel the Elder).

Recent analysis of instrumental documentary and proxy climate records, focussing on European temperatures (Luterbacher et al., 2006), have also pointed to the unprecedented warmth of the 20th century and shown that the extreme summer of 2003 was very likely warmer than any that has occurred in at least 500 years (IPCC, 2001; Luterbacher et al., 2004, 2006; Guiot et al., 2005).

If the behaviour of recent temperature change is to be understood, and the mechanisms and causes correctly attributed, parallel efforts are needed to reconstruct the longer and more widespread pre-instrumental history of climate variability, as well as the detailed changes in various factors that might influence climate (Bradley et al., 2003b; Jones and Mann, 2004). For example, major reorganizations in Holocene climate plus finer-scale climate fluctuations such as abrupt shifts in drought and flood frequency may be explained by a combination of climate forcings. For the Holocene such forcings may include (1) changes in thermohaline circulation; (2) changes in insolation, notably precession that may generate long-period El Niño-type reorganizations in moisture and temperature and changes in marine and land ice cover; (3) changes in solar output; (4)

changes in the concentrations of volcanic aerosols and dusts; and (5) anthropogenic impact. Of all the potential climate forcing mechanisms, solar variability superimposed on long-term changes in insolation (Bond et al., 1997, 2001; Denton and Karle´n, 1973; Mayewski et al., 1997; O'Brien et al., 1995; Stuvier et al., 1997, 1998; de Menocal et al., 2000, Desprat et al., 2003; Usoskin et al., 2003, 2006) seems to be the most likely important forcing mechanism for the Holocene climatic events.

Actually, a variety of paleo-records are available to test the impact of these forcing mechanisms, including, $\Delta^{14}C$ series in tree rings and ^{10}Be series from ice cores, gas content (CO_2, CH_4, SO_2, NH_4), from ice cores.

However, many important characteristics of the rapid climate change events are still not clearly understood. In order to understand the phasing and the cause of rapid climate change events from region to region, these events must to be documented through a series of multi-disciplinary investigations of very well-dated continuous records of key areas for paleoclimatic studies.

1.2 THE MEDITERRANEAN SEA

1.2.1 Why the Mediterranean Sea

During the last few years, a numerous group of researchers has focused their attention on the study of late-Quaternary climatic evolution, in sediments collected in the Mediterranean area (Fig. 1.6) (e.g., Emeis et al., 1996; Rohling et al., 2001).

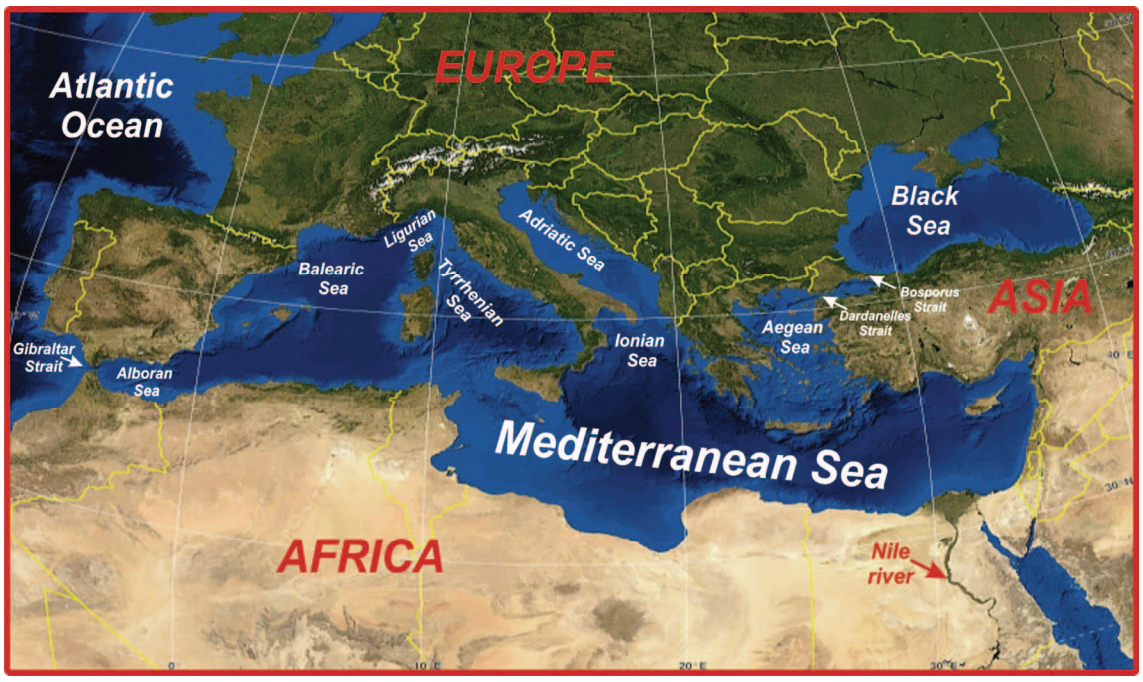

Fig. 1.5 Mediterranean Sea map.

The Mediterranean basin (Fig. 1.6), is considered one of the most complex marine environment on the Earth (Williams, 1998) for its geographic estension and hydrography. The Mediterranean represents an excellent 'natural laboratory' where processes can be studied in conveniently-reduced spatial scales and with a better signal to noise ratio than may be expected in the open ocean (Rohling, 2001).

The scientific community focused on the study of Late-Quaternary record to identify, in the geological record, paleo-analogues to the modern climatic condition and to better understand the future evolution of the climate.

Anyway, several uncertainties are still present, regarding the resolution of the chrono-stratigraphic scheme. The main problem is to find marine records and high-resolution proxies which are favourable for high-resolution paleoclimatic studies at decadal- to centennial-scale. In this context, the Mediterranean Sea due to the high sedimentation rates together with a continuous sedimentation, offers the unique opportunity to analyze global and regional climate changes at high resolution time scale.

Moreover, for a fine age control and for a high-resolution integrated stratigraphy, indipendent tie-points (e.g. tephra layers) are necessary. During the late-Quaternary, including prehistoric and historical times, several volcanoes have been active in the Mediterranean area (Fig. 1.7). In this context, the eruptive events can be considered as instantaneous geologic events, and then vitreous volcanic eject (tephra) can provide time-synchronous marker horizon within sediment sequence for over large areas.

Fig. 1.7 Mediterranean Sea map, with location of the main volcanic sources.

1.2.2 Climate

The Mediterranean region lies in an area of great climatic interest. It marks a transitional zone between the deserts of North Africa, which are situated within the arid zone of the subtropical high (Boucher, 1975), and Central and Northern Europe, influenced by the westerly flow during the whole year. In addition, the Mediterranean climate is influenced by the South Asian Monsoon, the Siberian High Pressure System, the Southern Oscillation and the North Atlantic Oscillation (Fig. 1.8). The climate of the Mediterranean is mild and wet during the winter and hot and dry during the summer. Winter climate is mostly dominated by the westward movement of storms originating over the Atlantic and impinging upon the western European coasts (Lolis et al., 2002). In the summer, high pressure and descending motions dominate over the region, leading to dry conditions particularly over the southern Mediterranean (Saaroni et al., 2003; Ziv et al., 2004).

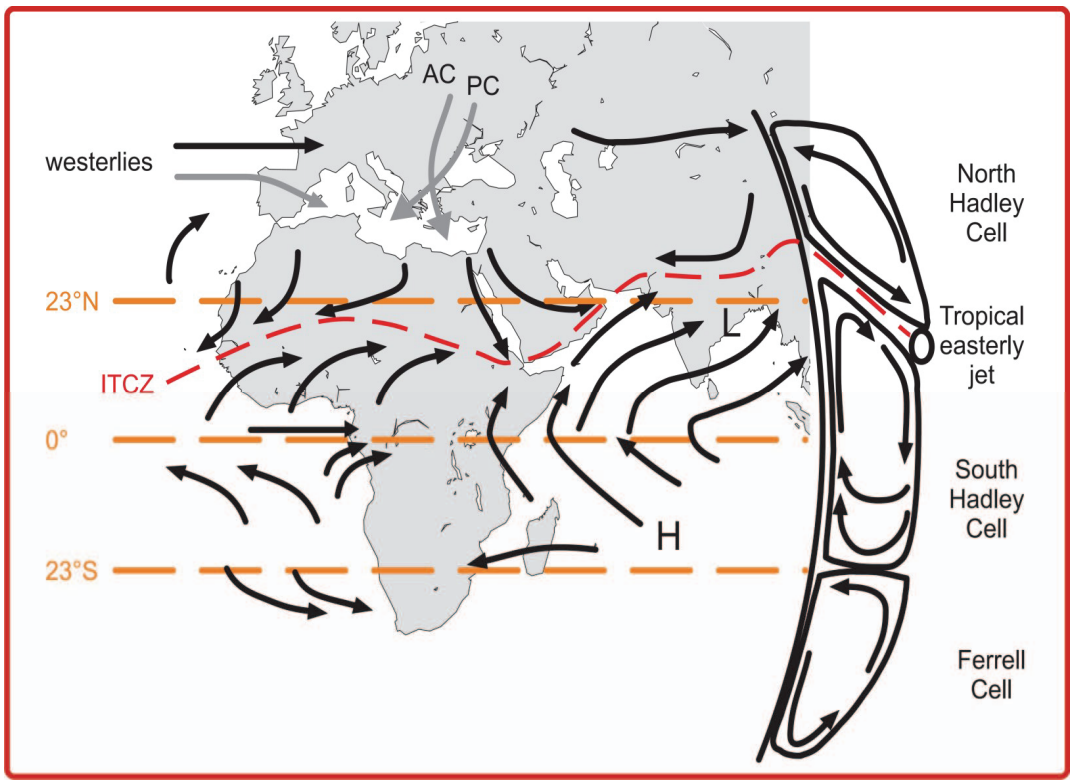

Fig. 1.8 Northern Hemisphere summer atmospheric circulation. Main winds are indicated as black arrows. ITCZ = intertropical convergence zone; H and L = areas of high and low sea level pressure, respectively. Main air masses reaching the eastern Mediterranean in winter as grey arrows. AC and PC = Arctic continental and Polar air masses, respectively (Reichart, 1997 and Rohling et al., 2008a; Marino, 2008).

1.2.3 Hydrography

The Mediterranean Sea is characterized by the presence of thresholds that separate the basin in a series of sub-basins. Mainly, from West to East, The Strait of Gibraltar, a threshold with a depth of 284 m (Fig. 1.9) (Bryden and Kinder,1991), which drives the exchange of Atlantic and Mediterranean waters, has an important role to play in the circulation and productivity of the Mediterranean Sea. Subsequently, the threshold of Strait of Sicily divides the Mediterranean into the main Western and Eastern basins, while several satellite basins and definite entities may be distinguished in more detail, such as the Alboran, Balearic, Ligurian, Tyrrhenian, Adriatic, Ionian and Aegean Seas (Fig. 1.6).

The Mediterranean circulation is anti-estuarine type. In particular, the Mediterranean circulation is driven by water exchange through the various straits, wind stress, and thermohaline fluxes, with the latter depending on the basin's freshwater and heat budgets (Robinson et al., 2001). In the northern sectors of the basin the surface pattenrs are dominated by cyclonic gyres. In the southern sectors surface waters derived from the Atlantic Ocean flow eastwards through currents, jets (Western basin) and anticyclonic gyres (Eastern basin) (Pinardi and Masetti, 2000).

In spite of the high fresh water input from rain or rivers in the region, the Mediterranean Sea is defined a concentration basin, with an excess of evaporation over freshwater input resulting in strong temperature and salinity gradients in surface waters from West to East (Wüst, 1961; Béthoux, 1979; Garrett, 1996; Gilman and Garrett, 1994). In this

context, the seasonality of water deficit plays an important role in controlling the water transported by the main currents.

The vertical distribution of the Mediterranean water masses includes the surface waters (0-200 m), the intermediate waters (200-600 m), and the deep waters (> 600 m) (Pinardi and Masetti, 2000; Tsimplis et al., 2005) (Fig. 1.9).

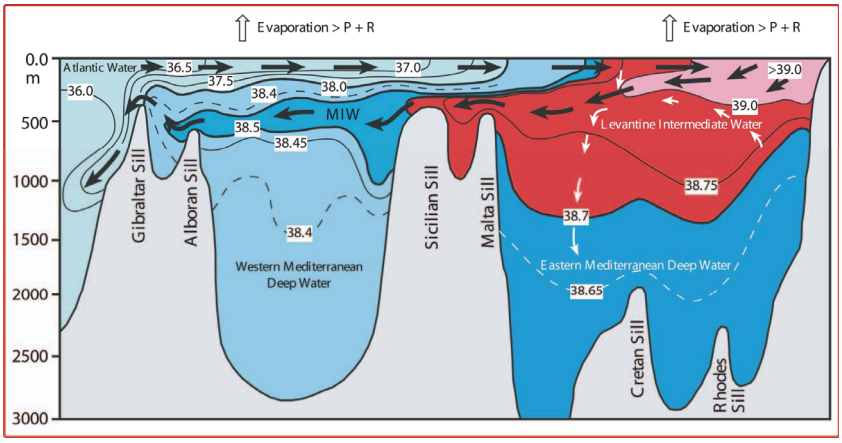

Fig. 1.9 West - East cross-section showing water mass circulation in the Mediterranean Sea during winter (after Wüst, 1961). Isolines indicate salinity values and arrows indicate the direction of water circulation in the Mediterranean Sea (Rohling et al., 2008a).

During its passage eastward, Atlantic water (AW, 0-200 m), already stripped of much of its nutrients by phytoplankton growth in the surface of the Atlantic Ocean, interacts and mixes with upwelled Levantine Intermediate Water (LIW) (Hayes, 1999).

Moreover, during its passage eastward, AW nutrients are decreased even more by phytoplankton (Bethoux et al., 1997), while climatic factors such as evaporation have resulted in its salinity increasing by up to 10% (Milliman et al., 1992) (Fig. 1.9, 1.10a).

Consequently, the Atlantic Water (AW) that eastward up inflow in the Mediterranean Sea is currently referred to as the Modified Atlantic Water (MAW) (Heburn and La Violette, 1990; Milliman et al., 1992; Millot, 1999).

In winter occasional outbreaks of cold, dry air masses over the northern Levantine basin severely cool the sea surface thereby leading to vertical convection of these cold and salty (dense) surface waters to form the Levantine Intermediate water (LIW, 200-600 m) in the Rhodes Gyre (Fig. 1.10b) (Malanotte-Rizzoli and Hecht, 1988; Georgopoulos et al., 1989; Buongiorno Nardelli and Salusti, 2000). This water mass subsequently settles between 200 and 600 m and spreads out in the entire Mediterranean basins and eventually enters the Atlantic Ocean, by Gibraltar Strait (Parrilla et al., 1986; Richez and Gascard, 1986; Marino, 2008) (Fig. 1.10b). The interaction of the LIW with cold surface waters in the Northern basins of the Mediterranean (the Gulf of Lions and the Adriatic Sea) governs deep-water (> 600 m) formation processes (Fig. 1.10b), which is responsible for the deep-sea ventilation of the entire basin (Pinardi and Masetti, 2000). Sites of deep water formation are the Gulf of Lions for the Western basin (Western Mediterranean Deep Waters, WMDW), while the sources of the Eastern Mediterranean Deep Water (EMDW) are the Adriatic and Aegean Seas (Schlitzer et al., 1991) (Fig. 1.10c).

The water flowing out of the Mediterranean, Levantine Intermediate Water (LIW) and the Mediterranean Deep Water (MDW) is denser and flows below the incoming lighter Atlantic water (Fig. 1.10b).

Finally, because of the West–East gradient in important life supporting nutrients such as nitrogen and phosphorus (Krom et al., 1991) there is West–East gradient in ocean productivity (Turley et al., in press). Within this framework the marine climate of the Mediterranean Sea is characterized by relatively warm and salty, nutrient-poor waters. It is important to note that the gradients are thought to exert the main control on present-day planktonic foraminiferal distribution patterns (e.g. Thunell, 1978; Pujol and Vergnaud-Grazzini, 1995). Therefore, it may be expected that temporal variations in the temperature and salinity gradients would be expressed by changes in the planktonic foraminiferal assemblage records as studied from sediment cores.

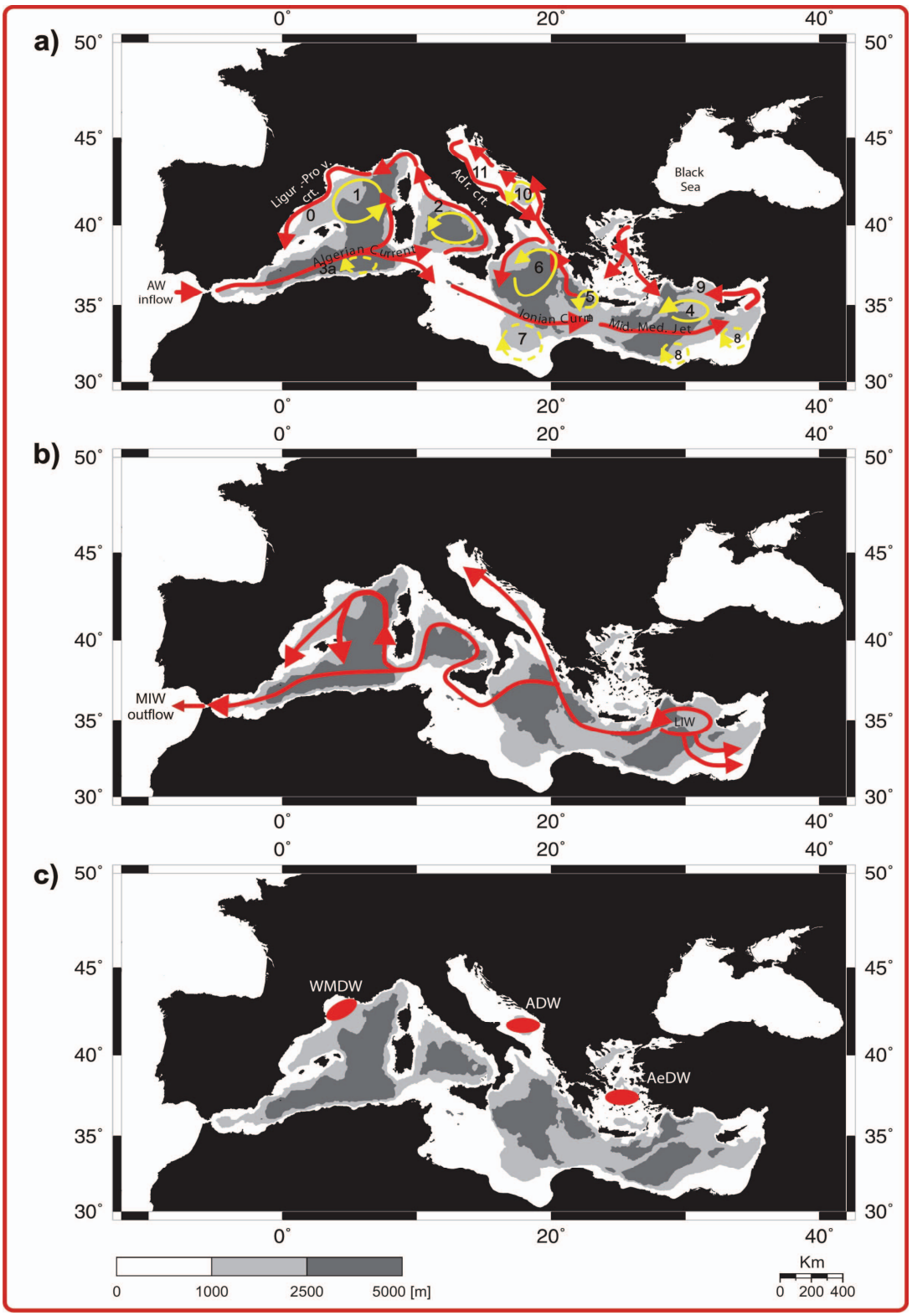
a)
b)
c)
0°
20°
40°
50°
45°
40°
35°
30°
Ligur.-Pro v. crt.
Adr. crt.
Black Sea
Algerian Current
AW inflow
Ionian Current
Mid. Med. Jet
0
1
2
3a
4
5
6
7
8
9
10
11
MIW outflow
LIW
WMDW
ADW
AeDW
0
1000
2500
5000 [m]
Km
0 200 400

Fig. 1.10 Water mass circulation in the Mediterranean Sea (**a**) The schematic of major basin current and gyres systems. **0** Ligurian-Provencal current; **1** Lion Gyre; **2** Thyrrenian cyclonic circulation; **3** Algerian current; **4** Rhodes Gyre; **5** Western Cretan Gyre; **6** Western Ionian Gyre; **7**Anticyclone in the Gulf of Syrte; **8** Shikmona and Mers a-Matruh gyres system; **9** Cilican and asia Minor current; **10** Southern Adriatic gyre; **11** Western Adriatic Coastal current. Ligur. - Prov. crt. = Ligurian-Provencal current; Adr. crt. = Adriatic current; Mid Med. Jet = Mid Mediterranean Jet. (**b**) ***LIW*** dispersal pathways. (**c**) Sites of deep water overturning. **WMDW** (western Mediterranean Deep Waters); ***ADW*** (Adriatic Deep Waters); ***AeDW*** (Aegean Deep Waters). (slightly modified after Pinardi and Masetti, 2000 and Marino, 2008).

1.3 PLANKTONIC FORAMINIFERA IN THE MEDITERRANEAN SEA

The salinity, temperature, nutrients gradients between Western to Eastern part of the Mediterranean basin, and the presence of gyre and eddies, exert the main control on present-day planktonic foraminiferal distribution patterns (e.g. Thunell, 1978; Pujol and Vergnaud-Grazzini, 1995). For this planktonic foraminifera fossil assemblages can be considered an excellent proxies for paleoclimatic and paleoceanografic investigations. Planktonic foraminifera in the Mediterranean have been extensively studied since the first piston cores were taken during the Swedish Deep Sea Expedition of 1946-47 (e.g. Kullenberg, 1952; Todd, 1958; Parker, 1958; Olausson, 1960, 1961; Herman, 1972; Cita et al., 1977; Thunell et al., 1977; Vergnaud-Grazzini et al., 1977; Thunell, 1978). Previous works performed on long sediement cores collected in the Western Mediterranean Sea primarily concerned stable oxygen isotope ($\delta^{18}O$) records rather than faunal variations (Paterne et al., 1986; Vazquez et al., 1990), while faunal abundance investigations were focussed specifically on the last deglaciation time interval (Pujol and Vergnaud-Grazzini, 1989; Rohling et al., 1995).

Meanwhile, the anoxic/dysoxic sedimentation during periods of sapropel deposition prevents bioturbation, thereby allowing highly resolved reconstructions of planktonic

foraminiferal changes in the time domain and providing important information on planktonic foraminiferal palaeoecological features (i.e., Thunell et al., 1977; Thunell and Williams, 1983; Ganssen and Troelstra, 1987; Tang and Stott, 1993; Rohling et al., 1997, Hayes, 1999).

1.3.1 Planktonic foraminiferal ecological features: state of the art

Globigerinoides ruber

This taxon (Fig. 1.11) is generally considered a mixed layer and omnivorous feeders bearing dinoflagellate symbiont (Be´ and Hamlin, 1967; Be´ and Tolderlund, 1971; Be´ and Hutson, 1977; Be´ et al., 1977; Fairbanks et al., 1982; Hemleben and Spindler, 1983; Almogi-Labin, 1984; Thunell and Reynolds, 1984; Bé et al., 1985; Vergnaud-Grazzini et al., 1986; Hemleben et al., 1989; Pujol and Vergnaud-Grazzini, 1989; Van Leeuwen, 1989; Hemleben et al., 1989; Pujol and Vergnaud-Grazzini, 1995). The temperature range for the *G. ruber* is 13.3°- 29.5°C, optimum above 21.3°C; in particular, pink variety is most abundant at T > 24.4°C (Tolderlund and Bé, 1971). Although this species is able to tolerate a broad range of temperatures and salinities, it usually thrive in the warm, nutrient-poor waters of the summer mixed layer well above the thermocline and nutricline (Hemleben et al., 1989). In the Mediterranean, the highest frequencies are found at the end of summer. At that time, it occurs all over the Mediterranean, but maximal densities are recorded east of the Sicilian Strait and in the Ionian basin at in the 50-100 m water-depth (Pujol and Vergnaud Grazzini 1995).

Globigerinoides quadrilobatus - Globigerinoides trilobus - Globigerinoides sacculifer

These tropical taxa (Fig. 1.11) occur in greatest abundance in the upper 50 m at the end of summer. They are rare (about 5% of the shallow assemblage) in the Alboran Sea, but are more prolific within the Balearic Basin and off the North African coast (Pujol and Vergnaud-Grazzini 1995). *G. sacculifer* may be considered a varietal form of *G. trilobus* characterized by a sac-like final chamber. These spinose and symbiont bearing species are usually found in shallow waters with relatively low densities. They appear associated with oligotrophic conditions, in the Gulf of Lion where a rapid nutrient

depletion occurs at the end of summer in the surface layers, and in the Levantine and Ionian Basins, where oligotrophic conditions are dominant all over the year. Moreover the association of these species is indicative of a well-stratified euphotic zone and an oligotrophic mixed layer.

In particular, Caron et al. (1981) demonstrated that symbiont photosynthesis (directly affected by light intensity) is important for the growth and survival of *G. quadrilobatus.* In this regard, *G. quadrilobatus* showed the highest feeding rate of copepods among spinose planktonic foraminifera (Anderson, 1983; Spindler et al., 1984; Hemleben et al., 1989).

Orbulina universa

This taxon (Fig. 1.11) lives in mixed layer (Bé et al., 1985; Vergnaud-Grazzini et al., 1986; Thunell and Reynolds, 1984) and deeper waters (Fairbanks et al., 1982; Almogi-Labin, 1984; Bé et al., 1985). It generally prefers surface waters with temperatures between 13°C and 19°C. Its symbiont activity may also partly control its distribution (Spero and Parker, 1985). In the Mediterranean, *O. universa* is more prolific at the end of summer in the 50-100 m depth interval along the North African coast and around the Balearic Isles (Pujol and Vergnaud-Grazzini 1995).

Globigerinella siphonifera – Globoturborotalita tenella – Globigerinella calida.

In the Mediterranean, they prefer the winter period and maximal abundances are found in the 100-200 m depth interval (Pujol & Vergnaud Grazzini 1995). Relative abundances reach 5% of the live assemblage in the Ionian Basin and off Tunisia.

Globigerina bulloides

G.bulloides inhabits both mixed layer (< 400 m water depth) (Bé, 1969; Bé et al., 1985; Hemleben et al., 1989; Reynolds and Thunell, 1989; Van Leeuwen, 1989) and deeper waters (mainly in and above the thermocline). Almogi-Labin,1984; Hemleben et al., 1989; Pujol and Vergnaud-Grazzini, 1989). *G. bulloides* (Fig. 1.11) is a species typical of the transitional to subpolar provinces in the north Atlantic and is therefore adapted to

cool surface waters (Tolderlund and Be, 1971; Be, 1977; Hemleben et al., 1989). Today, it reaches the highest concentrations in upwelling regions or in areas of vigorous vertical mixing in the water column (Reynolds and Thunell, 1985), where high phytoplankton productivity prevails. Moreover, in the Mediterranean Sea this species occurs in significant abundances in winter. High frequencies are observed in the western-south western Mediterranean (Pujol and Vergnaud-Grazzini 1995). between 50 and 200 m water depth.

Globorotalia inflata

G. inflata (Fig. 1.11) prefers cool and well-mixed waters with intermediate to high nutrient levels (Pujol and Vergnaud-Grazzini, 1995). It prefers cooling and/or increased seasonal contrast, with vertical mixing during winter. The absence of this species has been observed in many Late Quaternary sapropel layers and this pattern is interpreted as the response to a lack of mixing of the water column, with year-round stratification (Capotondi et al., 2000; Ariztegui et al., 2000; Principato et al., 2003). Temperature range between 2.2°C to 22.6°C, (Tolderlund and Bé, 1971).

Turborotalita quinqueloba

T. quinqueloba (Fig. 1.11) is a eurythermal (shallow dweller) species that increases production during diatom blooms (in spring) (Sautter and Thunell, 1991). The temperature range for this taxon is 2.2°C - 16°C, with optimum between 4.6°C and 10.8°C (Tolderlund and Bé, 1971). Is importane to note that the lower limit may even be about 1°C and upper limit 21.5°C according to sparse findings. Today, they reach the highest concentrations in upwelling regions or in areas of vigorous mixing in water column (Raynolds & Thunell 1985) where high phytoplankton productivity prevails.

Globigerinita glutinata

G. glutinata (Fig. 1.11) in the North Atlantic increases in percentages with the presence of a deep mixed layer (Fairbanks et al., 1980; Bé et al., 1985; Thunell and Reynolds, 1984; Hemleben et al., 1989; Reynolds and Thunell, 1989) and with a decrease in surface water temperature. This taxon displays a first reaction of the planktonic foraminiferal fauna to phytoplankton development during spring (Thunnell and Reynolds, 1984; Schiebel and Hemleben, 2000).

Globorotalia scitula

Little is known about the ecology of *G. scitula* (Fig. 1.11). Data based on sediment trap/plankton nets document that *G. scitula* lives in very deep waters (Bé, 1969). In particular, *G. scitula* appears near the surface as a very thin shelled specimen before. Subsequently, this taxon sinking to deeper water (Hemleben et al., 1989). Finally, *G. scitula* is considered a "deep-dwelling" subpolar species and commonly preferring a diatom-based diet. Actually, it is very scarse in the Mediterranean Sea (<5% East of the Sicily Straits, Geraga et al., 2005; Ducassou et al., 2007).

Globorotalia truncatulinoides

G. truncatulinoides is a very deep dwelling species (Tolderlund and Bé, 1971; Hutson, 1977; Hemleben and Spindler, 1983; Vergnaud-Grazzini et al, 1986; Hemleben et al.,1989) that live between 15.4°C to 22°C (Tolderlund and Bé, 1971; Brummer and Kroon, 1988; Hemleben et al., 1989). In the Mediterranean, this non-spinose taxon (Fig. 1.11) prevails during winter in deep waters of the western basin. It seems that the primary factor controlling the distribution of this species within the Mediterranean is the winter convection and vertical mixing whereas food availability and temperature are secondary limiting factors (Pujol and Vergnaud-Grazzini 1995).

Neogloboquadrinids (N. pachyderma and N. dutertrei)

This group comprises predominantly dextrally coiled *pachyderma* types and quite tightly coiled *dutertrei* types in agreement with Rohling and Gieskes, (1989). Abundance of Neogloboquadrinids is closely linked to the development of a Deep Chlorophyll Maximum (DCM; Rohling and Gieskes, 1989; and references therein: Fairbanks and Wiebe, 1982; Fairbanks et al., 1980, 1982; Hemleben and Spindler, 1983; Thunell and Reynolds, 1984; Bé et al., 1985; Hemleben et al., 1989; Pujol and Vergnaud-Grazzini, 1989; Reynolds and Thunell, 1989; Van Leeuwen, 1989; Rohling et al., 1995). This group have a very wide temperature range. In particular, This species occurs from subpolar to tropical regions but is most prolific when sub-thermocline temperatures are colder than 12 °C (Be and Tolderlund, 1971).

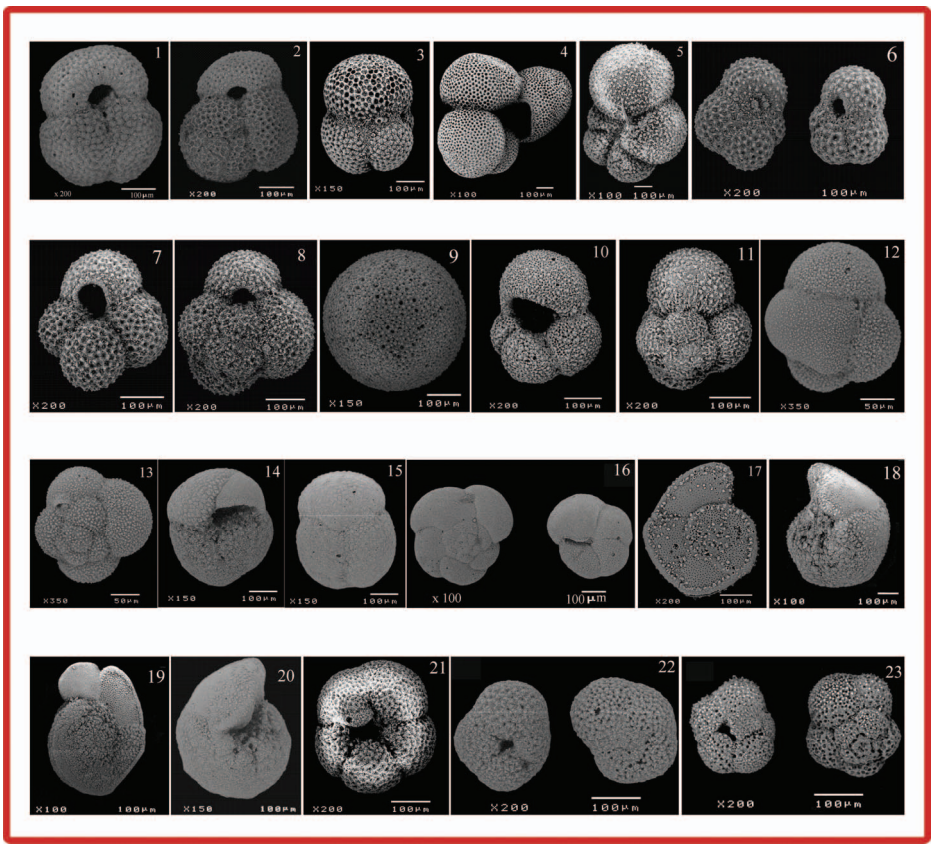

Fig. 1.11 **Image 1.** *Globigerinoides ruber* (x 200). Apertural view. **Image 2.** *Globigerinoides ruber* (x 200). Spiral view. **Image 3.** *Globigerinoides sacculifer*, without sac (x 150). Apertural view. **Image 4.** *Globigerinoides sacculifer*, with a sac (x 100). Apertural view. **Image 5.** *Globigerinella siphonifera* (x 100). **Image 6.** *Globoturborotalita rubescens* (x200). Apertural view. **Image 7.** *Globoturborotalita tenella* (x 200). Apertural view. **Image 8.** *Globoturborotalita tenella* (x 200). Spiral view. **Image 9.** *Orbulina universa* (x 150). **Image 10.** *Globigerina bulloides* (x 200). Apertural view. **Image 11.** *Globigerina bulloides* (x 200) Spiral view. **Image 12.** *Globigerinita glutinata* (x 350). Apertural view. **Image 13.** *Globigerinita glutinata* (x 350). Spiral view. **Image 14.** *Globorotalia inflata* (x 150). Apertural view. **Image 15.** *Globorotalia inflata* (x 150). Spiral view. **Image 16.** *Globorotalia scitula* (x 100). Spiral view and apertural view. **Image 17.** *Globorotalia truncatulinoides* (right-coiling) (x 200). Spiral view. **Image 18.** *Globorotalia truncatulinoides* (right-coiling) (x 100). Apertural view. **Image 19.** *Globorotalia truncatulinoides* (left-coiling) (x 150). Spiral view. **Image 20.** *Globorotalia truncatulinoides* (left-coiling) (x 150). Apertural view. **Image 21.** *Neogloboquadrina pachyderma* (right-coiling) (x 200). Apertural view. **Image 22.** *Neogloboquadrina pachyderma* (left-coiling) (x 200). Apertural and spiral view. **Image 23.** *Turborotalita quinqueloba* (x 200). Apertural and spiral view. (Images by Hayes, 1999).

1.4 OBJECTIVES

The present work is based on the study of four cores recovered in the Sardinia Channel (Tyrrhennian Sea) and in the continental shelf of Salerno Gulf (Tyrrhennian Sea) which span the last 80 kyr. In addition, in order to characterize in higher resolution the last 10 kyr, I considered three sedimentary cores collected from the continental shelf off the Tyrrhenian basin margin in a sedimentary area characterised by a very high sedimentation rates (Trincardi and Field, 1991; Budillon et al., 1994; 2005; Iorio et al., 2004; Sacchi et al., 2004).

Specifically this thesis aims to:

- Identification of events (Event Stratigraphy), from a super-expanded shallow water marine sedimentary record of the eastern Tyrrhenian Sea, which can be used to improve the resolution chronology over the last 500 years in the central Mediterranean basin.

- Improve the age model for the last 10 kyr in the Eastern Tyrrhenian Sea, by integration of a multi-proxy calcareous plankton (planktonic foraminifera and calcareous nannofossils), tephrostratigraphy and ^{14}C-AMS radiocarbon data in order to identify the main climatic changes and to improve the Event Stratigraphy during this time interval.

- Reconstruct the planktonic foraminiferal changes during the last 80 kyr in the central southern part of Tyrrhenian Sea (Sardinian Channel) in order to verify and to extend back in time the eco-biozonal scheme proposed by Sprovieri et al. (2003) for the Sicily Channel (for the last 23 kyr, central Mediterereanean). Secondly, the paleolatitudinal position of the studied site can offer the possibility to really proposed a comparison of planktonic foraminiferal changes investigated in western part of the Mediterranean along a west-east transect.

Following this approach one of the aim of this PhD thesis is to verify the validity of the available eco-biozonal schemes for the Mediterranean area and where possible to update or refine these eco-biozones. Moreover, using accurate independed ages we could proposed calibrated ages for the recognised eco-biozones.

REFERENCES

Aksu, A. E., Yasar, D.and Mudie, P. J., 1995. Paleoclimatic and paleoceanographic conditions leading to development of sapropel S1 in the Aegean Sea. Palaeogeogr. Palaeoclimatol. Palaeoecol., 116, 71-101.

Alley, R. B. and Agustsdottir, A. M., 2005: The 8 kyr event: cause and consequences of a major Holocene abrupt climate change. Quaternary Science Reviews, 24, 1123-1149.

Alley, R. B., Mayewski, P. A., Sowers, T., Stuiver, M., Taylor, K. C. and Clark, P. U., 1997: Holocene climatic instability: A prominent, widespread event 8200 yr ago. Geology, 25, 483-486.

Alley, R. B., 1993. In search of ice-stream sticky spots. Journal of Glaciology 39, 447-454.

Almogi-Labin, A., 1984. Population dynamics of planktonic foraminifera and pteropoda Gulf of Aqaba, Red Sea. Proc. K. Ned Akad. Wet. Ser. B, Phys. Sci., 87 481-511.

Ambrosiani, B., 1984. Settlement expansion—settlement contraction: a question of war, plague or climate? In: Morner, N. A., Karl!en, W. (Eds.), Climatic Changes on a Yearly to Millenial Basis. Reidel Publishing Company, Dordrecht, pp. 241–247.

Amore, F. O., Caffau, M., Massa, B., Morabito, S., 2004. Late Pleistocene–Holocene paleoclimate and related paleoenvironmental changes as recorded by calcareous nannofossils and planktonic foraminifera assemblages in the southern Tyrrhenian Sea (Cape Palinuro, Italy). Marine Micropaleontology 52, 255–276.

Anderson, D. E., Binney, H. A., Smith, M. A., 1998. Evidence for abrupt climatic change in northern Scotland between 3900 and 3500 calendar years BP. The Holocene 8, 97–103.

Aritzegui, D., Asioli, A., Lowe, J. J., Trincardi, F., Vigliotti, L., Tamburini, F., Chondrogianni, C., Accorsi, C. A., Bandini Mazzanti, M., Mercuri, A. M., Van der Kaars, S., McKenzie, J. A., Oldfield, F., 2000. Paleoclimate and the formation

of sapropel S1: inferences from Late Quaternary lacustrine and marine sequences in the central Mediterranean region. Palaeogeogr. Palaeoclimatol. Palaeoecol. 158, 215-240.

Asioli, A., Trincardi, F., Lowe, J. J., Ariztegui, D., Langone, L., Oldfield, F., 2001. Sub-millennial scale climatic oscillations in the central Adriatic during the Lateglacial. Paleoceanographic implications. Quarter. Sci. Rev., 20, 1201-1221.

Barber, D. C., 1999. Forcing of the cold event of 8,200 years ago by catastrophic drainage of Laurentide lakes. Nature, 400, 344–347.

Bard, E., Rostek, F., Turon, J. L. and Gendreau, S., 2000. Hydrological impact of Heinrich events in the subtropical northeast Atlantic. Science 289, 1321-1324.

Bard, E., 1998. Geochemical and geophysical implications of the radiocarbon calibration. Geochimica et Cosmochimica Acta 62, 2025–2038.

Bé, A. W.H., Bishop, J. K. B., Sverdlove, M. S. and Gardner, W. D., 1985. Standing stock, vertical distribution and flux of planktonic foraminifera in the Panama Basin. Mar. Micropalaeontol., 9, 307-333.

Bé, A. W. H., 1977. An ecological, zoogeographic and taxonomic review of recent planktonic foraminifera . In Ramsey, A.T.S., Ed., Oceanic Micropalaeontology. London: Academic Press,1-100.

Bé, A. W. H. and Tolderlund, D. S., 1971. Distribution and ecology of living planktonic foraminifera in surface waters of the Atlantic and Indian Oceans. In (Funnell, B.M. and Riedel, W.R., eds), The Micropalaeontology of Oceans, 105-149. Cambridge University Press.

Bé, A. W. H. and Hamlin, W. H., 1967. Ecology of Recent planktonic foraminifera: Part 3. Distribution in the North Atlantic during the summer of 1962. Micropaleontology 13, 87-106.

Bender, M., Sowers, T., Dickson, M. L., Orchardo, J., Grootes, P., Mayewski, P. and Meese. D., 1994. Climate correlations between Greenland and Antarctica during the past 100,000 years. Nature 372, 663-666.

Berglund, B. E, 2003. Human impact and climate changes—synchronous events and a causal link?. Quaternary International 105, 7–12.

Bethoux, J. P., Morin, P., Chaumery, C., Connan, O., Gentili B. and Ruiz-Pino, D., 1998. Nutrients in the Mediterranean Sea, mass balance and statistical analysis of concentrations with respect to environmental change. Marine Chemistry, 63: 155-169.

Bethoux, J. P., 1979. Budgets of the Mediterranean Sea. Their dependence on local climate and on characteristics of the Atlantic water. Oceanologica Acta, 2, 157-163.

Birks, H. J. B., 1986. Late-Quaternary biotic changes on terrestrial and lacustrine environments, with particular reference to northwest Europe. In: Berglund, B.E. (Ed.). Handbookof Holocene Palaeoecology and Palaeohydrology. Wiley, Chichester, pp. 743–774.

Bishop, J. K. B. and Rossow, W. B., 1991. Spatial and temporal variability of global surface solar irradiance. Journal of Geophysical Research, 96,16839-16858.

Blanc-Vernet, L., Sgarrella, F., Acquaviva, M., 1984. Evènements climatiques, hydrologie et foraminifèrs en Mèditerranè e au Quaternaire rècent. Bull. Soc. Ge´ol. Fr. 26, 1235–1243.

Bond, G., Showers, W., Cheseby, M., Lotti, R., Almasi, P., deMenocal, P., Priore, P., Cullen, H., Hajdas, I. and Bonani, G., 1997. A pervasive millennial-scale cycle in North Atlantic Holocene and glacial climates. Science, 278, 1257-1266.

Bond, G., Broecker, W. S., Johnsen, S. J,. McManus, J., Labeyrie, L. D., Jouzel, J. and Bonani, G., 1993. Correlations between climate records from North Atlantic sediments and Greenland ice. Nature 365, 143-147.

Bond, G., Heinrich, H., Broecker, W., Labeyrie, L., McManus, J., Andrews, J., Huon, S., Jantschik, R., Clasen, S., Simet, C., Tedesco, K., Klas, M., Bonani G. and Ivy. S., 1992. Evidence for massive discharges of icebergs into the North Atlantic Ocean during the last glacial period. Nature 360, 245-250.

Bradley, R. S., Briffa, K. R., Cole, and J. Osborn, T. J., 2003b. The climate of the last millennium. In: Paleoclimat. Global Change and the Future [Alverson, K.D., R.S. Bradley, and T.F. Pedersen (eds.)]. Springer, Berlin, pp. 105–141.

Boucher, K. 1975. Global climate - The English Univ. Press Ltd. (London): 326pp.

Bradley, R. and Jones, P., 1992. Climate since A.D. 1500, Routledge, London, 679 pp.

Bradley, R. S. and Jones, P. D., 1992."When was the Little Ice Age?. In: Proceedings International Symposium on the Little Ice Age Climate (Ed. T. Mikami), pp.1-4. Department of Geography, Tokyo Metropolitan University (keywords: historical climate temperature ice observations records).

Bradley, R. S. and Jones, P. D., 1992.Climate since A.D.1500: Introduction. In: Climate Since A.D.1500 (Eds. R.S. Bradley and P.D. Jones), pp.1-16 Routledge, London. (keywords: historical climate change book records observations).

Bradley, R. S. and Jones, P. D., 1992. Records of explosive volcanic eruptions over the last 500 years. In: Climate Since A.D.1600 (Eds. R.S. Bradley and P.D. Jones), pp.606-622 Routledge, London (keywords: volcanoes historical records climate change).

Bradley, R. S. and Jones, P. D. (Editors)., 1992. Climate Since A.D.1500. 679pp Routledge, London. (keywords: historical climate book records observations reconstructions).

Brewer, S., Alleaume, S., Guiot, J., Nicault A., 2007. Historical droughts in Mediterranean regions during the last 500 years: a data/model approach. Clim. Past 3, 355–366.

Broecker., W. S., 2006. Abrupt climate change revisited. Global and Planetary Change 54, 211–215.

Broecker, W. S., Bond, G., Klas, M., Clark, E. and Manus, J., 1992. Origin of the North Atlantic's Heinrich events. Climate Dynamics 6, 265-273.

Bryden, H. L. and Kinder, T. H., (1991). Steady two-layer exchange through the Strait of Gibraltar. Deep-Sea Research, 38, 445-463.

Brummer, G. J. A. and Kroon, D., 1988. Genetically controlled planktonic foraminiferal coiling ratios as tracers of past ocean dynamics. In: G.J. Brummer and D. Kroon (Editors), Planktonic Foraminifers as Tracers of Ocean-climate history. Free Univ. Press, Amsterdam, pp. 293-298.

Budillon, F., Lirer, F., Iorio, M., Macrì, P., Sagnotti, L., Vallefuoco, M., Ferraro, L., Garziglia, S., Innangi, S., Sahabi, M., Tonielli, R, 2008. Integrated stratigraphic reconstruction for the last 80 kyr in a deep sector of the Sardinia Channel (Western Mediterranean).Deep Sea Research 2008, in press.

Budillon, F., Violante, C., Conforti, A., Esposito, E., Insinga, D., Iorio, M., Porfido, S., 2005. Event beds in the recent prodelta stratigraphic record of the small flood-prone Bonea stream (Amalfi Coast, Southern Italy). Marine Geology 222–223 419–441.

Budillon, F., Esposito, E., Iorio, M., Pelosi, N., Porfido, S., Violante, C., 2005. The geological record of storm events over the last 1000 years in the Salerno Bay (Southern Tyrrhenian Sea): new proxy evidences, European Geoscience Union, Adv. Geosci., 2 1–8.

Budillon, F., Pescatore, T., Senatore, M. R., 1994. Cicli deposizionali del Pleistocene Superiore–Olocene sulla piattaforma continentale del Golfo di Salerno (Tirreno Meridionale). Boll. Soc. Geol. Ital. 113, 303–316.

Buongiorno Nardelli, B., and Salusti E., 2000. On dense water formation criteria and their application to the Mediterranean Sea. Deep-Sea Research I, 47, 193-221.

Cacho, I., Shackleton, N., Elderfield, H., Sierro, F. J., Grimalt, J. O., 2006. Glacial rapid variability in deep-water temperature and d18O from the Western Mediterranean Sea. Quaternary Science Reviews 25, 3294–3311.

Cacho, I., Grimalt, J. O., Canals, M., Sbaffi, L., Shackleton, N. J.,Schònfeld, J.,Zahn, R., 2001. Variability of the western Mediterranean Sea surface temperature during the last 25,000 years and its connection with the Northern Hemisphere climatic changes. Paleoceanography 16,40-52.

Cacho, I., Grimalt, J. O., Sierro, F. J., Shackleton, N. J. and Canals, M., 2000. Evidence for enhanced Mediterranean thermohaline circulation during rapid climatic coolings, Earth Planetary Science Letters, 183, 417– 429.

Cacho, I., Grimalt, J. O., Pelejero, C., Canals, M., Sierro, F. J., Flores, J. A. and Shackleton, N. J., 1999. Dansgaard-Oeschger and Heinrich event imprints in the Alboran Sea paleotemperatures. Paleoceanography 14, 698– 705.

Camuffo, D., 1987. Freezing of the Venetian Lagoon since the 9th century AD in comparison to the climate of Western Europe and England. Climatic Change, 10, 43.

Capotondi, L., Borsetti, A., Morigi, C., 1999. Foraminiferal ecozones, a high resolution proxy for the late Quaternary biochronology in the central Mediterranean Sea. Marine Geology 153, 253– 274.

Caron, D. A., Bé, A. W. H., 1984. Predicted and observed feeding rates of the spinose planktonic foraminifer Globigerinoides sacculifer. B. Mar. Sci., 35, 1–10.

Castradori, D., 1993. Calcareous nannofossils and the origin of eastern Mediterranean sapropels. Paleoceanography 8, 459-471.

Cita, M. B., Ciampo, G., Ferrone, E., Moncharmont Zei, M., Scorziello, R., Taddei Ruggiero, E., 1974. Il Quaternario del Tirreno abissale. Interpretazione stratigrafica e paleoclimatica del pozzo DSDP 132. Rev. Esp. Micropaleontol. 6, 257– 326.

Cita, M. B., Vergnaud-Grazzini, C., Robert, C., Chamley, H., Ciaranfi, N. and d'Onofrio, S., 1977. Palaeoclimatic record of a long deep sea core from the eastern Mediterranean. Quat Res., 8, 205-235.

Corselli, C., Principato, M. S., Maffioli, P., and Crudeli D.. 2002. Changes in planktonic assemblages during sapropel S5 deposition: Evidence from Urania Basin area, eastern Mediterranean. Paleoceanography, 17, 1029 doi:1029/2000PA000536.

Cortijo, E., Labeyrie, L., Vidal, L., Vautravers, M., Chapman, M., Duplessy, J. C., Elliot, M., Arnold, M., Turon, J. L. and Auffret, G., 1997. Changes in sea surface

hydrology associated with Heinrich event 4 in the North Atlantic Ocean between 40° and 60°N. Earth Planetary Science Letters 146, 29– 45.

Dansgaard, W., Johnsen, S. J., Clausen, H. B., Dahl-Jensen, D., Gundestrup, N. S., Hammer, C. U., Hvidberg, C. S., Steffensen, J. P., Sveinbjòrnsdottir, A. E., Jouzel, J., Bond, G., 1993. Evidence for general instability of past climate from a 250-ka ice-core record. Nature 364, 218–220.

De Lange, G. J. and Ten Haven, H. L., 1983. Recent sapropel formation in the eastern Mediterranean. Nature, 305, 797-798.

De Menocal, P. B., Ortiz, J., Guilderson, T. and Sarnthein, M., 2000. Coherent high- and low-latitude climate variability during the Holocene warm period. Science 288, 2198–2202.

Denton, G. H., and Karlen. W., 1973. Holocene climatic variations—their pattern and possible cause. Quaternary Research 3, 155-205.

De Rijk, S., Hayes, A., Rohling, E. J., 1999. Eastern Mediterranean sapropel S1 interruption: an expression of the onset of climatic deterioration around 7 ka BP. Mar.ineGeology 153, 337–343.

Desprat, S., Goni, M. F. S., & Loutre, M. F. 2003. Revealing climatic variability of the last three millennia in northwestern Iberia using pollen influx data. Earth Planetary Science Letters, 213, 63.

Duarte, C. M., Agustì, S., Kennedy, H., Vaqué, D., 1999. The Mediterranean climate as a template for Mediterranean marine ecosystems: the example of the northeast Spanish littoral. Progress in Oceanography 44, 245–270.

Ducassou, E., Capotondi, L., Murat, A., Bernasconi, S., Mulder, T., Gonthier, E., Migeon, S., Duprat, J., Giraudeau, J., Mascle, J. (2007, in press). Multiproxy Late Quaternary stratigraphy of the Nile deep-sea turbidite system- Towards a chronology of deep-sea terrigeneous systems. Sedimentary Geology, , doi:10.1016/j.sedgeo. 2007.01.023.

Dugdale, R. C., and Wilkerson, F. P. ,1988. "Nutrient sources and primary production in the Eastern Mediterranean.". Oceanologica Acta, 9,179-184.

Elliot,M., Labeyrie, L., Dokken, T. and Manthe, S., 2001. Coherent patterns of ice-rafted debris deposits in the Nordic regions during the last glacial (10–60 ka), Earth Planet. Sci. Lett. 194, 151-163.

Elliot, M., Labeyrie, L., Bond, G., Cortijo, E., Turon, J. L., Tisnerat, N. and Duplessy, J. C., 1998. Millennial-scale iceberg discharges in the Irminger Basin during the last glacial period: Relationship with the Heinrich events and environmental settings. Paleoceanography 13, 433-446.

Emeis, K. C., Sakamoto, T., Wehausen, R., Brumsack, H. J., 2000a. The sapropel record of the eastern Mediterranean Sea, results of Ocean Drilling Program Leg 160. Palaeogeogr. Palaeoclimatol. Palaeoecol. 158, 371-395.

Emeis, K. C., Struck, U., Schulz, H. M., Rosenberg, R., Bernasconi, S., Erlenkeuser, H., Sakamoto, T., Martinez-Ruiz, F., 2000b. Temperature and salinity variations of Mediterranean Sea surface waters over the last 16,000 years from records of planktonic stable oxygen isotopes and alkenone unsaturation ratios. Palaeogeogr. Palaeoclimatol. Palaeoecol. 158, 259-280.

Emeis, K. C., Robertson, A. H. F., Richter, C., 1996. Site 963. Proc. ODP Init. Rep. 160, Ocean Drilling Program,College Station, TX, pp. 55-84.

Eronen, M., Hyv.arinen, H., Zetterberg, P., 1999. Holocene humidity changes in northern Finnish Lapland inferred from lake sediments and submerged Scots pines dated by tree-rings. The Holocene 9, 569–580.

Fairbanks, R. G., Sverdlove, M., Free, R., Wiebe, P. H. and Bé, A. W. H., 1982. Vertical distribution of living planktonic foraminifera from the Panama Basin. Nature, 298, 841-844.

Fairbanks, R. G. and Wiebe, P. H., 1980. Foraminifera and chlorophyll maximum: Vertical distribution, seasonal succession and paleoceanographic significance. Science, 209, 1524-1526.

Fairbanks, R. G., Wiebe, P. H. and Bé, A. W. H., 1980. Vertical distribution and isotopic composition of living planktonic foraminifera in the western North Atlantic. Science, 207, 61-63.

Fleitmann, D. Burns, S. J., Mudelsee, M., Neff, U., Kramers, J., Mangini, A., Matter, A., 2003. Holocene forcing of the Indian monsoon recorded in a stalagmite from Southern Oman. Science 300, 1737–1739.

Flores, J. A., Sierro, F. J., Francès, G., Vasquez, A., Zamarreno, I., 1997. The last 100,000 years in the western Mediterranean: sea surface water and frontal dynamics as revealed by coccolithophores. Mar. Micropaleontol. 29, 351–366.

Frignani, M., Langone, L., Ravaioli, M., Sorgente, D., Alvisi, F., Albertazzi, S., 2005. Fine-sediment mass balance in the western Adriatic continental shelf over a century time scale. Marine Geology 222–223, 113–133.

Frignani, M., Sorgente, D., Langone, L., Albertazzi, S., Ravaioli, M., 2004. Behavior of Chernobyl radiocesium in sediments of the Adriatic Sea offshore the Po River delta and the Emilia-Romagna coast. Journal of Environmental Radioactivity 71, 299– 312.

Frignani, M., Langone, L., 1991. Accumulation rates and ^{137}Cs distribution in sediments off the Po River delta and the Emilia- Romagna coast (northwestern Adriatic Sea, Italy). Cont. Shelf Res. 11, 525– 542.

Ganssen, G and Troelstra, S. R., 1987. palaeoenvironmental changes from stable isotopes in planktonic foraminifera from eastern Mediterranean sapropels. Marine Geology, 75, 221-230.

Garrett, C. 1996. The role of the strait of Gibraltar in the evolution of Mediterranean water, properties and circulation. Bulletin de l'Institut Océanographique de Monaco, 17, 1-19.

Georgopoulos, D., Theocharis, A., and Zodiatis, G., 1989. Intermediate Water Formation in the Cretan Sea (S. Aegean Sea), Oceanologica Acta, 12, 353-359.

Geraga M., Tsaila-Monopolis S., Ioakim C., Papatheodorou G., Ferentinos G., 2005. Short-term climate changes in the southern Aegean Sea over the last 48,000 years. Palaeogeography, Palaeoclimatology, Palaeoecology 220, 311– 332.

Geraga, M., Tsaila-Monopolis, S., Ioakim, C., Papatheodorou, G., Ferentinos, G., 2000. Evaluation of palaeoenvironmental changes during the last 18,000 years in the Myrtoon basin, SW Aegean Sea. Palaeogeogr., Palaeoclimatol., Palaeoecol. 156, 1-17.

Gilmann, C., and Garrett, C., 1994. Heat flux parametrizations for the Mediterranean Sea: the role of atmospheric aerosols and constraints from water budget. Journal of Geophysical Research 99, 5119-5134.

Giordani, P., Hammond, D. E., Berelson, W. M., Montanari, G., Poletti, R., Milandri, A., Frignani, Langone, M. L., Ravaioli, M., Rovatti, G., Rabbi, E., 1992. Benthic fluxes and nutrient budgets for sediments in the Northern Adriatic Sea: burial and recycling efficiencies. The Science of the Total Environment, Supplement pp. 251–275.

Graslund, B., 1980. Climatic fluctuations in the Early Subboreal period. A preliminary discussion. Striae 14, 13–22.

GRIP members, 1993**.** Greenland Ice-Core Project (GRIP) members, Climate instability during the last interglacial period recorded in the GRIP ice core. Nature 364, 203–207.

Grousset, P. E., Labeyrie, L., Sinko, J. A., Cremer, M., Bond, G., Duprat, J., Cortijo, E. and Huon, S., 1993. Patterns of ice-rafted detritus in the glacial North Atlantic (40-55°N). Paleoceanography, 8, 175–192.

Guiot, J., Alleaume, S., Nicault, A., & Brewer, S., 2005. The Mediterranean droughts during the last 650 years: reconstruction from tree-rings and climate model simulation. Geophys. Res. Abstracts, 7, 02471, European Geosciences Union, Vienna, 24–29.

Guiot, J., Nicault, A., Rathgeber, C., Edouard, J. L., Guibal, F., Pichard, G., & Till, C.,2005. Last-millennium summer-temperature variations in Western Europe based on proxy data. Holocene, 15, 489, doi:10.1191/0959683605hl819rp.

Hagstrum, J. T., and Champion D. E., 2002. A Holocene paleosecular variation record from 14C-dated volcanic rocks in western North America, J. Geophys. Res., 107, 2025, doi:10.1029/2001JB000524.

Haug, G. H., Hughen, K. A., Peterson, L. C., Sigman, D. M. & Ròhl, U., 2001. Southward migration of the Intertropical Convergence Zone through the Holocene. Science 293, 1304–1308.

Hayes, A., Kucera, M., Kallel, N., Sbaffi, L., Rohling E. J., 2005. Glacial Mediterranean sea surface temperatures based on planktonic foraminiferal assemblages. Quaternary Science Reviews, 24, 999-1016.

Hayes, A., 1999. Late Quaternary palaeoclimatic and palaeoecological changes in the Mediterranean Sea. University of Southampton, Faculty of Science, Department of Oceanography, PhD *Thesis* pp.139.

Heburn, G. W. and La Violette, P. E., 1990. Variations in the structure of the anticyclonic gyres found in the Alboran Sea. J. Geophys. Res., 92, 2901-2906.

Hemleben, C. H., Spindler, M. and Anderson, O. R., 1989. Modern Planktonic Foraminifera. Springer, New York, 363 pp.

Hemleben, C. H. and Spindler, M., 1983. Recent advances in research on living planktonic foraminifera. In: J.E. Meulenkamp (Editor), Reconstruction of marine palaeoenvironments. Utrecht Micropaleontology G. bulloides., 30, 141-170.

Herman, Y., 1972. Quaternary eastern Mediterranean sediments: micropalaeontological climatic record: In: D.J. Stanley (Editor), The Mediterranean Sea. Dowden, Hutchinson & Ross, Stroudsburg, Pa; pp. 129-147.

Hilgen, F. J., 1991. Astronomical calibration of Gauss to Matuyama sapropels in the Mediterranean and implication for the geomagnetic polarity time scale. Earth Planetary Science Letters 104, 226-244.

Hoek, W. Z., 2008. The Last Glacial-Interglacial Transition. Episodes, 31, 226-229.

Hughen, K. A., Baillie, M. G. L., Bard, E., Beck, J. W., Bertrand, C. J. H., Blackwell, P. G., Buck, C. E., Burr, G. S., Cutler, K. B., Damon, P. E., Edwards, R. L., Fairbanks, R. G., Friedrich, M., Guilderson, T. P., Krom, B., MCcormac, G., Mannig, S., Rasmey, C. B., Reimer, P. J., Reimer, R. W., Remmele, S., Southon, J. R., Stuiver, M., Talamo, S., Taylor, F. W., Van Der Plicht, J. and Weyhenmeyer, C. E., 2004. Marine04 marine Radiocarbon Age Calibration, 0-26 Cal kyr BP. Radiocarbon, 46, 1059-1086.

Hughen, K. A., Overpeck, J. T., Peterson, L. C. & Trumbore, S., 1996.Rapid climate changes in the tropical Atlantic region during the last deglaciation. Nature 380, 51–54.

Jansen, E. and Koc, N., 2000. Century to decadal scale records of Norwegian sea surface temperature variations of the past 2 millenia. PAGES Newsletter 8 (1), 13–14.

Jing, Z., Sumin; W., Guishan; Y., Haifeng, X., 2007. Younger Dryas Event and Cold Events in Early-Mid Holocene: Record from the sediment of Erhai Lake. Advances in Climate Change Research 3 (Suppl.), 1673–1719.

Johnsen, S., Clausen, H., Dansgaard W,, Fuhrer, K., Gundestrup, N., Hammer, C., Iversen, P., Jouzel, J., Stauffer, B. and Steffensen. J., 1992. Irregular glacial interstadials recorded in a new Greenland ice core. Natur*e* 359, 311-313.

Jones, P. D., and Mann, M. E., 2004: Climate over past millennia. Rev. Geophys., 42, RG2002, doi:10.1029/2003RG000143.

Jones, P. D. and Bradley, R. S., 1992. Climatic variations over the last 500 years. In: Climate Since A.D.1500. (Eds. R.S. Bradley and P.D. Jones), pp.649-665 Routledge, London.

Jorissen, F. J., 1999. Benthic foraminiferal microhabitats below the sediment-water interface. In: B.K. Sen Gupta, Editor, *Modern Foraminifera*, Kluwer Academic Publishers, Dordrecht, The Netherlands, pp. 161–179.

Jorissen, F. J., Asioli, A., Borsetti, A. M., de Visser, L., Hilgen,J.P., Rohling, E.J., van der Borg, K., Vergnaud-Grazzini, C., Zachariasse, W.J., 1993. Late Quaternary central Mediterranean biochronology. Marine Micropaleontology 21, 169-189.

Jorissen, F. J., 1988. Benthic foraminifera from the Adriatic Sea; principles ofphenotypic variation. Utrecht Micropaleontol. Bull., 37, 176 pp.

Jorissen, F. J., 1987. The distribution of benthic foraminifera in the Adriaitic Sea. Mar. Micropaleontol,, 12, 21-48.

Jouzel, J., Lorius, C., Petit, J. R., Genthon, C., Barkov, N. I., Kotlyakov, V. M. and Petrov. V. M., 1987. Vostok ice core: A continuous isotope temperature record over the last climatic cycle (160,000 years). Nature 329, 403-418.

Incarbona, A., Di Stefano, E., Patti, B., Pelosi, N., Bonomo, S., Mazzola, S., Sprovieri, R., Tranchida, G., Zgozi, S. and Bonanno, A., 2008. Holocene millennial-scale productivity variations in the Sicily Channel (Mediterranean Sea). Paleoceanography, 23, PA3204, doi:10.1029/2007PA001581.

Incarbona, A., 2007. Paleoceanografia del Canale di Sicilia (Mediterraneo Centrale) durante gli ultimi 350 mila anni, rivelata dalle associazioni a nannofossili calcarei. PhD Thesis, Università degli Studi di Palermo, Italy, 1–127.

Insinga, D., Molisso, F., Lubritto, C., Sacchi, M., Passariello, I., Morra, V., 2008. The proximal marine record of Somma–Vesuvius volcanic activity in the Naples and Salerno bays, Eastern Tyrrhenian Sea, during the last 3 kyrs. Journal of Volcanology and Geothermal Research 177, 170–186.

Iorio, M., Sagnotti, L., Angelino, A., Budillon, F., D'Argenio, B., Turell Dinares, J., Macrı`, P., Marsella, E., 2004. High-resolution petrophysical and paleomagnetic study of late-Holocene shelf sediments, Salerno Gulf, Tyrrhenian Sea. Holocene 14, 433442.

IPCC, 2001. Climate Change 2001. The Scientific Basis. Contribution of Working Group I to the Third Assessment Report of the Intergovernmental Panel on Climate Change. Cambridge University Press, Cambridge, U.K.; New York, U.S.A.

Related online version. http://www.grida.no/climate/ipcc tar/wg1/index.htm. (Eds.) Houghton, J.T. and Ding, Y. and Griggs, D.J. and Noguer, M. and van der Linden, P.J. and Dai, X. and Maskell, K. and Johnson, C.A. 1, 2.

IPCC, 2007. Climate Change 2007: The Physical Science Basis. Contribution of Working Group I to the Fourth Assessment Report of the Intergovernmental Panel on Climate Change. Cambridge University Press, Cambridge, U.K.; New York, U.S.A. Related online version. http://ipcc-wg1.ucar.edu/wg1/wg1-report.html. (Eds.) Solomon, S. and Qin, D. and Manning, M. and Chen, Y. and Marquis, M. and Averyt, K.B. and Tignor, M. and Miller, H.L. 2.1, 19, 33.

Kallel, N., Paterne, M., Labeyrie, L., Duplessy, C., Arnold, M., 1997. Temperature and salinity records of the Tyrrhenian Sea during the last 18,000 years. Palaeogeogr. Palaeoclimatol. Palaeoecol. 135, 97–108.

Kidd, R. B., Cita, M. B. and Ryan, W. B. F., 1978. Stratigraphy of the eastern Mediterranean sapropel sequences recovered during DSDP Leg 42A and their environmental significance. Initial reports of the Deep Sea Drilling Project, v.42, pt 1, 421-443.

Klitgaard-Kristensen, D., Sejrup, H. P., Haflidason, H., Johnsen, S. and Spurk, M., 1998. A regional 8200 cal. Yr BP cooling event in northwest Europe, induced by final stages of the Laurentide ice-sheet deglaciation?. Journal of Quaternary Science 13**,** 165–169.

Kullenberg, B., 1952. On the salinity of the water contained in marine sediments. Medd. Oceanogr. Inst. Göteborg, 21, 1-38.

Lacombe, H., Gascard, J. C., Gonella, J. and Bethoux, J. P., 1981. Response of the Mediterranean to the water and energy fluxes across its surface, on seasonal and inter-annual scales. Oceanol. Acta, 4, 247-255.

Lamb, H. H., 1982. Climate, History and the Modern World. Methuen, London, 387pp.

Lamb, H. H., 1977. Climate: Past, Present and Future. II. Climatic History and the Future. Methuen, London, 835pp.

Leeman A. and Niessen, F., 1994. Holocene glacial activity and climatic variations in the Swiss Alps: reconstructing a continuous record from proglacial lake sediments. The Holocene 4, 259–268.

Lirer, F., Sprovieri, M., Pelosi, N., Ferraro, L., 2007. Clues of solar forcing from a 2000 years long sedimentary record from the eastern tyrrhenian margin. Clima e cambiamenti climatici: le attività di ricerca del CNR pp. 209-212.

Lolis, C. Bartzokas, J., A. and Katsoulis, B. D., 2002. Spatial and temporal 850 hPa air temperature and sea-surface temperature covariances in the Mediterranean region and their connection to atmospheric circulation. International Journal of Climatology, 22, 663-676.

Lowe, J. J., Hoek, W. Z., INTIMATE group, 2001. Inter-regional correlation of palaeoclimatic records for the Last Glacial–Interglacial Transition: a protocol for improved precision recommended by the INTIMATE project group. Quaternary Science Reviews 20, 1175–1187.

Lowe, J. J. and Walker, M. J. C., 2000. Reconstructing Quaternary Environments (2nd edition ed.), Addison-Wesley-Longman, London.

Luterbacher, J., Xoplaki, E., Casty, C., Wanner, H., Pauling, A., Kùttel, M., Rutishauser, T., Brònnimann, S., Fischer, E., Fleitmann, D., Gonzàlez-Rouco, F. J., Garcìa-Herrera, R., Barriendos, M., Rodrigo, F., Gonzalez-Hidalgo, J. C., Saz, M. A., Gimeno, L., Ribera, P., Brunet, M., Paeth, H., Rimbu, N., Felis, T., Jacobeit, J., Dù nkeloh, A., Zorita, E., Guiot, J., Tùrkes, M., Alcoforado, M. J., Trigo, R., Wheeler, D., Tett, S., Mann, M. E., Touchan, R., Shindell, D. T., Silenzi, S., Montagna, P., D.,Camuffo, Mariotti, A., Nanni, T., Brunetti, M., Maugeri, M., Zerefos, C., De Zolt, S., Lionello, P., Nunes, M. F.,Rath, V., Beltrami, H., Garnier, E. and Le Roy Ladurie, E., 2006. Mediterranean Climate Variability. Chapter1: Mediterranean Climate Variability Over the Last Centuries: A Review Elsevier Oxford pp. 27–143.

Luterbacher, J., Dietrich, D., Xoplaki, E., Grosjean, M., Wanner, H., 2004. European Seasonal and Annual Temperature Variability, Trends, and Extremes Since 1500. Science 303, 1499-1503.

Luterbacher, J., Xoplaki, E.. 500-year winter temperature and precipitation variability over the Mediterranean area and its connection to the large-scale atmospheric circulation. *In* Bolle, H.-J. (Ed): Mediterranean Climate Variability and Trends. Springer Verlag, in press.

Malanotte-Rizzoli, P., and Hecht A., 1988. Large-scale properties of the eastern Mediterranean: a review. Oceanologica Acta, 11, 323-335.

Mangerud J., Andersen, S.T., Berglund, B.E., and Donner, J.J., 1974. Quaternary stratigraphy of Norden, a proposal for terminology and classification. Boreas, 3, 109-128.

Marino, 2008. Palaeoceanography of the interglacial eastern Mediterranean Sea. PhD Thesis, ISBN 978-90-393-4762-1 NSG publication No. 2008 02 21 LPP Contributions Series No. 24.

Martinson, D. G., Pisias, N. G., Hays, J. D., Imbrie, J., Moore, T. C., Shackleton, N. J.,1987. Age dating and the orbital theory of the ice ages: development of a high-resolution 0 to 300,000-year chronoestratigraphy. Quat. Res. 27, 1-29.

Martrat, B., Grimalt, J. O., Lopez-Martinez, C., Cacho, I., Sierro, F. J., Flores, J. A., Zahn, R., Canals, M., Curtis J.H. and Hodell, D. A., 2004. Abrupt temperature changes in the Western Mediterranean over the past 250,000 years. Science 306, 1762–1765.

Masson-Delmotte, V., Landais, A., Stiévenard, M., Cattani, O., Falourd, S. Jouzel, J., Johnsen, S. J., Dahl-Jensen, D., Sveinbjornsdottir, A., White, J. W. C., Popp T. and Fischer, H., 2005. Holocene climatic changes in Greenland : different deuterium excess signals at Greenland Ice Core Project (GRIP) and North GRIP. Journal of Geophysical Research 110, p. D14102.

Masson-Delmotte, V., Jouzel, J., Landais, A., Stiévenard, M., Johnsen, S. J., White, J. W. C., Werner M.,, Sveinbjornsdottir A. and Fuhrer, K., 2005. GRIP deuterium excess reveals rapid and orbital changes of Greenland moisture origin, Science 309, 118–121.

Matthes, F. E. 1939. Report of the Committee on Glaciers**.** Transactions of the American Geophysical Union; 518-523.

Mayewski, P. A., Rohling, E. E., Stager, J. C., Karlen, W., Maasch, K. A., Meeker, L. D., Meyerson, E. A., Gasse, F., van Kreveld, S., Holmgren, K., Lee-Thorp, J., Rosqvist, G., Rack, F., Staubwasser, M., Schneider, R. R., Steig, E. J., 2004. Holocene climate variability. Quaternary Research 62, 243-255.

Mayewski, P. A., Meeker, L. D., Twickler, M. S,. Whitlow, S. I., Yang, and Q. Prentice. M., 1997. Major features and forcing of high latitude northern hemisphere atmospheric circulation over the last 110,000 years. Journal of Geophysical Research 102, 345-366.

Mayewski, P. A., Twickler, M. S., Whitlow, S. I., Meeker, L. D., Yang, Q., Thomas, J., Kreutz, K., Grootes, P., Morse, D., Steig, E. and Waddington. E. D., 1996. Climate change during the last deglaciation in Antarctica. Scienc*e* 272,1636-1638.

Mercone, D., Thomson, J., Croudace, I. W., Siani, G., Paterne, M., Troelstra, S. R., 2000. Duration of S1, the most recent sapropel in the eastern Mediterranean Sea, as indicated by accelerator mass spectrometry radiocarbon and geochemical evidence. Paleoceanography 15, 336–347.

Milliman, J. D., 1992. Sea-level rise response to climatic change and tectonics in the Mediterranean Sea. In L. Jeftic, J. D. Milliman, & G. Sestini. Climate change in the Mediterranean pp. 45–56. (London).

Millot, C., 1999. Circulation in the Western Mediterranean Sea. J. Mar. Syst., 20, 423-442.

Moberg, A., Sonechkin, D. M., Holmgren, K., Datsenko N. M. and Karlén W., 2005. Highly variable Northern Hemisphere temperatures reconstructed from low- and high-resolution proxy data. Nature 443, 613-617.

Molero, J., Sanchez-Cabeza, J. A., Merino, J., Mitchell, P. I., Vidal-Quadras, A., 1999. Impact of ^{134}Cs and ^{137}Cs from the Chernobyl reactor accident on the Spanish Mediterranean marine environment. Journal of Environmental Radioactivity 43,357-370.

Molloy, K., O'Connell, M., 1995. Palaeoecological investigations towards the reconstruction of environment and land-use changes during the prehistory at Cèide Fields, western Ireland. Probleme der Kustenforschung im s .udlichen Nordseegebiet 23, 187–225.

Myers, P. G., and Haines K., 2002. Stability of the Mediterranean's thermohaline circulation under modified surface evaporative fluxes, Journal of Geophysical Research, 107, 7-1 to 7-10.

Myers, P. G., and Rohling, E. J., 2000. Modelling a 200 year interruption of the Holocene sapropel S1. Quaternary Research, 53, 98-104.

Murray, J. W., 1991. Ecology and Palaeocology of Benthic Foraminifera. Longman Scientific & Technical, New York. 312 pp.

Nesje, A., Dahl, S.O., Andersson, C. and Matthews, J. A., 2000: The lacustrine sedimentary sequence in Sygneskardvatnet, western Norway: a continuous, high-resolution record of the Jostedalsbreen ice cap during the Holocene. Quaternary Science Review 19, 1047–1065.

NGRIP members, 2004. High-resolution record of Northern Hemisphere climate extending into the last interglacial period. Nature 431, 147-151.

Nilsson, T., 1964. Standardpollendiagramme und ^{14}C datierungen aus dem Ager.ods Mosse im mittleren Schonen. Lunds Universitets A(rsskrift, N.F 2 (59), 52.

O'Brien, S. R., Mayewski, P. A., Meeker, L. D., Meese, D. A., Twickler, M. S. and Whitlow, S. I., 1996. Complexity of Holocene climate as reconstructed from a Greenland ice core. Science 270, 1962-1964.

Olaf, D. S., 2002. Timing, equilibrium-line altitudes and climatic implications of two early-Holocene glacier readvances during the Erdalen Event at Jostedalsbreen, western Norway. The Holocene 12, 17–25.

Olausson, E., 1961. Studies of deep sea cores. Rep. Swedish Deep-sea Exped., 1947-48, 8 (4): 353-391.

Olausson, E., 1960. Descriptions of sediment from the Mediterranean and Red Sea. Rep. Swedish Deep-Sea Exped., 1947-48, 8, 287-334.

Papucci, C., Charmasson, S., Delfanti, R., Gasco, C., Mitchell, P. and Sanchez-Cabeza, J. A., 1996. Time evolution and levels of man-made radioactivity in the Mediterranean Sea. In: Guegueniat, P. et al., 1996. Radionuclides in the oceans inputs and inventories Les Editions de Physique, Les Ulis, pp. 176–197.

Parker, F. L., 1958. Eastern Mediterranean foraminifera. Rep. Swedish Deep-sea Exped., 1947-48, 8, 217-283.

Parrilla, G., Kinder, T. H. and Preller, R. H., 1986. Deep and intermediate Mediterranean water in the western Alboran Sea. Deep-Sea Research, 33, 55-88.

Paterne, M., Guichard, F., Labeyrie, J., Gillot, P. Y. and Duplessy, J. C., 1986. Tyrrhenian Sea tephrochronology of the oxygen isotope record for the past 60,000 years. Marine Geology, 72, 259-285.

Pedersen, T. F. and Calvert, S. E., 1990. Anoxia vs. productivity ,what controls the formation of organic-carbon-rich sediments and sedimentary-rocks. AAPG Bull. 74, 454-466.

Pérez-Folgado, M., Sierro, F. J., Flores, J. A., Grimalt, J .O., Zahn, R., 2004. Paleoclimatic variations in foraminifer assemblages from the Alboran Sea (Western Mediterranean) during the last 150 ka in ODP Site 977. Marine Geology 212, 113–131.

Pérez-Folgado, M., Sierro, F. J., Flores, J. A., Cacho, I., Grimalt, J. O., Zahn, R., Shackleton, N. 2003. Western Mediterranean planktonic foraminifera events and millennial climatic variability during the last 70 kyr. Marine Micropaleontology, 48, 1-2, 49-70.

Pinardi, N. and Masetti, E., 2000. Variability of the large scale general circulation of the Mediterranean Sea from observations and modeling: a review. Paleogeography, Paleoclimatology, Paleoecology, 158, 153-173.

Piva, A., Asioli, A., Trincardi, F., Schneider, R. R., Vigliotti, L., 2008. Late-Holocene climate variability in the Adriatic Sea (Central Mediterranean). The Holocene 18 153 DOI: 10.1177/0959683607085606.

POEM Group, 1992. General circulation of the eastern Mediterranean. Earth Science Reviews 32, 285–309.

Principato, M. S., Giunta, S., Corselli, C., Negri, A., 2003. Late Pleistocene-Holocene planktonic assemblages in three box-cores from the Mediterranean Ridge area (west-southwest of Crete):palaeoecological and palaeoceanographic reconstruction of sapropel S1 interval. Palaeogeography, Palaeoclimatology, Palaeoecology 190, 61-77.

Pujol, C. and Vergnaud-Grazzini, C., 1995. Distribution patterns of live planktic foraminifers as related to regional hydrography and productive systems of the Mediterranean Sea. Mar. Micropaleontol., 25: 187-217.

Pujol, C and Vergnaud-Grazzini, C., 1989. Paleoceanography of the last deglaciation in the Alboran Sea (Western Mediterranean). Stable isotopes and planktonic foraminiferal records. Mar. Micropaleontol., 15, 253-267.

Raffi, I. and Rio, D., 1979. Calcareous nannofossil biostratigraphy of the DSDP Site 132-Leg 13 (Tyrrhenian Sea-Western Mediterranean). Riv. Ital. Paleontol. 85, 127–172.

Rasmussen, S. O., Seierstad, K. K., Andersen, I. K. Bigler, M., Dahl-Jensen, D., Johnsen, S. J., 2008. Synchronization of the NGRIP, GRIP, and GISP2 ice cores across MIS2 and palaeoclimatic implications. Quaternary Science Reviews, 27, 18–28.

Rasmussen, S. O., Andersen, K. K., Svensson, A. M., Steffensen, J. P., Vinther, B., Clausen, H. B., Siggaard-Andersen, M. L., Johnsen, S. J., Larsen, L. B., Dahl-Jensen, D., Bigler, M., Ròthlisberger, R., Fischer, H., Goto-Azuma, K., Hansson, M., Ruth, U., 2006. A new Greenland ice core chronology for the last glacial termination. Journal of Geophysical Research 111, D06102.

Richez, C. and Gascard, J. C., 1986. Mediterranean water flows when approaching the Strait of Gibraltar. Deep Sea Research, 135-137.

Robinson, S. A., Black, S., Sellwood, B. W., Valdes P. J., 2006. A review of palaeoclimates and palaeoenvironments in the Levant and Eastern Mediterranean from 25,000 to 5000 years BP: setting the environmental background for the evolution of human civilisation. Quaternary Science Reviews 25, 1517–1541.

Robinson, A. R., Golnaraghi, M., Leslie, W. G., Artegiani, A., Hecht, A., Lazzoni, E., Michelato, A., Sansone, E., Theocharis, A. and Ünlüata, Ü., 1991. Structure and variability of the Eastern Mediterranean circulation. Dyn. Atmos. Oceans, 15, 215-240.

Rohling, E. J., Cane, T. R., Cooke, S., Sprovieri, M., Boulabassi, I., Emeis, K. C., Schiebel, R., Kroon, D., Jorissen, F. J., Lorre A. and Kemp, A. E. S., 2002. African monsoon variability during the previous interglacial maximum, Earth and Planetary Science Letters 202, 61–75.

Rohling, E. J. 2001. The dark secret of the Mediterranean - a case history in past environmental reconstruction. http://www.noc.soton.ac.uk/soes/staff/ejr/DarkMed /ref-cond.html.

Rohling, E. J. and De Rijk, S., 1999. The Holocene Climate Optimum and Last Glacial Maximum in the Mediterranean: the marine oxygen isotope record. Marine Geology 153, 57-75.

Rohling, E. J., Jorissen, F. J., de Stigter, H. C., 1997. 200 year interruption of Holocene sapropel formation in the Adriatic Sea. J. Micropaleontol. 16, 97–108.

Rohling, E. J., den Dulk, M., Pujol, C. and Vergnaud-Grazzini, C., 1995. Abrupt hydrographic changes in the Alboran Sea (Western Mediterranean) around 8000 yrs BP. Deep-sea Research, 42, 1609-1619.

Rohling, E. J. and Hilgen, F. J., 1994. The eastern Mediterranean climate at times of sapropel formation: a review. Geologie en Mijnbouw, 70, 253-264.

Rohling, E. J., and Bryden, H. L. 1992. Man-induced salinity and temperature increases in western Mediterranean Deep Water, Journal of Geophysical Research, 97, 11191-11198.

Rohling, E. J., 1991b. Shoaling of the eastern Mediterranean pycnocline due to reduction of excess evaporation: implications for sapropel formation. Palaeoceanography, 6, 747-753.

Rohling, E. J and Gieskes, W. W. C, 1989. Late Quaternary changes in Mediterranean Intermediate Water density and formation rate. Paleoceanography, 4, 531-545.

Ruddiman W. F., 2001. Earth's Climate Past and Future. United States - W.H.Freeman &amp, Co Ltd - New York.

Ruddiman, W. F., 1977. Late Quaternary deposition of ice-rafted sand in the sub-polar North Atlantic (40–60 N). Geological Society of America Bulletin **88,** 1813–1827.

Saaroni, H., B. Ziv, J. Edelson, and P. Alpert, Long-term variations in summer temperatures over the Eastern Mediterranean, Geophysical Research Letters, 30, 1946.

Sacchi, M., Insinga, D., Milia, A., Molisso, F., Raspini, A., Torrente, M. M., Conforti, A., 2005. Stratigraphic signature of the Vesuvius 79 AD event off the Sarno prodelta system, Naples Bay. Marine Geology 222–223, 443–469.

Sagnotti, L., Budillon, F., Dinares-Turell, J., Iorio, M., Macrì, P., 2005. Evidence for a variable paleomagnetic lock-in depth in the Holocene sequence from the Salerno

Gulf (Italy): implications for "high-resolution" paleomagnetic dating. Geochem., Geophys., Geosyst. 6 (Q11013). doi:10.1029/2005GC001043.

Sancetta, C., 1994. Mediterranean sapropels: Seasonal stratification yields high production and carbon flux. Paleoceanography 9, 195–196.

Sanchez-Cabeza, J. A., Masqué, P., Ani-Ragolta, I., Merino, J., Frignani, M., Alvisi, F., Palanques, A., Puig, P., 1999. Sediment accumulation rates in the southern Barcelona continental margin (NW Mediterranean Sea) derived from 210Pb and 137Cs chronology. Progress in Oceanography 44 313–332.

Sandweiss, D. H., Maasch, K. A., Anderson, D. G., 1999. Transitions in the mid-Holocene. Science 283, 499–500.

Sautter, L. R., Thunell, R. C., 1989. Seasonal succession of planktonic foraminifera: results from a four-year time-series sediment trap experiment in the northeast Pacific, J. Foramin. Res. 19, 253–267.

Sbaffi, L., Wezel, F. C., Curzi, G., Zoppi, U., 2004. Millennial- to centennial-scale palaeoclimatic variations during Termination I and the Holocene in the central Mediterranean Sea. Global and Planetary Change 40, 201–217.

Schiebel, R., Hiller, B., Hemleben, C., 1995. Impacts of storms on recent planktic foraminiferal test production and $CaCO_3$ flux in the north Atlantic at 47°N, 20°W (JGOFS). Marine Micropaleontology 26, 115–129.

Schlitzer, R., Roether, W., Oster, H., Junghaus, H. G., Hausmann, M., Johannesen, J., Michelato, A., 1991. Chlorofluoro methane and oxygen in the Eastern Mediterranean. Deep Sea Research 38, 1531–1551.

Schònfeld, J., Zahn, R. and De Abreu L., 2003. Surface and deep water response to rapid climate changes at the Western Iberian Margin. Global Planetary Change 36, 237-264.

Schònfeld, J. and Zahn, R., 2000. Late glacial to Holocene history of the Mediterranean Outflow: Evidence from benthic foraminiferal assemblages and stable isotopes at the Portuguese margin. Palaeogeogr. Palaeoclimatol. Palaeoecol. 159, 85-111.

Severinghaus, J. P. and Brook, E. J., 1999. Abrupt climate change at the end of the last glacial period inferred from trapped air in polar ice. Science 286, 930–934.

Sgarrella, F. and Moncharmont Zei, M., 1993. Benthic foraminifera of the Gulf of Naples (Italy): systematic and autoecology. Bollettino della Societa` paleontologica Italiana 32, 145– 264.

Shackleton, N. J., Hall, M. A., Vincent, E., 2000. Phase relationships between millennial-scale events 64,000–24,000 years ago. Paleoceanography 15, 565–569.

Siani, G., Paterne, M., Miche, E., Sulpizio, R., Sbrana, A., Arnold, M., Haddad, G., 2001. Mediterranean sea surface radiocarbon reservoir age changes since the Last Glacial Maximum. Science, 294, 1917-1920.

Sierro, F. J., Hodell, D. A., Curtis, J. H., Flores, J. A. , Reguera, I., Colmenero-Hidalgo, E. M., Bàrcena, A., Grimalt, J. O., Cacho, I., Frigola, J. and Canals, M., 2005. Impact of iceberg melting on Mediterranean thermohaline circulation during Heinrich events. Paleoceanography, 20, PA2019, doi:10.1029/2004PA001051.

Sierro, F. J., Krijgsman, W., Hilgen, F. J., Flores, J. A., 2001. The Abad composite (SE Spain): Mediterranean reference section for the Messinian and the Astronomical Polarity Time Scale (APTS). Palaeogeography Palaeoclimatology Palaeoecology 168, 143–172.

Spahni, R., 2003: The attenuation of fast atmospheric CH_4 variations recorded in polar ice cores. Geophys. Res. Lett., 30, doi:10.1029/2003GL017093.

Spindler, M., Hemleben, C., Salomons, J. B., Smit, L. P., 1984. Feeding behavior of some planktonic foraminifers in laboratory cultures. J. Foramin. Res. 14, 237–249.

Spero, H. J., Parker, S. L., 1985. Photosynthesis in the symbiotic planktonic foraminifer Orbulina universa and its potential contribution to oceanic primary productivity. J. Foraminiferal Res., 15, 273-281.

Sprovieri, R., Di Stefano E., Incarbona A., Gargano M. E., 2003. A high-resolution of the last deglaciation in the Sicily Channel based on foraminiferal and calcareous

nannofossil quantitative distribution. Palaeogeography, Palaeoclimatology, Palaeoecology 202, 119-142.

Sprovieri, R., Sprovieri, M., Caruso, A., Pelosi, N., Bonomo, S., Ferraro, L., 2006. Astronomic forcing on the planktonic foraminifera assemblage in the Piacenzian Punta Piccola section (southern Italy). Paleoceanography. 21 PA4204.

Stager, J. C. and Mayewski**,** P. A., 1997**.** Abrupt mid-Holocene climatic transitions registered at the equator and the poles. Science 276, 1834-1836.

Steig, E. J., Brook, E. J., White, J. W. C., Sucher, C. M., Bender, M. L., Lehman, S. J., Waddington, E. D., Morse, D. L. and Clow, C. D., 2000. Synchronous climate changes in Antarctica and the North Atlantic. Science 282, pp. 92–95.

St-Onge, G., Stoner, J. S. and Hillaire-Marcel, C., 2003. Holocene paleomagnetic records from the St. Lawrence Estuary, eastern Canada: Centennial to millennial-scale geomagnetic modulation of cosmogenic isotopes, Earth Planet. Sci. Lett., 209, 113–130.

Stuiver, M., Reimer, P. J., Reimer, R. W., 2005. CALIB 5.0. In www.program and documentation.

Stuiver, M., Reimer, P. J., Bard, E. Beck, J. W., Burr, G. S., Hughen, K. A., Kromer, B., McCormac, F. G., van der Plicht, J. and Spurk M., 1998. INTCAL98 Radio carbon age calibration 24,000 - 0 cal BP, Radiocarbon, 40,1041-1083.

Stuiver, M., Braziunas, T. F., Grootes, P. M. and Zielinski, G. A. 1997. Is there evidence for solar forcing of climate in the GISP2 oxygen isotope record?. Quaternary Research 48, 259-266.

Stuiver, M., and T. F. Braziunas. 1993. Sun, ocean, climate and atmospheric 14CO2: An evaluation of causal and spectral relationships. The Holocene 3, 289-305.

Stuiver, M. and Kra, R.S., 1986. Calibration issue, Proceedings of the 12th International 14C conference. Radiocarbon 28, 805-1030.

Tang, C. M. and Stott, L. D., 1993. Seasonal salinity changes during Mediterranean sapropel deposition 9000 years BP.: evidence from isotopic analyses of individual planktonic foraminifera. Paleoceanography, 8, 473-493.

Thompson L. G., Davis M. E., Mosley-Thompson E., Sowers T. A., Henderson K.A., Zagorodnov V. S., Lin P.-N., Mikhalenko V. N., Campen R. K., Bolzan J. F., Cole-Dai J., 1998. A 25,000 year tropical climate history from Bolivian ice cores. Science 282, 1858–1864.

Thunell, R. C. and Williams, D. F., 1989. Glacial-Holocene salinity changes in the Mediterranean Sea: hydrographic and depositional effects. Nature, 338, 493-496.

Thunell, R. C and Reynolds, L. A., 1984. Sedimentation of planktonic foraminifera: seasonal changes in species flux in the Panama Basin. Micropalaeontology, 30, 243-262.

Thunell, R. C and Williams, D. F., 1983. Paleotemperature and paleosalinity history of the eastern Mediterranean during the Late Quaternary. Palaeogeogr., Palaeoclimatol., Palaeoecol., 44, 23-39.

Thunell, R. C., 1978. Distribution of recent planktonic foraminifera in surface sediments of the Mediterranean Sea. Mar Micropaleontol., 3: 147-173.

Todd, R., 1958. Foraminifera from western deep-sea cores. Rep. Swedish Deep-sea Exped., 8, 169-215.

Tolderlund, D. S. and Bé, A. W. H., 1971. Seasonal distribution of planktonic foraminifera in the western North Atlantic. Micropalaeontology, 17, 297-329.

Trincardi, F. and Field, M.E., 1991. Geometry, lateral variation, and preservation of downlapping regressive shelf deposits: eastern Tyrrhenian Sea margin, Italy. J. Sediment. Petrol. 61, pp.775–790.

Tsimplis, M. N., Zervakis, V., Josey, S., Peeneva, E., Struglia, M. V., Stanev, E., Lionello, P., Malanotte-Rizzoli, P., Artale, V., Theocharis, A., Tragou, E. and Oguz, T., 2006. Changes in the oceanography of the Mediterranean Sea and their

link to climate variability. In: P. Lionello, P. Malanotte-Rizzoli & R. Boscolo (Eds), Mediterranean Climate Variability, Amsterdam, Elsevier, pp. 227-282.

Turley, C. M., 1999. "The changing Mediterranean Sea — a sensitive ecosystem?". Progress in Oceanography, 44, 387-400.

Turner, G. M., and Thompson, R., 1982. Detransformation of the British geomagnetic secular variation record for Holocene times, Geophys. J. R. Astron. Soc., 70, 789–792.

Usoskin, I. G., Solanki, S. K., Korte, M., 2006. Solar activity reconstructed over the last 7000 years: The influence of geomagnetic field changes. Geophysical Research Letters vol. 33 L08103.

Usoskin, I. G., Solanki, S. K., Schùssler, M., Mursula, K., Alanko, K., 2003. A millennium scale sunspot number reconstruction: Evidence for an unusually active Sun since the 1940's. Phys. Rev. Lett., 91, 211101.

Van der Zwaan, G. J. and Jorissen, F. J., 1991. Biofaciat patterns in river-induced shelf anoxia. In: R.V. Tyson and T.H. Pearson (Editors), Modern and Ancient Continental Shelf Anoxia. Geol. Soc. Spec. PUN., 58, 65-82.

Van Geel, B., van der Pflicht, J., Kilian, M. R., Klaver, E. R., Kouwenberg, J. H. M., Renssen, H., Reynaud-Farrera, I., Waterbolk, H. T., 1998. The sharp rise of ^{14}C ca. 800 cal BC: possible causes, related climatic teleconnections and the impact on human environments. Radiocarbon 40, 535–550.

Van Geel, B., Buurman, J., Waterbolk, H. T., 1996. Archaeological and palaeoecological indications of an abrupt climate change in The Netherlands, and evidence for climatological teleconnections around 2650 BP. Journal of Quaternary Science 11, 451–460.

Van Leeuwen, R. J. W., 1989. Sea-floor distribution and Late Quaternary faunal patterns of planktonic and benthic foraminifera in the Angola Basin. Utrecht Micropalaeontol. G. bulloides., 38, 288 pp.

Vargas-Yáñez, M., García, M., Salat, J., García-Martínez, M. C., Pascual, J., Moya, F., 2007. Warming trends and decadal variability in the Western Mediterranean shelf. Global and Planetary Change doi:10.1016/j.gloplacha.2007.09.001.

Vazquez, A., Zamarreño, I., Reyes, E. and Linares, J., 1991. Late Quaternary climatic changes on the south-western Balearic slope (Western Mediterranean): isotopic, faunal and mineralogical relationships, Palaeogeogr., Palaeoclimatol., Palaeoecol., 81, 215-227.

Verngnaud-Grazzini, C., Borsetti, A. M., Cati, F., Colantoni, P., Siesser, W. G., Saliege, J. F., Sartori, R., Tampieri, R., 1988. Paleoceanographic record of the last deglaciation in the Strait of Sicily. Mar. Micropaleontol. 13, 1– 21.

Vergnaud-Grazzini, C., Glaçon, G., Pierre, C., Pujol, C. and Urrutiaguer, M. J., 1986. Foraminiferes planctoniques de Méditerranée en fin d'été. Relations avec les structures hydrologiques. Mem. Soc. Geol. Ital., 36, 175-188.

Vergnaud-Grazzini, C., Ryan, W. B. F. and Cita, M. B., 1977. Stable isotope fractionation, climatic change and episodic stagnation in the eastern Mediterranean during the Late Quaternary. Marine Micropaleontology 2, 353-370.

Violanti, D., Parisi, E., Erba, E., 1987. Fluttuazioni climatiche durante il Quaternario nel Mar Tirreno, Mediterraneo Occidentale (Carota PC-19 BAN 80). Riv. Ital. Paleontol. Stratigr. 92, 515–570.

Von Grafenstein, U., Erlenkeuser, H., Muller, J., Jouzel J. and Johnsen, S., 1998. The cold event 8200 years ago documented in oxygen isotope records of precipitation in Europe and Greenland. Climate Dynamics 14, 73–81.

Walker, M. J. C., Bjòrck, S., Lowe, J. J., Cwynar, L. C., Johnsen, S., Knudsen, K. L., Wohlfarth, B., 1999. Isotopic 'events' in the GRIP ice core: a stratotype for the late Pleistocene. Quaternary Science Reviews, 18, 1143–1150.

Warning B. and Brumsack, H. J., 2000. Trace metal signatures of eastern Mediterranean sapropels, Palaeogeography, Palaeoclimatology, Palaeoecology 158, 293–309.

Williams, N., 1998. The Mediterranean Beckons to Europe's oceanographers. Science, 229, 463-464.

Wolf-Welling, T. C. W., Cowan, E. A., Daniels, J., Eyles, N., Maldonado, A., Pudsey, C. J., 2001. Diffuse spectral reflectance data from rise Sites 1095, 1096, 1101 and Palmer Deep Sites 1098 and 1099 (Leg 178, Western Antarctic Peninsula). In: Barker, P.F., Camerlenghi, A., Acton, G.D., Ramsay, A.T.S. (Eds.), Proceeding Ocean Drilling Program, Scientific Results, 178, 1-22.

Wüst, G., 1961. On the vertical circulation of the Mediterranean Sea. J. Geophys. Res., 66, 3261-3271.

Ziv, B., Saaroni, H. and Alpert P., 2004. The factors governing the summer regime of the eastern Mediterranean, International Journal of Climatology, 24, 1859-1871.

Chapter 2

MATERIALS AND SITE SETTING

2 MATERIALS AND SITE SETTING

For this study different marine cores have been selected from the Western Mediterranean Sea.

Based on literature data, the studied sites were expected to offer a high resolution record for paleo-environmental reconstruction during the latest Quaternary, as well as for reconstruction of circulation patterns in the Mediterranean basins. In fact, previous literature data from western to eastern Mediterranean Sea (Perez-Folgado et al., 2003, 2004; Sprovieri et al., 2003, 2006; Lirer et al., 2007; Incarbona et al., 2008, in press) clearly suggest that the following Mediterranean sites represent key areas for this research (Fig. 2.1).

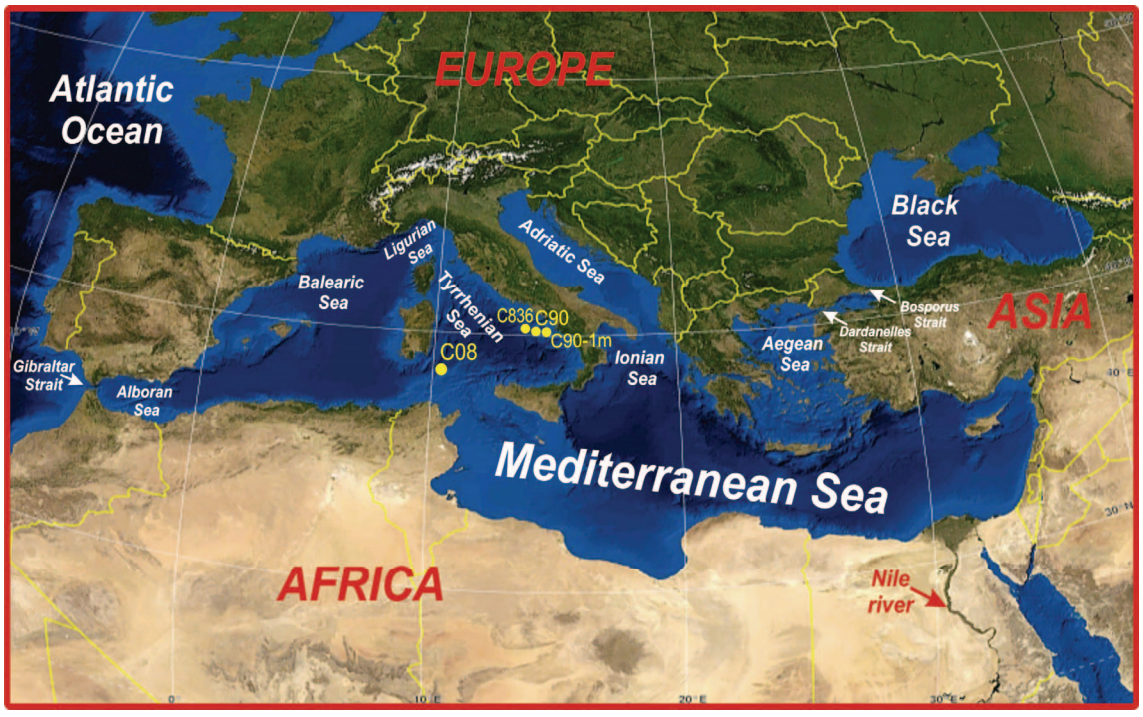

Fig. 2.1 Location map of the investigated area with the position of the studied gravity cores.

2.1.1 Core C08

The gravity core C08, is located in the Sentinelle Valley of the Sardinia Channel (Fig. 2.1) at 2370 m below sea level. This core has been recovered during the cruise CIESM Sub2 onboard the R/V Urania in December 2005 (Tab. 2.1).

The sedimentary sequence (Fig. 2.2) consists on 5.40 m of hemipelagic mud interbedded with three turbiditic fine sand layers and one tephra layer in the lower part (see, Budillon et al. 2008, in press).

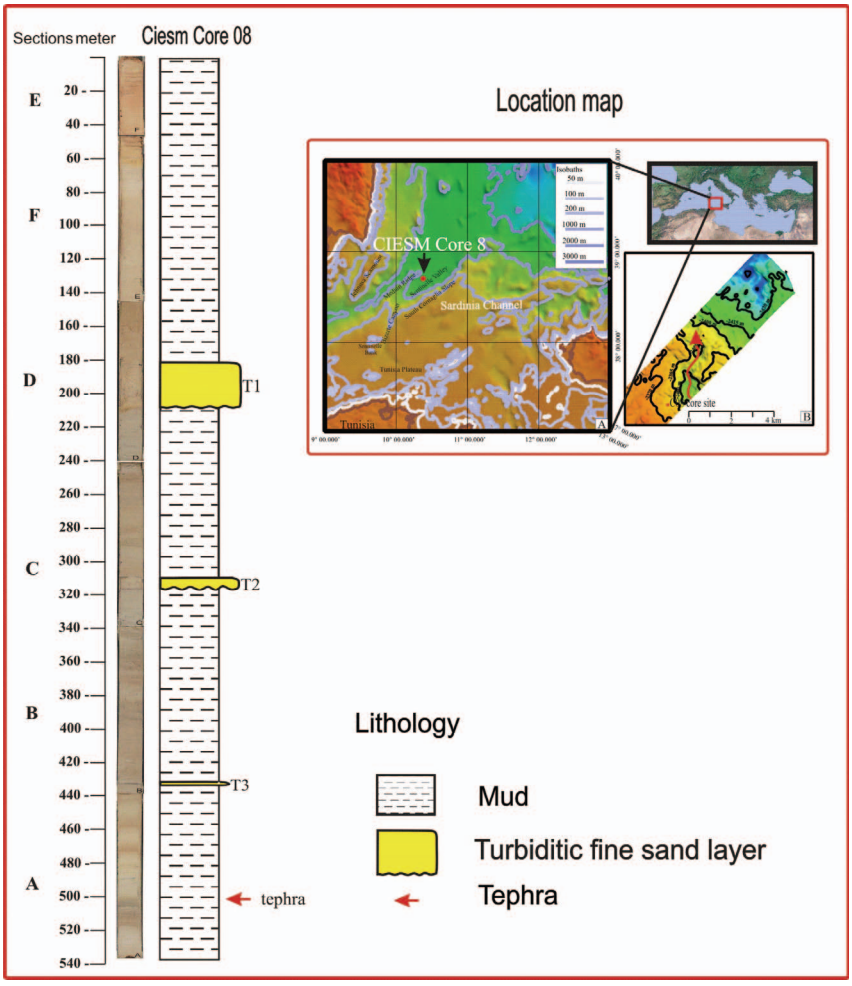

Fig. 2.2 Location map and lithology of the core **C08**

2.1.2 Core C90-1m

The gravity core C90-1m (Tab. 2.1), is located close to the shelf break of the northern Salerno Bay, at water depth of 103.4 m (Fig. 2.1). This core has been recovered during the cruise onboard the R/V Tethis in June 2006. The sedimentary sequence was recovered with SW104 drill-system of ISMAR-CNR.

The continental shelf off the Tyrrhenian basin margin is characterised by high sediment accumulation rate (Trincardi and Field, 1991; Budillon et al., 1994; Sacchi et al., 2004) and the occurrence of several tephra layers.

The sedimentary succession, consists on 106 cm thick (Fig. 2.3), of hemi-pelagic marls punctuated by a tephra layer between 55 and 66 cm b.s.f. (Fig. 2.3). This tephra represents a lithostratigraphic marker in this area as evidenced by Iorio et al. (2004), Budillon et al. (2005) and Sagnotti et al. (2005) (Fig. 2.6).

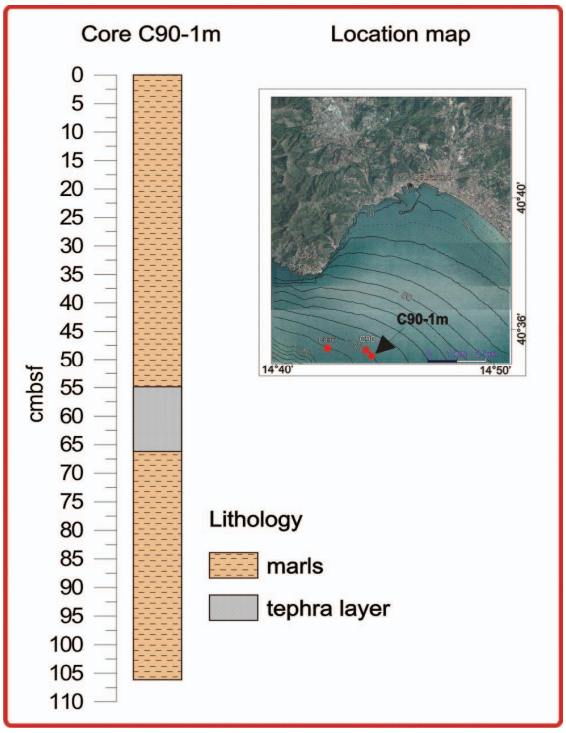

Fig. 2.3 Location map and lithology of the core **C90-1m**

2.1.3 Core C90

The gravity core C90 (Tab. 2.1) is located close to the shelf break of the northern Salerno Bay (eastern Tyrrhenian margin), at a water depth of 103.4 m (Fig. 2.1). This core has been recovered, during the cruise GMS97_01, onboard of the R/V Urania, within the frame of a national CARG project, by the Istituto per l'Ambiente Marino Costiero (IAMC – CNR) of Naples. The cored succession consists on 4.87 m thick, of undisturbed and well preserved hemi-pelagic deposits (Fig. 2.4) punctuated by a number of volcaniclastic layers occurring as cm-thick horizons.

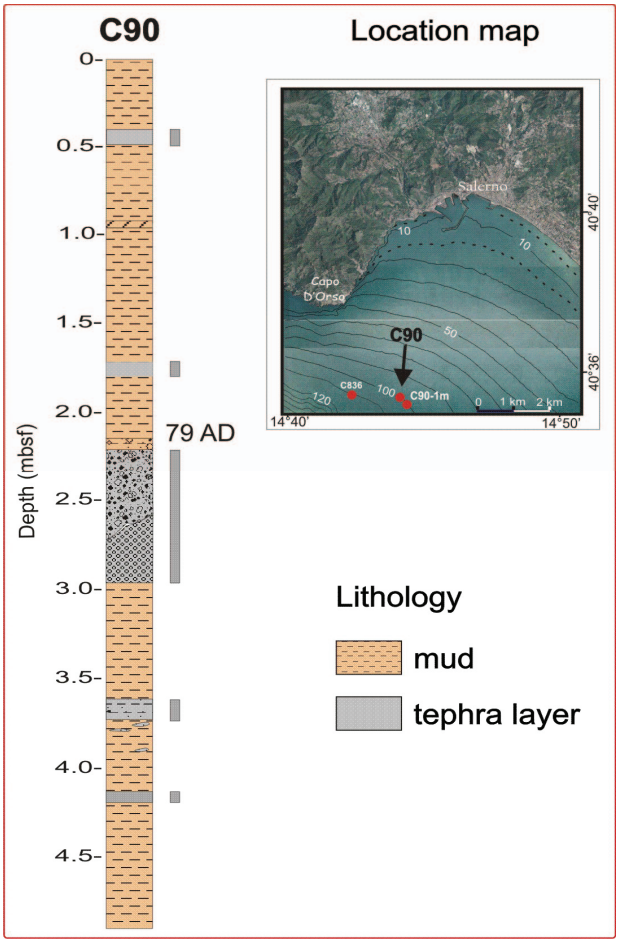

Fig. 2.4 Location map and Lithology of the core **C90**.

2.1.4 Core C836

The gravity core C836 (Tab. 2.1) is collected in the outer shelf of the Salerno Gulf at about 110 m of depth, off the Amalfi coast (Fig. 2.1). This core has been recovered during the cruise GMS00_05 onboard of the R/V Urania, within the frame of a national CARG project by the Istituto per l'Ambiente Marino Costiero (IAMC – CNR) of Naples.

Core C836 consists on 5.74 m thick of homogeneous mud (Fig. 2.5) interdedded by 6 tephra centimetres layers (Fig. 2.5, 2.6). A distinct bioclastic interval (between 523 cm b.s.f. and 544 cm b.s.f.) is evident in the C836 core (Fig. 2.5).

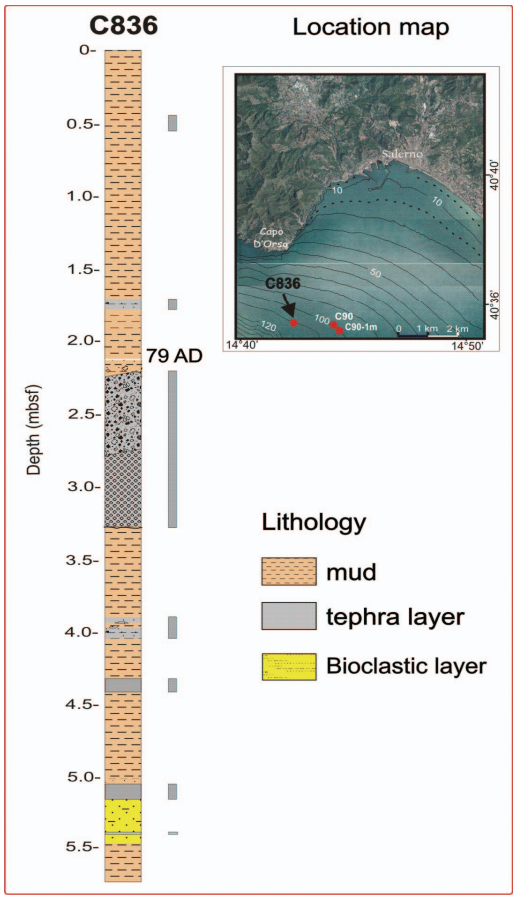

Fig. 2.5 Location map and lithology of the core **C836**.

2.1.5 Composite core C90-1m_C90_C836

The constructed composite succession is based on the three previously described gravity cores C90-1m, C90 and C836 (Fig. 2.6). The resulting composite record is constructed from the top down to the base as following: sea-floor down to base of tephra V0 (core C90-1m), from the base of tephra V0 down to top of tephra V2 (core C90) and from top of tephra V2 down to the base core (core C836) (Fig. 2.6).

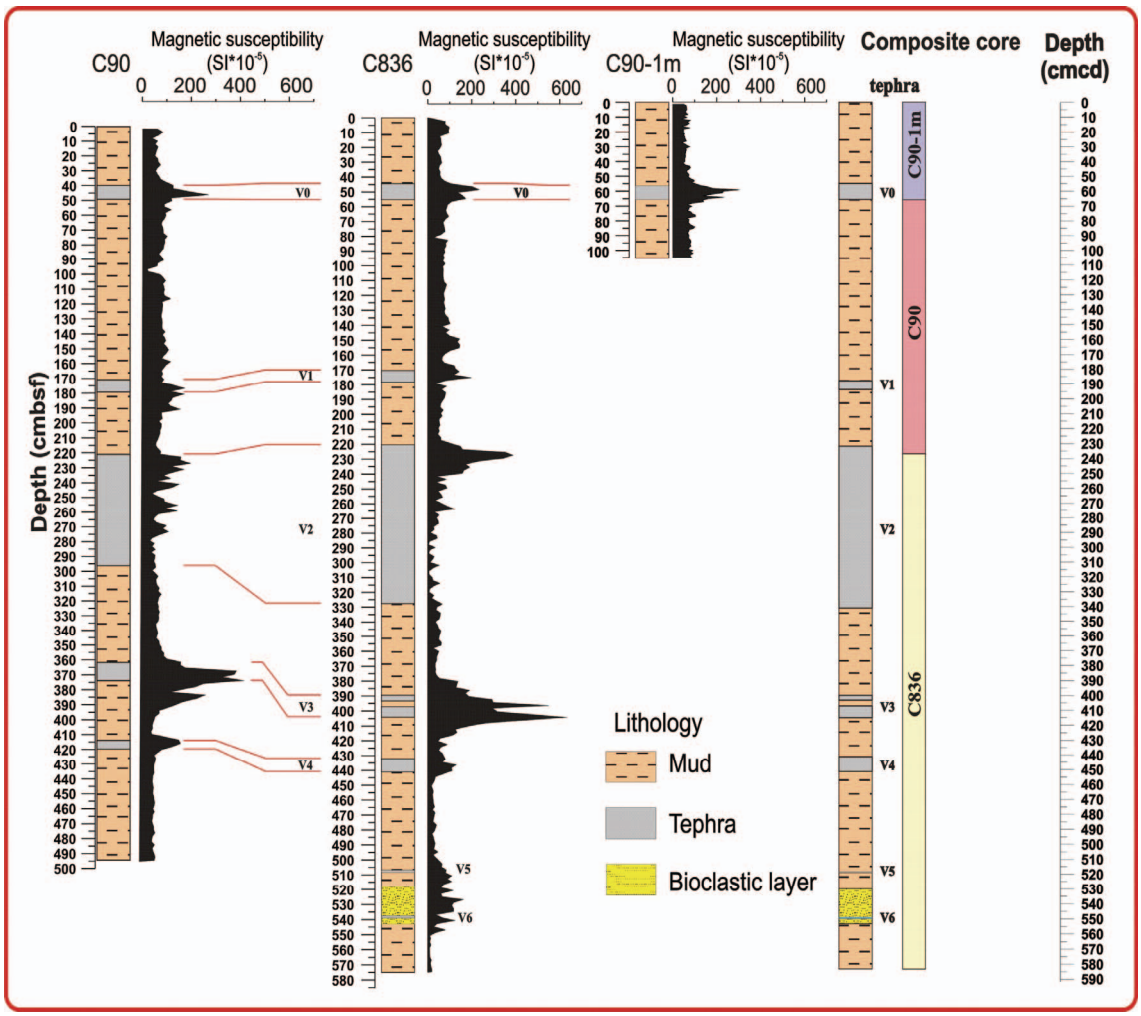

Fig. 2.6 Correlation of the three studied cores **C90-1m**, **C90** and **C836**. Magnetic susceptibility data for **C90** and **C836** cores are from Iorio *et al.* (2004) and for **C90-1m** core from this work.

Station	Latitude	Longitude	Water Depth (m)	Length (m)	Age model Source
Core C08	38°38.536'N	10°21.558'E	2370	5.40	**This study**
Core C90-1m	40°35.760'N	14°42,480'E	103.4	1.06	**This study**
Core C90	40°35.760'N	14°42.380'E	103.4	4.87	**This study**
Core C836	40°35.980'N	14°40.470'E	110	5.74	**This study**

Table 2.1. detail of the studied cores (**C08**, **C90-1m**, **C90**, **C836**) in the Western Southern Mediterranean Sea. In particular the cores are situated in the Southern Tyrrhenian Basin.

REFERENCES

Budillon, F., Lirer, F., Iorio, M., Macrì, P., Sagnotti, L., Vallefuoco, M., Ferraro, L., Garziglia, S., Innangi, S., Sahabi, M., Tonielli, R, 2008. Integrated stratigraphic reconstruction for the last 80 kyr in a deep sector of the Sardinia Channel (Western Mediterranean).Deep Sea Research 2008, in press.

Budillon, F., Violante, C., Conforti, A., Esposito, E., Insinga, D., Iorio, M., Porfido, S., 2005. Event beds in the recent prodelta stratigraphic record of the small flood-prone Bonea stream (Amalfi Coast, Southern Italy). Marine Geology 222–223 419–441.

Budillon, F., Esposito, E., Iorio, M., Pelosi, N., Porfido, S., Violante, C., 2005. The geological record of storm events over the last 1000 years in the Salerno Bay (Southern Tyrrhenian Sea): new proxy evidences, European Geoscience Union, Adv. Geosci., 2 1–8.

Budillon, F., Pescatore, T., Senatore, M. R., 1994. Cicli deposizionali del Pleistocene Superiore–Olocene sulla piattaforma continentale del Golfo di Salerno (Tirreno Meridionale). Boll. Soc. Geol. Ital. 113, 303–316.

Incarbona, A., Di Stefano, E., Patti, B., Pelosi, N., Bonomo, S., Mazzola, S., Sprovieri, R., Tranchida, G., Zgozi, S. and Bonanno, A., 2008. Holocene millennial-scale productivity variations in the Sicily Channel (Mediterranean Sea). Paleoceanography, 23, PA3204, doi:10.1029/2007PA001581.

Iorio, M., Sagnotti, L., Angelino, A., Budillon, F., D'Argenio, B., Turell Dinares, J., Macrı`, P., Marsella, E., 2004. High-resolution petrophysical and paleomagnetic study of late-Holocene shelf sediments, Salerno Gulf, Tyrrhenian Sea. Holocene 14, 433442.

Lirer, F., Sprovieri, M., Pelosi, N., Ferraro, L., 2007. Clues of solar forcing from a 2000 years long sedimentary record from the eastern tyrrhenian margin. Clima e cambiamenti climatici: le attività di ricerca del CNR pp. 209-212.

Pérez-Folgado, M., Sierro, F. J., Flores, J. A., Grimalt, J .O., Zahn, R., 2004. Paleoclimatic variations in foraminifer assemblages from the Alboran Sea (Western Mediterranean) during the last 150 ka in ODP Site 977. Marine Geology 212, 113–131.

Pérez-Folgado, M., Sierro, F. J., Flores, J. A., Cacho, I., Grimalt, J. O., Zahn, R., Shackleton, N. 2003. Western Mediterranean planktonic foraminifera events and millennial climatic variability during the last 70 kyr. Marine Micropaleontology, 48, 1-2, 49-70.

Sacchi, M., Insinga, D., Milia, A., Molisso, F., Raspini, A., Torrente, M. M., Conforti, A., 2005. Stratigraphic signature of the Vesuvius 79 AD event off the Sarno prodelta system, Naples Bay. Marine Geology 222–223, 443–469.

Sagnotti, L., Budillon, F., Dinares-Turell, J., Iorio, M., Macrì, P., 2005. Evidence for a variable paleomagnetic lock-in depth in the Holocene sequence from the Salerno Gulf (Italy): implications for "high-resolution" paleomagnetic dating. Geochem., Geophys., Geosyst. 6 (Q11013). doi:10.1029/2005GC001043.

Sprovieri, R., Di Stefano, E., Incarbona, A., Gargano, M. E., 2003. A high-resolution of the last deglaciation in the Sicily Channel based on foraminiferal and calcareous nannofossil quantitative distribution. Palaeogeography, Palaeoclimatology, Palaeoecology 202, 119-142.

Sprovieri, R., Sprovieri, M., Caruso, A., Pelosi, N., Bonomo, S., Ferraro, L., 2006. Astronomic forcing on the planktonic foraminifera assemblage in the Piacenzian Punta Piccola section (southern Italy). Paleoceanography. 21 PA4204.

Trincardi, F. and Field, M.E., 1991. Geometry, lateral variation, and preservation of downlapping regressive shelf deposits: eastern Tyrrhenian Sea margin, Italy. J. Sediment. Petrol. 61, pp.775–790.

Chapter 3

METHODS

3 METHODS

This chapter describes the different methods and procedures used for this study (planktonic foraminifera, calcareous nannofossils, benthic foraminifera, tefrostratigraphy, AMS-^{14}C data, ^{210}Pb and ^{137}Cs radionuclide and petrophisical properties), from the studied marine records (Tab. 3.1).

Station	Micropaleontological Analysis	Size mesh	Adopted taxonomy	Petrophysical properties and Magnetostratigraphy	Radionuclide Dating (^{210}Pb and ^{137}Cs)	Radiocarbon Dates (^{14}C)	Tephrostratigraphy	References
Core C08	planktonic foraminifera*	>125 µm	Jorissen et al. (1993) Capotondi et al. (1999)	Magnetic susceptibility * Colour Reflectance* Paleomagnetism*		*Globigerina bulloides* * *Globorotalia inflata* *		This study, Budillon et al. (2008)
Core C90-1m	planktonic foraminifera* benthic foraminifera*	>90 µm	Jorissen et al. (1993) Capotondi et al. (1999	Magnetic susceptibility* Colour Reflectance*	^{210}Pb and ^{137}Cs activity*	*Planktonic foraminifera mixing*	Tephra layers analysis (EDS)*	This study
Core C90	planktonic foraminifera* Calcareous nannofossils*	>90 µm	Jorissen et al. (1993) Capotondi et al. (1999	Magnetic susceptibility Colour Reflectance		*Globigerinoides ruber* * *Globorotalia inflata* *	Tephra layers analysis (EDS)*	Lirer et al. (2007); Insinga et al. (2008), This study
Core C836	planktonic foraminifera* Calcareous nannofossils*	>90 µm	Jorissen et al. (1993) Capotondi et al. (1999	Magnetic susceptibility Colour Reflectance		*Globigerinoides ruber* * *Globorotalia inflata* *	Tephra layers analysis (EDS)*	Lirer et al. (2007); Insinga et al. (2008), This study

Tab. 3.1 Different methods and procedures used for micropaleontological analysis (planktonic foraminifera, calcareous nannofossils, benthic foraminifera), petrophysical properties, ^{137}Cs and ^{210}Pb radionuclide, AMS ^{14}C dates and tefrostratigraphy on the studied marine core records (**C08**, **C90-1m**, **C90**, **C836**). The star shows the data from this study.

3.1 CORE ANALYSIS

Cores were split in two halves, photographed, described for lithology and finally measured for petrophysical parameters.

3.1.1 Magnetic Susceptibility and Colour Reflectance

The physical properties of the cores were measured at 1 cm step in a fully automated GEOTEK Multi-Sensor Core Logger (MSCL), in the petrophysical laboratory of IAMC in Naples (Italy). The MSCL system includes a Bartington MS2E Point sensor, to measure the low-field magnetic susceptibility (MS) with a spatial resolution of 0.1 cm and a Minolta Spectrophotometer CM 2002 which records at 0.8 cm step, the percentage of reflected energy (RSC) at 31 wavelengths in 10-nm steps, over the visible spectrum (from 400 to 700 nm). MS and RSC measurements were taken on the archive half, ~1 hr after the core had been split. The split core was covered with cling film to protect the glass cover of the Minolta aperture while measuring. Both measurements, log plotted, were visually compared in order to detect similar trends and tentatively group the data according to their physical properties and corresponding stratigraphy (Wolf Welling et al., 2001).

3.1.2 Paleomagnetic Secular Variation (PSV)

Paleomagnetic secular variation (PSV) records obtained from sediments and volcanic rocks provide the main source of information to extend the direct observations on directional variations of the Earth's magnetic field to recent geological past.

In this research, for the paleomagnetic study, 1-m-long u-channel specimens were sampled from archive halves of the CIESM C08 core. The u-channels, were measured in a magnetically shielded room at the paleomagnetic laboratory at the Istituto Nazionale di Geofisica e Vulcanologia in Rome, using an automated pass through a 2-G Enterprises DC SQUID cryogenic magnetometer system. For each u-channel the natural remanent magnetization (NRM) was measured at 1-cm steps. It is emphasized, however, that, due to the intrinsic response functions of the SQUID sensors, remanence

measurements may be considered truly independent only every ca. 5 cm. The NRM was progressively demagnetized by the alternating field (AF) in nine steps up to a maximum field peak of 100 mT, by translating the u-channel through a set of three perpendicular AF coils at a speed of 10 cm/s. The remanence was measured at the same 1-cm spacing after each demagnetization step. Demagnetization data from u-channels were analysed on orthogonal vector projections and the paleomagnetic data obtained generally provided straightforward demagnetization diagrams, indicating that the sediments carry an almost single-component NRM. In fact, during the AF demagnetization a complete removal of any coring overprint and/or laboratory-induced remanences was achieved at low AF peaks (10 mT), and the characteristic remanent magnetization (ChRMs) of the sediments was clearly identified and determined by principal component analysis (Kirschvink, 1980). For each u-channel the uppermost and lowermost few centimeters were disregarded for the paleomagnetic analysis, to avoid any deflection to the remanence direction due to disturbances that may have been introduced during sampling.

3.2 CORE SAMPLING

3.2.1 Sampling

The sampling spacing is of 1 cm for cores C90-1m, C90 and C836 resulting a total number of 106 samples for the core C90-1m, and 468 samples for the composite core C90-1m_C90_C836 (Salerno Gulf). For the core C08 (Sardinia Channel), the sampling spacing is of 2 cm, for a total of 216 samples.

In terms of micropaloentological analysis, the planktonic foraminiferal study was been performed on all the samples, the calcareous nannofossil study was been performed for the composite core C90-1m_C90_C836 on 187 samples and finally benthic foraminiferal study was been performed on 43 samples from core C90-1m.

Tephrostratigraphic study was carried out on 5 tephra layers of composite core C90-1m_C90_C836.

3.3 MICROPALEONTOLOGICAL ANALYSIS

3.3.1 Planktonic foraminifera

Each wet sample of about 20 g was dried at 50° and washed over sieves with mesh-width size of 63 microns. Quantitative planktonic foraminiferal analysis were carried out on the fractions >125μm (core C08) and >90μm (Cores C90-1m, C90, C836) to avoid juvenile specimens.

All taxa are quantified as percentages of the total number of planktonic foraminifera. The concentration is reported as number of specimens per gram of dry sediment. Regarding the adopted taxonomy, some planktonic species or morphotypes are lumped together according to the following scheme (Jorissen et al., 1993, Capotondi et al., 1999):

- *Globigerinoides ruber* includes *Globigerinoides ruber* (variety rosea and alba) and *Globigerinoides elongatus*;
- *Orbulina* spp. includes both *Orbulina universa* and *Orbulina suturalis*;
- *Globigerinoides quadrilobatus* includes *Globigerinoides trilobus* and *Globigerinoides sacculifer*;
- *Globigerina bulloides* (including extremely rare specimens of *Globigerina falconensis)*;
- *Globorotalia truncatulinoides* left coiling;
- *Globorotalia inflata*;
- *Globigerinita glutinata*;
- *Turborotalita quinqueloba*;
- *Hastigerina siphoniphera* includes *Globigerinella calida*.

3.3.2 Calcareous nannofossil

For the calcareous nannofossils 187 samples were prepared as "smear slides" (Bown 1998) and analysed using a light microscope (transmitted light and crossed nicols) at about 1250X magnification. Abundance data were collected performing an approximately 500 specimen count and plotted as percentage values. The abundances of *Florisphaera profunda* was calculated with respect to 500 specimens of all other species. Reworked taxa (of Mesozoic and Cenozoic age) abundance was estimated by counting the specimens found in fields observed to count 500 nannofossils and plotted as percentage values. Selected warm-water taxa (*Discosphaera tubifera*, *Rhabdosphaera* spp., *Syracosphaera* spp. and *Umbellosphaera* spp.), were separately plotted and in a cumulative curve, and the *Gephyrocapsa oceanica*/*Gephyrocapsa muellerae* ratio (*G.oceanica*/*G. oceanica* + *G. muellerae*) were used to document climatic fluctuations (Sprovieri et al., 2003; Sierro et al. 2001).

3.3.3 Benthic foraminifera

Analysis of benthic foraminifera was carried out on 43 samples. Sampling spacing was 2 cm from the top of the core C90-1m (seafloor) down to the base. Each wet sample of about 20 g was dried at 50° and washed over sieves with mesh-width size of 63 microns. Quantitative benthic foraminiferal analysis was carried out on the fractions >90μm (core C90-1m) to avoid juvenile specimens. All taxa are quantified as percentages of the total number of benthic foraminifera. The concentration is reported as number of specimens per gram of dry sediment. In nine samples within the tephra layer, between 55 and 66 cmbsf, the total number of benthic individuals appears very low. Generally, less than 95 individuals were counted every sample and a total of 58 benthic foraminiferal species were identified. The generic attribution of benthic taxa was made following Loeblich and Tappan classification (1987); species were mainly determined on the basis of conspicuous studies on the Mediterranean benthic species (Cimerman and Langer, 1991; Sgarrella and Moncharmont-Zei, 1993).

Quantitative analysis has been performed on eight selected species showing the most relative abundace in the assemblages:

- *Bulimina aculeata*;
- *Bulimina marginata*;
- *Bolivina alata*;
- *Cassidulina carinata*;
- *Hyalinea baltica*;
- *Uvigerina mediterranea*;
- *Melonis padanum*;
- *Valvulineria bradyana*.

3.3.4 Late Quaternary high-resolution eco-biostratigraphy

In the Holocene and latest Pleistocene stratigraphic interval (about the last 22 kyr) the classical biostratigraphy cannot be used, because common used biostratigraphic events (FAD and LAD) are not present in the this short time interval. Consequently, in the last years some authors (e.g. Capotondi et al., 1999; Asioli et al., 2001; Sprovieri et al., 2003) proposed for the Mediterranean region a sequence of eco-biozones based on relative abundance fluctuations of planktonic foraminifera.

More recently some papers appeared (Sbaffi et al., 2001; Giunta et al., 2003; Principato et al., 2003; Sprovieri et al., 2003) which report a sequence of eco-biozones also based on abundance fluctuations in the calcareous nannofossil assemblage. The integrated calcareous plankton eco-biostratigraphy provides an high resolution subdivision of this geological record if a detailed set of samples is studied from a quantitative point of view. Recently, Ducassou et al. (2007) and Perez-Folgado et al. (2003, 2004) proposed for the Alboran Sea and Nile deep-sea area, respectively, the extension of eco-biostratigraphy back to ~250 kyr.

The identification of these eco-bioevents is clearly associated to the Quaternary climatic record wich is characterised by significant fluctuation from glacial to interglacial conditions that affected the global planktonic foraminiferal distribution. Moreover, data on living planktonic foraminifera show a seasonal and geographical variability in their distribution. This variability may be associated to different parameters (nutrient, food availability, hydrographical patterns) which can be taken in account for biostratigraphic and biochronological meaning and useful for regional correlation.

Anyway, at present, it is clearly evident that it does not exist a complete and unanimously accepted eco-biotratigraphic scheme, which can allowed an easily correlation between different sectors of the Mediterranean Sea.

In this study, the planktonic eco-biostratigraphic scheme proposed by Sprovieri et al. (2003) for the Sicily Channel has been adopted for the last 23 kyr. According to this scheme 9 eco-biozones (labelled from 1F to 9F) have been identified. Downwards to ~80 kyr only a further eco-biozone (labelled 10F) has been recognised in core C08 (see chapter 6 for details). In addition, for the two last millennia, the first eco-biozone 1F has been subdivided in two sub-eco-biozones 1Fa and 1Fb (see chapter 5 for details). Furthermore, for the last 500 years in this thesis a subdivision informally labelled with A, B and C intervals have been proposed for core C90-1m (see chapter 4 for details).

According to Sprovieri et al. (2003), the concept followed to identify the sequence of eco-biozones, is well comparable with the concept of Event Stratigraphy, as recently proposed by the INTIMATE working group (Walker et al., 1999; Lowe et al., 2001) that in the last years studied the Greenland ice cores (GRIP and GISP).

The Event Stratigraphy proposed for this study allows to identify a sequence of events (or climatic events), regionally recorded in the western part of the Mediterranean area, which may be associated (or correlated) to the events recorded in to the type section (the oxygen isotopic profile of the GRIP/GISP ice cores). Finally, an independently obtained age model of the studied records could offer the possibility to identify diachroneity among the different sites.

3.4 TEPHROSTRATIGRAPHY

In the studied cores C90-1m, C90, C836 (Gulf of Salerno), on the basis of sedimentological description, have been identified the presence and thickness of tephra layers. In particular, tephra abundance peaks were firstly identified from magnetic susceptibility measurements, then from semi-quantitative counting on microscope slides. The tephra layers, not all visible by naked eye in the cored sediments, were identified by a peak of abundance of glass fragments above the background in the whole detritic material coarser than 40 micron. They were oven-dried, sieved with 1phi interval sieves, for defining grain-size distribution, and at least 100 fragments for each sample were counted under a binocular microscope, in order to determine lithological components content. For each sample, at least 30 juvenile fragments were embedded in epoxy resin and suitably polished for microprobe analysis. On the same embedded fragments, qualitative SEM EDS observation was used to define the mineralogical content. Major-element analysis on pumice fragments, glass shards and crystals were performed on a SEM JEOL JSM 5310 (15kV, ZAF Correction Routine) with EDS at CISAG (Centro Interdipartimentale di Servizio per Analisi Geomineralogiche) at the University of Naples Federico II. Instrument calibration was based on international mineral and glass standards. Individual analysis of glass shards with total oxide sums lower than 95% were excluded.

3.5 DATING (^{14}C, ^{210}Pb and ^{137}Cs)

3.5.1 Radionuclide dating (^{210}Pb and ^{137}Cs)

The uppermost 40 cm of core C90-1m were dated using the short-lived radionuclide ^{210}Pb by alpha spectrometry measurements.

The natural radionuclide ^{210}Pb (t1/2=22.26 yr) is originating from the ^{238}U series and is continuously introduced into the marine environment from:

i) the atmosphere, after decay from ^{222}Rn exhaled from the continental crust ;

ii) within the water column, mainly through the radioactive decay of dissolved ^{226}Ra.

Because of its reactivity, it rapidly becomes associated with suspended matter and, therefore, subject to sedimentation.

^{210}Pb has been widely used as geo-chronometer for age dating on 100-yr time scale over the last 40 yr. ^{137}Cs (t1 /2=30.2 yr) is a short-lived artificial radionuclide delivered to the aquatic environment by fallout from atomic weapon testing starting in 1954 A.D. and peaking in 1963 A.D., when the maximum global fallout occurred. ^{137}Cs presence in the Mediterranean Sea has recently been reviewed by (Papucci et al., 1996). Later, the Chernobyl accident added significantly to the total ^{137}Cs inventory in the Mediterranean Sea (Molero et al., 1999).

^{210}Pb and ^{137}Cs have been used in the Western Mediterranean to study water mass transport (Sanchez-Cabeza et al., 1995) and sedimentation processes (Sanchez-Cabeza et al., 1993; Palanques et al., 1998). Several studies have been carried out to quantify sedimentation rates in various areas in the Mediterranean, such as the Gulf of Lyons (e.g., Zuo, Eisma & Berger, 1991; Zuo et al., 1997, Buscail et al., 1997), in the Western Mediterranean (Budillon et al., 2005), the Ebro river area (Palanques & Drake, 1990) and the Adriatic Sea (Frignani et al., 1990; Frignani & Langone, 1991).

Analysis were been performed on the uppermost 40 cm of core C90-1m (Salerno Bay-southern Tyrrhenian) at Istituto Scienze Marine - Sezione di Geologia Marina (ISMAR – CNR) radiometric laboratory. ^{210}Pb by alpha spectrometry measurements following the procedure based on the measurement of its daughter nuclide ^{210}Po outlined in Frignani and Langone (1991). In addition, several levels were prepared for ^{210}Pb counting via gamma spectrometry using a gamma-x type germanium detector (Giordani et al., 1992) in order to check the assumption of constant activity of the supported ^{210}Pb. Briefly, sediment was dried at 60 °C, 3 g were leached with hot 8N HNO_3 and 30% H_2O_2 after spiking with ^{209}Po tracer. The leaching solution was evaporated to a small volume. The HNO_3 was eliminated using concentrated HCl, and the volume was made

up to 60 ml with 1.5 N HCl. Iron was reduced using ascorbic acid. ^{210}Po was plated onto a silver disc overnight at room temperature.

For additional details for methodology see Frignani et al.(1993). Sediment porosity was determined according to Berner (1971) from the water content, assuming a mineral density of 2.5 g cm^{-3}. Supported ^{210}Pb (in equilibrium with ^{226}Ra in sediments) was obtained from the constant activity in the samples of core measured by alpha spectrometry, and was subtracted from the measured total activities.

^{137}Cs was counted to support ^{210}Pb. Dry sediment samples weighing 12–24 g in aliquots of 10–20 ml were analysed for ^{137}Cs by gamma spectrometry using coaxial intrinsic germanium detectors (Giordani et al., 1992). Efficiency calibrations were periodically carried out against multipeak commercial standards.

The short-lived radionuclides ^{137}Cs and ^{210}Pb, enabled the calculation of sediment accumulation rates for approximately the last 50–150 yr.

3.5.2 Radiocarbon dates (^{14}C)

The method most routinely employed to date marine fossils and sediments spanning the last ca. 50,000 years is radiocarbon dating. It is now evident that this method cannot normally provide age estimates for Holocene events at greater than a centennial precision, while true uncertainties of the older of millennia will commonly constrain dates for pre-Holocene events (see below). The general sources of uncertainty constrain the precision and accuracy of radiocarbon dates obtained from marine samples, are:

- ✓ analytical precision (laboratory),
- ✓ factor affecting the geological integrity of dated materials (stratigraphy). The geological integrity of samples must always be evaluated independently, though contamination of samples may not always be readily apparent, and its effects difficult to define statistically.
- ✓ *"marine reservoir errors*",
- ✓ calibration procedures.

Currently two techniques are possible in order to determine the relationship between ^{14}C of a sample:

- ✓ Method of Libby, that it is the dating with a conventional method for the measure of the radioactive activity β of the champion,
- ✓ Method AMS, based on the Atomic Mass Spectroscopy (AMS) with particle accelerators of type Tandem, that it allows the direct measurement of the relationship between Carbon atoms and of its radioisotope.

Dating has been performed on planktonic and benthic foraminifera carbonate shells. Shells were cleaned in ultrasonic bath, and later, washed and dried.

Furthermore, in order to compare our data with literature, all ^{14}C-AMS ages were calibrated to calendar years (cal. BP).

In particular, in the core C08 (Sardinia Channel, Western Mediterranean), the AMS ^{14}C analysis were performed on the planktonic foraminifers *Globigerina bulloides* and *Globorotalia inflata* at the Centre for Isotopic Research on Cultural and Environmental Heritage (CIRCE) radiocarbon laboratory, Caserta, (Italy*)*. All radiocarbon dates were corrected using a reservoir age of 48 +/- 21 yr (a mean ΔR value calculated among six of the Tyrrhenian Sea) and calibrated using the marine data base and the CALIB 5.0 Program (Stuiver and Reimer, 1993), (this study).

For the cores C90-1m, C90, C836 (Salerno Bay, Tyrrhenian basin), the AMS ^{14}C radiocarbon data have been performed on mixed planktonic foraminifera (*Globigerinoides ruber* and *Globorotalia inflata*) and one on bivalve (Insinga et al., 2008) at the CIRCE laboratory in Caserta (Italy). The data were then calibrated using CalPal 2005 (Weninger et al., 2004). The reservoir correction ΔR (reservoir age) used for calibration is 400 yr (Siani et al. 2001). The calibrated age ranges are reported in years BP (and AD) and referred to 2σ. The small differences between the AMS ^{14}C radiocarbon data obtained using different reservoir correction ΔR (reservoir age) and

different programs clearly suggested that the both methods are valid for the last 25 kyr of marine Tyrrhenian records.

Diagram 3.1. Followed methodology resume.

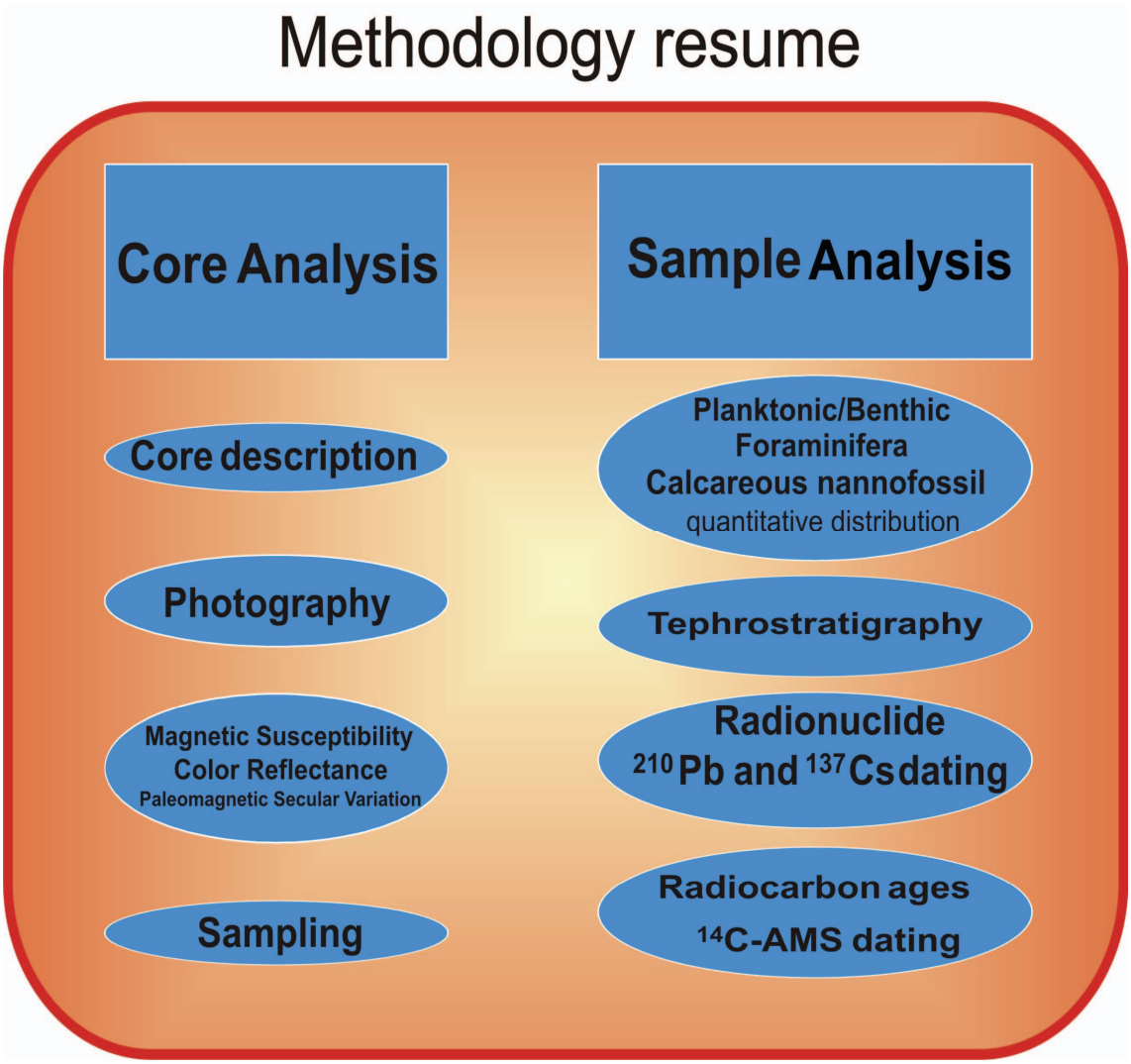

Fig. 3.1 Methodology Resume Scheme.

REFERENCES

Asioli, A., Trincardi, F., Lowe, J. J., Ariztegui, D., Langone, L., Oldfield, F., 2001. Sub-millennial scale climatic oscillations in the central Adriatic during the Lateglacial. Paleoceanographic implications. Quarter. Sci. Rev., 20, 1201-1221.

Berner, R. A., 1971. Principles of chemical sedimentology. McGraw-Hill, NewYork, pp. 240.

Budillon, F., Lirer, F., Iorio, M., Macrì, P., Sagnotti, L., Vallefuoco, M., Ferraro, L., Garziglia, S., Innangi, S., Sahabi, M., Tonielli, R, 2008. Integrated stratigraphic reconstruction for the last 80 kyr in a deep sector of the Sardinia Channel (Western Mediterranean).Deep Sea Research 2008, in press.

Buscail, R., Pocklington, R., Daumas, R., Guidi, L., 1990. Fluxes and budget of organic matter in the benthic boundary layer over the Northwestern Mediterranean margin. Continental Shelf Research, 10 (9-11), 1089-1122.

Buscail, R., Ambatsian, P., Monaco, A., Bernat, M., 1997. ^{210}Pb, manganese and carbon: indicators of focussing processes on the nortwestern Mediterranean continental margin. Marine Geology, 137, 271-286.

Capotondi, L., Borsetti, A., Morigi, C., 1999. Foraminiferal ecozones, a high resolution proxy for the late Quaternary biochronology in the central Mediterranean Sea. Marine Geology 153, 253– 274.

Cimerman, F., Langer, M., 1991. Mediterranean Foraminifera. Slovenska Akademija Znanosti in Umetnosti, Academia Scientiarum Artium Slovenica, Classis IV, Historia Naturalia 30, Ljubliana.

Ducassou, E., Capotondi, L., Murat, A., Bernasconi, S., Mulder, T., Gonthier, E., Migeon, S., Duprat, J., Giraudeau, J., Mascle, J. (2007, in press). Multiproxy Late Quaternary stratigraphy of the Nile deep-sea turbidite system- Towards a chronology of deep-sea terrigeneous systems. Sedimentary Geology, , doi:10.1016/j.sedgeo. 2007.01.023.

Frignani, M., Langone, L., 1991. Accumulation rates and ^{137}Cs distribution in sediments off the Po River delta and the Emilia- Romagna coast (northwestern Adriatic Sea, Italy). Cont. Shelf Res. 11, 525– 542.

Frignani M., Langone. L., Ravaioli M. and Cadonna A., 1990. Sediment Fluxes on 100 VR Time Scale in Different Environments of the Adriatic Sea (ltaly). Rapp.Comm.int.Mer Medit., 32, 1, 284.

Giordani, P., Hammond, D. E., Berelson, W. M., Montanari, G., Poletti, R., Milandri, A., Frignani, Langone, M. L., Ravaioli, M., Rovatti, G., Rabbi, E., 1992. Benthic fluxes and nutrient budgets for sediments in the Northern Adriatic Sea: burial and recycling efficiencies. The Science of the Total Environment, Supplement pp. 251–275.

Giunta S., Negri, A., Morigi, C., Capotondi, L., Combourieu Nebout, N., Emeis, K. C., Sangiorgi, F. and Vigliotti, L., 2003. Coccolithophorid ecostratigraphy and multi-proxy paleoceanographic reconstruction in the Southern Adriatic Sea during the last deglacial time (Core AD91-17). Palaeogeography, Palaeoclimatology, Palaeoecology, 190, 39-59.

Hagstrum, J. T., and Champion D. E., 2002. A Holocene paleosecular variation record from 14C-dated volcanic rocks in western North America, J. Geophys. Res., 107, 2025, doi:10.1029/2001JB000524.

Insinga, D., Molisso, F., Lubritto, C., Sacchi, M., Passariello, I., Morra, V., 2008. The proximal marine record of Somma–Vesuvius volcanic activity in the Naples and Salerno bays, Eastern Tyrrhenian Sea, during the last 3 kyrs. Journal of Volcanology and Geothermal 177, 170–186.

Kirschvink, J. L., 1980. The least-square line and plane and the analysis of paleomagnetic data. Geophysical Journal of the Royal Astronomical Society 62, 699-718.

Jorissen, F. J., 1999. Benthic foraminiferal microhabitats below the sediment-water interface. In: B.K. Sen Gupta, Editor, *Modern Foraminifera*, Kluwer Academic Publishers, Dordrecht, The Netherlands, pp. 161–179.

Jorissen, F. J., Asioli, A., Borsetti, A. M., de Visser, L., Hilgen,J.P., Rohling, E.J., van der Borg, K., Vergnaud-Grazzini, C., Zachariasse, W.J., 1993. Late Quaternary central Mediterranean biochronology. Marine Micropaleontology 21, 169-189.

Jorissen, F. J., 1988. Benthic foraminifera from the Adriatic Sea; principles ofphenotypic variation. Utrecht Micropaleontol. Bull., 37, 176 pp.

Jorissen, F. J., 1987. The distribution of benthic foraminifera in the Adriaitic Sea. Mar. Micropaleontol,, 12, 21-48.

Lirer, F., Sprovieri, M., Pelosi, N., Ferraro, L., 2007. Clues of solar forcing from a 2000 years long sedimentary record from the eastern tyrrhenian margin. Clima e cambiamenti climatici: le attività di ricerca del CNR pp. 209-212.

Lowe, J. J., Hoek, W. Z., INTIMATE group, 2001. Inter-regional correlation of palaeoclimatic records for the Last Glacial–Interglacial Transition: a protocol for improved precision recommended by the INTIMATE project group. Quaternary Science Reviews 20, 1175–1187.

Molero, J., Sanchez-Cabeza, J. A., Merino, J., Mitchell, P. I., Vidal-Quadras, A., 1999. Impact of ^{134}Cs and ^{137}Cs from the Chernobyl reactor accident on the Spanish Mediterranean marine environment. Journal of Environmental Radioactivity 43,357-370.

Murray, J. W., 1991. Ecology and Palaeocology of Benthic Foraminifera. Longman Scientific & Technical, New York. 312 pp.

Palanques, A. and Guillén, J., 1998. Coastal changes on the Ebro Delta: natural and human factors. Journal of Coastal Conservation 4, pp. 17–26.

Papucci, C., Charmasson, S., Delfanti, R., Gasco, C., Mitchell, P. and Sanchez-Cabeza, J. A., 1996. Time evolution and levels of man-made radioactivity in the

Mediterranean Sea. In: Guegueniat, P. et al., 1996. Radionuclides in the oceans inputs and inventories Les Editions de Physique, Les Ulis, pp. 176–197.

Pérez-Folgado, M., Sierro, F. J., Flores, J. A., Grimalt, J. O., Zahn, R., 2004. Paleoclimatic variations in foraminifer assemblages from the Alboran Sea (Western Mediterranean) during the last 150 ka in ODP Site 977. Marine Geology 212, 113–131.

Pérez-Folgado, M., Sierro, F. J., Flores, J. A., Cacho, I., Grimalt, J. O., Zahn, R., Shackleton, N. 2003. Western Mediterranean planktonic foraminifera events and millennial climatic variability during the last 70 kyr. Marine Micropaleontology, 48, 1-2, 49-70.

Principato, M. S., Giunta, S., Corselli, C., Negri, A., 2003. Late Pleistocene-Holocene planktonic assemblages in three box-cores from the Mediterranean Ridge area (west-southwest of Crete):palaeoecological and palaeoceanographic reconstruction of sapropel S1 interval. Palaeogeography, Palaeoclimatology, Palaeoecology 190, 61-77.

Sanchez-Cabeza, J. A., Masqué, P., Ani-Ragolta, I., Merino, J., Frignani, M., Alvisi, F., Palanques, A., Puig, P., 1999. Sediment accumulation rates in the southern Barcelona continental margin (NW Mediterranean Sea) derived from ^{210}Pb and ^{137}Cs chronology. Progress in Oceanography 44 313–332.

Sanchez-Cabeza, J. A., Masqué, P., Mir, J., Martínez-Alonso, M., Esteve, I., 1999b. ^{210}Pb atmospheric flux and mat growth rates of a microbial mat from the northwestern Mediterranean Sea area (Ebro river delta). Environmental Science and Technology, 33, 3711-3715.

Sanchez-Cabeza, J. A., Masqué, P., Ani-Ragolta, I., 1998. ^{210}Pb and ^{210}Po analysis in sediments and soils by microwave acid digestion, Journal of Radioanalytical and Nuclear Chemistry, 227, 19-22.

Sanchez-Cabeza, J. A., J. Molero, J. Merino, L. Pujol, and P. I. Mitchell. 1995. ^{137}Cs as a tracer of the Catalan current. Oceanologica Acta 18:221-226.

Sbaffi, L., Wezel, F. C., Curzi, G., Zoppi, U., 2004. Millennial- to centennial-scale palaeoclimatic variations during Termination I and the Holocene in the central Mediterranean Sea. Global and Planetary Change 40, 201–217.

Schroder, C. J., Scott B. D. & Medioli, F. S., 1987. Can smaller benthic Foraminifera be ignored in paleoenvironmental analysis? J. foramin. Res. 17: 101–105.

Sgarrella, F. and Moncharmont Zei, M., 1993. Benthic foraminifera of the Gulf of Naples (Italy): systematic and autoecology. Bollettino della Societa` Paleontologica Italiana 32, 145– 264.

Siani G., Paterne, M., Miche, E., Sulpizio, R., Sbrana, A., Arnold, M., Haddad, G., 2001. Mediterranean sea surface radiocarbon reservoir age changes since the Last Glacial Maximum. Science, 294, 1917-1920.

Sierro, F. J., Krijgsman, W., Hilgen, F. J., Flores, J. A., 2001. The Abad composite (SE Spain): Mediterranean reference section for the Messinian and the Astronomical Polarity Time Scale (APTS). Palaeogeography Palaeoclimatology Palaeoecology 168, 143–172.

Sprovieri, R., Di Stefano, E., Incarbona, A., Gargano, M. E., 2003. A high-resolution of the last deglaciation in the Sicily Channel based on foraminiferal and calcareous nannofossil quantitative distribution. Palaeogeography, Palaeoclimatology, Palaeoecology 202, 119-142.

St-Onge, G., Stoner, J. S. and Hillaire-Marcel, C., 2003. Holocene paleomagnetic records from the St. Lawrence Estuary, eastern Canada: Centennial to millennial-scale geomagnetic modulation of cosmogenic isotopes, Earth Planet. Sci. Lett., 209, 113–130.

Stuiver, M. and T. F. Braziunas. 1993. Sun, ocean, climate and atmospheric 14CO2: An evaluation of causal and spectral relationships. The Holocene 3, 289-305.

Turner, G. M. and Thompson, R., 1982. Detransformation of the British geomagnetic secular variation record for Holocene times, Geophys. J. R. Astron. Soc., 70, 789–792.

Van der Zwaan, G. J. and Jorissen, F. J., 1991. Biofaciat patterns in river-induced shelf anoxia. In: R.V. Tyson and T.H. Pearson (Editors), Modern and Ancient Continental Shelf Anoxia. Geol. Soc. Spec. PUN., 58, 65-82.

Walker, M. J. C., Bjørck, S., Lowe, J. ., Cwynar, L. C., Johnsen, S., Knudsen, K.-L.INTIMATE group and Wohlfarth, B., 1999. Isotopic "events" in the GRIP ice core: a stratotype for the Late Pleistocene. *Quat. Sci. Rev.* 18, pp. 1143–1150.

Weninger, B., Jöris, O. and Danzeglocke, U., 2004. Calpal—the Cologne radiocarbon CALibration and PALeoclimate research package (http://www.calpal.de).

Wolf-Welling, T. C. W., Cowan, E. A., Daniels, J., Eyles, N., Maldonado, A., Pudsey, C. J., 2001. Diffuse spectral reflectance data from rise Sites 1095, 1096, 1101 and Palmer Deep Sites 1098 and 1099 (Leg 178, Western Antarctic Peninsula). In: Barker, P.F., Camerlenghi, A., Acton, G.D., Ramsay, A.T.S. (Eds.), Proceeding Ocean Drilling Program, Scientific Results, 178, 1-22.

Zuo, Z., Eisma, D., Gieles, R. and Beks, J., 1997. Accumulation rates and sediment deposition in the northwestern Mediterranean. Deep-Sea Res II 44 3-4, pp. 597–609.

Zuo, Z. Z., Eisma, D. and Berger, G. W., 1991. Determination of sediment accumulation and mixing rates in the Gulf of Lyons, Mediterranean Sea. Oceanologica Acta 14, 253-263.

Chapter 4

ECO-BIOSTRATIGRAPHIC SCHEME FOR THE LAST 520 YR IN THE SOUTHERN TYRRHENIAN SEA

Based on

Vallefuoco, M.[(1)], Lirer, F. [(1)], Ferraro, L.[(1)], Sprovieri, M.[(1)], Bellucci, L.[(2)], Albertazzi, S.[(2)], Capotondi, L.[(2)], Giuliani, S.[(2)], Angelino, A.[(1)], Iorio, M.[(1)]

1) Istituto per l'Ambiente Marino Costiero (IAMC) – CNR, Calata Porta di Massa, Interno Porto di Napoli, 80133, Napoli, Italy

2) Istituto Scienze Marine (Sezione di Geologia Marina), ISMAR – CNR, Consiglio Nazionale delle Ricerche, Via Gobetti 101 40129 Bologna, Italy

to be submitted to The Holocene

ABSTRACT

High-resolution study of Southern Tyrrhenian marine record from continental shelf of Salerno Gulf, provides a unique opportunity to identify the main events occurring during the last 520 years within a well constrained chronological framework based on ^{210}Pb and ^{137}Cs radiometric dating method. The obtained age model shows an accurate definition of a constant sedimentation rate of 0.20 cm/yr for the last 520 yr.

Combining planktonic and benthonic foraminifera, three eco-intervals have been detected and dated. Furthermore, the boundaries of these eco-intervals resulted almost coincident suggesting a similar response to climate forcing.

Finally, a possible human impact on planktonic and benthic foraminiferal fauna, associated to the building dam on Sele River at 1934 AD, may be suggested.

Key words: Planktonic and benthic foraminifera, last 500 years, Eastern Tyrrhenian Sea

4.1 INTRODUCTION

The Mediterranean region lies in an area of great climatic interest. It marks a transitional zone between the deserts of North Africa, which are situated within the arid zone of the subtropical high, and the Central-Northern Europe, which is influenced by the westerly flow during the whole year. In addition, the Mediterranean region is exposed to effects of the South Asian Monsoon, the Siberian High Pressure System, the Southern Oscillation and the North Atlantic Oscillation (Boucher, 1975). As a consequence the Mediterranean area, associated with the semi-enclosed environment of the Mediterranean basin, which is connected with the Atlantic Ocean through the Strait of Gibraltar, is considered a natural laboratory to document the climatic events records in the North Hemisphere.

Furthermore, human activity in the Mediterranean region is documented since about 3000 years with a potential anthropic impact on watersheds through forest clearances, intense agriculture and artificial damming. Consequently, the freshwater budget of the basin and the river load of material to the sea was drastically modified, acting as a major factor regulating the climate in the basin (cf. Rohling & Bryden, 1992; Martin & Milliman, 1997).

Within this framework, an increasing number of multiproxy studies focused on the past climate variability in the Mediterranean area documented intense climate oscillations in that area during the last millemium. Major climatic changes occurring during the last millennium are the Little Ice Age (LIA) and Medieval Warm Period (MWP). These events were reliably recorded in Mediterranean archives by Mann et al. (1999) and Esper et al. (2002). Concerning the MWP, there is not universally accepted, precise definition for duration of the Medieval Warm Period (~800 – ~1300 AD), it was a time of warm climate in Europe with temperatures allegedly comparable with the present-day conditions (Maasch et al., 2005). Contrarily, the LIA appears characterized by a intense widespread cooling (on the order of 0.5 – 1.0°C) associated to evident lowering of the

equilibrium line altitude of mountain glaciers around the world of about 100 m (e.g. Broecker 2001). From A.D. 1500 to 1850, climate was characterized by an abrupt cooling phase considered the most intense since the Last Glacial Maximum.

Although the climate of the last millennium has sustained the growth and development of modern society, there is surprisingly little systematic knowledge about marine climate variability during this period and mainly of the last 500 years. This is probably associated to fact that the time resolution of studied marine records was minor respect to the climate changes. So that this work offers the unique opportunity to study expanded marine records where it is possible to combine planktonic and benthonic foraminifera within a well constrained chronological framework.

The aim of the present paper is focused on the identification of events (Event Stratigraphy), from a super-expanded shallow water marine sedimentary record of the eastern Tyrrhenian Sea, which can be used to improve the resolution chronology over the last 500 years in the central Mediterranean basin.

4.2 MATERIAL AND METHODS

4.2.1 The C90-1m core

The studied gravity core C90-1m (40°35.76'N; 14°42.48'E) has been recovered, through the coring system SW104 of ISMAR – CNR of Bologna. This system allowed to recover the water-sediment interface producing an undisturbed (without sediment deformation) and very well preserved marine record. This core is collected close to the shelf break of the Northern Salerno Bay, at a water depth of 103.4 m (Fig. 4.1). The sedimentary succession, consists on 106 cm thick of hemi-pelagic marls with a tephra layer between 55 and 66 cm b.s.f. (Fig. 4.2).

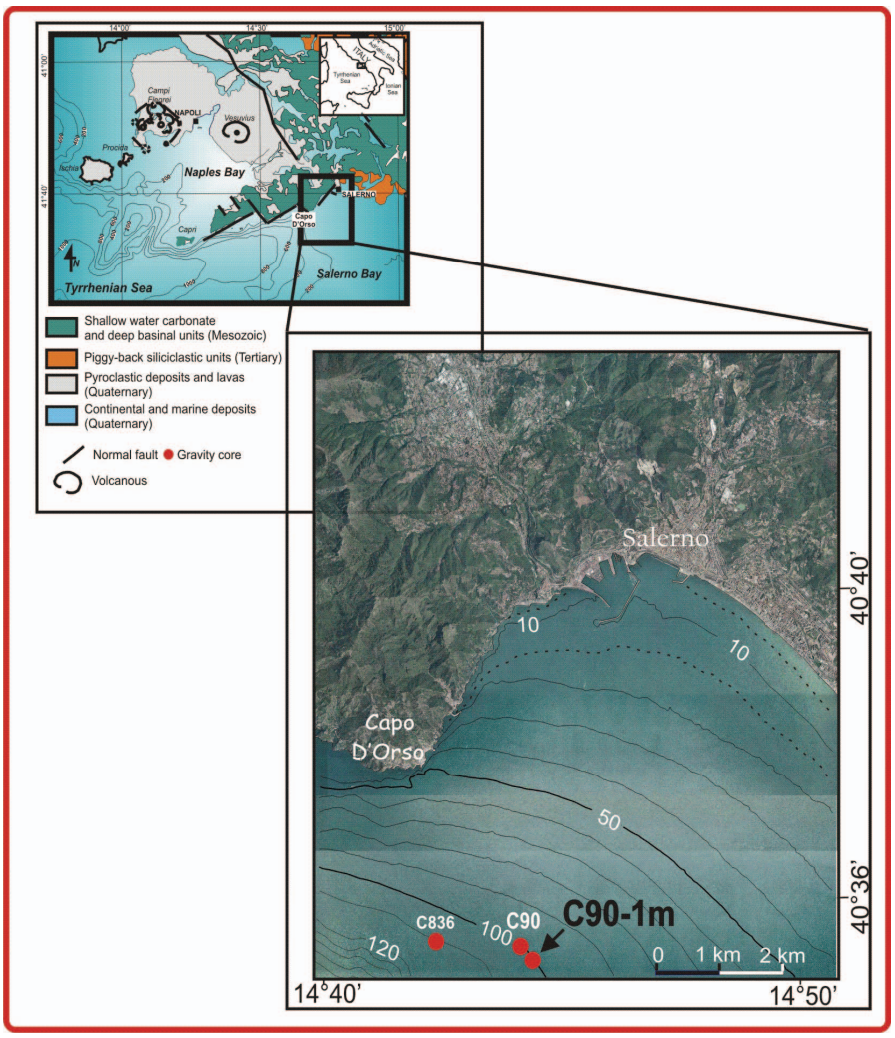

Fig. 4.1 Location map of the studied core (**C90-1m**) and of other very close cores (C836 and C90).

4.2.2 Petrophysical properties

Physical properties of the core C90-1m were measured at 1 cm step in a fully automated GEOTEK Multi-Sensor Core Logger (MSCL), in the petrophysical laboratory of IAMC-CNR in Naples (Italy). The MSCL system includes a Bartington MS2E Point sensor to measure the low-field magnetic susceptibility (MS) with a spatial resolution of

0.1 cm and a Minolta Spectrophotometer CM 2002 which records at 0.8 cm step, the percentage of reflected energy (RSC) at 31 wavelengths in 10-nm steps, over the visible spectrum (from 400 to 700 nm).

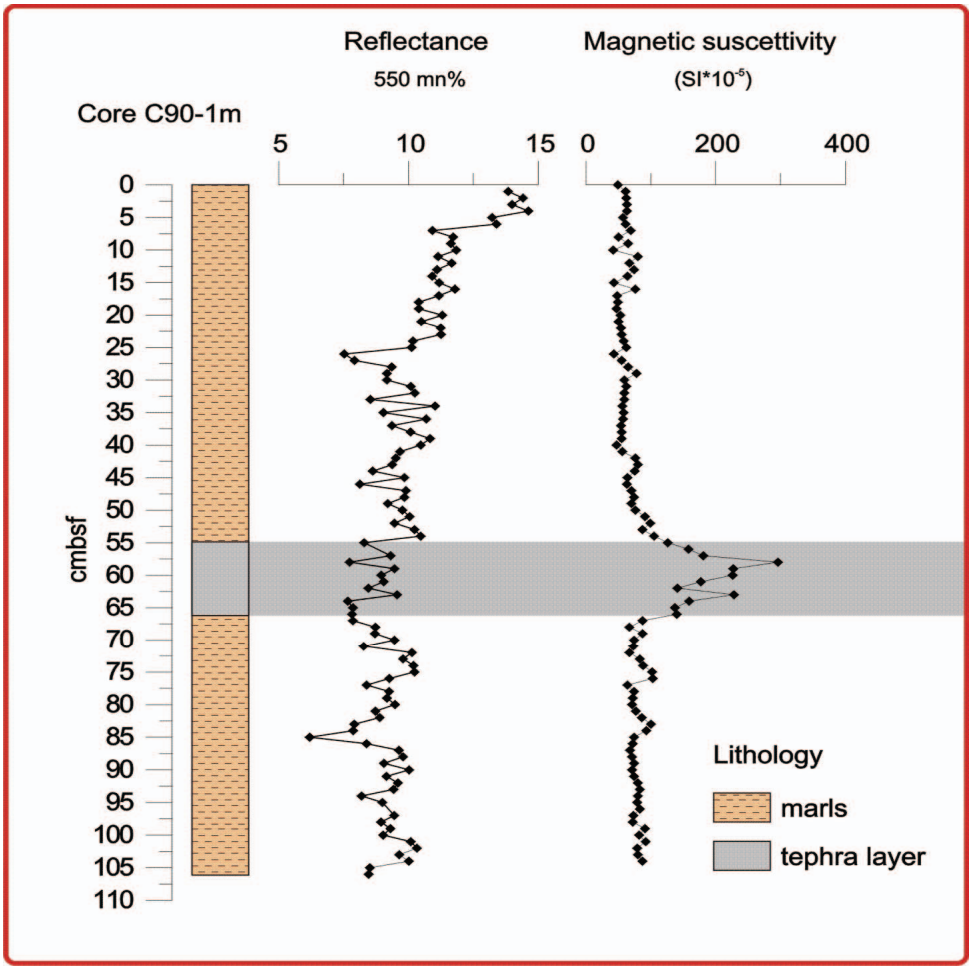

Fig. 4.2 Lithology, Reflectance and Magnetic Susceptibility of the studied core (**C90-1m**).

MS and RSC measurements were carried out ~1 hr after the core split. The split core was covered with cling film to protect the glass cover of the Minolta aperture while measuring. Core logs of the MS and RSC were visually compared in order to detect

similar trends and tentatively gather data according to their physical properties and corresponding stratigraphy (Wolf Welling et al., 2001) (Fig. 4.2).

4.2.3 Radionuclides ^{137}Cs and ^{210}Pb

The uppermost 40 cm b.s.f. of core C90-1m were dated by short-lived radionuclide ^{210}Pb alpha spectrometry measurements, at the ISMAR – CNR radiometric laboratory of Bologna, following the procedures proposed by Frignani and Langone (1991). In addition, a number of levels were prepared for ^{210}Pb counting via gamma spectrometry using a gamma-x type germanium detector (Giordani et al. 1992) in order to check the assumption of constant activity of the supported ^{210}Pb. Activity of ^{137}Cs was measured to support ^{210}Pb via gamma spectrometry using coaxial intrinsic germanium detectors (Giordani et al. 1992).

4.2.4 Tephrostratigraphy

Tephrostratigraphic analysis, for the present paper, was carried out on the layer recorded at 55-66 cm b.s.f.. The tephra layer was identified by a peak of abundance of glass fragments above the background in the whole detritic material coarser than 40 μm. Two samples (at 55 and 58 cm) were oven-dried, sieved at 1ϕ interval sieves, for defining grain-size distribution, and about 100 fragments were counted and picked under a binocular microscope for accurate lithological investigation. On the whole, the two layers resulted mainly made up of pumice and minor scoria fragments. For each sample, at least 30 juvenile fragments were embedded in epoxy resin and suitably polished for microprobe analysis. On the same embedded fragments, qualitative SEM EDS observation was used to define the mineralogical assemblage. Major-element analysis on pumice fragments, glass shards and crystals were performed on a SEM JEOL JSM 5310 (15kV, ZAF Correction Routine) with EDS at CISAG (Centro Interdipartimentale di Servizio per Analisi Geomineralogiche) at the University of Naples Federico II. Instrument calibration was based on international mineral and glass standards. Individual analysis of glass shards with total oxide sums lower than 95% were excluded.

Results of chemical analysis reported in Table 4.1 as average values of about 10 point analysis of each sample, recalculated to 100% water free. The chemical composition of the pumice fragments has been classified according to Total Alkali - Silica plot (TAS - Le Bas et al., 1986).

Sample	depth (cm)	SiO_2	TiO_2	Al_2O_3	FeO	MnO	MgO	CaO	Na_2O	K_2O
C90-1m	55-58	48,69	1,26	17,47	10,45	0,19	3,68	9,48	3,84	8,30
		0,34	*0,08*	*0,21*	*0,22*	*0,09*	*0,15*	*0,18*	*0,30*	*0,40*

Tab.4.1 Major (wt %) element composition of the tephra

4.2.5 Analysis of planktonic and benthic foraminifera

Analysis of planktonic foraminifera was performed on 104 samples. Sampling spacing was 1 cm from the top of the core (seafloor) down to the base. Each wet sample of about 20 g was dried at 50°C and washed over sieves with mesh-width size of 63 microns. Quantitative planktonic foraminiferal analysis were carried out on the fraction >90μm to avoid juvenile specimens. The adopted taxonomy is in agreement with Jorissen et al. (1993), Capotondi et al. (1999). Some planktic species or morphotypes are lumped together according to the following scheme: *Globigerinoides ruber* includes *G. ruber* (variety rosea and alba) and *G. elongatus*; *Orbulina* spp. includes both *Orbulina universa* and *O. suturalis*; *Globigerinoides quadrilobatus* includes *G. trilobus* and *G. sacculifer*; *G. bulloides* (including extremely rare specimens of *G. falconensis)*; *Globorotalia truncatulinoides* left coiling; *G. inflata* left coiling; *Globigerinita glutinata*; *Turborotalita quinqueloba*; *Globigerinatella siphoniphera* (rare) includes *G. calida* (rare). All taxa are quantified as percentages of the total number of planktic foraminifera, while the concentration is reported as number of specimens per gram of dry sediment.

Analysis of benthic foraminifera was conducted on 43 samples. Sampling spacing was 2 cm from the top of the core (seafloor) down to the base. Each wet sample of about 20 g was dried at 50° and washed over sieves with mesh-width size of 63 microns. For the benthic quantitative analysis, approximately 300 specimens were counted from the entire fraction >90μm to avoid juvenile specimens, and then their percentages of frequency were calculated. In nine samples within the tephra layer, located between 55 and 66 cm b.s.f., the total number of benthic individuals appears very low. Generally, less than 95 individuals were counted every sample and a total of 58 benthic foraminiferal species were identified. The generic attribution of benthic taxa was made following Loeblich and Tappan classification (1987); species were mainly determined on the basis of conspicuous studies on the Mediterranean benthic species (Cimerman and Langer, 1991; Sgarrella and Moncharmont-Zei, 1993).

Quantitative analysis has been performed on eight selected species showing the most relative abundace in the assemblages: *Bulimina aculeata*; *Bulimina marginata*; *Bolivina alata*; *Cassidulina carinata*; *Hyalinea baltica*; *Uvigerina mediterranea*; *Melonis padanum*; *Valvulineria bradyana*.

All taxa are quantified as percentages of the total number of benthic foraminifera, while the concentration is reported as number of specimens per gram of dry sediment.

4.3 RESULTS

4.3.1 ^{137}Cs and ^{210}Pb radiometric chronology

A high-resolution age model of the C90-1m core is based on the ^{210}Pb and ^{137}Cs radiometric dating with an accurate definition of the sediment chronology for the upper 40 cm b.s.f.. Lower part of the core was dated by extrapolation of the overlying sediments.

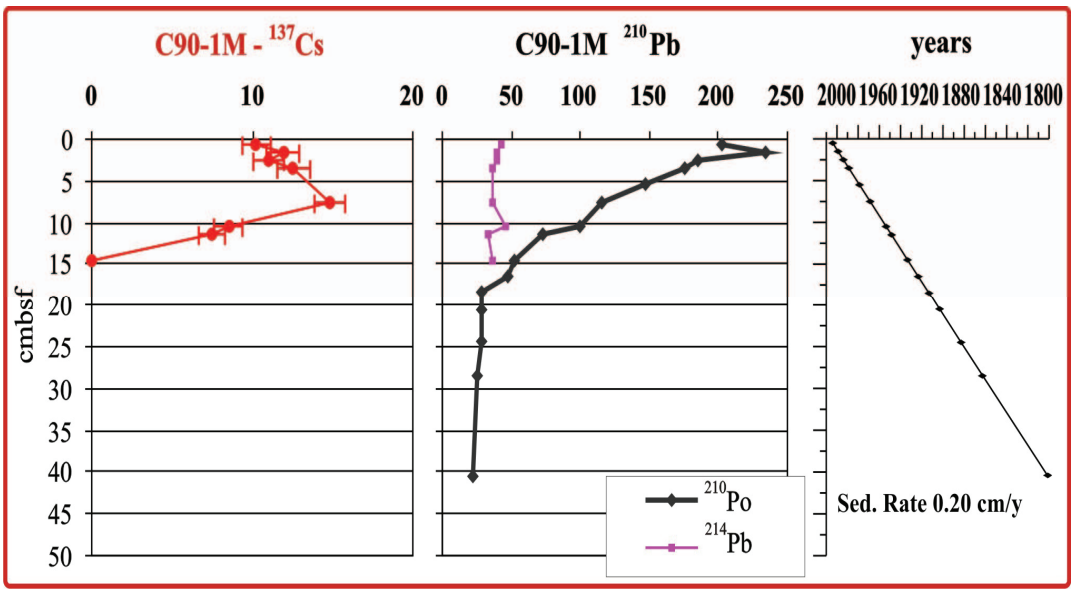

Fig. 4.3 The **^{210}Pb** and **^{137}Cs** activity–depth profiles in core **C90-1m** with the age-depth profile for the first 40 cmbsf.

The ^{210}Pb activity–depth profile in core C90-1m shows an exponential decline with depth (Fig. 4.3), suggesting a constant sediment accumulation over the last century.

The application of dating models is not straightforward because there is no simple mechanism that describes the delivery of sedimentary material and ^{210}Pb to the bottom. Furthermore, the effects of mixing might add complexity to the process of profile formation. In fact, the application of simple dating models in presence of mixing would provide overestimated sedimentation rates. Nevertheless, the excess ^{210}Pb profile shows no evidence of superficial mixed layer. Consequently, the sediment accumulation rate was calculated for the first 40 cm b.s.f. by applying a Constant Flux–Constant Sedimentation model (Robbins, 1978) to the activity–depth profile of excess ^{210}Pb. A mean sediment accumulation rate of 0.20 cm yr^{-1} was obtained with age of 1802 AD at 40.5 cm b.s.f. (Fig. 4.3).

The measured ^{137}Cs activities are low compared to those measured in the Northern Adriatic sediments (Frignani et al., 2004), but show a clear trend detectable down to 15 cm (Fig. 4.3). Assuming that the following peaks at 11.5 cm b.s.f. and at 7.5 cm b.s.f. can be associated to caesium activity onsets dated 1954 AD and to the caesium fallout dated at 1963 AD, respectively, and that 2006.5 AD represents the data of recovering core, the resulting mean sedimentation rate is 0.18 cm/yr (Fig. 4.3 and 4.4). These values are in good agreement with those obtained from ^{210}Pb activity–depth profile. The preservation of a clear curve trend of ^{137}Cs activity suggests that the sedimentation rate has been mostly constant for the last fifty years at the C90-1m core site.

Linear interpolation back to 100 cm b.s.f. (base of core C90-1m), of the obtained 0 - 40 cm b.s.f. age-depth profile (0.20 cm/yr, see Fig. 4.4), suggested a constant sedimentation rate for the last 520 years.

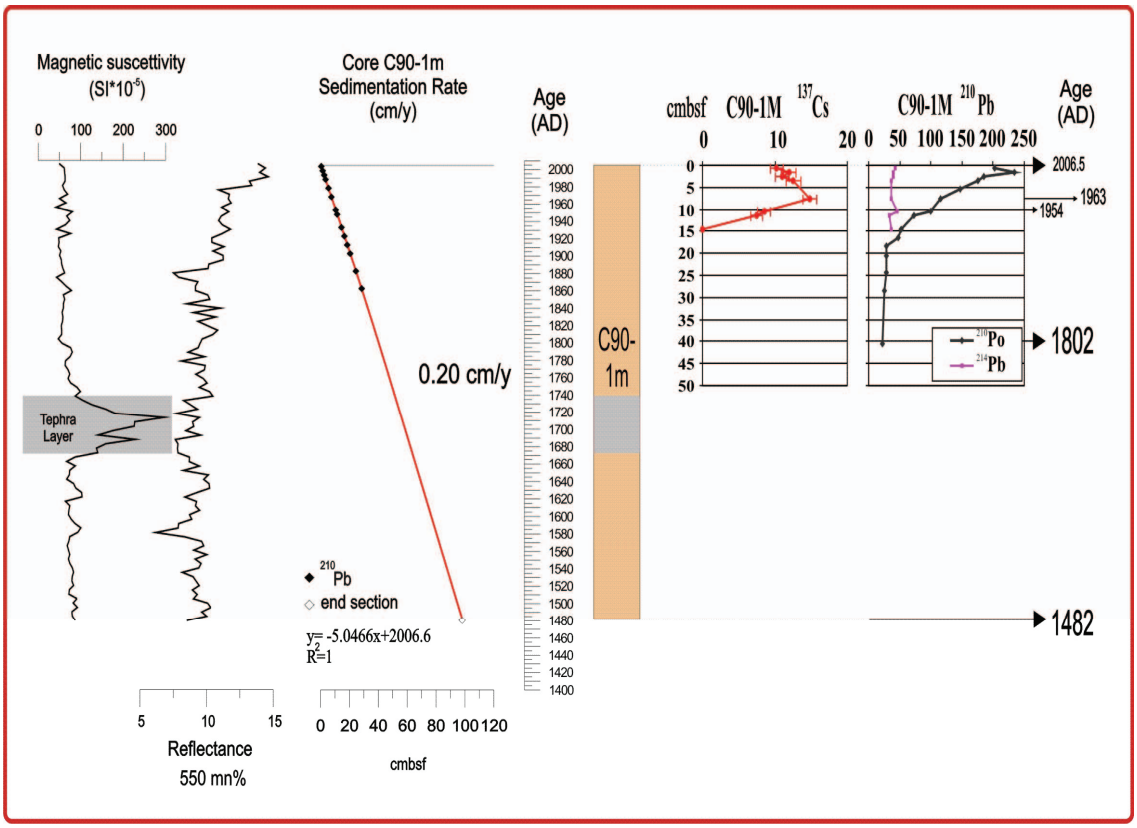

Fig. 4.4 Magnetic Susceptibility, Colour Reflectance, Age-depth profile for the core **C90-1m**, with the position of the tie points. The numbers in black colour on the right side are the radiometric tie-points.

4.3.2 Tephrostratigraphic results

The sample (55-58) of the tephra layer, recorded between 55 and 66 cm b.s.f., is mainly made up of well preserved leucite-rich scoria fragments (ϕ_{max} 0.5mm). Glass composition is phono-tephritic (Fig. 4.5). As far as mineralogical assemblage is concerned, the phono-tephrites contain leucite and green clinopyroxene. The lithological component distribution, the mineralogical assemblage and the chemical composition of juvenile fragments have been used to correlate, where possible, the pyroclastic layer to specific eruptive episodes of the two campanian volcanic sources. The obtained chemical composition is compared with those available in literature (Rolandi et al., 1998; Insinga et al. 2008; Turney et al., 2008) and with unpublished data (P.P.).

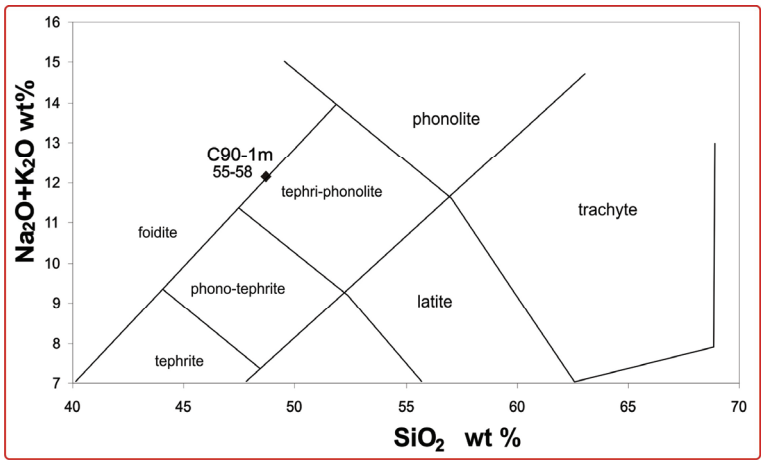

Fig. 4.5 The chemical compositions of the pumice fragments of investigated tephra layer have been classified according to Total Alkali - Silica plot (TAS - Le Bas et al., 1986).

Insinga et al. (2008) reported a radiocarbon calibrated age of 1809±97 AD at the top of the same tephra layer (V0) (this assumption is based on the petrochemical composition) recorded in the core C90 (Fig. 4.1 and 4.6), that suggests that this deposit can be attributed to the main explosive eruption at the Somma-Vesuvius recorded at 1822 AD (see Budillon et al., 2005 for details). Although a limited number of data is available about the chemical composition of glasses related to post-1631 AD vesuvian strombolian events, sample C90-1m_55-58 can be definitely correlated with the recent activity. In particular, as suggested by stratigraphic results coming from ^{210}Pb profiles acquired along the C90-1m sedimentary record, is possible to correlate the tephra with the activity younger than 1631 AD and older than 1822 AD eruptions. (Fig. 4.4).

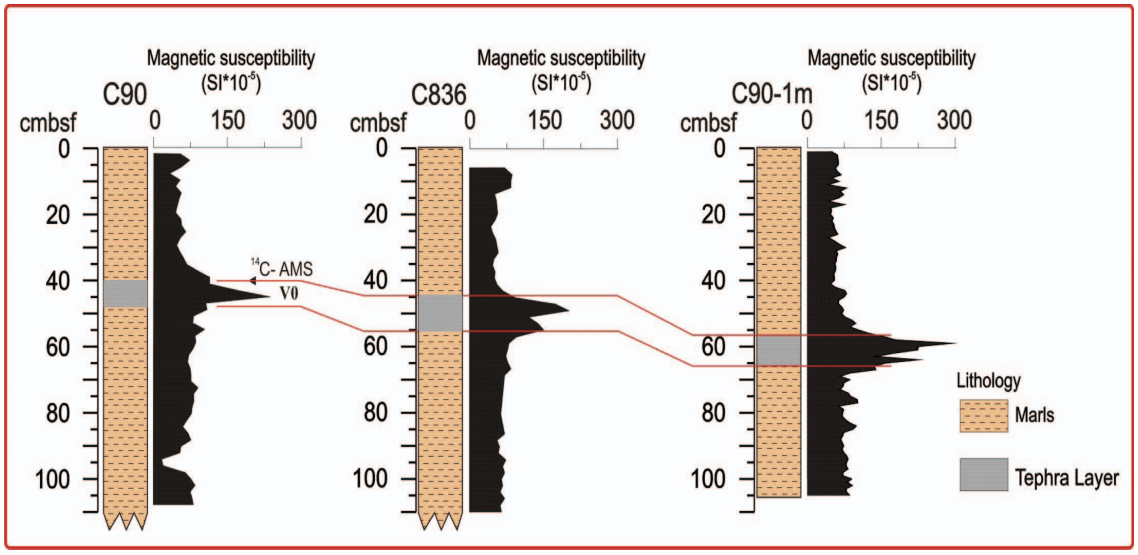

Fig. 4.6 Correlation of recognized tephra layer with very close gravity cores **C90** and **C836** (Fig. 1). The correlation is based on lithology and magnetic susceptibility data. Radiocarbon calibrated age (^{14}C-AMS on the top of the tephra **V0**) by Insinga et al., (2008). Magnetic susceptibility profile for cores **C90** and **C836** are from Iorio et al., (2004). Magnetic susceptibility profile of the core **C90-1m,** is from this work.

4.3.3 Planktonic foraminifera assemblage

The planktonic foraminifera, characterized by modern assemblages, are abundant and well-preserved and the percentages of foraminiferal fragments are very low and do not alter the composition of the planktonic assemblage.

The long-term trend in planktonic foraminifera reveal that the faunal composition of the studied interval does not show drastic changes in the abundance patterns (Fig. 4.7). In particular, among the taxa that have a continuous distribution patterns, *G. ruber* shows a progressive decrease in abundance from the base up to the top core (Fig. 4.7) where three discrete intervals have been detected as following: 1410-1680 AD, 1680-1960 AD and 1960 -2006 AD. Contrarily *T. quinqueloba* and *G. glutinata* show a progressive increase upwards with a drastic increase in abundance at 1680 AD and 1740 AD, respectively (Fig. 4.7). *G. truncatulinoides* left coiled has a long-term trend (mean average value of 3% of the total planktonic foraminiferal fauna) and only at 1670 AD (mid-point) reaches high abundance values (>15% of the total planktonic foraminiferal fauna). *G. quadrilobatus* gr. starts to be important at 1640 AD and shows a progressive increase upwards (Fig 4.7) with three distinct peaks at 1750 AD (mid-point), at 1860 AD (mid-point) and 1990 AD (Fig. 4.7). *G. bulloides* and *G. inflata* left coiled show long-term oscillation superimposed on short-term fluctuations possibly related to high-frequency climatic oscillations (Fig. 4.7). In particular, *G. bulloides* shows a strong increase in abundance from 20% up to 40% of the total planktonic foraminiferal fauna at 1930 AD (Fig. 4.7).

4.3.4 Benthic foraminifera assemblage

The distribution of benthic foraminifera assemblage in the C90-1m well reflects that commonly distributed in the modern Mediterranean areas in depth range of 40–100 m (Murray, 1991; Sgarrella and Moncharmont Zei, 1993). The abundance and vertical distribution of the eight most abundant species is reported in Fig. 4.7. In particular, *Bulimina aculeata* is present only in the upper part of the core, with a strong increase in abundance from 1920 AD upwards with a sharp peak at 1940 AD (>20% of the total

benthic foraminiferal fauna). *B. marginata* is well represented in the lower part of the record reaching abundance values >10% (Fig. 4.7), while upwards resulted constantly present (mean average value of 5%) reaching a minimum at 1940 AD with a following increase up to the top (Fig. 4.7). *Cassidulina carinata* shows a progressive decrease in abundance from the base of the core up to 1620 AD. From that point it shows relatively constant abundance up to the top of core (Fig. 4.7). *Bolivina alata*, *Hyalinea baltica* and *Valvulineria bradyana* show similar long-term trends with progressive increase in abundance from the base of the Maunder event (1660 AD) upwards to about 1920 AD where a drastic drop in abundance is recorded (Fig 4.7). *Uvigerina mediterranea* has a very discontinuous trend throughout the section with a maxima abundance values in the lower part of the core up to the base of Maunder event. In the uppermost part of the core this taxon shows a sudden increase in abundance from 1920 AD with two distinct peaks at 1940 AD and at 2005 AD (Fig. 4.7). *Melonis padanum* generally shows low abundance values, generally <10% of the total benthic foraminiferal fauna, with a steadily peak at 1670 AD during the Maunder event (Fig. 4.7).

4.4 HIGH-RESOLUTION EVENT STRATIGRAPHY FOR THE TYRRHENIAN REGION

4.4.1 Planktonic foraminiferal discussion

Evident changes in quantitative distribution patterns of different planktonic foraminifera species allowed several authors (Ducassou et al. 2007; Sprovieri et al. 2003; Principato et al. 2003; Casford et al. 2002; Asioli et al. 1999, 2001; Capotondi et al. 1999) to define a number of eco-biozones used to subdivide the Mediterranean Holocene-late Pleistocene stratigraphic record. The eco-biozone boundaries are identified by events of temporary appearance or disappearance and/or evident abundance peaks of selected species. At present, the Holocene eco-biostratigraphic schemes are generally accepted with modification associated to the mainly division between Western, Eastern Mediterranean areas and Adriatic sea, while for the last 500 years no data are available for eco-biostratigraphic subdivision of this time interval.

In this paper, based on a high-resolution age model, we tentatively proposed a subdivision of this time interval in three intervals A, B and C (Fig. 4.7).

From the base to the top the identified intervals, plotted *vs* the solar variability proxies $\Delta^{14}C$ and TSI (Stuiver et al.,1998; Bard et al., 2000), are as following:

The first eco-interval A, from base core to 1720 AD, is mainly characterised by the absence (or very low abundance) of *G. quadrilobatus* and high abundance in *G. ruber* distribution pattern associated with *G. bulloides* and *G. truncatulinoides* l.c. which show two distinct peaks during solar activity minima Sporer and Maunder events (Fig. 4.7). Consequently, this interval falls within the middle-upper part of LIA event.

Moreover, the concurrence during this interval A of *G. inflata* and *G. truncatulinoides* seems to suggest a deep high phytoplankton productivity. This condition is supported by the ecological features of these two taxa, considered as high dietary dependence on phytoplankton. In fact, *G. inflata* and *G. truncatulinoides* are considered indicative of deep mixed layer during winter (Pujol & Vergnaud-Grazzini 1995) for the Mediterranean area, but *G. truncatulinoides* always lives at greater depth than *G. inflata*. Moreover, it lives in phosphate-rich waters and is a good recorder of thermocline nutrient levels (Mulitza et al. 1999).

Upwards, the eco-interval B, from 1720 AD to 1920 AD, is dominated by *T. quinqueloba* and *G. glutinata* associated with a strong decrease in abundance of *G. ruber* and *G. bulloides* (Fig. 4.7). As consequence, according to the ecological features of these taxa (Raynolds & Thunell 1985; Schiebel & Hemleben, 2000), during this time interval a turnover between herbivore and opportunistic species and carnivore planktonic foraminifera is recorded (Fig. 4.7). This turnover occurs after the Maunder event, during which historical chronicle reports at 1708-09 AD, the occurrence of the coldest winter in Europe for the least half millennium (Luterbacher et al. 2006). Furthermore, within this interval B, *G. quadrilobatus* increased only during warm intervals (Fig. 4.7). In particular, the two strong peaks, centred at about 1860 AD and 1760 AD, well correspond to the warm intervals between the Damon and Dalton and between the Maunder and Dalton events, respectively (Fig. 4.7). This trend suggests a

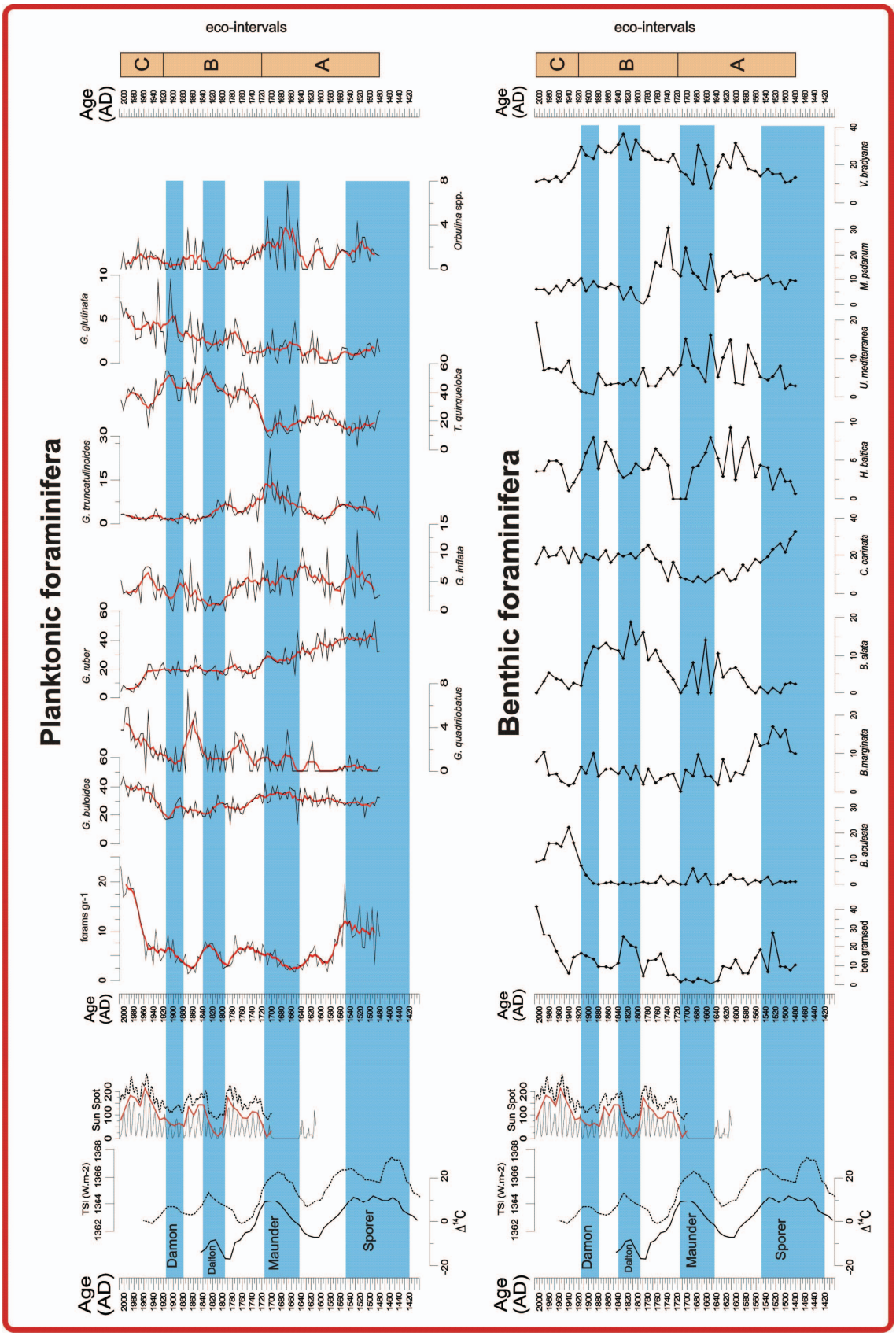
eco-intervals
C
B
A
Age (AD)
Planktonic foraminifera
forams gr-1
G. bulloides
G. ruber
G. quadriloboatus
G. truncatulinoides
G. inflata
G. glutinata
T. quinqueloba
Orbulina spp.
Sun Spot
TSI (W.m-2)
Δ14C
Damon
Dalton
Maunder
Sporer
Benthic foraminifera
ben gramsed
B. aculeata
B.marginata
B. alata
C. carinate
H. balfica
U. mediterranea
M. padanum
V. bradyana

Fig. 4.7 Distribution of selected species of planktonic and benthic foraminifera of the studied core **C90-1m,** with the position of the recognised eco-intervals. Correlation between the planktonic and benthic foraminifera species (as number of specimens per gram of dry sediment) with tree-ring $\Delta^{14}C$ (Stuiver et al., 1998), Total Solar Irradiance (TSI) (Bard et al., 2000) and sun spot data (Usoskin et al., 2002). The blue band correspond to the time of the solar activity minima, for the last 550 years. In particular, the ***Sporer Minimum*** (AD 1420–1540), the ***Maunder Minimum*** (AD 1645–1715), ***Dalton Minimum*** (AD 1790-1830), ***Damon Minimum*** (AD 1880-1900) that occur in the ***Little Ice Age*** (LIA, AD 1450–1900) (Stuiver and Kra, 1986; Stuvier et al., 1997, 1998; Bard et al., 2000; Desprat et al., 2003; Luterbacher et al., 2006; Usoskin et al., 2003, 2007).

strong relationship between oligotrophic conditions and warm periods as reported by Piva et al. (2008) in the Adriatic Sea and by Poor et al. (2004) in the Caribbean area.

Finally, the eco-interval C, from 1920 AD to 2006 AD, is characterised by the progressive decrease in abundance of *G. ruber* and by a further increased of *T. quinqueloba*, *G. bulloides* and of *G. quadrilobatus* (Fig. 4.7). The planktonic foraminiferal assemblage of interval C suggested a very high surface water phytoplankton productivity. This condition could be associated to the building dam of Sele river (the Sele river represents one of the main river which flow in the Salerno Gulf) at 1934 AD, which produced the end of the bottom solid transport and only the fine fraction arrive in the sea water system with an concentration of the nutrient.

4.4.2 Benthic foraminiferal discussion

The distribution pattern of the benthic foraminifera assemblage shows an evident three-partition (eco-intervals) of the sedimentary record.

Eco-interval A, at the base of section (1480 AD), is characterised by common occurrence of *H. balthica*, *U. mediterranea* and *V. bradyana* associated to low percentages of *B. marginata* and *C. carinata* and to relativly increase of *B. alata* in the uppermost part of the interval (Fig. 4.7). The ecological features of these species suggest more oligotrophic conditions at the base of the interval A, well confirmed by

the higher abundance values of *B. marginata* which is a shallow-intermediate infaunal species, opportunistic, but less resistant for low oxygen conditions. At the top of the interval A, the increase of *B. alata*, species with shallow infaunal microhabitat and adapted to live in environment with oxygen depletion in bottom and poor water and with meso-eutrophic conditions (Murray, 1991; Schmiedl et al., 2003; and references therein), and the constant presence of the above mentioned taxa, suggest an progressive increase of organic matter to the seafloor. At that time (upper part of interval A) *M. padanum* shows the two strong peaks in abundance at 1665 AD and 1680 AD during Maunder event (Fig. 4.7).

The second eco-interval B, spans from1720 AD to 1920 AD, is characterized by the dominance of *B. alata* and *V. bradyana*, associated to reoccurrence of *H. baltica*, after its minima during the Maunder event (Fig. 4.7). By contrast *U. mediterranea* shows an antithetic distribution pattern respect to *B. alata* and *V. bradyana* . *M. padanum* shows the third strong peak at 1740 AD in the uppermost part of Maunder event (lowermost part of interval B) (Fig. 4.7).

The strong dominance *H. baltica* and *V. bradyana* in interval B, suggests moderate oxygenated environments and medium/high trophic levels (Jorissen, 1987; Bergamin et al., 1999; Schmiedl et al, 2003 and references therein).

According to several studies (Jorissen et al., 1992; Hohenegger et al., 1993) based on ecological observation on living benthic foraminiferal associations, *M. padanum* appears to have an intermediate deep infaunal microhabitat, and usually indicate a high, continuous flux of organic matter to seafloor. The slight changes in the composition of the faunal abundances, suggest a shift to more eutrophic condition to the seafloor respect to interval A.

Finally, the eco-interval C characterizes the uppermost part of the core, from 1920 AD to the top and is dominated by *B. aculeata* and by the reoccurrence of *U. mediterranea*, which increases after its minima at the end of interval B (during Damon event) (Fig.

4.7). Contrarily, the strong decrease in abundance of *B. alata* and *V. bradyana* is recorded (Fig. 4.7).

These benthic turnover, suggests a more oligothrophic condition at seafloor, confirming by the ecological features of *U. mediterranea* and *B. aculeta*. In particular, *B. aculeata* is a dominant constituent of benthic faunas in high-productivity areas where organic matter fluxes are enhanced, often combined with suboxic or disoxy conditions in the pore and bottom water (Corliss, 1985; Mackensen and Douglas, 1989; Jorissen et al., 1992; Sen Gupta and Machin-Castillo, 1993; Rathburn and Corliss, 1994). The strong increase in abundance at 1930 AD, from about 0% up to 25% of the total benthic foraminiferal fauna, suggests a very high content of organic matter to the sea floor. This event can be probably associated to the building dam of the Sele river at 1934 AD, which caused the ended of the bottom transport to the sea floor with a dominance of the fine fraction with a higher concentration of nutrients. Simultaneously, the stratification of the water column caused a severe decrease in the ventilation of the subsurface waters. In such conditions *B. aculeata* appears proliferate and seems to be highly adaptable to changes in oxygenation and food availability and quality (Linke and Lutze, 1993).

4.5. CONCLUSION

A detailed age model for the studied shallow water marine sediments of the continental shelf of Salerno Gulf (Tyrrhenian Sea), based on the ^{210}Pb and ^{137}Cs radiometric dating, shows an accurate definition of a constant sedimentation rate of 0.20cm/yr for the last 520 yr. Moreover, high-resolution analysis of planktonic and benthic fauna seem to reflect the main climate change recorded in the last 520 years.

Tentatively three eco-intervals have been detected and dated for planktonic and benthic foraminifera. The boundaries of these intervals resulted almost coincident suggesting a similar response to climate forcing.

In term of benthic foraminiferal ecosystem the studied record is relatively enriched in infaunal species that tend to dominate under more eutrophic conditions. On the other hand the planktonic foraminifera seem to suggest a drastic turnover between carnivore and herbivore-opportunistic foraminifera consequently to the Maunder event and a possible and progressive swallowing of the phytoplankton productivity as indicated by the increase of *G. bulloides* in the last century. The change between carnivore and herbivore may be associated to a possible change in the water column food availability successively to the Maunder event. Finally, the strong increase in abundance of *G. quadrilobatus* during the warm intervals reflect the present day Mediterranean oligotrophic conditions.

Finally, a clear human impact on the marine environmental ecosystem associated to the building dam on Sele River (Salerno Gulf) at 1934 AD, which possibly changed the amount of grain-size river transport and the nutrient budge in the sea water. This hypothesis seems to be support to the strong and progressive increased in abundance in *G. bulloides* distribution pattern, to the sudden increase in benthic foraminifer *B. aculeata* and further to the prominent increase in of benthic and planktonic foraminifera (as number of specimens per gram of dry sediment) after 1934 AD.

ACKNOWLEDGMENTS

This paper is financially supported by VULCOST project (Team leader Prof. Bruno D'Argenio). This project represents the Line2 of this Italian project VECTOR.

REFERENCES

Appleby, P. G., 2001. Chronostratigraphic techniques in recent sediments. In Last W.M. & Smol J.P. (eds.), 2001. Tracking environmental change using lake sediments. Vol.1: Basin analysis, coring and chronological techniques. Kluwer Academic Published, Dordrecht.

Bard, E., Raisbeck, G., Yiou, F., Jouzel, J., 2000. Solar irradiance during the last 1200 years based on cosmogenic nuclides. Tellus 52B, 985–992.

Berkeley , A., Perry , C. T., Smithers , S. G., Horton , B. P., Taylor, K. G., 2007. A review of the ecological and taphonomic controls on foraminiferal assemblage development in intertidal environments. Earth-Science Reviews 83, 205–230.

Boucher, K. 1975. Global climate - The English Univ. Press Ltd. (London): 326pp.

Broecker, W. S., 2001. Was the Medieval Warm Period global?. Science 291, 1497-1499.

Budillon, F., Esposito, E., Iorio, M., Pelosi, N., Porfido, S., Violante, C., 2005. The geological record of storm events over the last 1000 years in the Salerno Bay (Southern Tyrrhenian Sea): new proxy evidences, European Geoscience Union, Adv. Geosci., 2, 1–8.

Budillon, F., Violante, C., Conforti, A., Esposito, E., Insinga, D., Iorio, M., Porfido, S., 2005. Event beds in the recent prodelta stratigraphic record of the small flood-prone Bonea stream (Amalfi Coast, Southern Italy). Marine Geology 222–223, 419–441.

Capotondi, L., Borsetti, A. M., Morigi, C., 1999. Foraminiferal ecozones, a high resolution proxy for the late Quaternary biochronology in the central Mediterranean Sea. Marine Geology 153, 253-274.

Caron, D. A., Bé, A.W. H., 1984. Predicted and observed feeding rates of the spinose planktonic foraminifer Globigerinoides sacculifer. B. Mar. Sci., 35, 1–10.

Cimerman, F., Langer, M., 1991. Mediterranean Foraminifera. Slovenska Akademija Znanosti in Umetnosti, Academia Scientiarum Artium Slovenica, Classis IV, Historia Naturalia 30, Ljubliana.

Corliss, B. H., 1985. Microhabitats of benthic foraminifera within Mediterranean Sea during times of sapropel S5 and S6 deposition. Palaeogeography, Palaeoclimatology, Palaeoecology 190, 139– 164.

Esper, J., Cook, E. R. and Schweingruber, F. H., 2002. Low-frequency signals in long tree-ring chronologies for reconstructing past temperature variability. Science, 295, 2250.

Fairbanks, R. G., Sverdlove, M., Free, R., Wiebe, P. H., Bé, A. W. H., 1982. Vertical distribution of living planktonic foraminifera from the Panama Basin. Nature 298, 841-844.

Fairbanks, R. G. and Wiebe, P. H., 1980. Foraminifera and chlorophyll maximum: vertical distribution, seasonal succession, and paleoceanographic significance. Science 209,1524–1526.

Frignani, M., Langone, L., 1991. Accumulation rates and ^{137}Cs distribution in sediments off the Po River delta and the Emilia- Romagna coast (northwestern Adriatic Sea, Italy). Cont. Shelf Res. 11, 525– 542.

Frignani, M., Langone, L., Ravaioli, M., Sorgente, D., Alvisi, F., Albertazzi, S., 2005. Fine-sediment mass balance in the western Adriatic continental shelf over a century time scale. Marine Geology 222–223, 113–133.

Frignani, M., Sorgente, D., Langone, L., Albertazzi, S., Ravaioli, M., 2004. Behavior of Chernobyl radiocesium in sediments of the Adriatic Sea offshore the Po River

delta and the Emilia-Romagna coast. Journal of Environmental Radioactivity 71, 299– 312.

Giordani, P., Hammond, D. E., Berelson, W. M., Montanari, G., Poletti, R., Milandri, A., Frignani, M., Langone, L., Ravaioli, M., Rovatti, G., Rabbi, E., 1992. Benthic fluxes and nutrient budgets for sediments in the Northern Adriatic Sea: burial and recycling efficiencies. The Science of the Total Environment, Supplement pp. 251–275.

Hayes, A., 1999. Late Quaternary palaeoclimatic and palaeoecological changes in the Mediterranean Sea. University of Southampton, Faculty of Science, Department of Oceanography, PhD Thesis pp.139.

Hemleben, C., Spindler, M., Anderson, O. R., 1989. Modern Planktonic Foraminifera. Springer pp 363.

Hohenegger, J., Piller, W. E., Baal, C., 1993. Horizontal and vertical spatial microdistribution of foraminifera in the shallow subtidal gulf of Trieste, Northern Adriatic Sea. J. For. Res. 23, 79-101.

Insinga, D., Molisso, F., Lubritto, C., Sacchi, M., Passariello, I., Morra, V., 2008. The proximal marine record of Somma–Vesuvius volcanic activity in the Naples and Salerno bays, Eastern Tyrrhenian Sea, during the last 3 kyrs. Journal of Volcanology and Geothermal 177, 170–186.

Iorio, M., Sagnotti, L., Angelino, A., Budillon, F., D'Argenio, B., Turell Dinares, J., Macrı`, P., Marsella, E., 2004. High-resolution petrophysical and paleomagnetic study of late-Holocene shelf sediments, Salerno Gulf, Tyrrhenian Sea. Holocene 14, 433-442.

Jorissen, F. J., 1999b. Benthic foraminiferal microhabitats below the sediment–water interface. In: Sen Gupta, B.K. (Ed.), Modern Foraminifera.KluwerAcademic publishers,Dordrecht, pp. 161–179.

Jorissen, F. J., de Stigter, H. C., Vidmark, J. V., 1995. A conceptual model explaining benthic foraminiferal microhabitats. Marine Micropaleontology 26, 3 –15.

Jorissen, F. J., Asioli, A., Borsetti, A. M., de Visser, L., Hilgen,J. P., Rohling, E. J., van der Borg, K., Vergnaud-Grazzini, C., Zachariasse, W. J., 1993. Late Quaternary central Mediterranean biochronology. Marine Micropaleontology 21, 169-189.

Jorissen, F. J., Barmawidjaja, D.M., Puskaric, S., van der Zwaan, G.J., 1992. Vertical distribution of benthic foraminifera in the northern Adriatic Sea: the relation with the organic flux. Marine Micropaleontology 19, 131– 146.

Jorissen, F. J., 1988. Benthic foraminifera from the Adriatic Sea: principles of phenotypic variations. Utrecht Micropaleontological Bulletins 34, 177 pp.

Jorissen, F. J., 1987. The distribution of benthic foraminifera in the Adriatic Sea. Marine Micropaleontology 12, 21– 48.

Linke. P. and Lutze, G. F.. 1993. Microhabitat preferences of benthic foraminifera - a static concept or a dynamic adaptation to optimize food acquisition?. Mar. Micropaleontol. 20, 215-234.

Lirer, F., Sprovieri, M., Pelosi, N., Ferraro, L., 2007. Clues of solar forcing from a 2000 years long sedimentary record from the eastern tyrrhenian margin. Clima e cambiamenti climatici: le attività di ricerca del CNR pp. 209-212

Loubere, P., 1997. Benthic foraminiferal assemblages formation, organic carbon flux and oxygen concentration on the outer continental shelf and slope. Journal of Foraminiferal Research, 27, 93-100.

Luterbacher, J., Xoplaki, E., Casty, C., Wanner, H., Pauling, A., Kùttel, M., Rutishauser, T., Brònnimann, S., Fischer, E., Fleitmann, D., Gonzàlez-Rouco, F. J., Garcìa-Herrera, R., Barriendos, M., Rodrigo, F., Gonzalez-Hidalgo, J. C., Saz, M. A., Gimeno, L., Ribera, P., Brunet, M., Paeth, H., Rimbu, N., Felis, T., Jacobeit, J., Dù nkeloh, A., Zorita, E., Guiot, J., Tùrkes, M., Alcoforado, M. J., Trigo, R., Wheeler, D., Tett, S., Mann, M. E., Touchan, R., Shindell, D. T., Silenzi, S., Montagna, P., D.,Camuffo, Mariotti, A., Nanni, T., Brunetti, M., Maugeri, M., Zerefos, C., De Zolt, S., Lionello, P., Nunes, M. F.,Rath, V.,

Beltrami, H., Garnier, E. and Le Roy Ladurie, E., 2006. Mediterranean Climate Variability. Chapter1: Mediterranean Climate Variability Over the Last Centuries: A Review Elsevier Oxford pp. 27–143.

Luterbacher, J., Dietrich, D., Xoplaki, E., Grosjean, M., Wanner, H., 2004. European Seasonal and Annual Temperature Variability, Trends, and Extremes Since 1500. Science vol 303, 14991503.

Mackensen. A. and Douglas. R.G., 1989. Down-core distribution of live and dead deep-water benthic foraminifera in box cores from the Weddell Sea and the California Borderland. Deep-Sea Res. 36, 879-900.

Mann, M., Bradley, R., Hughes, M., 1999. Northern Hemisphere temperatures during the past millennium: inferences, uncertainties, and limitations, Geophys. Res. Lett. 26, 759–762.

Martin, J. M., Milliman, J. D., 1997. EROS 2000 (European River Ocean System). The western Mediterranean: an introduction. Deep-Sea Research II 44, 521–529.

Maasch, K. A., Mayewski, P. A., Rohling, E. J., Stager, J. C., Karlen, W., Meeker, L. D. and Meyerson, E. A.,2005. A 2000 year context for modern climate change. Geografiska Annaler, 87A, 7-15.

Milliman, J. D., Syvitski, J. P. M., 1992. Geomorphic/tectonic control of sediment discharge to the ocean: the importance of small mountainous rivers. Journal of Geology 100, 525–544.

Murray, J. W., 1991. Ecology and Palaeocology of Benthic Foraminifera. Longman Scientific & Technical, New York. 312 pp.

Piva, A., Asioli, A., Trincardi, F., Schneider, R. R., Vigliotti, L., 2008. Late-Holocene climate variability in the Adriatic Sea (Central Mediterranean). The Holocene 18 153 DOI: 10.1177/0959683607085606.

Pujol, C. and Vergnaud-Grazzini, C., 1989. Paleoceanography of the last deglaciation in the Alboran Sea (Western Mediterranean). Stable isotopes and planktonic foraminiferal records. Marine Micropaleontology, 15, 253-267.

Pujol, C. and Vergnaud Grazzini, C., 1995. Distribution patterns of live planktic foraminifera as related to regional hydrography and productive systems of the Mediterranean sea. Marine Micropaleontology 25, 187–217.

Rathburn, A. E. and Corliss, B. H., 1994. The ecology of living (stained) deep-sea benthic foraminifera from the Sulu Sea. Paleoceanography, 9, 87-150.

Reynolds, L. and Thunell, R. C., 1989. Seasonal succession of planktonic foraminifera: results from a four year time series sediment trap experiment in the northeast Pacific. J. Foraminiferal Res. 19, 253-267.

Robbins, J. A., 1978. Geochemical and geophysical application of radioactive lead. In: Nriagu, J.O. (Ed.), The Biogeochemistry of Lead in the Environment. Elsevier, Amsterdam, pp. 285– 393.

Rohling, E. J. and Bryden, H. L., 1992. Man-induced salinity and temperature increases in western Mediterranean Deep Water. Journal of Geophysical Research 97, 11191-11198.

Rolandi, G., Petrosino, P., Mc Geehin, J., 1998. The Interplinian activity at Somma–Vesuvius in the last 3500 years. Journal Volcanology Geotherm. Res. 82, 19–52.

Sagnotti, L., Budillon, F., Dinares-Turell, J., Iorio, M., Macrì, P., 2005. Evidence for a variable paleomagnetic lock-in depth in the Holocene sequence from the Salerno Gulf (Italy): implications for "high-resolution" paleomagnetic dating. Geochem., Geophys., Geosyst. 6 (Q11013). doi:10.1029/2005GC001043.

Schiebel, R., Hiller, B., Hemleben, C., 1995. Impacts of storms on recent planktic foraminiferal test production and CaCO3 flux in the north Atlantic at 47°N, 20°W (JGOFS). Marine Micropaleontology 26, 115–129.

Schmiedl, G., Mitschele, A., Bec, S., Emeis, K. C., Hemleben, C., Schulz, H., Sperling, M., Weldeab, S., 2003. Benthic foraminiferal record of ecosystem variability in the eastern Mediterranean Sea during times of sapropel S5 and S6deposition. Palaeogeog. Palaeoclimatol. Palaeoecol. 190, 139– 164.

Sen Gupta, B. K. and Machain-Castillo, M.L., 1993. Benthic foraminifera in oxygen poor habitats. Marine Micropaleontology 20, 183– 201.

Sgarrella, F. and Moncharmont Zei, M., 1993. Benthic foraminifera of the Gulf of Naples (Italy): systematic and autoecology. Bollettino della Societa` Paleontologica Italiana 32, 145– 264.

Stuiver, M., Reimer, P. J., Bard, E., Beck, J. W., Burr, G. S., Hughen, K. A., Kromer, B., McCormac, F. G., van der Plicht, J. and Spurk. M., 1998. INTCAL98 Radiocarbon age calibration 24,000 - 0 cal BP. Radiocarbon, 40,1041-1083.

Stuiver M. and Kra, R.S., 1986. Calibration issue, Proceedings of the 12th International 14C conference. Radiocarbon 28, 805-1030.

Turney, C. S. M., Blockley, S. P. E., Lowe, J. J., Wulf, S., Branch, N. P., Mastrolorenzo, G., Swindle, G., Nathan, R., Pollard, A. M., 2008. Geochemical characterization of Quaternary tephras from the Campanian Province, Italy . Quaternary International 178, 288–305.

Usoskin, I. G., Solanki, S. K., Korte, M., 2006. Solar activity reconstructed over the last 7000 years: The influence of geomagnetic field changes. Geophysical Research Letters vol. 33 L08103.

Usoskin, I. G., Solanki, S. K., Schùssler, M., Mursula, K., Alanko, K., 2003. A millennium scale sunspot number reconstruction: Evidence for an unusually active Sun since the 1940's. Phys. Rev. Lett., 91, 211101.

Wolf-Welling, T. C. W., Cowan, E. A., Daniels, J., Eyles, N., Maldonado, A., Pudsey, C. J., 2001. Diffuse spectral reflectance data from rise Sites 1095, 1096, 1101 and Palmer Deep Sites 1098 and 1099 (Leg 178, Western Antarctic Peninsula). In: Barker, P.F., Camerlenghi, A., Acton, G.D., Ramsay, A.T.S. (Eds.), Proceeding Ocean Drilling Program, Scientific Results, 178, 1-22.

Chapter 5

HIGH RESOLUTION STRATIGRAPHY IN THE EASTERN TYRRHENIAN SEA DURING THE LAST 10 KYR

Based on

Lirer, F.[(1)], Sprovieri, M.[(1)], Ferraro, L.[(1)], **Vallefuoco**, **M.**[(1)], Cascella, A.[(2)], Petrosino, P.[(3)], Tamburrino, S.[(1)], Lubritto, C.[(4)], Pelosi, N.[(1)]

1) Istituto per l'Ambiente Marino Costiero (IAMC) – CNR, Calata Porta di Massa, Interno Porto di Napoli, 80133, Napoli, Italy
2) Istituto Nazionale di Geofisica e Vulcanologia (INGV), Via della Faggiola 32, 52126 Pisa, Italy
3) Dipartimento di Scienze della Terra – Università degli Studi "Federico II" di Napoli. Largo S. Marcellino 10, 80138, Napoli, Italy
4) Dipartimento di Scienze Ambientali, Seconda Università di Napoli, Via Vivaldi 47 – Caserta, Italy

to be submitted to Quaternary Science Review

ABSTRACT

We present a detailed chronology for the last 10 kyr performed on composite core collected in the Tyrrhenian sea based on the integration of AMS ^{14}C measurements, ^{210}Pb and ^{137}Cs radionuclides,tephrostratigraphy and calcareous plankton assemblages. The compositional changes on micropaleontological content (planktonic foraminifera and calcareous nannoplancton) allowed the identification of 4 main biozones.

In terms of climatic variability was possible to recognize the sapropel S1 equivalent event, the Medieval Warm Period and the Little Ice Age

The MWP-LIA transition, here dated at 1480 AD, was marked by a progressive turnover between carnivore species and herbivore-opportunistic ones suggesting a variation in the nutrient content. The Little Ice Age event, spanning from 1500 AD to 1905 AD, was marked by a planktonic foraminiferal assemblages mainly controlled by a strong increase in abundance of Turborotalita quinqueloba. T. quinqueloba reached highest abundance prominent solar activity minima. Finally, data suggest a clear human impact on the marine environmental ecosystem associated to the building dam on Sele River (Salerno Gulf) at 1934 AD.

Key words: planktonic foraminifera and calcareous nannofossils, tephrostratigraphy, Holocene, climatic changes, Tyrrhenian Sea.

5.1 INTRODUCTION

Climate variability reflects complex interactions between external forcing, hydrosphere-atmosphere-biosphere-cryosphere dynamics. Astronomical cycles modulate the long-term patterns of solar energy impinging on the Earth, thus providing a clock for the onset of major glacial episodes although changes in solar irradiance operate also to century-decadal timescales thus interfering with a wide range of internal climatic processes, that arise from feedbacks and system responses to external forcing (e.g., Trenberth, 1992 and references therein).

In the last decade a large number of climate sensitive proxy records have become available to investigate paleoclimatic variability at human time scale.

In particular, the Mediterranean Sea due its land-locked configuration represents a key area to explore paleoclimate evolution of the Northern Hemisphere. This basin marks a transitional zone between the deserts of North Africa, which are situated within the arid zone of the subtropical high, and central and northern Europe, which is influenced by the westerly flow during the whole year. In addition, the Mediterranean climate is exposed to the South Asian Monsoon, the Siberian High Pressure System, the Southern Oscillation and the North Atlantic Oscillation.

Several high-resolution biostratigraphic works have aimed at monitoring the climatic variation concerning the Holocene of the Mediterranean. The investigations are based on compositional changes in the planktonic foraminifera and/or calcareous nannoplancton assemblages (e.g. Rohling et al., 2002; Cacho et al., 1999, 2000, 2001; Sprovieri et al. 2003; Incarbona et al. 2008). These authors proposed for the Mediterranean region a sequence of "ecozones" based on evidence of abundance fluctuations of planktonic foraminifera as an appropriate tool to subdivide the stratigraphic record in shorter time intervals (Asioli, 1996; Capotondi et al., 1999; Sbaffi et al., 2001; Asioli et al., 2001; Sprovieri et al., 2003; Perez-Folgado et al., 2003;

Piva et al., 2008; Di Donato et al., 2008). The boundaries of the "ecozones" coincide with abrupt relative abundance changes of a number of selected species.

The goal of the present paper is to define a biostratigraphy at millennial scale during the last 10 kyr in the Tyrrhenian basin margin characterised by a very high sedimentation rates (Trincardi and Field, 1991; Budillon et al., 1994; 2005; Iorio et al., 2004; Sacchi et al., 2004). In addition we aim to reconstruct the climatic history in this region based on quantitative distribution of foraminifera and nannoplanton taxa.

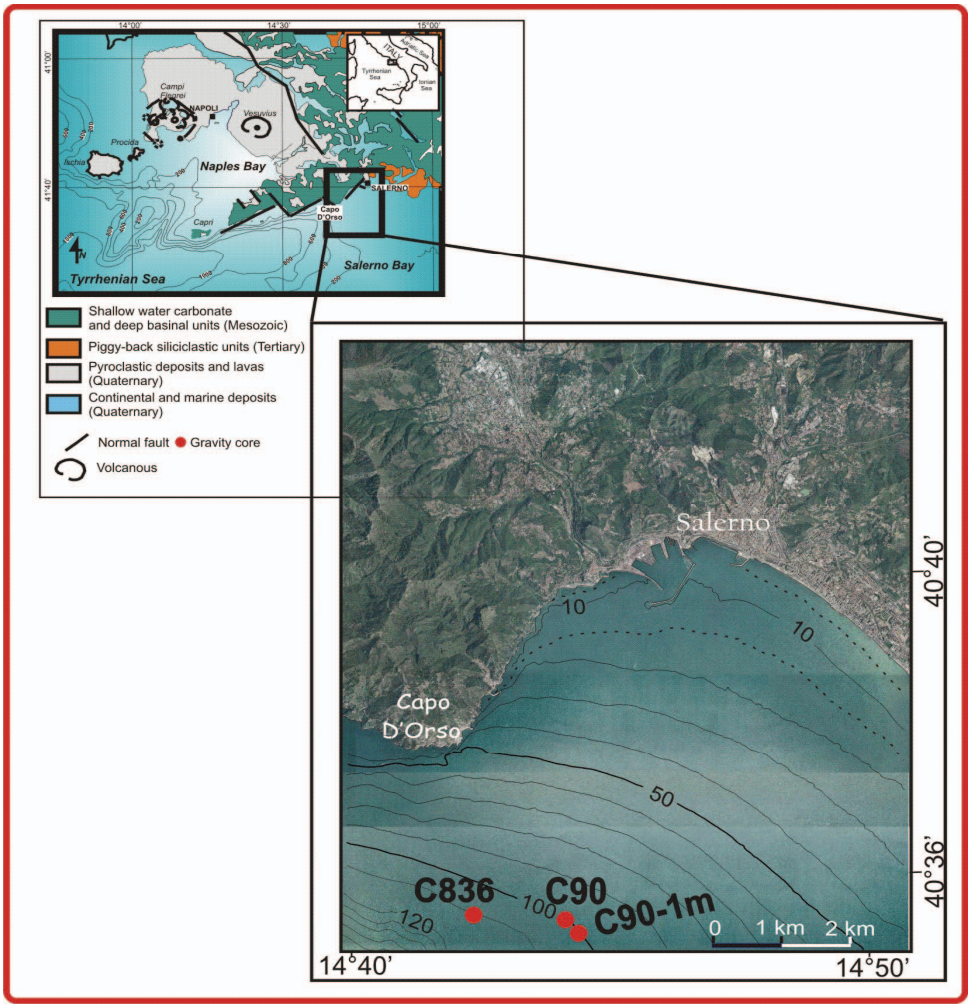

Fig. 5.1 Location map of the studied cores.

5.2 MATERIALS AND METHODS

5.2.1 Lithology

The constructed composite succession is based on the three gravity cores C90-1m (40°35.76' N;14°42,48'E), C90 (40°35,76' N; 14°42,38'E) and C836 (40°35,980' N; 14°42,470'E). These cores have been recovered close to the shelf break of the northern Salerno Bay, at a water depth of 103.4m, 105m and 110m, respectively (Fig. 5.1).

The resulting composite record is composed from the top down to the base as following: sea-floor down to base of tephra V0 (core C90-1m), from the base of tephra V0 down to top of tephra V2 (core C90) and from top of tephra V2 down to the base core (core C836) (Fig. 5.2 and 5.3). The correlation of the cores (~2 km close each other) has been performed by Iorio et al. (2004) and Budillon et al. (2005). This correlation is based on the magnetic susceptibility records, the occurrence of the tephra layer associated to 79 AD eruption (Iorio et al., 2004; Insinga et al., 2008) and the paleomagnetic secular variation (Iorio et al., 2004) (see Fig. 5.3, 5.4).

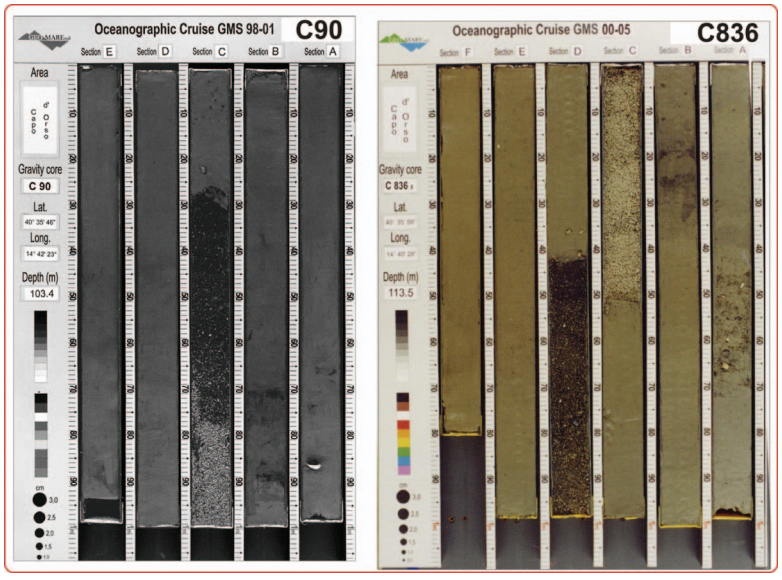

Fig. 5.2 Pictures of cores C90 and C836.

The resulting sedimentary succession consist on 5.85 m of undisturbed and well preserved hemi-pelagic deposits punctuated by a total of seven volcaniclastic layers occurring as cm-thick horizons (Fig. 5.2). The four tephra labelled from V0 to V3 can be correlated to the volcanic levels reported by Iorio et al. (2004). From V4 to V6 we labelled three unprecedented reported tephra layers. In addition, a distinct bioclastic interval (between 533 cm b.s.f. and 554 cm b.s.f.) is recorded in the composite core (Fig. 5.3).

In the Table 5.1, are listed all the tephra layers recorded throughout the composite succession.

C90-1m	C90	C836	Cores	Composite Core	Label according to Iorio et al., (2004)	Label according to Insinga et al., (2008)	Attributed volcanic event	
55-66cm	39-48cm	45-55cm	**C90-1m**	55-66cm	**V0**	**tS1**	1822 AD or 1631AD?	**Insinga et al. (2008)**
	172-178cm	170-180cm	**C90**	188-194 cm	**V1**		472AD	**Iorio et al. (2004) and Sagnotti et al. (2005)**
	216-295cm	220-328cm	**C836**	232-341 cm	**V2**	**tS2**	79AD	**Insinga et al. (2008)**
	360-372cm	390-405cm	**C836**	400-415 cm	**V3**	**tS3-tS3a**	AP1-AP2	**Insinga et al. (2008)**
	412-420cm	431-441cm	**C836**	441-451 cm	**V4 (this work)**	**V4 (this work)**		
		508-509cm	**C836**	518-519 cm	**V5 (this work)**	**V5 (this work)**		
		539-540cm	**C836**	549-550 cm	**V6 (this work)**	**V6 (this work)**		

Tab. 5.1 Position in cm and labels of the recognised tephra layers.

5.2.2 Analysis of planktonic foraminifera

Analysis of planktonic foraminifera has been carried out on a total of 452 samples at a continuous 1 cm sampling rate. About were dried at 50°C and washed with a 63 μm microns mesh-width size. Planktonic foraminifera, are abundant and well-preserved while percentages of foraminiferal fragments are very low and do not alter the composition of the planktonic assemblage.

Quantitative planktonic foraminiferal analysis were carried out on the fraction >90μm to avoid juvenile specimens. The adopted taxonomy is in agreement with Jorissen et al. (1993), Capotondi et al. (1999). Some planktic species or morphotypes are lumped together as following: *Globigerinoides ruber* includes *G. ruber* (variety rosea and alba) and *G. elongatus*; *Orbulina* spp. includes both *Orbulina universa* and *O. suturalis*; *Globigerinoides quadrilobatus* includes *G. trilobus* and *G. sacculifer*; *G. bulloides* (includes *G. falconensis)*; *Globorotalia truncatulinoides* left and right coiling; *Globigerinita glutinata*; *Turborotalita quinqueloba*; *Globigerinatella siphoniphera* includes *G. calida*; *Neogloboquadrina pachyderma* (right and left coiling). Data are reported in percentages.

5.2.3 Calcareous nannofossil analysis

For calcareous nannofossile analysis, a total of 187 samples were prepared as "smear slides" (Bown 1998) and analysed using a light microscope (transmitted light and crossed nicols) at about 1250X magnification. Abundance data were collected performing an approximately 500 specimens count and plotted as percentage values. The abundances of *Florisphaera profunda* were calculated with respect to 500 specimens of all other species. Abundance of reworked taxa (of Mesozoic and Cenozoic age) was reported as percentage values by counting specimens in all the fields considered for a total of ~500 nannofossils. According to Sprovieri et al. (2003) and Sierro et al. (2001), selected warm-water taxa (*Discosphaera tubifera*, *Rhabdosphaera* spp., *Syracosphaera* spp. and *Umbellosphaera* spp.), plotted separately and in cumulative curves, and the *Gephyrocapsa oceanica*/ *Gephyrocapsa muellerae* ratio (*G.oceanica* / *G. oceanica* + *G. muellerae*) were used to document climatic fluctuations.

5.2.4 Tephrostratigraphic analysis

The studied tephra layers, clearly identified by magnetic susceptibility (Fig. 5.3), were successively identified by a peak of abundance of glass fragments above the background in the whole detritic material coarser than 40μm. Samples were oven-dried, sieved at 1ϕ interval sieves, for defining grain-size distribution, and at least 100 fragments for each

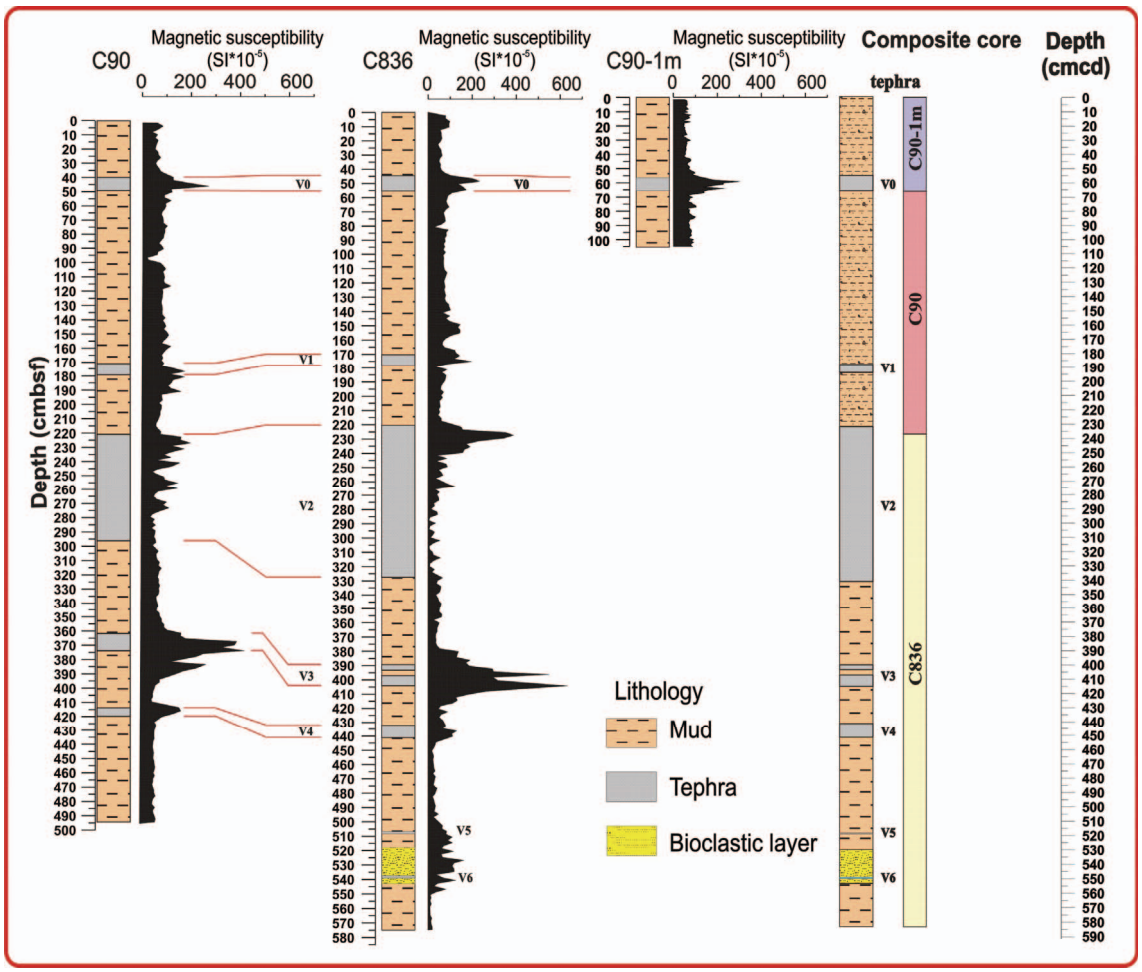

Fig. 5.3 Correlation of the three studied cores with the constructed composite core. **V0-V6** are labelled all the recognised tephra layers. Magnetic susceptibility for cores **C90** and **C836** are from Iorio et al., 2004). Magnetic susceptibility from core **C90-1m** is from this work.

sample were counted under a binocular microscope, in order to determine lithological components. On the whole, the layers resulted mainly made up of pumice and minor scoria fragments. For each sample, at least 30 juvenile fragments were embedded in epoxy resin and suitably polished for microprobe analysis. On the same embedded fragments, qualitative SEM EDS observation was made to define the mineralogical

content. Major-element analysis on pumice fragments, glass shards and crystals were performed on a SEM JEOL JSM 5310 (15kV, ZAF Correction Routine) with EDS at CISAG (Centro Interdipartimentale di Servizio per Analisi Geomineralogiche) at the University of Naples "Federico II". Instrument calibration was based on international mineral and glass standards. Individual analysis of glass shards with total oxide sums lower than 95% were excluded.

The results of chemical analysis are reported in Table 5.2 as average values of about 10 point analyses for each sample, recalculated to 100% water free. The chemical compositions of the pumice fragments of investigated tephra layers have been classified according to Total Alkali - Silica plot (TAS - Le Bas et al., 1986).

Tephra	V6		V5		V4		V3						V0	
core sample	C836		C836		C836		C836		C836		C836		C90	
depth (cm)	539-540		508-509		435-436		399-400a		399-400b		390-391		45-48	
SiO_2	60,87	0,22	59,77	0,28	60,73	0,37	56,00	0,61	52,42	0,58	54,60	0,70	48,69	0,34
TiO_2	0,47	0,01	0,57	0,10	0,47	0,08	0,62	0,06	0,73	0,03	0,84	0,09	1,26	0,08
Al_2O_3	18,63	0,17	18,23	0,15	18,39	0,22	19,89	0,21	19,37	0,14	18,34	0,06	17,47	0,21
FeO	3,45	0,11	4,31	0,12	3,70	0,23	4,88	0,14	6,95	0,18	5,67	0,42	10,45	0,22
MnO	0,21	0,09	0,15	0,06	0,09	0,08	0,16	0,10	0,24	0,07	0,31	0,03	0,19	0,09
MgO	0,54	0,12	0,95	0,14	0,59	0,15	0,77	0,07	1,93	0,09	8,00	0,43	3,68	0,15
CaO	2,49	0,08	3,35	0,10	2,49	0,05	4,64	0,09	7,15	0,33	1,65	0,46	9,48	0,18
Na_2O	5,04	0,43	3,99	0,23	4,72	0,20	5,19	0,54	4,39	0,58	6,33	0,23	3,84	0,30
K_2O	8,38	0,20	8,68	0,11	8,82	0,50	7,86	0,49	6,81	0,17	4,30	0,44	8,30	0,40

Tab. 5.2 Major (wt%) element composition of the tephra V0, V3, V4, V5 and V6.

5.2.5 Radiocarbon analysis

The AMS ^{14}C radiocarbon data, have been performed on mixed planktonic foraminifera (*G. ruber* and *G. inflata*) at the CIRCE (Centre for Isotopic Research for Cultural and Environmental heritage) laboratory in Caserta (Italy). The data were calibrated using CalPal (Cologne Radiocarbon Calibration & Paleoclimate Research Package) 2005 (Weninger et al., 2004). The reservoir correction ΔR (reservoir age) used for calibration

is 400 yr (Siani et al. 2001). The calibrated age ranges are reported in years BP (and AD) and referred to 2σ. Table 5.3 reports the AMS ^{14}C dates available and their respective calibrated ages.

Cores	depth (cm)	Radiocarbon Age	Calibrated Age	Composite core depth (cm)
C90	40	484 ± 29	1802 ± 97yr AD	55
C90	157	1662 ± 23	720 ± 40yr AD	173
C836	384	3559 ± 46	3390 ± 50yr BP	394
C836	443	4382 ± 32	4470 ± 70yr BP	453
C836	504	7967 ± 98	8360 ± 110yr BP	514
C836	527	12004 ± 48	13490 ± 70yr BP	537
C836	573	41777 ± 481	44930 ± 560yr BP	583

Tab.5.3 ^{14}C-AMS radiocarbon data available for the composite core.

5.2.6 Radionuclides ^{137}Cs and ^{210}Pb analysis

The uppermost 40 cm b.s.f. of core C90-1m were dated by short-lived radionuclide ^{210}Pb alpha spectrometry measurements at the ISMAR – CNR radiometric laboratory of Bologna following the procedures proposed by Frignani and Langone (1991). In addition, a number of levels were prepared for ^{210}Pb counting via gamma spectrometry using a gamma-x type germanium detector (Giordani et al. 1992) in order to check the assumption of constant activity of the supported ^{210}Pb. Activity of ^{137}Cs was measured to support ^{210}Pb via gamma spectrometry using coaxial intrinsic germanium detectors (Giordani et al. 1992).

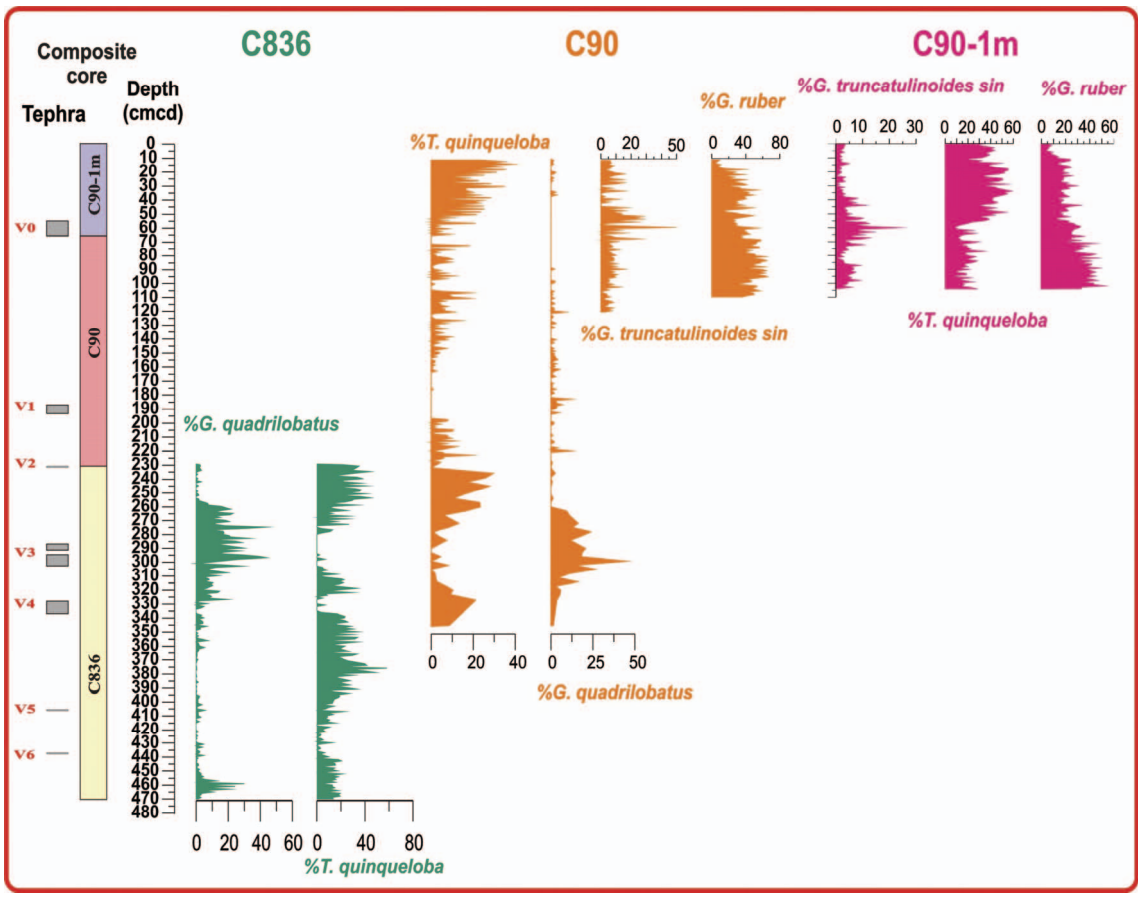

Fig. 5.4 Correlation of the studied cores based on the distribution patterns of selected planktonic foraminifera (*Turborotalita quinqueloba, Globigerinoides quadrilobatus* and *Globorotalia truncatulinoides left coiled*). The thickness of tephra associated to 79 AD volcanic event has been excluded in the construction of the composite core.

5.3. RESULTS

5.3.1 Quantitative distribution of planktonic foraminifera

The quantitative distribution patterns of selected planktonic foraminifera (*G. quadrilobatus*, *T. quinqueloba*, *G. truncatulinoides* l.c. and *G. ruber*) clearly confirm the good correlation between the three cores (Fig. 5.4).-*G. inflata* shows two main drops

in abundance at 325 cmcd (from 30% to 3%) and at 180 cmcd (from 20% to 3%) (Fig. 5.5). *G. ruber* show short term oscillation with mean value of ~30% up to 200 cmcd (Fig. 5.5), successively this taxon clearly shows a progressive upwards decrease in abundance (Fig. 5.5).

T. quinqueloba and *G. glutinata* are characterized by the same trend from the base up to 200 cmcd even if *T. quinqueloba*, from 160 cmcd upwards, shows a progressive increase when *G. glutinata* document values less than 5% (Fig. 5.5).

O. universa and *G. siphoniphera* reach high abundance values in the middle part of the section, while *G. bulloides* shows long-term oscillations with a progressive upwards increased from 170 cmcd to 60 cmcd (Fig. 5.5) and a further increased from 20 cmcd to top core (Fig. 5.5).

G. truncatulinoides (l.c.), *N. pachyderma* (r.c.), *G. quadrilobatus*, and *G. tenellus*, only occasionally reach significant percentages (Fig. 5.5). In particular, *G. truncatulinoides* (r.c.) shows a very reduced values (from 7% to 0), from 360 up to 260 cmcd, *N. pachyderma* (r.c.) is continuously present (with variable percentage from 5 to 10%) from 360 cmcd downwards (Fig. 5.5) and *G. quadrilobatus* which generally reaches very low abundance values (less than 5%) has a distinct acme interval from 260 down to 335 cmcd with values higher that 20% (Fig. 5.5) and a further peak in abundance (higher than 20%) in the lowermost part of the studied record (Fig. 5.5). Finally, *G. tenellus* distribution is discontinuously recorded only between 325 cmcd downwards with values variable among 1 to 4% (Fig. 5.5).

5.3.2 Quantitative distribution of calcareous nannofossils

Throughout the whole composite record, calcareous nannofossils are generally abundant and well preserved. Reworked species are continuously present along the record (Fig. 5.6). The assemblages are dominated by *Emiliania huxleyi* and small–sized *Reticulofenestra* spp. Subordinate and generally rare are *Gephyrocapsa oceanica*, *G. muellerae*, *Florisphaera profunda*, *Discosphaera tubifera, Rhabdosphaera* spp., *Syracosphaera* spp. and *Umbellosphaera sibogae*, *Helicosphaera carteri*,

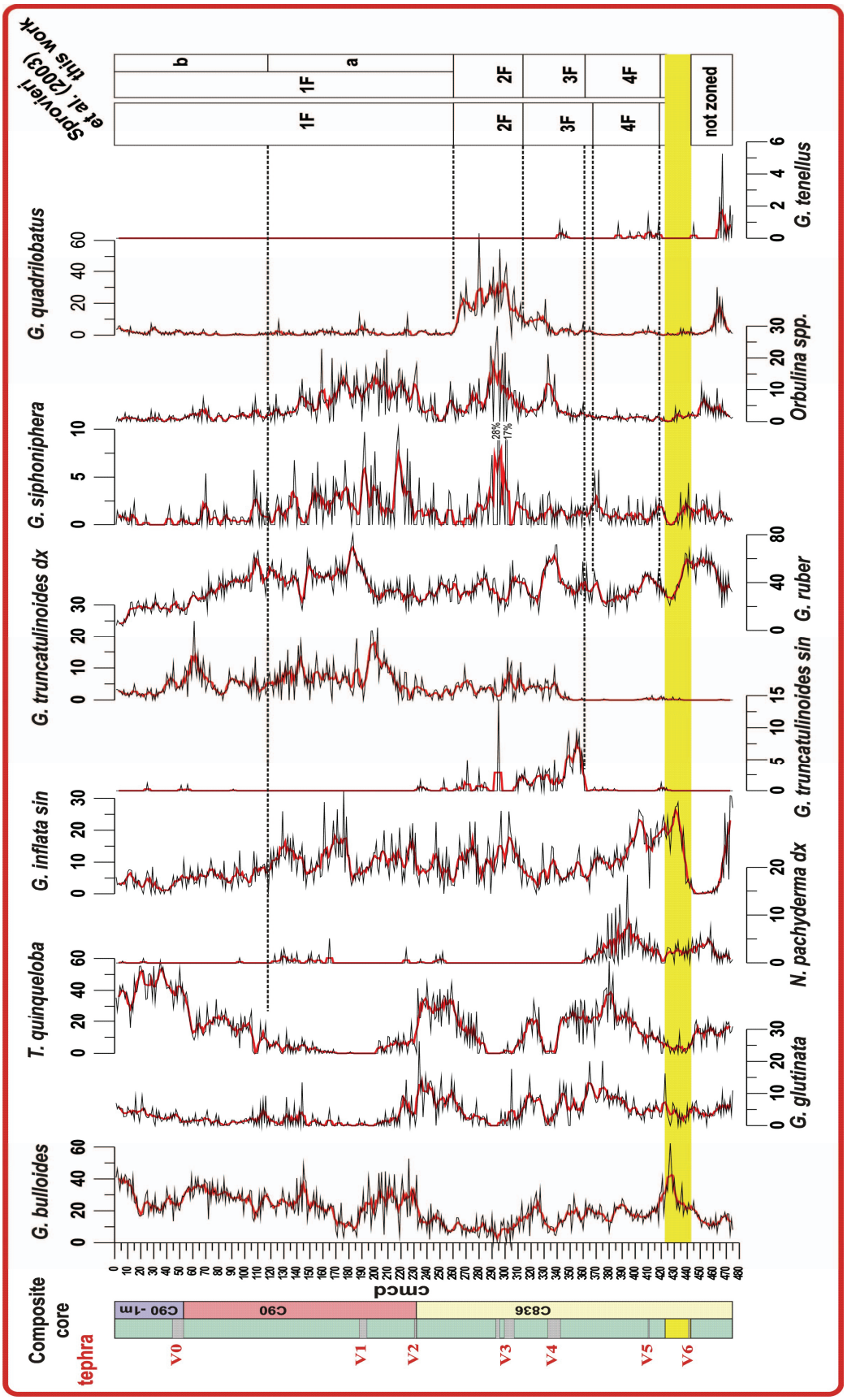
Sprovieri et al. (2003)
this work
b
a
1F
2F
3F
4F
not zoned
G. quadrilobatus
G. tenellus
Orbulina spp.
G. siphoniphera
28%
17%
G. truncatulinoides dx
G. ruber
G. truncatulinoides sin
G. inflata sin
N. pachyderma dx
T. quinqueloba
G. glutinata
G. bulloides
cmcd
Composite core
C90 -1m
C90
C836
tephra
V0
V1
V2
V3
V4
V5
V6

Fig. 5.5 Quantitative distribution of planktonic foraminifera with the position of the recognised eco-biozones. **V0-V6** are labelled all the tephra layers. The yellow band represent the bioclastic layer.

Braarudosphaera bigelowii, *Coccolithus pelagicus*. In the lowermost portion of the core (from ~442 cmcd down to the bottom) assemblages are characterized by abundant *G. muellerae*, *G. oceanica* and frequent specimens of *Emiliania huxleyi*, *F. profunda*, *D. tubifera, Rhabdosphaera* spp., *Syracosphaera* spp. and *U. sibogae*, *H. carteri* (Fig. 5.6). From about 442 cmcd to the base of the deposition Sapropel S1 equivalent interval (419 cmcd) nannofossile assemblages are characterized by dominant abundances of *E. huxleyi*. Similar distribution patterns were reported from the South Adriatic and the Tyrennean Sea by Sbaffi et al. (2001) and Giunta et al. (2003). In particular, the abundance peak of *E. huxley* at 435 cmcd could be correlated with the one reported by Sbaffi et al (2001) at the base of their Biozone 5 (15 kyr BP).

The Gephyrocapsa group shows a decreasing abundance from the base to the top of the composite core. *G. muellerae* is abundant only at the base of the studied interval. *G. oceanica* shows an increase in abundance from 430 cmcd to the top of the phase S1a of Sapropel S1 and a sudden decrease up to the top of sapropel event (Fig. 5.6). In the sapropel S1 interval the *Gephyrocapsa oceanica/ Gephyrocapsa muellerae* ratio has fluctuations similar to the ones described by Sprovieri et al (2003) in the Sicily Channel (Fig. 5.6).

The warm-water taxa show a progressive increasing trend toward 266 cmcd and upwards this index show short term oscillation (Fig. 5.6). A nearly sharp increase in abundance during the phases S1and S1b interrupted by a drop in warm water taxa during the cold phase S1i is recorded (Fig. 5.6).

The distribution pattern of *F. profunda* is similar to the warm-water taxa one. *F. profunda* increases at the base of both S1a and S1b segments, and slightly decreases in abundance during the S1i phase (Fig. 5.6).

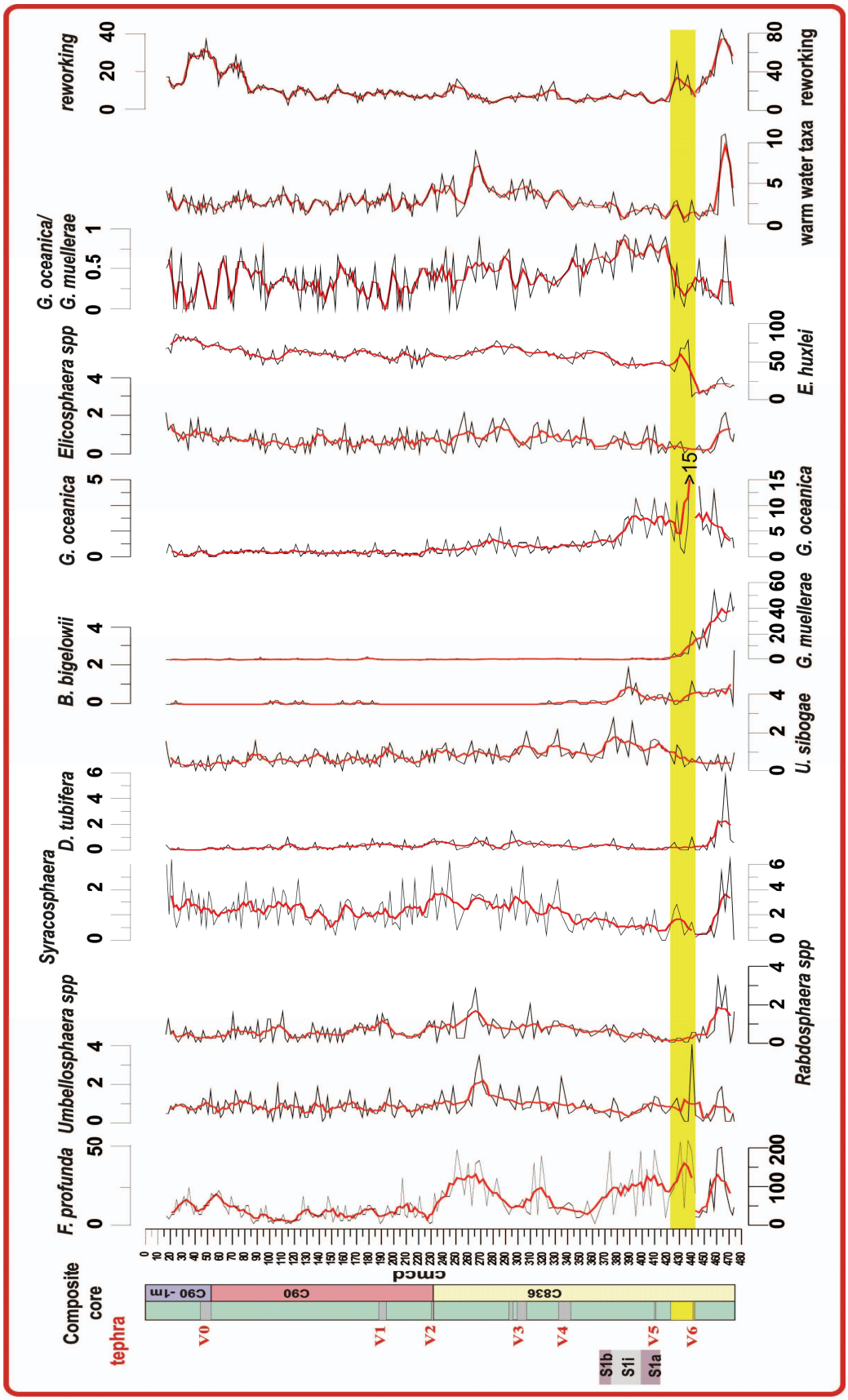
reworking
warm water taxa
G. oceanica/ G. muellerae
E. huxlei
Elicosphaera spp
G. oceanica
>15
G. muellerae
B. bigelowii
U. sibogae
Syracosphaera
D. tubifera
Rabdosphaera spp
Umbellosphaera spp
F. profunda
Composite core
tephra
cmcd
C90 -1m
C90
C836
V0
V1
V2
V3
V4
V5
V6
S1b
S1i
S1a

Fig. 5.6 Quantitative distribution of calcareous nannofossils with the position of the recognised eco-biozones. **V0-V6** are labelled all the tephra layers. The yellow band represent the bioclastic layer. For *F. Profunda, Siracosphaera spp* and *G. Oceanica,* the reference scales (% of the taxon), below the yellow layer (yellow band) is different from that reported for the upper interval (above yellow band).

The abundance curve of *B. bigelowii* displays an distinctive peak in the middle part of the S1i interval. An abundance spike is reported also in the upper part of the S1i segment of the core ODP Leg 160 963D (Sprovieri et al., 2003) and during the S1b in the Ionian Sea (Negri and Giunta, 2001). The increased abundance of *B. bigelowii* testifies less saline conditions during the deposition of the S1i (Sprovieri et al., 2003) (Fig. 5.6).

Helicosphaera spp. clearly shows a progressive increase in abundance toward the top of the composite core.

Due to the high diversity in abundance of calcareous nannofossil species resulted very difficult to apply the calcareous nannofossils eco-biostratigraphic scheme proposed by Sprovieri et al. (2003). In terms of eco-bioevents the distinct peak in *B. bigelowii* distribution pattern seems to be a good regionally recorded events.

5.3.3 Tephra layers

The chemical composition of the investigated tephra layers fall into the compositional fields of Somma-Vesuvio products (C90_45-46-48, C90_175-176, C836_390-391 and C836_399-400, C836_508-509, C836_539-540) and Campi Flegrean products (C836_435-436) (Fig. 5.7). Mineralogical analysis, the lithological component distribution and the chemical composition of juvenile fragments have been used to correlate, where possible, the single pyroclastic layers to specific eruptive episodes of the two campanian volcanic sources. The obtained chemical compositions were compared with those available in literature (Rolandi et al., 1998; Insinga et al., 2008; Turney et al., 2008) and with unpublished data (P.P.).

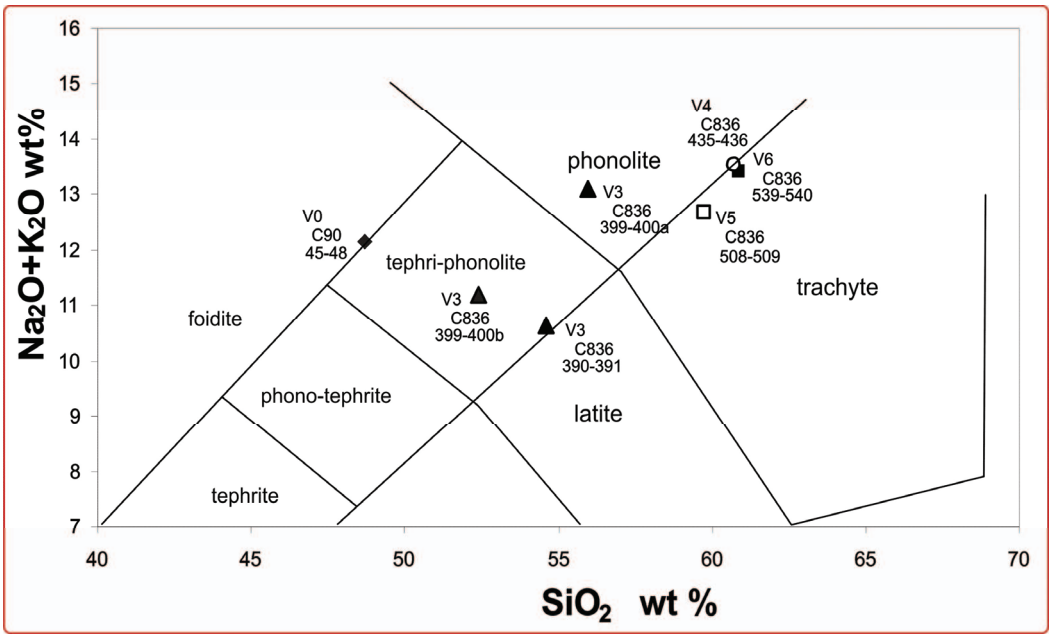

Fig. 5.7 The chemical compositions of the pumice fragments of investigated tephra layers have been classified according to Total Alkali - Silica plot (TAS - Le Bas et al., 1986).

Tephra V0-sample C90_45-46-48

The sample is mainly composed by preserved leucite-rich scoria fragments (ϕ_{max} 0.5mm). Glass composition is phono-tephritic. Insinga et al. (2008) reported a radiocarbon calibrated age of 1809±97yr AD at the top of the same tephra layer (correlation based on the petrochemical composition) recorded in the core C90 (Fig. 5.3) that suggests that this deposit can be attributed to the main explosive eruption at the Somma-Vesuvius recorded at 1822 AD (see Budillon et al., 2005 for details). Although a limited number of data is available about the chemical composition of glasses related to post-1631 AD vesuvian strombolian events, sample C90_45-46-48 can be definitely correlated with that recent activity. and in particular younger than 1631 AD (i.e. 1794

AD event) and older than 1822 AD eruptions as suggested by stratigraphic results coming from ^{210}Pb profiles acquired along the C90-1m sedimentary record.

Tephra V1- sample C90_175-176.

The layer is mainly composed by loose leucite crystals and scoria fragments (ϕ_{max}=1mm) containing leucite micro-crystals. The scoria glasses resulted generally analcimized, so no chemical data are available from this layer. It is characterized by a huge presence of a fassaitic clinopyroxene, and no davyne, almost ubiquitous in 472 AD products, was identified among its phenocrystals. Starting from this consideration, and carefully taking into account the Somma-Vesuvius products cropping on land in the Salerno area, we can quite confidently exclude the correlation with the 472 AD products. Similarly to the Mercato-Ottaviano and Avellino eruption fall products, in fact, the 472 AD showed a E oriented dispersal axis, which does not make their presence probable in the Salerno Gulf. Mediaeval eruptions, on the contrary, rely to a strombolian size generally implying a sub-circular distribution and, as a consequence, their products can have been emplaced in the Salerno area. So this layer could represent one of the mediaeval eruptions of Rolandi et al. (1998), all characterized by the huge presence of leucite and fassaitic clinopyroxene. Chemical data obtained from the same tephra recovered offshore Sele river do exclude a possible correlation of this layer with the 472 AD products while they confirm an early mediaeval eruption as the better source event (VI century, Insinga and Budillon, pers. comm.).

Tephra V2

This tephra layer has been studied in core C90 by Insinga et al. (2008) and has been associated to 79 AD eruption.

Tephra V3-samples C836_390-391 and C836_399-400

These two layers are quite similar to each other. They are mainly made up of dark glassy fragments (ϕ_{max}=0.5mm and 1mm, respectively) and contain leucite microlites. Their composition is tephry-phonolitic and well resembles that of the products of the third protohistoric eruption of Rolandi et al. (1998). More precisely, the tephra layers

can be respectively correlated with the layer A and layer D of Rolandi et al. (1998), which correspond to the AP3 and AP6 of Andronico et al. (2002). The age of protohistoric eruptions is not well constrained on land by ^{14}C dating.According to Rolandi et al. (1998), the only reliable age datum is available for the paleosol underlying the layer A, and is 2829±50 cal years BP. The authors, however, hypothesize only slight age differences between the single phases of the third protohistoric eruption, which they consider an eruptive cycle interrupted by short lived repose times, during which mainly mud flow activity occurred on the slopes of the Somma-Vesuvio volcano.

Tephra V4–sample C836_435-436

It is a well preserved pumice rich (ϕ_{max}=0.5mm) tephra layer. Pumice composition is trachytic and, compared with the composition of glasses from main Campi Flegrei explosive events, makes the correlation with the Astroni (4062±72 cal. years – Alessio et al., 1977) eruption products quite reliable.

Tephra V5-sample C836_508-509

It is a well preserved pumice rich (phi max 2mm) tephra layer. Pumice fragments are almost aphiric and trachytic in composition. For the juvenile fragments of this tephra layer the correlation with the Campi Flegrei Fondi di Baia products (8400 ka – Alessio et al., 1977) fits the best.

Tephra V6-sample C836_539-540

It is a pumice rich tephra layer visible by naked eye. Maximum diameter of pumice fragments is 0.5 mm. Pumice composition is trachytic and the compositional range obtained for the fragments extracted from this layer well fits the compositional range of Neapolitan Yellow Tuff juvenile fragments, dated at ca 15 kyr B.P. (Deino et al., 2004).

5.3.4 Radionuclides ^{137}Cs and ^{210}Pb results

A high-resolution age model for the first 40cmcd (upper part of core C90-1m, Fig. 5.3) is based on ^{210}Pb and ^{137}Cs radiometric dating. These two signals enabled the calculation of sediment accumulation rates for approximately the last 150 yr at the site of C90-1m core.

The ^{210}Pb activity–depth profile in core C90-1m shows an exponential decline with depth (Fig. 5.8), suggesting a constant sediment accumulation over the last century. The application of dating models is not straightforward because there is no simple mechanism that describes the delivery of sedimentary material and ^{210}Pb to the bottom. Furthermore, the effects of mixing might add complexity to the process of profile formation. In fact, the application of simple dating models in presence of mixing would provide overestimated sedimentation rates. Nevertheless, the excess ^{210}Pb profile shows no evidence of superficial mixed layer. Consequently, the sediment accumulation rate was calculated for the first 40 cmbsf by applying a Constant Flux–Constant Sedimentation model (Robbins, 1978) to the activity–depth profile of excess ^{210}Pb. A mean sediment accumulation rate of 0.20 cm yr^{-1} was obtained with age of 1802 AD at 40.5 cm b.s.f. (Fig. 5.8).

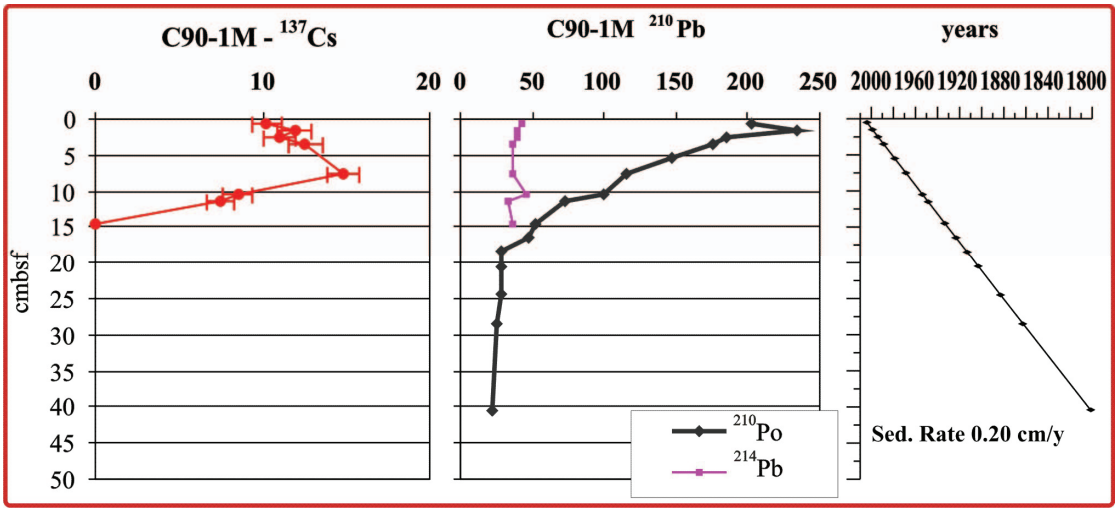

Fig. 5.8 The **^{210}Pb** and **^{137}Cs** activity–depth profiles in core **C90-1m** with the age-depth profile for the first 40 cmcd.

The measured ^{137}Cs activities are low compared to those measured in the Northern Adriatic sediments (Frignani et al., 2004), but show a clear trend detectable down to 15

cm (Fig. 5.8). Assuming that the following peaks at 11.5 cmcd and at 7.5 cmcd can be associated to caesium activity onsets dated 1954 AD and to the caesium fallout dated at 1963 AD, respectively, and that 2006.5 AD represents the data of recovering core, the resulting mean sedimentation rate is 0.18 cm/yr. These values are in good agreement with those obtained from ^{210}Pb-activity–depth-profile. The preservation of a clear curve trend of ^{137}Cs activity suggests that the sedimentation rate has been mostly constant for the last fifty years at the C90-1m core site.

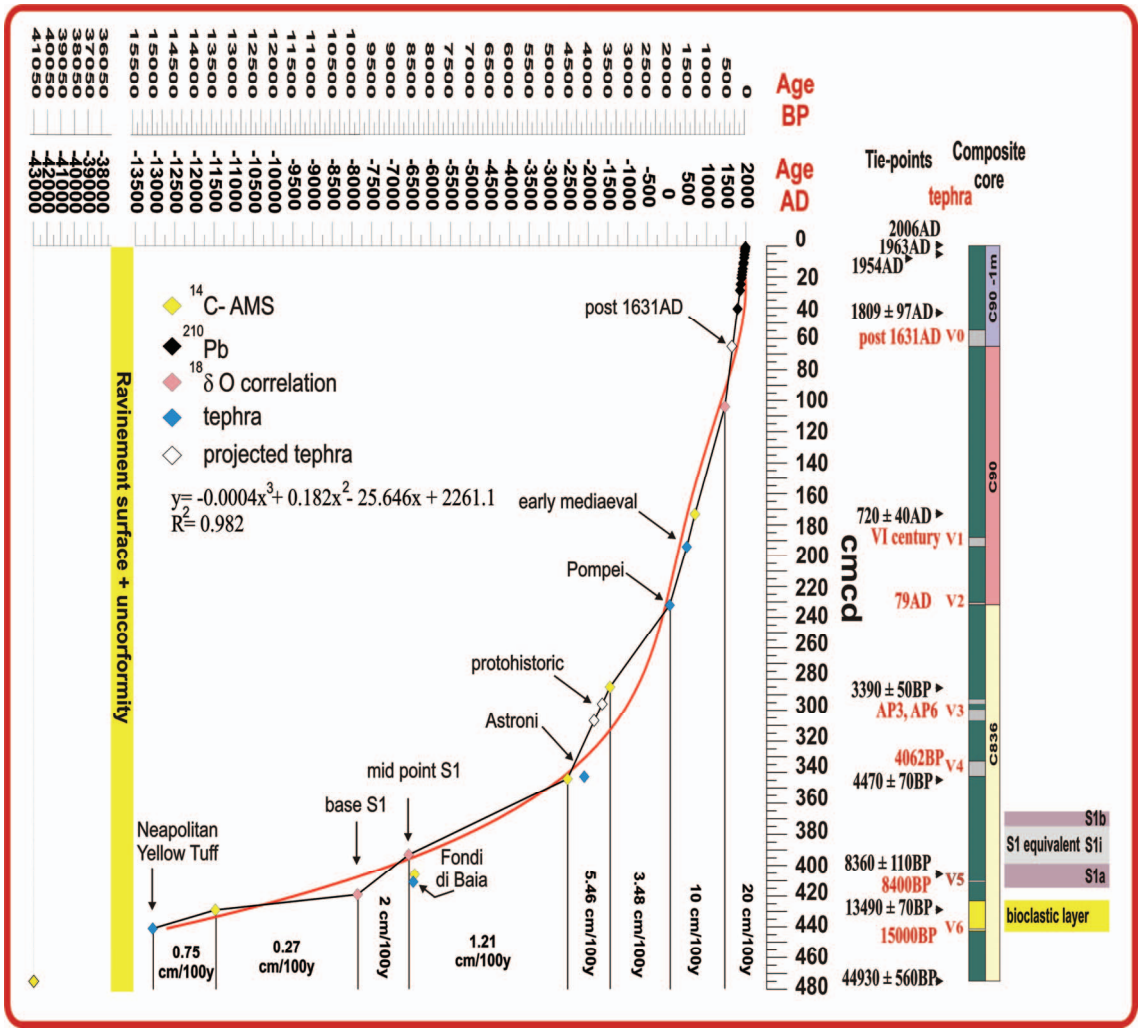

Fig. 5.9 Age-depth profile for the composite core with the position of all the tie.points. The numbers in black colour close to composite core are the radiometric tie-points while the red numbers represent the age of volcanic events after the tephrostratigraphic study. Red curve is a third order polynomial used to interpolated the tie-points. Yellow diamonds are the AMS ^{14}C radiocarbon data, the black diamonds are the ^{210}Pb tie-points, the pink diamonds are the mid-point of sapropel S1 equivalent (astronomically data at 8.5 kyr, Lourens 2004) and the base of sapropel S1 equivalent (dated at 9.8 kyr, Casford et al., 2002, 2007).

5.4 AGE DEPTH MODEL

Age depth model for the investigated composite section is based on the integration of several approaches: AMS ^{14}C radiocarbon data, ^{210}Pb and ^{137}Cs radionuclides and tephrostratigraphy. The complete list of the tie-points used for constructing the age depth model is reported in table 5.4. A third-order polynomial is needed to describe the age-depth relationship for the studied record, indicating a progressive decrease in average sedimentation rate from top core down to the base from 20cm/100yr to 0.75cm/100yr (Fig. 5.9). This age model shows the sedimentary gap of about 25 kyr between 423 and 443 cmcd (Fig. 5.9) in correspondence of the major unconformities (yellow band in figure 5.9) associated with the sea-level fall in the last glacial age. The identification of this sedimentary gap resulted by the attribution of the studied record comprise between the base core (475cmcd) and the base of bioclastic layer (at 443cmcd), to the time interval between Heinrich event HE4 and HE5 (between ~40 kyr and ~46 kyr), and by the assignment mean age of ~15 kyr to the lower part of the bioclastic layer. In particular, the age attribution to the sedimentary interval below the bioclastic layer is based on the combination of the AMS ^{14}C radiocarbon datum at 475 cmcd (44930 ± 560 yr BP) and of the planktonic foraminiferal signature, while for the bioclastic layer the proposed age resulted by combining the AMS ^{14}C radiocarbon datum (13409 ± 70yr BP) at 429 cmcd, within the bioclastic layer (lower part), and the

occurrence of the tephra layer associated to Neapolitan Yellow Tuff (dated at 15 kyr BP between 549 and 550 cmcd) in the middle part of the bioclastic interval.

cmcd	Core	Method	Volcanic event	Age (years)	Age (years) tephra BP	Remarks	Reference
0,5	C90-1m	^{210}Pb and ^{137}Cs		2004 AD			
1,5	C90-1m	^{210}Pb and ^{137}Cs		1998.9 AD			
2,5	C90-1m	^{210}Pb and ^{137}Cs		1993.9 AD			
3,5	C90-1m	^{210}Pb and ^{137}Cs		1988.9 AD			
5,5	C90-1m	^{210}Pb and ^{137}Cs		1978.8 AD			
7,5	C90-1m	^{210}Pb and ^{137}Cs		1968.7 AD			
10,5	C90-1m	^{210}Pb and ^{137}Cs		1953.6 AD			
11,5	C90-1m	^{210}Pb and ^{137}Cs		1948.5 AD			
14,5	C90-1m	^{210}Pb and ^{137}Cs		1933.4 AD			
16,5	C90-1m	^{210}Pb and ^{137}Cs		1923.3 AD			
18,5	C90-1m	^{210}Pb and ^{137}Cs		1913.2 AD			
20,5	C90-1m	^{210}Pb and ^{137}Cs		1903.2 AD			
24,5	C90-1m	^{210}Pb and ^{137}Cs		1883 AD			
28,5	C90-1m	^{210}Pb and ^{137}Cs		1862.8 AD			
66	C90-1m	base tephra	Vesuvian Strobolian event	between 1631 AD and 1822 AD		not used for age model	
173	C90	^{14}C-AMS		720 ± 40 AD			
194	C90	tephra	Mediaeval eruptions	early Mediaeval			
232	C90	tephra	Pompei	79 AD			
285	C836	^{14}C-AMS		1440 ± 50 BC	3390 ± 50 BP		
403	C836	base tephra	protohistoric AP6			not used for age model	
415	C836	base tephra	protohistoric AP3	880 ± 50 BC		not used for age model	Age by Santacroce et al. (2008)
343	C836	tephra	Astroni	Astroni	4062 BP	not used for age model	Age by Alessio et al. (1977)
344	C836	^{14}C-AMS		2520 ± 70 BC	4470 ± 70 BP		
393	C836	middle point Sapropel S1equivalent		6550 BC	8500 BP		Age by Lourens (2004)
406	C836	^{14}C-AMS		6410 ± 110 BC	8360 ± 110 BP		
410	C836	base tephra	Fondi di Baia	6450 BC	8400 BP		Age by Alessio et al. (1977)
419	C836	base Sapropel S1equivalent		7850 BC	9800 BP		Age by Casford et al. (2002, 2007)
429	C836	^{14}C-AMS		11459 ± 70 BC	13409 ± 70 BP		
441	C836	base tephra	Neapolitan Yellow Tuff	13050 BC	15000 BP		Age by Deino et al. (2004)
475	C836	^{14}C-AMS		42988 ± 560 BC	44930 ± 560 BP		

Tab. 5.4 List of the tie-points used for constructing the age depth model.

5.5Discussion

5.5.1 Planktonic foraminiferal ecozones

Evident changes in quantitative distribution patterns of different planktonic foraminifera species in different basins of the Mediterranean sea allowed several authors (Ducassou et al., 2007; Sprovieri et al. 2003; Principato et al. 2003; Asioli et al. 1999, 2001; Capotondi et al. 1999; Casford et al. 2002) to define a number of ecobiozones usefull for chronological subdivision of the Holocene-late Pleistocene time interval. The eco-biozone boundaries are identified by events of temporary appearance or disappearance and/or evident abundance peaks of selected species. In this work we adopted as basic scheme the eco-biostratigraphic subdivision of Sprovieri et al. (2003).

In particular four eco-biozones have been identified and dated above the bioclastic layer to the top core as following. In terms of age, only the base of eco-biozone 4F of Sprovieri et al. (2003), which virtually coincides with the base of sapropel S1 (Sprovieri et al., 2003), has been reported the age proposed by Casford et al. (2002; 2007) for the Aegean Sea.

The identification of the lower and upper boundaries of eco-biozone 4F of Sprovieri et al. (2003), slight above the bioclastic layer, allowed the attribution of the lower most record to the uppermost part of eco-biozone 5F of Sprovieri et al. (2003). This eco-biozone is characterised by the occurrence of *G. truncatulinoides* l.c., the absence of *N. pachyderma* r.c., the high percentages of *G. inflata* l.c. and decreasing abundances of *G. ruber* (Fig. 5.5).

Upwards, the eco-biozone 4F of Sprovieri et al. (2003), identified between 419cmcd (lower boundary dated at 9.8 kyr BP, this age is by Casford et al., 2007) and 367cmcd (upper boundary dated at 6.3 kyr BP), is characterised by the progressive upwards increased in abundance of *N. pachyderma* r.c., by absence of *G. truncatulinoides* and by two strong positive fluctuations in *G. ruber* abundance in the upper (S1b) and lower part (S1a) of the eco-biozone 4F (Fig. 5.5). Additional planktonic foraminiferal features like

low abundance values in *G. ruber* distribution pattern between 375 and 400 cmcd (Fig. 5.5) and the highest values (>5%) of *N. pachyderma* r.c. (reached between 375 and 400 cmcd) associated with *G. tenellus* mark the interruption (S1i) of sapropel S1 equivalent event (Fig. 5.5). Moreover, following the distribution patterns of the planktonic foraminifera, we proposed to move the top of this eco-biozone in correspondence of the sudden increase in abundance of *G. truncatulinoides* l.c. at 360 cmcd (7 cm above the top of eco-biozone 4F) and here dated at 5.8 kyr BP (Fig. 5.5).

The following eco-biozone 3F of Sprovieri et al. (2003) was identified between 360 cmcd (dated at 5.8 kyr BP) and 314 cmcd (dated at 3.9 kyr BP). The lower boundary of this eco-biozone is clearly marked by the sudden increase of *G. truncatulinoides* l.c. at 360 cmcd associated to the concomitant rapid downwards decrease in abundance of *N. pachyderma* r.c. (Fig. 5.5). The main feature of this eco-biozone is the presence of *G. truncatulinoides* l.c. which reaches abundances >10% and the progressive upwards increase in abundance of *G. quadrilobatus* and the abrupt onset of *G. truncatulinoides* r.c. at 346 cmcd (dated at 4.6 kyr BP) (Fig. 5.5).

The eco-biozone 2F of Sprovieri et al. (2003) defined by an acme interval of *G. quadrilobatus* in our record was identified between 260 cmcd (dated at 2.7 kyr BP) and 314 cmcd (dated at 3.9 kyr BP) (Fig. 5.5). The eco-biozone is also characterised by concomitant abundance of *G. truncatulinoides* r.c. (and l.c.<2%), *Orbulina* spp. and *G. siphoniphera* and very low abundance of *T. quinqueloba*, *G. glutinata* and *G. bulloides* (Fig. 5.5).

Finally, the middle to uppermost part of the studied composite record has been correlated to the eco-biozone 1F (Sprovieri et al. 2003) which base is marked at 260 cmcd (dated at 2.7 kyr BP) by the abrupt upwards decrease in abundance of *G. quadrilobatus* (<2%) (Fig. 5.5). This eco-biozone is characterized by high abundance of *G. truncatulinoides* (r.c.), *G. inflata* (l.c.), *G. ruber* and by the absence/very low abundance of *G. glutinata*, *G. quadrilobatus*, *G. truncatulinoides* (l.c.) and a progressive decrease upwards of *Orbulina* spp. and *G. siphoniphera*. Furthermore, *T.*

quinqueloba shows two peaks in abundance between 200 - 260 cmcd and between 120 cmcd – topcore (Fig. 5.5). In the present work we suggest a further subdivision of the eco-biozone 1F in two sub-eco-biozones 1F*a* and 1F*b* which boundary at 120 cmcd is dated at 1270 AD (680 yr BP).

5.5.2 Paleoclimatic and paleoceanographic reconstruction

The lowermost part of the studied record can be tentatively associated to the warm interval between Heinrich event HE4 and HE5 (between ~40 kyr and ~46 kyr),

The bioclastic interval between 423 cmcd and 443 cmcd (Fig. 5.5) can be reasonably correlated to the regional ravinement surface, recognised in all the Salerno Bay (Budillon et al., 1994 and Conforti, 2003) above the major unconformity associated with the seal-level fall of the last glacial age (Budillon et al.,1994; Conforti, 2003).

Between 367-419 cmcd we identified the calcareous plankton signatures (planktonic foraminifera and calcareous nannofossils) documented in litterature as diagnostic of the S1 sapropel deposition. Several authors (i.e. Piva et al., 2008; Sprovieri et al., 2003; Cramp and O'Sullivan 1999) clearly suggested that lithological signature (dark organic rich and laminated layer) of sapropel deposition is not always recognisable, so that particular micropaleontological features, geochemical and paleomagnetic parameters may be used to identify this oceanographic phase. For these reasons we name this eastern Tyrrhenian layer as sapropel S1 equivalent (Fig. 5.10).

In the studied marine record the distribution patterns of calcareous plankton assemblage combined to a single AMS ^{14}C radiocarbon datum clearly mark the interval of humid climate (Rohling et al., 2002) in temperate region associate to deposition of the anoxic sediments of sapropel S1 in the eastern Mediterranean basin. Casford et al. (2002; 2007) defined an age of 6.5 kyr and 9.8 kyr for top and base of sapropel S1 in the Aegean Sea with an intermediate cold event (S1i) (associated to an interruption of the sapropel deposition) centred at a calibrated age of about 8.2 kyr BP (Rohling & Palike (2005) and that De Rijk et al. (1999), Myers and Rohling (2000), Ariztegui et al. (2000) and Mercone et al. (2000) estimated in terms of duration between 200 and 500 years. In, our

data two distinct peaks in *G. ruber* distribution evidence the occurrence of S1a and S1b phases while the drastic increase of *N. pachyderma* and *T. quinqueloba* (Fig. 5.10) document an interruption of this deposition as evidenced already in literature (Sprovieri et al., 2003). In terms of calcareous nannofossils, this interval is marked by an increase in abundance of *F. profunda*, which indicates seasonal stratification of the photic zone (Sprovieri et al., 2003; Castradori 1993). Furthermore, the interruption phase S1i is marked by a drastic peak in calcareous nannofossils species *B. bigelowii* and by a decrease in abundance of *F. profunda* (Fig. 5.10). This calcareous nannofossil features combined with the strong increase in abundance of *N. pachyderma* seem to confirm the occurrence of cool water condition during the interruption phase S1i. These data confirms those obtained by Sprovieri et al. (2003) in ODP-Site 963 (Sicily Channel).

Based on the age model the sapropel S1 equivalent layer spans from 6.3 kyr BP to 9.8 kyr BP and the interruption correspond to the cold global event centred at 8.2 kyr BP (i.e. Rohling and Palike 2005).

Above the sapropel S1 equivalent, the planktonic foraminiferal fauna during the entire interval (between 6.3 kyr BP and 3.9 kyr BP) indicates the presence of a distinct seasonal contrast with a water column ventilation. This interval falls in the uppermost part of eco-biozone 4F and within eco-biozone 3F (Fig. 5.10). This interval is characterised by a strong decrease in abundance of typical planktonic warm oligotrophic taxa (i.e. *G. quadrilobatus*, *Orbulina* spp., *G. siphoniphera*) and by concurrence in abundance of taxa which indicates deep mixed layer during winter (i.e. *G. inflata* and *G. truncatulinoides*). The waters were been well stratified and oligotrophic during summer, when *G. ruber* was dominant and *Umbellosphaera* spp. and *Rhabdosphaera* spp. increased in abundance as recorded between 327-343 cmcd (Figs. 5.6 and 5.10). Colder productive surface waters and well-mixed deep layers occur in the lower and upper part of this interval (Fig. 5.10). Chronologically, these two cold events may be tentatively associate to Bond cycle 4 and 3 (Fig. 5.10). The cold event (Bond cycle 3) centred at 4 kyr BP can be correlated with the cold event recorded by Sangiorgi et al. (2003) in the

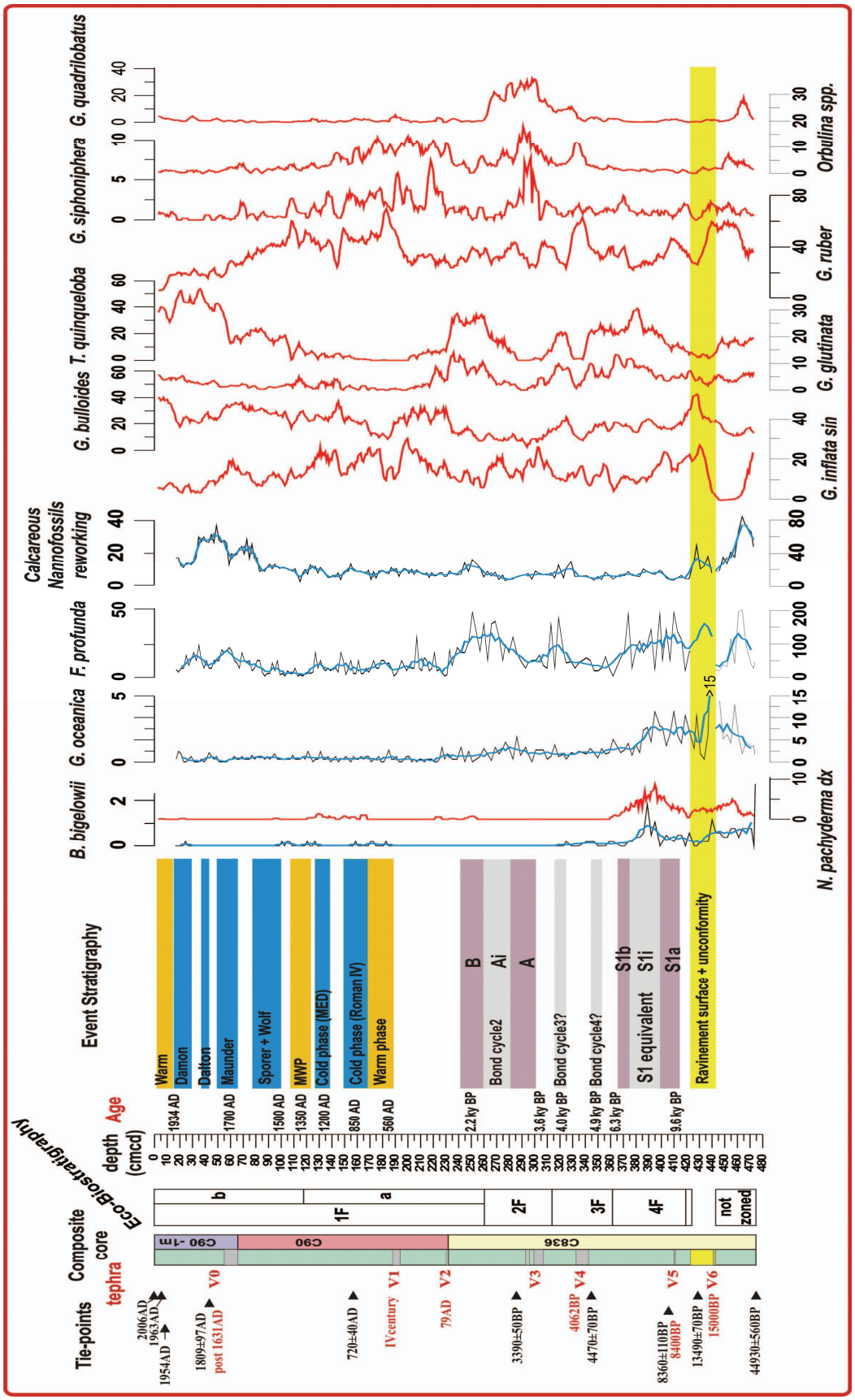
Tie-points
tephra
Composite core
Eco-Biostratigraphy
depth (cmcd)
Age
Event Stratigraphy
B. bigelowii
G. oceanica
F. profunda
Calcareous Nannofossils reworking
G. bulloides
T. quinqueloba
G. siphonifera
G. quadrilobatus
N. pachyderma dx
G. inflata sin
G. glutinata
G. ruber
Orbulina spp.
2006AD
1963AD
1954AD
1809±97AD
post 1631AD
720±40AD
IVcentury
79AD
3390±50BP
4062BP
4470±70BP
8360±110BP
8400BP
13490±70BP
15000BP
44930±560BP
V0
V1
V2
V3
V4
V5
V6
C90 -1m
C90
C836
1F
2F
3F
4F
not zoned
Warm
Damon
Dalton
Maunder
Sporer + Wolf
MWP
Cold phase (MED)
Cold phase (Roman IV)
Warm phase
B
Bond cycle2
Ai
A
Bond cycle3?
Bond cycle4?
S1b
S1 equivalent
S1i
S1a
Ravinement surface + unconformity
>15

Fig. 5.10 Quantitative distribution patterns of selected planktonic foraminifer and calcareous nannofossils species, superimposed to 3 point-moving average, plotted vs depth (cmcd) used for Event Stratigraphy. The black arrows and numbers close to composite core are the radiometric tie-points while the red numbers represent the age of volcanic events after the tephrostratigraphic study (tephra layers labelled from **V0** to **V6**). The blue and orange bands represent the cold (blue) and warm (orange) climatic events according to the solar variability proxy $\Delta^{14}C$, measured in tree rings (Stuiver te al., 1998). The Bond cycles are following Bond et al. (2001).

Adriatic Sea (and dated at 3.9 kyr BP). The warm phase which separate the Bond cycles 4 and 3 can be associated to the warm Copper Age interval.

Upwards, between 240-300 cmcd (Fig. 5.10), the calcareous plankton signals indicates the occurrence of two distinct warm/humid phases (A and B) separated by a colder/drier event (Ai). According to the adopted age-model this event was restricted between 2.25 kyr BP and 3.625 kyr BP (Fig. 5.10). The planktonic foraminifera assemblage shows two distinct peaks of *G. ruber* during the warmer phases separated by an interval with lower abundances of the same species and an increase of *G. inflata* l.c. and *T. quinqueloba*. The calcareous nannofossil assemblage shows a distinct peak in abundance of *F. profunda* and *G. oceanica.* This humid phase which clearly spans from eco-biozone 3F to the lowermost part of eco-biozone 2F (Fig. 5.10), is characterised by an acme of *G. quadrilobatus* (>30%), a typical surface Mediterranean water dweller and prolific at the end of summer (i.e. Be´ and Hamlin, 1967; Be´ and Tolderlund, 1971; Be´ and Hutson, 1977; Be´ et al., 1977; Hemleben et al., 1989; Pujol and Vergnaud-Grazzini, 1995). We speculate that the first of these two warm/humid phases correspond to the prominent solar activity maxima between Egyptian and Homeric (corresponding to the Bronze Age). Also Schilman et al. (2001) interpreted an abrupt negative excursion in the $\delta^{18}O_{G.\ ruber}$ signal off of Israel coastal area, between 3.6 and 3.0 kyr BP as response to the relatively short humid event of the late Bronze Age (Issar, 1990;

Frumkin et al., 1991; Issar et al., 1991; Schoell, 1978; Degens et al., 1984). On the other hand, the second warm/humid peak falls within the Golden Age, from the Latin Literature, which corresponds to a humid and mild climate regime (Lamb, 1982).

After the famous Pompei volcanic event (79 AD), which represents one of the main chronostratigraphic marker of the eastern part of the southern Tyrrhenian area, the historical chronicles indicate the occurrence between the 3rd and 5th century of the Decline and Fall of the Roman Empire. During that time the increase in deforestation, associated to the urbanistic expansion of Roman culture, potentially provided an increase of continental runoff, which may have produced a drastic change in the continental water budge which flows in the Mediterranean. This interval falls within the lower part of the eco-biozone 1Fa, during which the planktonic foraminiferal assemblage shows a low diversity and is dominated by *G. inflata* and *G. bulloides* and subordinate *Orbulina* spp. (Fig. 5.10).

Following this time interval, the successive main climatic events which experienced the Mediterranean area in the last millennium are the following: the Medieval Warm Period (MWP), the Little Ice Age (LIA) and the modern warm period.

At present, there is not universally accepted, precise definition for duration of the Medieval Warm Period (~800-~1300 AD); it was a time of warm climate in Europe with temperatures allegedly comparable with the present-day conditions (Maasch et al., 2005).

In terms of planktonic foraminiferal assemblage there is not clear signature of the MWP, but the time interval spanning from ~560 AD to ~1300 AD (from 190 cmcd to 120 cmcd, see Fig. 5.10), which falls within the upper part of eco-biozone 1Fa (Fig. 5.10), clearly show a dominance of warm carnivore species (*G. ruber*, *G. siphoniphera* and *Orbulina* spp.. Within this long interval the concurrence of *G. inflata* and *G. ruber* indicates deep vertical mixing in water column during winter and less cooler water (Fig. 5.10). During this warmest time interval two very short cold events may be reasonably identified in correspondence of the two peaks in abundance of *N. pachyderma* r.c. (at

1204 AD and at 840 AD) (Fig. 5.10). These events can be associated with the MED and Roman IV cold events according to the solar variability proxy $\Delta^{14}C$, measured in tree rings (Stuiver te al., 1998). Tentatively, we placed the MWP event just above the cold MED event in correspondence of a strong increase in abundance of *G. ruber* (Fig. 5.10). This MWP event has been also recorded by Schilman et al (2001) off of Israel coastal area through $\delta^{18}O_{\ G.\ ruber}$ signal between ~1100 and ~1350 AD.

Following ~1300 AD the progressive turnover between carnivore species (strong reduction) and herbivore-opportunistic ones is recorded (Fig. 5.10). This progressively change in planktonic foraminiferal fauna can be reasonably associate to the Medieval Warm Period-Little Ice Age transition, here dated at 1480 AD (this transition culminated at around 1400 ± 40 yr AD according to Maasch et al., 2005), which represents one of several global-scale rapid climate change (RCC) events to have occurred in the Holocene (Mayewski et al. 2004).

In terms of temperatures and glaciers fluctuations, the subsequently Little Ice Age has four phases (Wolf, Sporer, Maunder and Dalton events), according to the solar variability proxy $\Delta^{14}C$, measured in tree rings (Stuiver te al., 1998). The planktonic foraminiferal assemblage during that time is characterised by two sudden and strong increases in abundance of *T. quinqueloba* at 100 cmcd (>20%) and 60cmcd (>40%) associated with two drops in *G. ruber* abundance and absence of the other carnivore species (Fig. 5.10). At same time *G. bulloides* (>30%) increased in abundance from 100 cmcd to 50 cmcd and decreased from 50cmcd to 15cmcd (Fig. 5.10).

Chronologically, in the studied record the LIA onset starts at 1500 AD, which coincides with the first increase in *T. quinqueloba* abundance (at 100 cmcd >20%). At ~1700 AD the further and sudden increase in *T. quinqueloba* abundance (at 60 cmcd >40%) and the drastic drop in *G. ruber* abundance pattern may be associated to the Maunder event (Fig. 5.10). At that time *G. truncatulinoides* l.c. and *G. inflata* l.c. show a distinct peak in abundance (Fig. 5.10). Historical chronicle reports at 1708-09 AD,

during Maunder event, the occurrence of the coldest winter in Europe for the least half millennium (Luterbacher et al. 2006) during which the Venice Lagoon was freeze.

The end of LIA event has been tentatively placed at 1905 AD in correspondence of the distinct drop (at 20 cmcd) in abundance of *T. quiqueloba* (Fig. 5.10). We tentatively speculate that the four distinct peaks recorded in *T. quiqueloba* distribution pattern may correspond to the cold phases corresponding to the prominent solar activity minima Wolf, Sporer, Maunder, Dalton and Damon events (Fig. 5.10).

In terms of ecological niches, *T. quinqueloba* has to be considered herbivore and opportunistic species that has favorable conditions when high phytoplankton productivity prevails during spring (Raynolds & Thunell 1989; Schiebel and Hemleben, 2000). *G. bulloides*, today reaches the highest concentrations in upwelling regions or in areas of vigorous vertical mixing in the water column (Reynolds and Thunell, 1989), where high phytoplankton productivity prevails. Moreover, in the Mediterranean Sea this species occurs in significant abundances in winter.

On the other hand, *G. inflata* and *G. truncatulinoides*, which show in the studied record high abundance values during the Maunder event (Fig. 5.10), are considered as indicative of deep mixed layer during winter as reported by Pujol and Vergnaud-Grazzini (1995) for the Mediterranean area and show a generally high dietary dependence on phytoplankton, but *G. truncatulinoides* always lives at greater depth than *G. inflata*. Moreover, it lives in phosphate-rich waters and is a good recorder of thermocline nutrient levels (Mulitza et al 1998).

These data seem to suggest that from the base of LIA (1500 AD) to the Maunder event (~1700 AD) we have a deep high phytoplankton productivity, while following Maunder event upwards the high phytoplankton productivity is strongly concentrated in the shallow part of the water column.

In terms of calcareous nannofossil fauna, following ~1500 AD a progressive increase in reworking species may be associated to the LIA onset. According to Incarbona et al. (in press), in ODP-Site 963 (Sicily Channel), during glacial phases the runoff increased

during glacial cycles resulting in reworking increased. Moreover, enrichment and depletion in warm water calcareous nannofossil taxa may be suggested the cyclic alternation of warm and cold (Wolf, Sporer, Maunder and Dalton events) intervals according to solar variability proxy $\Delta^{14}C$.

The last climatic event which experienced the Mediterranean area is represented by the onset of modern warm condition. Following ~1900 AD the planktonic foraminiferal assemblage shows very low values in *G. ruber* (<3%) and a further progressive increased (from 1934AD) in abundance in *G. bulloides* (>30%) distribution pattern associated with a slightly increase in abundance (from 1934 AD) of *G. quadrilobatus* (>5%) is recorded (Fig. 5.10). In the same time benthic fauna shows the sudden increase (from 1934AD) in abundance of *B. aculeata* from 2-3% up to 20% of the total benthic fauna. Apparently, these data seem to not reflect the modern global warming. Contrarily, official documents report that at 1934 the dam on Sele River (Salerno Gulf) was built. From 1934 AD, the dam building produced a strong reduction of coarse-grained materials which flow in the sea water producing a change in grain size framework of the sea-bottom and a possible change in nutrient support. At that time a strong increase in number of planktonic and benthic foraminifer per gram of sediment is recorded. All these data seem to suggest a strong human impact on the marine environmental ecosystem.

5.6 CONCLUSION

The present study reports a detailed chronological framework and a high-resolution Event Stratigraphy for the Eastern Tyrrhenian region during the last 10 kyr from continental shelf marine record. The detailed chronology for the Tyrrhenian composite core based on the integration of AMS ^{14}C radiocarbon data ^{210}Pb and ^{137}Cs radionuclides and tephrostratigraphic studies allowed us to date four eco-biozones and the main climatic changes occurring during the Holocene. From the base to the top, the eco-biozone 4F spans from 9.8 kyr to 5.8 kyr, the eco-biozone 3F spans from 5.8 kyr to 3.9 kyr, the eco-biozone 2F spans from 3.9 kyr to 2.7 kyr and finally the eco-biozone 1F spans from 2.7 kyr to present day. The eco-biozone 1F presents two subeco-biozone 1Fa and 1Fb which boundary is placed at 1270 AD.

In terms of climate events, two distinct humid phases have been recorded during the early and middle part of the Holocene, as well as the Medieval Warm Period (MWP), the Little Ice Age (LIA) and the modern warm period in the latest part of the Holocene. In particular, the well-known early Holocene humid phase, reported by Rohling et al. (2002), associated to the deposition in the Mediterranean Area of Sapropel S1, is recorded. Chronologically, the sapropel S1 equivalent event spans from 6.3 kyr BP to 9.8 kyr BP. We can clearly confirm the identification of this event by calcareous plankton (planktonic foraminifera and calcareous nannofossils) signatures, according to Sprovieri et et. (2003). Furthermore, the cold global event centred at 8.2 kyrBP (i.e. Rohling and Palike 2005) is recorded by the strong increase in abundance of cold planktonic foraminiferal species *N. pachyderma* r.c..

The successive important humid phase recorded between 2.25 kyrBP and 3.625 kyrBP (spanning from Bronze to Golden age) is well detected through calcareous plankton signature. This humid phase presents the similar calcareous plankton signature of the sapropel S1 equivalent, supporting the hypothesis that during that time the climate (and

or the solar forcing) has to be the same of the early Holocene humid phase (Sapropel S1).

The MWP does not show a distinct planktonic foraminiferal features. Tentatively, this warm interval may coincide with time interval spanning from ~560 AD to ~1300 AD, where is clearly evident a dominance of warm carnivore species *G. ruber*, *G. siphoniphera* and *Orbulina* spp.. Within this long interval two distinct warm water taxa oscillations are present. The uppermost can really associated to the historically warmest part of the MWP (~900-1300 AD).

The subsequently MWP-LIA transition, which represents a global-scale rapid climate change (RCC) event, is strongly marked by a progressive turnover between carnivore species and herbivore-opportunistic ones and is dated at 1480 AD.

The LIA event spans from at 1500 AD to 1905 AD and is marked by a planktonic foraminiferal assemblages mainly controlled by a strong increase in abundance of *T. quinqueloba*. During this time interval the Maunder event is here centred at ~1700 AD. This cold event is characterised by the definitive decrease in abundance of warm water taxa and by the further increase of herbivore-opportunistic species. At that time, in northern part of Italy, during 1708-09 AD is reported the occurrence of the coldest winter in Europe for the least half millennium during which the Venice Lagoon was freeze.

Finally, the uppermost climatic event which experienced the Mediterranean area is represented by the onset of modern warm condition. Our data do not show a clear relationship with the modern global warming. Contrarily, they suggest a clear human impact on the marine environmental ecosystem associated to the building dam on Sele River (Salerno Gulf) at 1934 AD.

ACKNOWLEDGMENTS

This paper is financially supported by VULCOST project (Team leader Prof. Bruno D'Argenio). This project represents the Line2 of this Italian project VECTOR.

REFERENCES

Alessio, M., Bella, F., Belluomini, G., Calderoni, G., Cortesi, C., Fornaseri, M., Franco, M., Improta, F., Scherillo, A., Turi, B., 1971. Datazioni con il metodo C-14 di carboni e di livelli humificati-paleosuoli. intercalati nelle formazioni piroclastiche dei Campi Flegrei- Napoli. Rend. Soc. Ital. Mineral. Petrol. 27–2, 305–317.

Alessio, M., Bella, F., Improta, S., Belluomini, G., Calderoni, G., Cortesi, C., Turi, B., 1976. University of Rome carbon-14 dates XIV. Radiocarbon 18, 321–349.

Andronico, D. and Cioni, R., 2002. Constrating styles on Mount Vesuvius activity in the period between the Avellino and Pompei Plinian eruptions, and some implicatis for assessment of future hazards. Bull. Volcanol. 64, 372–391.

Ariztegui, D., Asioli, A., Lowe, J. J., Trincardi, F., Vigliotti, L., Tamburini, F., Chondrogianni, C., Accorsi, C.A., Bandini Mazzanti, M., Mercuri, A. M., Van der Kaars, S., McKenzie, J. A., Oldfield, F., 2000. Palaeoclimate and the formation of sapropel S1: inferences from Late Quaternary lacustrine and marine sequences in the central Mediterranean region. Palaeogeography, Palaeoclimatology, Palaeoecology, 158, 215– 240.

Asioli, A., 1996. High resolution foraminifera biostratigraphy in the Central Adriatic basin during the last deglaciation: a contribution to the PALICLAS Project. In: Oldfield, F., Guilizzoni P. (Eds.), Palaeoenvironmental Analysis of Itlian Crater Lake and Adriatic Sediments. Memorie dell'Istituto Italiano di Idrobiologia 55, 197-218.

Asioli, A., Trincardi, F., Lowe, J. J., Ariztegui, D., Langone, L. and Oldfield, F., 2001. Sub-millennial scale climatic oscillations in the central Adriatic during the Lateglacial: Palaeoceanographic implications. Quaternary Science Review, 20, 1201–1221.

Bé, A. W. H., 1977. An ecological, zoogeographic and taxonomic review of recent planktonic foraminifera . In Ramsey, A.T.S., Ed., Oceanic Micropalaeontology. London: Academic Press,1-100.

Bé, A. W. H. and Tolderlund, D. S., 1971. Distribution and ecology of living planktonic foraminifera in surface waters of the Atlantic and Indian Oceans. In (Funnell, B.M. and Riedel, W.R., eds), The Micropalaeontology of Oceans, 105-149. Cambridge University Press.

Bé, A. W. H. and Hamlin, W. H., 1967. Ecology of Recent planktonic foraminifera: Part 3. Distribution in the North Atlantic during the summer of 1962. Micropaleontol. 13, 87-106.

Bé, A. W. H. and Tolderlund, D. S., 1971. Distribution and ecology of living planktonic foraminifera in surface waters of the Atlantic and Indian Oceans. In (Funnell, B.M. and Riedel, W.R., eds), The Micropalaeontology of Oceans, 105-149. Cambridge University Press.

Bown, P. R. and Young, J. R., 1998. Techniques. In: Bown, P.R. (Ed.), Calcareous Nannofossil Biostratigraphy, Kluwer Academic Publishers, Dordrecht, Boston, London: 16-32.

Budillon, F., Pescatore, T., Senatore, M. R., 1994. Cicli deposizionali del Pleistocene Superiore–Olocene sulla piattaforma continentale del Golfo di Salerno (Tirreno Meridionale). Boll. Soc. Geol. Ital. 113, 303–316.

Budillon, F., Violante, C., Conforti, A., Esposito, E., Insinga, D., Iorio, M., Porfido, S., 2005. Event beds in the recent prodelta stratigraphic record of the small flood-prone Bonea stream (Amalfi Coast, Southern Italy). Marine Geology 222–223, 419–441.

Budillon, F., Esposito, E., Iorio, M., Pelosi, N., Porfido, S., Violante, C., 2005. The geological record of storm events over the last 1000 years in the Salerno Bay (Southern Tyrrhenian Sea): new proxy evidences, European Geoscience Union, Adv. Geosci., 2, 1–8.

Cacho, I., Grimalt, J.O., Pelejero, C., Canals, M., Sierro, F. J., Flores, J.A., Shackleton, N. J., 1999a. Dansgaard–Oeschger and Heinrich event imprints in the Alboran Sea paleotemperatures. Paleoceanography 14, 698–705.

Cacho, I., Pelejero, C., Grimalt, J. O., Calafat, A. M., Canals, M., 1999b. C37 alkenone measurements of sea surface temperature in the Gulf of Lions (NW Mediterranean). Org. Geochem. 33, 557– 566.

Cacho, I., Grimalt, J. O., Sierro, F. J., Shackleton, N. J., Canals, M., 2000. Evidence of enhanced Mediterranean thermohaline circulation during rapid climatic coolings. Earth Planet. Sci. Lett. 183, 417–429.

Cacho, I., Grimalt, J. O., Canals, M., Sbaffi, L., Shackleton, N. J., Schònfeld, J., Zahn, R., 2001. variability of the western Mediterranean Sea surface temperatures during the last 25,000 years and its connection with the northern hemisphere climatic changes. Paleoceanography 16, 40– 52.

Capotondi, L., Borsetti, A. M., Morigi, C., 1999. Foraminiferal ecozones, a high resolution proxy for the late Quaternary biochronology in the central Mediterranean Sea. Marine Geology 153, 253-274.

Caron, D. A. and Bé, A. W. H., 1984. Predicted and observed feeding rates of the spinose planktonic foraminifer Globigerinoides sacculifer. B. Mar. Sci., 35, 1–10.

Casford, J. S. L., Rohling, E. J., Abu-Zied, R. H., Cooke, S., Fontanier, C., Leng, M. and Lykousis, V., 2002. Circulation changes and nutrient concentrations in the late Quaternary Aegean Sea: A nonsteady state concept for sapropel formation. Paleoceanography, 17, 1024, DOI:10.1029/2000PA000601.

Casford, J. S. L., Abu-Zied, R. H., Rohling, E. J., Cooke, S., Fontanier, C., Leng, M. J., Millard, A. and Thomson, J., 2007. A stratigraphically controlled multiproxy chronostratigraphy for the eastern Mediterranean. Paleoceanography, 22, PA4215, DOI:10.1029/2007PA001422.

Castradori, D,. 1993. Calcareous nannofossil biostratigraphy and biochronology in eastern Mediterranean deep-sea cores. Rivista Italiana di Paleontologia e Stratigrafia 99, pp. 107–126.

Conforti, A., 2003. Stratigrafia integrata della sequenza Tardo–Quaternaria del settore settentrionale del Golfo di Salerno e di quello meridionale del Golfo di Napoli. PhD Thesis, University of Naples Federico II, 144 pp.

Cramp, A. and O'Sullivan, G., 1999. Neogene sapropels in the Mediterranean: a review. Mar. Geol**.** 153, pp. 11–28.

Crowley, T. J., & Lowery, T. S., 2000. How warm was the Medieval Warm period? A comment on man-made versus natural climate change. Ambio, 39, 51.

Degens, E. T., Wong, H. K., Kempe, S., Kurtman, F., 1984. A geological study of Lake Van, eastern Turkey. Geol. Rundsch. 73, 701-734.

Deino, A., Orsi, G., de Vita, S., Piochi, M., 2004. The age of Neapolitan Yellow Tuff caldera-forming eruption (Campi Flegrei caldera—Italy) assessed by $^{40}Ar/^{39}Ar$ dating method. J. Volcanol. Geotherm. Res. 133, 157–170.

De Rijk, S., Rohling, E. J. and Hayes, A., 1999. Onset of climatic deterioration in the eastern Mediterranean around 7 ky BP; micropalaeontological data from Mediterranean sapropel interruptions. Marine Geology, 153, 337-343.

Di Donato, V., Esposito, P., Russo Ermolli, E., Scarano, A., Cheddadi, R., 2008. Coupled atmospheric and marine palaeoclimatic reconstruction for the last 35 ka in the Sele Plain-Gulf of Salerno area (southern Italy). Quaternary International, this volume, doi:10.1016/j.quaint.2008.05.006.

Ducassou, E., Capotondi L., Murat , A., Bernasconi, S. M., Mulder, T., Gonthier, E., Mignon, S., Duprat, J., Giraudeau, J., Mascle, J., 2007. Multiproxy Late Quaternary stratigraphy of the Nile deep-sea turbidite system. Towards a chronology of deep-sea terrigeneous systems. Sedimentary Geology 200, 1–13.

Frignani, M., Langone, L., 1991. Accumulation rates and ^{137}Cs distribution in sediments off the Po River delta and the Emilia- Romagna coast (northwestern Adriatic Sea, Italy). Cont. Shelf Res. 11, 525– 542.

Frignani, M., Langone, L., Ravaioli, M., Sorgente, D., Alvisi, F., Albertazzi, S., 2005. Fine-sediment mass balance in the western Adriatic continental shelf over a century time scale. Marine Geology 222–223, 113–133.

Frignani, M., Sorgente, D., Langone, L., Albertazzi, S., Ravaioli, M., 2004. Behavior of Chernobyl radiocesium in sediments of the Adriatic Sea offshore the Po River delta and the Emilia-Romagna coast. Journal of Environmental Radioactivity 71, 299– 312.

Frumkin, A., Magaritz, M., Carmi I. and Zak, I., 1991. The Holocene climatic record of the salt caves of Mount Sedom. Israel. Holocene 1, 191–200.

Giordani, P., Hammond, D. E., Berelson, W. M., Montanari, G., Poletti, R., Milandri, A., Frignani, M., Langone, L., Ravaioli, M., Rovatti, G., Rabbi, E., 1992. Benthic fluxes and nutrient budgets for sediments in the Northern Adriatic Sea: burial and recycling efficiencies. The Science of the Total Environment, Supplement pp. 251–275.

Giunta S., Negri, A., Morigi, C., Capotondi, L., Combourieu Nebout, N., Emeis, K. C., Sangiorgi, F. and Vigliotti, L., 2003. Coccolithophorid ecostratigraphy and multi-proxy paleoceanographic reconstruction in the Southern Adriatic Sea during the last deglacial time (Core AD91-17). Palaeogeography, Palaeoclimatology, Palaeoecology, 190, 39-59.

Hemleben, C., Spindler, M., Anderson, O. R., 1989. Modern Planktonic Foraminifera. Springer pp 363.

Hughes, M. and Diaz, H., 1994. Was there a "Medieval Warm Period", and if so, where and when?. Clim. Change, 26, 109–142.

Jorissen, F. J., Asioli, A., Borsetti, A. M., de Visser, L., Hilgen,J. P., Rohling, E. J., van der Borg, K., Vergnaud-Grazzini, C., Zachariasse, W. J., 1993. Late

Quaternary central Mediterranean biochronology. Marine Micropaleontology 21, 169189.

Incarbona, A., Di Stefano, E., Patti, B., Pelosi, N., Bonomo, S., Mazzola, S., Sprovieri, R., Tranchida, G., Zgozi, S. and Bonanno, A., 2008. Holocene millennial-scale productivity variations in the Sicily Channel (Mediterranean Sea). Paleoceanography, 23, PA3204, doi:10.1029/2007PA001581.

Insinga, D., Molisso, F., Lubritto, C., Sacchi, M., Passariello, I., Morra, V., 2007. The proximal marine record of Somma–Vesuvius volcanic activity in the Naples and Salerno bays, Eastern Tyrrhenian Sea, during the last 3 kyrs. Journal of Volcanology and Geothermal Research doi:10.1016/j.jvolgeores.2007.07.011.

Iorio, M., Sagnotti, L., Angelino, A., Budillon, F., D'Argenio, B., Turell Dinares, J., Macrı`, P., Marsella, E., 2004. High-resolution petrophysical and paleomagnetic study of late-Holocene shelf sediments, Salerno Gulf, Tyrrhenian Sea. Holocene 14, 433442.

Issar, A. S. 1990. Water Shall Flow from the Rock. Springer-Verlag, Heidelberg.

Issar, A. S., Govrin, Y., Geyh, M. A., Wakshal E. and Wolf, M., 1992. Climate changes during the upper Holocene in Israel. Israel Journal of Earth Sciences 40, 219–223.

Lamb, H. H., 1982. Climate, History and the Modern World. Methuen, London, 387pp.

Lirer, F., Sprovieri, M., Pelosi, N., Ferraro, L., 2007. Clues of solar forcing from a 2000 years long sedimentary record from the eastern tyrrhenian margin. Clima e cambiamenti climatici: le attività di ricerca del CNR pp. 209212.

Luterbacher, J., Xoplaki, E., Casty, C., Wanner, H., Pauling, A., Kùttel, M., Rutishauser, T., Brònnimann, S., Fischer, E., Fleitmann, D., Gonzàlez-Rouco, F. J., Garcìa-Herrera, R., Barriendos, M., Rodrigo, F., Gonzalez-Hidalgo, J. C., Saz, M. A., Gimeno, L., Ribera, P., Brunet, M., Paeth, H., Rimbu, N., Felis, T., Jacobeit, J., Dù nkeloh, A., Zorita, E., Guiot, J., Tùrkes, M., Alcoforado, M. J.,

Trigo, R., Wheeler, D., Tett, S., Mann, M. E., Touchan, R., Shindell, D. T., Silenzi, S., Montagna, P., D.,Camuffo, Mariotti, A., Nanni, T., Brunetti, M., Maugeri, M., Zerefos, C., De Zolt, S., Lionello, P., Nunes, M. F.,Rath, V., Beltrami, H., Garnier, E. and Le Roy Ladurie, E., 2006. Mediterranean Climate Variability. Chapter1: Mediterranean Climate Variability Over the Last Centuries: A Review. In: the Mediterranean Climate: an Overview of the main characteristics and issues. Eds. Lionello, P., Malanotte-Rizzoli, P., and Boscolo, R., Elsevier, Amsterdam, the Netherlands, 27-148.

Maasch, K. A., Mayewski, P. A., Rohling, E. J., Stager, J. C., Karlen, W., Meeker, L. D. and Meyerson, E. A.,2005. A 2000 year context for modern climate change. Geografiska Annaler, 87A, 7-15.

Mayewski, P. A., Rohling, E. J., Stager, J. C., Karlen, W., Maasch, K. A., Meeker, L. D., Meyerson, E. A., Gasse, F., van Kreveld, S., Holmgren, K., Lee-Thorp, J., Rosqvist, G., Rack, F., Staubwasser, M., Schneider, R. R. and Steig, E. J., 2004. Holocene climate variability. Quaternary Research, 62, 243-255.

Mercone, D., Thomson, J., Croudace, I. W., Siani, G., Paterne, M. and Troelstra, S., 2000. Duration of S1, the most recent sapropel in the eastern Mediterranean Sea, as indicated by accelerator mass spectrometry radiocarbon and geochemical evidence. Paleoceanography, 15, 336-347.

Mulitza, S., Wolff, T., Pätzold, J., Hale W. and Wefer, G., 1998. Temperature sensitivity of planktic foraminifera and its influence on the oxygen isotope record, Marine Micropalaeontology 33 pp. 223–240.

Myers, P. G. and Rohling, E. J., 2000. Modelling a 200 year interruption of the Holocene sapropel S1. Quaternary Research, 53, 98-104.

Negri, A. and Giunta, S., 2001. Calcareous nannofossil paleoecology in the sapropel S1 of the eastern Ionian Sea: Paleoceanographic implications. Palaeogeography Palaeoclimatology Palaeoecology 169, 101-112.

Pérez-Folgado, M., Sierro, F. J., Flores, J. A., Cacho, I., Grimalt, J. O., Zahn, R., Shackleton, N. 2003. Western Mediterranean planktonic foraminifera events and millennial climatic variability during the last 70 kyr. Marine Micropaleontology, 48, 1-2, 49-70.

Piva, A., Asioli, A., Trincardi, F., Schneider, R. R., Vigliotti, L., 2008. Late-Holocene climate variability in the Adriatic Sea (Central Mediterranean). The Holocene 18 153 DOI: 10.1177/0959683607085606.

Principato, M. S., Giunta, S., Corselli, C., Negri, A., 2003. Late Pleistocene-Holocene planktonic assemblages in three box-cores from the Mediterranean Ridge area (west-southwest of Crete): palaeoecological and palaeoceanographic reconstruction of sapropel S1 interval. Palaeogeography, Palaeoclimatology, Palaeoecology 62 190, 6177.

Pujol, C. and Vergnaud Grazzini, C., 1995: Distribution patterns of live planktic foraminifera as related to regional hydrography and productive systems of the Mediterranean sea. Marine. Micropaleontology 25, 187–217.

Reynolds, L., and Thunell, R. C., 1985. Seasonal succession of planktonic foraminifera in the subpolar North Pacific. J. Foraminiferal Res., 15:282-301.

Reynolds, L. A. and Thunell, R. C., 1989. Seasonal succession of planktonic foraminifera: results from a four year time series sediment trap experiment in the northeast Pacific. J. Foraminiferal Res. 19, 253-267.

Robbins, J. A., 1978. Geochemical and geophysical application of radioactive lead. In: Nriagu, J.O. (Ed.), The Biogeochemistry of Lead in the Environment. Elsevier, Amsterdam, pp. 285– 393.

Rohling, E. J., Jorissen, F. J. and De Stigter, H. C., 1997. A 200 Year interruption of Holocene sapropel formation in the Adriatic Sea. Journal of Micropaleontology, 16, 97-108.

Rohling, E. J., Mayewski, P. A., Hayes, A., Abu-Zied, R. H. and Casford, J. S. L., 2002a. Holocene atmosphere-ocean interactions: records from Greenland and the Aegean Sea, Climate Dynamics, 18, 587-593.

Rohling, E. J., and Pälike, H., 2005. Centennial-scale climate cooling with a sudden cold event around 8,200 years ago. Nature, 434, 975-979.

Rolandi, G., Petrosino, P., Mc Geehin, J., 1998. The Interplinian activity at Somma–Vesuvius in the last 3500 years. J. Volcanol. Geotherm. Res. 82, 19–52.

Sacchi, M., Insinga, D., Milia, A., Molisso, F., Raspini, A., Torrente, M.M., Conforti, A., 2005. Stratigraphic signature of the Vesuvius 79 AD event off the Sarno prodelta system, Naples Bay. Marine Geology 222–223, 443–469.

Sangiorgi, F., Capotondi, L., Combourieu Nebout, N., Vigliotti, L., Brinkhuis, H., Giunta, S., Lotter, A. F., Morigi, C., Negri, A., and Reichart, G. J.,2003. Holocene seasonal sea-surface temperature variations in the southern Adriatic Sea inferred from a multiproxy approach. Journal of Quaternary Science, 18, 723-732.

Sbaffi,L., Wezel,F. C., Kallel, N., Paterne,M.,Cacho,I., Ziveri,P., Shackleton,N., 2001. Response of the pelagic environment to paleoclimatic changes in the central Mediterranean Sea during the Late Quaternary. Marine Geology 178, 39-62.

Schiebel, R., Hiller, B., Hemleben, C., 1995. Impacts of storms on recent planktic foraminiferal test production and CaCO3 flux in the north Atlantic at 47°N, 20°W (JGOFS). Marine Micropaleontology 26, 115–129.

Schiebel, R. and Hemleben, C., 2000. Interannual variability of planktonic foraminiferal populations and test flux in the eastern North Atlantic Ocean (JGOFS), Deep-Sea Research II **47**, 1809–1852.

Schilman, B., Almogi-Labin, A., Bar-Matthews, M., Labeyrie, L., Paterne M. and Luz, B., 2001. Long- and short-term carbon fluctuations in the Eastern. Mediterranean during the late Holocene. Geology 29, 1099–1102.

Schoell, M., 1978. Oxygen isotope analysis on authigenic carbonates from Lake Van sediments and their possible bearing on the climate of the past 10,000 years. In: Degens, E.T. (Ed.), The Geology of Lake Van, Kurtman. The Mineral Research and Exploration Institute of Turkey, Ankara, pp. 92-97.

Siani G., Paterne, M., Miche, E., Sulpizio, R., Sbrana, A., Arnold, M., Haddad, G., 2001. Mediterranean sea surface radiocarbon reservoir age changes since the Last Glacial Maximum. Science, 294, 1917-1920.

Sierro, F. J., Krijgsman, W., Hilgen, F. J., Flores, J. A., 2001. The Abad composite (SE Spain): Mediterranean reference section for the Messinian and the Astronomical Polarity Time Scale (APTS). Palaeogeography Palaeoclimatology Palaeoecology 168, 143–172.

Sprovieri R., Di Stefano E., Incarbona A., Gargano M. E., 2003. A high-resolution of the last deglaciation in the Sicily Channel based on foraminiferal and calcareous nannofossil quantitative distribution. Palaeogeography, Palaeoclimatology, Palaeoecology 202, 119-142.

Stuiver, M., Reimer, P. J., Bard, E., Beck, J. W., Burr, G. S., Hughen, K. A., Kromer, B., McCormac, F. G., van der Plicht, J. and Spurk. M., 1998. INTCAL98 Radiocarbon age calibration 24,000 - 0 cal BP. Radiocarbon, 40,1041-1083.

Trenberth, K. E., Editor, 1992. Climate System Modeling, C.U.P., p. 772.

Trincardi, F. and Field, M. E., 1991. Geometry, lateral variation, and preservation of downlapping regressive shelf deposits: eastern Tyrrhenian Sea margin, Italy. J. Sediment. Petrol. 61, 775–790.

Turney, C. S. M., Blockley, S. P. E., Lowe, J. J., Wulf, S., Branch, N. P., Mastrolorenzo, G., Swindle, G., Nathan, R., Pollard, A. M., 2008. Geochemical characterization of Quaternary tephras from the Campanian Province, Italy . Quaternary International 178, 288–305.

Weninger, B., Jöris, O. and Danzeglocke, U., 2004. Calpal-the Cologne radiocarbon CALibration and PALeoclimate research package (http://www.calpal.de).

Wolf-Welling, T.C.W., Cowan, E. A., Daniels, J., Eyles, N., Maldonado, A., Pudsey, C. J., 2001. Diffuse spectral reflectance data from rise Sites 1095, 1096, 1101 and Palmer Deep Sites 1098 and 1099 (Leg 178, Western Antarctic Peninsula). In: Barker, P.F., Camerlenghi, A., Acton, G.D., Ramsay, A.T.S. (Eds.), Proceeding Ocean Drilling Program, Scientific Results, 178, 1-22.

Chapter 6

INTEGRATED STRATIGRAPHIC RECONSTRUCTION FOR THE LAST 80 KYR IN A DEEP SECTOR OF THE SARDINIA CHANNEL (WESTERN MEDITERRANEAN)

Based on:

Budillon F.[(1)], Lirer F.[(1)], Iorio M.[(1)], Macrì P.[(2)], Sagnotti L.[(2)], **Vallefuoco M.**[(1)], Ferraro L.[(1)], Garziglia S.[(3)], Innangi S.[(1)], Sahabi M.[(4)], Tonielli R.[(1)]

1) Istituto per l'Ambiente Marino Costiero, IAMC, Consiglio Nazionale delle Ricerche, Calata Porta di Massa 80, I-80133 Napoli, Italy

2) Istituto Nazionale di Geofisica e Vulcanologia, INGV, Via di Vigna Murata 605, I-00143 Rome, Italy

3) Géosciences-Azur, CNRS, BP 48,Fr-06235,Villefranche sur Mer, France

4) Faculté des Sciences, BP 20, 24000 El Jadida, Morocco

Published in Deep Sea RsearchII, 2008, in press

ABSTRACT

A quantitative analysis of planktonic foraminifera, coupled with petrophysical and paleomagnetic measurements and ^{14}C-AMS calibrations, was carried out on a deep core recovered in the Sardinia Channel (Western Mediterranean Sea), during the CIESM Sub2 survey, providing an integrated stratigraphic time-framework over the last 80 kyr.

Significant changes in the quantitative distribution of planktonic foraminifera allowed the identification of several eco-bioevents useful to accurately mark the boundaries of the eco-biozones widely recognised in the Western Mediterranean records and used for large-scale correlations. Namely, 10 eco-biozones were identified based on the relative abundance of selected climate sensitive planktonic foraminiferal species. Sixteen codified eco-bioevents were correlated with the Alboran Sea planktonic foraminiferal data and four climatic global events (Sapropel S1, Younger Dryas, Greenland Isotope Interstadial 1, Greenland Isotope Stadial 2, Heinrich events H1-H6) were recognized.

The eco-bioevents together with the ^{14}C AMS calibrations allowed us to define an accurate age model, spanning between 2 and 83 kyr cal. BP. The reliability of the age model was confirmed by comparing the colour reflectance (550 nm%) data of the studied record with the astronomically tuned record from the Ionian Sea (ODP-Site 964). A mean sedimentation rate of about 7 cm/kyr included three turbidite event beds that were chronologically constrained within the relative low stand and regressive sea-level phases of the MIS 4 and MIS 3. The deep-sea sedimentary record includes a distinct tephra occurring at the base of the core that dates 79 ka.

The paleomagnetic data provide a well-defined record of the characteristic remanent magnetization that may be used to reconstruct the geomagnetic paleosecular variation for the Mediterranean back to 83 kyr. BP.

Key words: integrated stratigraphy, late Neogene marine record, eco-bio-events, reflectance 550 nm %, Sardinia Channel, Western Mediterranean.

6.1 INTRODUCTION

Since climate excursions recorded in Northern Hemisphere in the Greenland GISP and GRIP ice cores (GRIP members, 1993) over the last 100 kyr had more or less synchronous effects in the Mediterranean area, many researches have focused on Mediterranean marine cores, with the aim to detect their intensity and the impact on the marine environment. During the last glacial period the Mediterranean region experienced rapid modifications in hydrographic conditions in response to fast climatic excursions, such as Heinrich events (HE) and Dansgaard-Oeschger (D-O) Stadials (cold) and Interstadials (warm) (Heinrich, 1988; Dansgaard et al., 1993). In particular, Rohling *et al*. (1998) and Cacho *et al*. (1999, 2000) have proved that the millennial scale D-O and HE directly control the winds and precipitation system on the northern Mediterranean basin. Even during the Holocene the principal climatic events and oscillations of the northern Hemisphere have been clearly traceable in different sectors of the Mediterranean basin sedimentary records (Cacho *et al.*, 1999, 2000, 2001; Rohling *et al*., 2002; Sprovieri *et al.,* 2003, 2006; Perez-Folgado et al., 2003, 2004; Geraga et al., 2005). A very detailed outline of the paleo-environmental changes and their control on marine communities, calibrated by several independent proxies (tephra, sapropel, ^{14}C geochronology), is now available for the Mediterranean area (Buccheri et al., 2002; Ducassou et al., 2007; Emeis et al., 2003; Narcisi and Vezzoli, 1999; Lourens, 2004; Principato et al., 2003; Rohling et al., 2003; Sangiorgi et al., 2006; Sprovieri et al., 2003; 2006, and reference therein). Several codified eco-bioevents, if clearly detected in marine records, can be used as tie points to chronologically constrain the late Pleistocene-Holocene Mediterranean marine sequences. Nevertheless, even if many reference records are available from deep-sea sites, most of them span a short time interval and lack a high resolution detail of the paleo-environmental and paleo-ecological changes before 40 kyr BP. Recently, Perez-Folgado et al. (2003, 2004) carried out a high-resolution study of the tuned ODP-Site 977, located in the western

part of the Alboran Sea, and identified several planktonic foraminiferal eco-bioevents that occurred during the marine isotope stages (MIS) 1-5. These eco-bioevents represent the best tool to correlate deep marine records from different Mediterranean sites.

Many recent studies emphasize the challenge when studying deep-sea records to establish a reliable chronology, even for the deposition of turbidites (Walker 1992; Beaudouin et al., 2004; Ducassou et al., 2007) and underline the utility to support conventional dating methodologies with different constraints. It is widely accepted that one of the main factors controlling and enhancing turbidite deposition along deep-sea fan is the regression and low stand of sea-level, whereas sea-level rise and highstand phases reduce terrigenous supply to deep-sea systems (Walker et al., 1992; Richards et al., 1998; Normark et al., 1998).

The CIESM core C08 is located at the mouth of the Bizerte Canyon in the Sentinelle Valley in a key position of paleoceanographic and geological significance (Fig. 6.1). The Sardinia Channel connects the Alboran to the Tyrrhenian Basin and offers a stratigraphic record with the potential to link the eco-stratigraphic and paleoceanographic observations between the Western, the Central and Eastern Mediterranean late Pleistocene-Holocene marine records (Perez-Folgado et al., 2004; Sbaffi et al., 2004; Geraga et al., 2005; Asioli et al., 2001; Ariztegui et al., 2000). In fact, a portion of the Modified Atlantic Water (MAW) coming from the Strait of Gibraltar (Bryden and Kinder, 1991), diverges from the part that enters the Eastern Mediterranean and flows through the Sardinia Channel into the Tyrrhenian Sea along the northern Sicilian coast (Millot, 1987), forming a secondary circulation gyre. The circulation system in this sector of the Tyrrhenian Sea is counter-clockwise, with the Levantine Intermediate Water (LIW) inflows lapping on the northern Sicilian coast and the outflow occurring along the eastern Sardinia coast (Pinardi and Masetti, 2000 and references therein). The core site is also in a strategic position to check the efficiency of a submarine canyon in driving density flow to the deep-sea environment (see below), even if not directly connected to any emerged sector nor to continental shelf areas

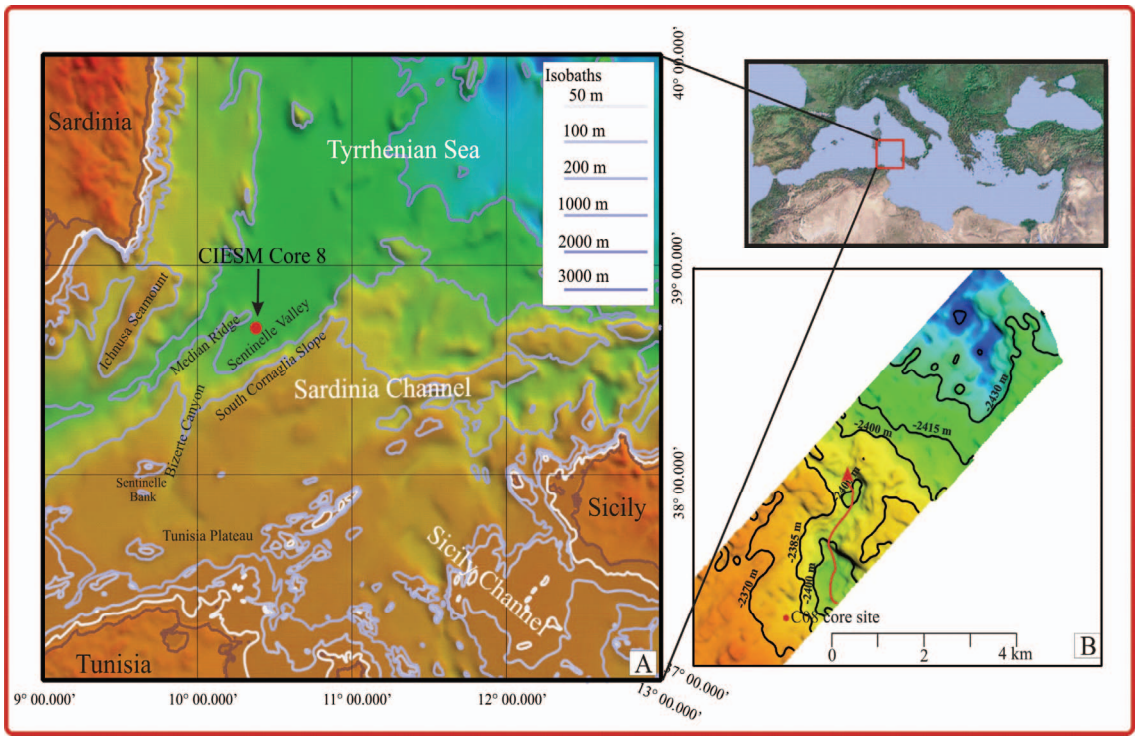

Fig. 6.1 A) Location map of CIESM core **C08**. Bathymetry from The General Bathymetric Chart of the Oceans (GEBCO, 1997); B) bathymetric detail of core site, close to a channel South-North oriented (red arrow).

(Reading and Richards, 1994). Thus the possibility that such a type of canyon would form a fan can be evaluated, even verifying the significance and the timing of the turbidite deposition.

The aim of this study is to provide a record of integrated stratigraphic data spanning back to about 80 kyr, relatively to a deep basin area, based on eco-biozones, ^{14}C-dated ages, event stratigraphy, lithostratigraphy, petrophysical properties and paleomagnetic measurements. Furthermore, the reliability of the reflectance parameter 550 nm % is evaluated as an independent correlation tool for tuning marine records.

6.2 GEOLOGICAL SETTING

Core C08 was collected in the Sentinelle Valley of the Sardinia Channel, 55 km from the mouth of the Bizerte Canyon, equidistant from Sicily, Sardinia and Tunisia (Fig. 6.1), during the cruise CIESM Sub2 onboard the R/V Urania in December 2005 (38°38.5364'N, 10°21.5576'E - 2370 m water depth). In this area a 400 km long submerged sector of the Apennine-Maghrebian branch of the Alpine orogen separates the Tyrrhenian (Plio-Pleistocene in age) and the Algero Provencąl (Miocene in age) oceanic basins. This sector of the chain was not completely fragmented during the opening of the basins (Mascle et al., 2004). Due to the relatively minor post-orogenic extension and the good preservation of morpho-structural features, the Sardinia Channel is an important area for the reconstruction of the geodynamic evolution of the Western Mediterranean sector and was recently investigated through submersible surveys (Mascle et al., 2001a; Mascle et al., 2004). The triangular-shaped valley is bounded by a NE-SW-oriented Median Ridge on its north-western side and by the South Cornaglia slope to the south-east. The south-western sector of the Sentinelle Valley receives the sedimentary contribution from the Bizerte Canyon, which cuts the Tunisian Plateau and the south margin of the Sentinelle Bank (Mascle et al., 2001b). The canyon head appears disconnected from the Tunisian shelf margin and extends over an area of about 1000 km^2 at an average depth of about 500 m (Fig. 6.1). It represents a particular type of canyon since it is not fed by an emerged areas or by a fluvio-deltaic systems (Reading and Richards, 1994; Prins et al., 2000; Kenyon et al., 2002;), but it drains a wide submarine plateau.

6.3 MATERIAL AND METHODS

The gravity corer entered the uppermost portion of a sedimentary sequence made up with lateral continuous parallel and thin reflectors (Sartori et al., 2001), possibly related

to hemipelagic and turbiditic deposition. It recovered about 5.40 m of hemipelagic mud interlayered with three fine-to-medium sand turbidite layers of increasing thickness towards the top of the core (Fig. 6.2).

6.3.1 Physical property measurements

The physical properties of the core were measured at 1-cm steps in a fully automated GEOTEK Multi-Sensor Core Logger (MSCL), in the petrophysical laboratories of IAMC in Naples (Italy). The MSCL system includes a Bartington MS2E Point sensor, to measure the low-field magnetic susceptibility (MS) with a spatial resolution of 0.4 cm and a Minolta Spectrophotometer CM 2002 that records at 0.8-cm steps, the percentage of reflected energy (RSC) at 31 wavelengths in 10-nm steps, over the visible spectrum (from 400 to 700 nm). MS and RSC measurements were taken on the archive half, ~1 h after the core had been split. The split core was covered with cling film to protect the glass cover of the Minolta aperture while measuring. Both measurements, log plotted, were visually compared in order to detect similar trends and tentatively group the data according to their physical properties and corresponding stratigraphy (Wolf-Welling et al., 2001).

6.3.2 Paleomagnetic analysis

For the paleomagnetic study, 1-m-long u-channel specimens were sampled from archive halves of the CIESM 08 core. Only the turbiditic sandy interval at 182-208 cm depth was not suitable for u-channel sampling due to its coarse-grained and unconsolidated texture. The u-channels, sampled from the archive sections of the core, were measured in a magnetically shielded room at the paleomagnetic laboratory at the Istituto Nazionale di Geofisica e Vulcanologia in Rome, using an automated pass through a 2-G Enterprises DC SQUID cryogenic magnetometer system. For each u-channel the natural remanent magnetization (NRM) was measured at 1-cm steps. It is emphasized however, that, due to the intrinsic response functions of the SQUID sensors, remanence measurements may be considered truly independent only every ca. 5 cm. The NRM was progressively

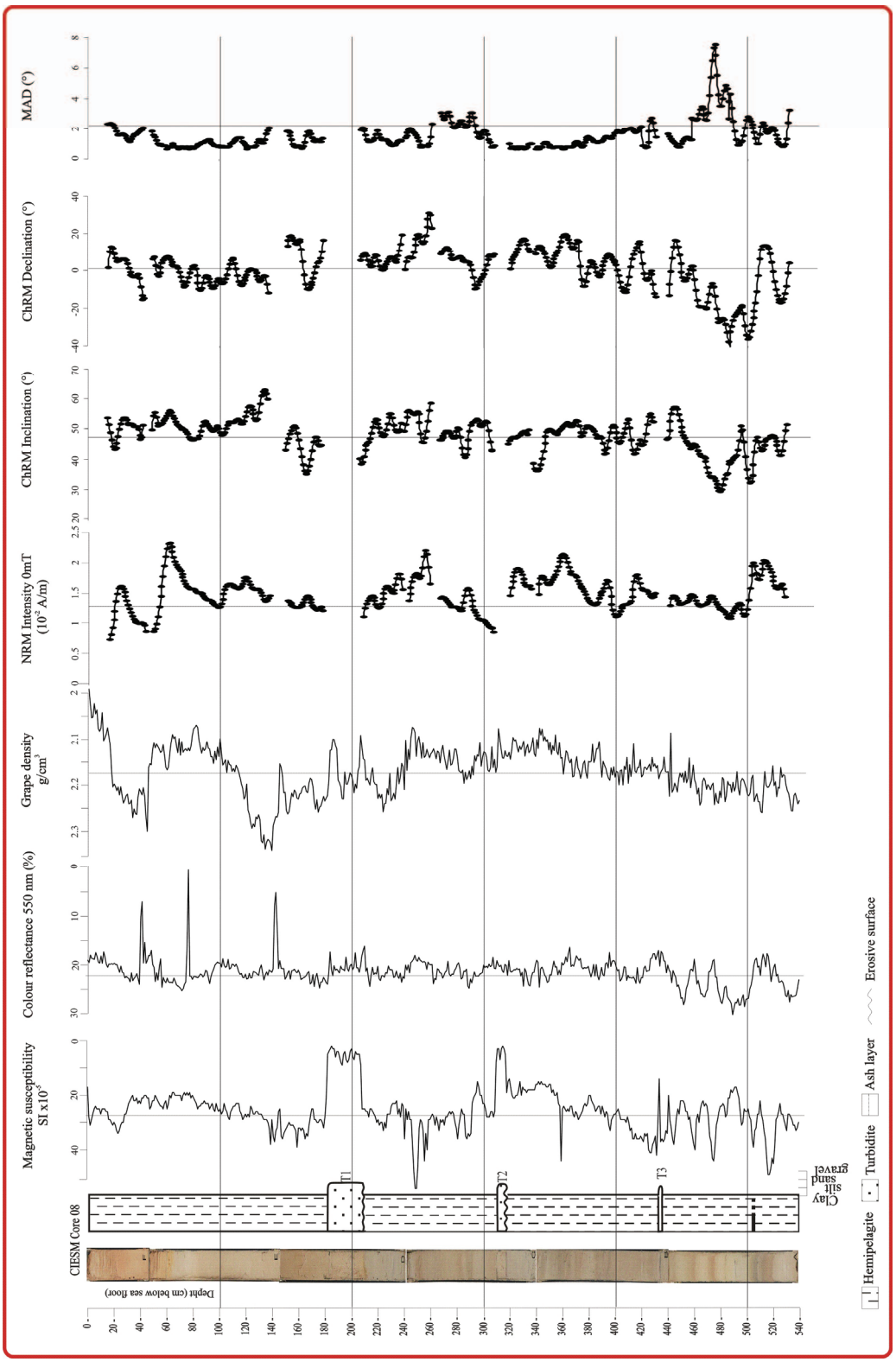
MAD (°)
ChRM Declination (°)
ChRM Inclination (°)
NRM Intensity 0mT (10⁻² A/m)
Grape density g/cm³
Colour reflectance 550 nm (%)
Magnetic susceptibility SI x10⁻⁶
CIESM Core 08
T1
T2
T3
Depth (cm below sea floor)
Clay
silt
sand
gravel
Hemipelagite
Turbidite
Ash layer
Erosive surface

Fig. 6.2 Core CIESM **C08**: photography, lithologic log, petrophysical properties curves (magnetic susceptibility, Grape density, reflectance 550 nm%), paleomagnetic measurements curves (Normalized intensity, **ChRM** inclination, **ChRM** declination, **MAD**) plotted against depth (cm below sea floor). In the paleomagnetic curves each dot represents a single measurement taken at 1-cm spacing. **NRM**: natural remanent magnetization; **ChRM**: characteristic remanent magnetization determined by principal component analysis on the demagnetization data; **MAD**: maximum angular deviation. The piston core was not azimuthally oriented, but a fiducial mark ensured the reciprocal orientation of each section from which u-channels were collected. The declination of each u-channel was rotated to bring the average value at 0°.

demagnetized by the alternating field (AF) in nine steps up to a maximum field peak of 100 mT, by translating the u-channel through a set of three perpendicular AF coils at a speed of 10 cm/s. The remanence was measured at the same 1-cm spacing after each demagnetization step. Demagnetization data from u-channels were analysed on orthogonal vector projections and the paleomagnetic data obtained generally provided straightforward demagnetization diagrams, indicating that the sediments carry an almost single-component NRM. In fact, during the AF demagnetization a complete removal of any coring overprint and/or laboratory-induced remanences was achieved at low AF peaks (10 mT), and the characteristic remanent magnetization (ChRMs) of the sediments was clearly identified and determined by principal component analysis (Kirschvink, 1980). For each u-channel the uppermost and lowermost few centimeters were disregarded for the paleomagnetic analysis, to avoid any deflection to the remanence direction due to disturbances that may have been introduced during sampling. As stated before, no paleomagnetic data were collected for the coarse-grained level at 181-207 cm depth, and the NRM demagnetization diagrams did not allow a clear identification of a ChRM at 137-151 cm and 309-317 cm depth intervals.

6.3.3 Planktonic assemblage analysis

The analysis of planktonic foraminifera was conducted on 216 samples. Sampling spacing was 2 cm from the top of the core down to the base. Each wet sample of about 20 g was dried at 50° C and washed over sieves with mesh-width size of 63 μm. Quantitative planktonic analysis were carried out on the fraction >125μm. The adopted taxonomic units were those reported by Jorissen et al. (1993), Capotondi et al. (1999). According to Jorissen et al. (1993) and Capotondi et al. (1999), we introduced some supraspecific categories (which remain unchanged even under bad preservation conditions), reducing the number of species actually occurring in the planktonic foraminiferal assemblages.

6.3.4 ^{14}C Radiocarbon calibrations

About 10 mg of *Globigerina bulloides* and *Globorotalia inflata* were picked from three samples in the first 2 m beneath the sea floor (at the core top, at 0.44 and 1.43 mbsf) and were AMS radiocarbon dated at the Centre for Isotopic Research on Cultural and Environmental Heritage (CIRCE) radiocarbon laboratory, Caserta, (Italy*)*. The CIRCE Accelerator Mass Spectrometry (AMS) system, based on the 3MV 9SDH-2 Pelletron accelerator, provides a mean overall precision of 0.63% (Terrasi et. al, in press). All radiocarbon dates were corrected using a reservoir age of 48 +/- 21 yr (a mean DR value calculated among six of the Tyrrhenian Sea) and calibrated using the marine data base and the CALIB 5.0 Program of Stuiver and Reimer (1993). The AMS RC age at 1.430 mbsf (21.590 ± 120 yr) close to the lower limit of the calibration curves, was not used for the age model.

6.4 RESULTS

6.4.1 Lithostratigraphy and petrophysical properties

The sediment consists for the 95 % of hemipelagic mud, ranging in colour from reddish and ochre to light, olive and dark grey, and for the remaining 5 % are turbiditic sand

layers (Fig. 6.2). The uppermost 0.50 m consists of a reddish mud pervasively oxidized, then about 0.11 m of alternating dark grey and ochre laminated mud, and further below, 0.05 m of fine laminated ochre mud occurs. From about 0.66 m down to 2.40 m olive grey mud occurs with rare dark patches, probably due to bioturbation, while from 2.40 m to the bottom of the core an alternation of several mud intervals occur, whose thickness range from centimeters to decimeters, showing different shades from light grey to dark grey. Three turbidite sand beds are interlayered in the mud sequence and occur from 1.82 to 2.08 m (T1), 3.10 to 3.17 m (T2), and 4.33 to 4.34 m (T3). They constitute the 5% of the whole stratigraphic thickness of the core and are all characterized by low values of magnetic susceptibility. The turbidite layer T1 is marked by a sharp erosive contact and consists of a thin layer of oxidized sand, and then of a massive fine to medium sand with a high percentage of shell fragments; the upper boundary is sharp and the grain-size populations comprised between fine sand and clay, which usually pertains to "b, c, d, e" divisions of the classical Bouma sequence (Bouma, 1962), are missing, as evidenced by the abrupt decrease of MS and Grape density values, which are a function of grain size and lithology. A sharp contact marks the onset of the turbidite layer T2, which contains a thin layer of well-sorted dark fine sand passing to a massive, well-sorted bioclastic fine sand; also in this case the upper boundary is sharp and the passage from massive and structureless sand to the hemipelagic mud is abrupt. Turbidite layer T3 has well-defined sharp boundaries and starts at the base with a thin layer of dark sand passing to light grey bioclastic sand. The thickness of the turbidites increases upward, but no sand layers occur in the uppermost 0.18 m of the core. A discrete fine ash layer, dark stained and characterized by diffuse boundaries occurs at 5.08 m and is marked by a MS peak value of 37 SI $x10^{-5}$. This tephra layer consists mainly of white pumices, dark green to yellowish glass shards, and few dark scorias, while lithic elements are scarce (Stella Tamburrino, pers. comm. 2007).

The lithologic features of the cored sediment are clearly detected by the petrophysical properties measured with at 1-cm steps: the volume magnetic susceptibility (MS) traces even thin tephra layers (Iorio et al., 2004), the GRAPE density is a compelling proxy for lithology and grain size (Wolf-Welling et al., 2001) and the reflectance at 550 nm % wavelength provides a quantitative evaluation of variations in sediment colour and can serve as a powerful correlation tool between long-distance core sites (Peterson et al., 2000). For instance, the meter composite depth of ODP-Sites records (ODP- Leg 154, Curry et al., 1995), is composed on the variation in natural gamma rays, reflectance and magnetic susceptibility parameters, to identify sedimentary patterns and to calibrate marine records to the standard variation of astronomical parameters (Lourens et al., 1998; Palike et al., 2006).

The three turbidites are well evidenced by low MS values (T1 and T2 measuring less than 5 SIx10^{-5}, T3 of 12 SI x10^{-5}) and by GRAPE density value (close to 2.1 gr/cm^3), but are not highlighted by RSC. The RSC parameter traces well the changes in shade colour throughout the core, and in particular it points out those occurring at the core top (due to the pervasive seabed sediment oxidation) and in the deepest 1.4 m (Fig. 6.2). Along this latter interval the wide oscillations in the RSC parameter, ranging between 15% and 30%, correspond to analogous oscillations in MS values**.**

6.4.2 Paleomagnetism

The main paleomagnetic results are plotted in Fig 6.2, which shows the stratigraphic trend of the NRM intensity, the ChRM inclination and declination and the maximum angular deviation (MAD). The NRM is weak and unstable in the topmost 0.15 m of the core and will not be discussed in the following. The data from below 0.15 m show that NRM intensity is relatively high and characterized by a limited variation, with values oscillating between 0.6 and 2.3 (10^{-2} A/m). The ChRM inclination oscillates from 30° to 60º with an average value of 48° that is ca. 10° lower than the expected value (58°) at the latitude of the coring site. Such a kind of shallow bias, or inclination error, has been found in laboratory redeposition experiments and in some modern natural sediments.

The sedimentary inclination shallowing is a well-known process linked to the deposition of magnetic particles and subsequent sediment compaction (see Tauxe and Kent, 1984; 2004; Arason and Levi, 1990; Deamer and Kodama 1990; Tan et al., 2003a; 2003b). The piston core was not azimuthally oriented, but a fiducial mark ensured the reciprocal orientation of each section from which u-channels were collected. The ChRM declination of each u-channel was rotated to bring the core average at 0°. Under this transformation the ChRM declination oscillates between -30° and + 30°, which is in the range of the expected geomagnetic secular variation. The principal component analysis of the demagnetization data shows a MAD always well below 3.3° along the core, which indicates a well-defined paleomagnetic direction, except a positive peak, up to a maximum of 7.5°, measured in the 0.47 – 0.48 m interval. This interval corresponds to the largest oscillations in the ChRM inclination and declination values, suggesting that some uncompensated lithological factor affects the paleomagnetic signal in that stratigraphic interval.

6.4.3 Quantitative distribution of planktonic foraminifera

A number of 13 species or groups of species were distinguished: *G. bulloides* (including extremely rare specimens of *G. falconensis)*; *G. quadrilobatus* (including *G. trilobus* and very subordinate *G. sacculifer)*; *G. ruber* (including white and pink varieties, the latter extremely rare), *G. elongatus* (very rare) and *G. gomitolus* (very rare); *Globorotalia truncatulinoides* sl. right (very rare) and left coiling; *G. tenellus* (rare); *Neogloboquadrina pachyderma* right and left coiling (extremely rare); *Globigerinita glutinata*; *Orbulina universa*; *Turborotalita quinqueloba*; *Globigerinatella siphoniphera* (rare) including *G. calida* (very rare); *Globoturborotalita rubescens* (rare). The planktonic foraminifera, characterized by modern assemblages, are abundant and well-preserved, and the percentages of foraminiferal fragments are very low and do not alter the composition of the planktonic assemblage.

The long-term trend in planktonic foraminifera reveal that the faunal composition of the studied interval does not show drastic changes in the abundance patterns (Fig. 6.3).

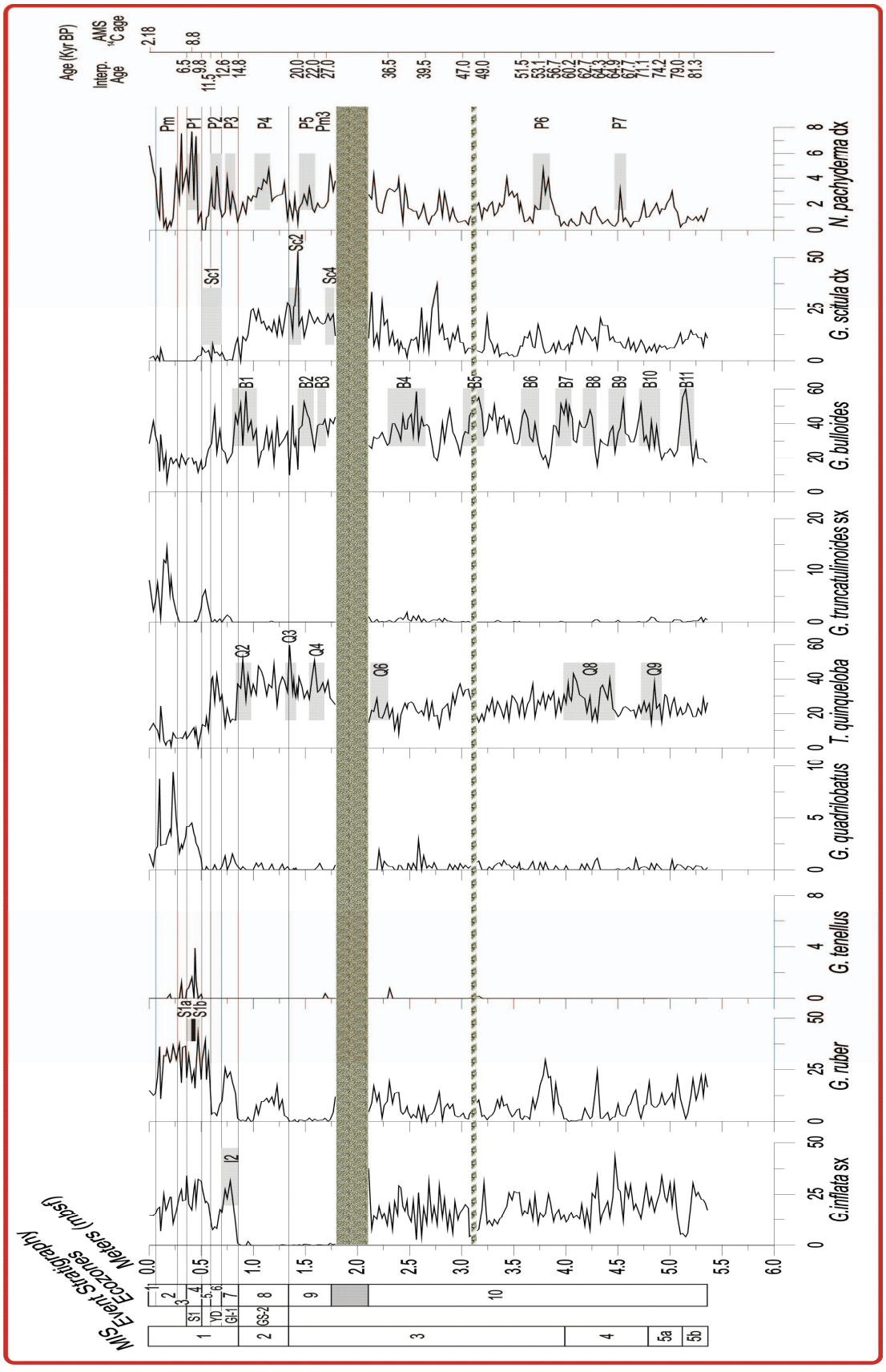
Age (Kyr BP)
Interp. Age
AMS ¹⁴C age
Pm
P1
P2
P3
P4
P5
Pm3
P6
P7
Sc1
Sc2
Sc4
B1
B2
B3
B4
B5
B6
B7
B8
B9
B10
B11
Q2
Q3
Q4
Q6
Q8
Q9
S1a
S1b
I2
N. pachyderma dx
G. sctula dx
G. bulloides
G. truncatulinoides sx
T. quinqueloba
G. quadrilobatus
G. tenellus
G. ruber
G.inflata sx
MIS Event Stratigraphy
Ecozones
Meters (mbsf)

Fig. 6.3 Relative abundance of selected planktonic foraminifera from core C08 plotted vs depth (m bsf). Eco-biozones 1-10 are identified, according to Sprovieri et al. (2003) slightly modified. Grey bands show the selected eco-bioevents proposed by Perez-Folgado et al. (2003, 2004). Event stratigraphy according to GRIP. MIS and age scale according to Perez-Folgado et al. (2003, 2004). Associated with the *G. ruber* curve, two grey bands interbedded with the black one correspond to the position of sapropel 1 equivalent with S1a and S1b. The two banded areas indicate the position of the turbidite layers.

In particular, among the taxa that have a continuous distribution patterns, *G. bulloides*, *G. ruber* gr., *G. inflata* left coiled, *G. scitula* right coiled, *G. glutinata*, *N. pachyderma* right coiled and *T. quinqueloba* show long-term oscillation (trend) superimposed on short-term fluctuations possibly related to high-frequency climatic oscillations (Fig. 6.3). Among the planktonic species having discontinuous distribution, *G. quadrilobatus* gr., *O. universa*, *G. truncatulinoides* left coiled, *G tenellus*, *G. rubescens* only occasionally reach significant percentages (Fig. 6.3).

6.5 DISCUSSION

6.5.1 Planktonic foraminiferal eco-biozonation

Significant changes in the quantitative distribution of the planktonic foraminifera species allowed several authors (Asioli et al., 1999, 2001; Capotondi et al., 1999; Casford et al., 2002; Principato et al., 2003; Sprovieri et al., 2003; Ducassou et al., 2007) to define eco-biozones useful for fine-scale subdividing of the stratigraphic record. The eco-biozone boundaries are characterized by the temporary appearance or disappearance and/or evident abundance peaks of different taxa. In the present work, we refer the stratigraphic record to a slightly modified eco-biostratigraphic classification by Sprovieri et al. (2003). At present, the eco-biostratigraphic classification of Sprovieri et al. (2003) proposes nine eco-biozones over the last 23 kyr. Here, we propose to mark

the base of eco-biozone nine with the strong increase of *G. inflata,* occurring in the Mediterranean area at about 30 kyr (Ducassou et al., 2007; Geraga et al., 2005), and to extend the eco-biozone 10 back to ~80 kyr. Actually, using the quantitative distribution pattern of the most abundant planktonic foraminifera species counted throughout the C08 core, we identified 10 evident eco-biozones from top to bottom (Fig. 6.3).

The uppermost part of the studied record attributed to the eco-biozone 1, which extend down to 0.08 m, is characterized by a decrease in abundance of *G. quadrilobatus* and the end of *G. truncatulinoides* right coiled. This attribution is also supported by a ^{14}C–AMS calibration, which dates 2.18 kyr cal. BP (Fig. 6.3; Tab. 6.1).

Eco-biozone 2 is defined by the concomitant abundance of *G. quadrilobatus* and *G. truncatulinoides* left and right coiled and by low abundance values of *N. pachyderma* right coiled in the lower part. Besides, the strong increase of *G. truncatulinoides* left coiled marks the base of the eco-biozone (Fig. 6.3).

The short interval represented by eco-biozone 3, whose base is at 0.31 m, is marked by the end of micropaleontological signature of sapropel S1 and is characterized by low abundances of *T. quinqueloba, G. quadrilobatus*, and *G. truncatulinoides* left coiled.

Eco-biozone 4 corresponds to the time interval of sapropel S1 deposition, although no lithological evidence was found, except for colour shades (Fig. 6.2). *G. ruber* oscillations allowed a reliable identification of the faunal signature of the climatic events associated with the deposition of sapropel S1 (Fig. 6.3). In particular, two distinct peaks in *G. ruber* mark the two short-term warm oscillations (S1a and S1b, Sprovieri et al., 2003), separated by a cold phase between them (Fig. 6.3). A ^{14}C-AMS datum at 0.44 m b.s.f. (within the cold phase) gives an age of 8.79 kyr cal. BP (Tab.6.1) coincident with an increase in abundance of *G. tenellus* and *G. quadrilobatus* (Sprovieri et al., 2003).

Eco-biozone 5 is defined by the concomitant occurrence of *G. ruber* and *G. inflata*, by a distinct peak of *G. truncatulinoides* left coiled, and by the absence of *N. pachyderma* right coiled and very low amounts of *T. quinqueloba*. The eco-biozone 6 is marked by

the absence of *G. ruber* and *G. inflata* left coiled, by distinct peaks of *T. quinqueloba* and *N. pachyderma* right coiled. This eco-biozone corresponds to the Younger Dryas event, according to Sprovieri et al., (2003). Eco-biozone 7 is defined by the increase in the abundance of *G. ruber* and *G. inflata*, by the absence of *T. quinqueloba,* and by a distinct peak of *G. quadrilobatus* corresponding to the warmer (interstadial) GI-1. According to Sprovieri et al., (2003) in the eco-biozone 8 the persistent high abundance of cold species permit correlation of this interval with the GRIP GS-2 period. In particular this eco-biozone is dominated by *T. quinqueloba*, *N. pachyderma* right coiled, *G. scitula,* and by absence of *G. inflata* left coiled and rare *G. ruber*. The base of this eco-biozone approximates to the base of MIS 2 (Pérez-Folgado et al., 2003) (Fig.6.3).
Eco-biozone 9 is characterized by the concomitant absence of *G. inflata* left coiled and *G. ruber*, by low abundance value of *N. pachyderma* right coiled, and by high abundance of *T. quinqueloba* and *G. scitula* right coiled. Eco-biozone 10 is clearly marked by the progressive downward increase in abundance of *G. inflata* left coiled and *G. ruber* and the progressive decrease of *G. scitula* right coiled, *T. quinqueloba*, *N. pachyderma* right coiled and *N. dutertrei* right coiled (Fig. 6.3). No distinctive or drastic events in the planktonic faunal patterns are visible towards the base of the studied record but only short-term oscillation in *G. bulloides* (B3-B11 eco-bioevents; the adopted sampling resolution unfortunately did not allow the recognition of the *G. bulloides* B8 eco-bioevent), *G. inflata* left coiled (I3-I5 eco-bioevents), *T. quinqueloba* (Q4-Q9 eco-bioevents) and *N. pachyderma* right coiled (P5-P7 eco-bioevents), clearly associated to the millennial climatic oscillations occurring in the last 80 kyr (Perez-Folgado et al., 2004). According to Perez-Folgado et al. (2004) *G. bulloides* eco-bioevents B7 and B10 are placed the MIS 4/MIS 3 and MIS4/MIS 5a transitions, respectively. Finally, also according to Perez-Folgado et al. (2004) the lowermost part of the studied record lies within the eco-bioevent B11 and within the uppermost part of MIS 5b (Fig. 6.3).

Events	mbsf	Age (Ka cal. BP)	References
AMS ^{14}C –	0	2,18	This work
Top S1	0,360	6,5	Casford et al. (2002) (Aegean Sea)
AMS ^{14}C –	0,440	8,8	This work
Base S1	0,470	9,8	Casford et al. (2002) (Aegean Sea)
TopYD	0,570	11,5	Asioli et al. (2001) (Adriatic Sea)
Base YD	0,700	12,6	Asioli et al. (2001) (Adriatic Sea)
Base GI-1	0,850	14,8	Asioli et al. (2001) (Adriatic Sea)
Base GS-2	1,350	20	Andersen et al. (2006) (Greenland Ice core)
AMS ^{14}C –	1,430	25,1	This work (not used in the age model)
Base B2	1.540	22	Perez-Folgado et al. (2003) (Alboran Sea)
Top B3	1.620	25.3	Perez-Folgado et al. (2004) (Alboran Sea)
Base B3	1.720	27	Perez-Folgado et al. (2003) (Alboran Sea)
Top B4	2,360	36,50	Perez-Folgado et al. (2004) (Alboran Sea)
Base B4	2,690	39.50	Perez-Folgado et al. (2004) (Alboran Sea)
Top B5	3.040	47,00	Perez-Folgado et al. (2004) (Alboran Sea)
Base B5	3,200	49,00	Perez-Folgado et al. (2004) (Alboran Sea)
Top B6	3,570	51,50	Perez-Folgado et al. (2004) (Alboran Sea)
Base B6	3,740	53,10	Perez-Folgado et al. (2004) (Alboran Sea)
Top B7	3,875	56,70	Perez-Folgado et al. (2004) (Alboran Sea)
Base B7	4.075	60,20	Perez-Folgado et al. (2004) (Alboran Sea)
Top B8	4.125	62.70	Perez-Folgado et al. (2004) (Alboran Sea)
Base B8	4.275	64.30	Perez-Folgado et al. (2004) (Alboran Sea)
Top B9	4.430	64,90	Perez-Folgado et al. (2004) (Alboran Sea)
Base B9	4.610	67,70	Perez-Folgado et al. (2004) (Alboran Sea)
Top B10	4,680	71,10	Perez-Folgado et al. (2004) (Alboran Sea)
Base B10	4,910	74,20	Perez-Folgado et al. (2004) (Alboran Sea)
Top B11	5.080	79,00	Perez-Folgado et al. (2004) (Alboran Sea)
Base B11	5.210	81,30	Perez-Folgado et al. (2004) (Alboran Sea)

Tab. 6.1 Tie-points used for age-depth profile of core **C08**. The *Globigerina bulloides* eco-bioevents **B3** to **B11** follow Perez-Folgado et al. (2003, 2004).

6.5.2 Age model

The identified foraminiferal marker events, regarded to reflect major changes in oceanographic conditions and already recognised in the Central and Western Mediterranean (Jorissen et al., 1993; Capotondi et al., 1999; Asioli et al., 2001; Sbaffi et

al., 2004; Sprovieri et al., 2003; Perez-Folgado et al., 2004; Geraga et al., 2005) were used, together with two ^{14}C–AMS dates (Tab. 6.1), to constrain the age of core CIESM C08 and strengthen the correlations between the various Mediterranean sites. In particular, we used the age model proposed by Perez-Folgado et al. (2003, 2004) for the Alboran Sea to recognize the top and base of the eco-bioevents recorded in the core C08, the age model proposed by Asioli et al. (2001) for the Adriatic Sea, to identify the Younger Dryas and the base of the Greenland isotope interstadial 1 (GI-1), and the age model of Andersen et al. (2006) for the N-GRIP record to distinguish the Greenland isotope stadial 2 (GS-2) (Tab. 6.1).

During the recovery of the core, a small amount of the core top may have been lost, which is seen by the ^{14}C – AMS dating of 2.18 kyr cal. BP at the top of the core and by comparing the planktonic foraminiferal contents of the studied record with those reported by Sprovieri et al. (2003) for ODP-Site 963 (Sicily Channel). This seems to confirm that the sedimentation of the last 2000 years is not preserved in CIESM C08 core.

The turbidite layers T1, T2 and T3 have been taken into account to construct the age model curve and to estimate sedimentation rates. A second-order polynomial is needed to describe the age-depth relationship for the studied record, indicating an average sedimentation rate of ~7 cm/kyr from the base to the top and four main excursions (Fig. 6.4).

In order to confirm the reliability of the proposed age model, a three-step validation process was performed. First, the visual comparison, in time domain, between *G. bulloides* distribution pattern of Perez-Folgado et al. (2004) for the Alboran Sea and the patterns in core CIESM C08 (Fig. 6.4), confirmed the tuning accuracy.

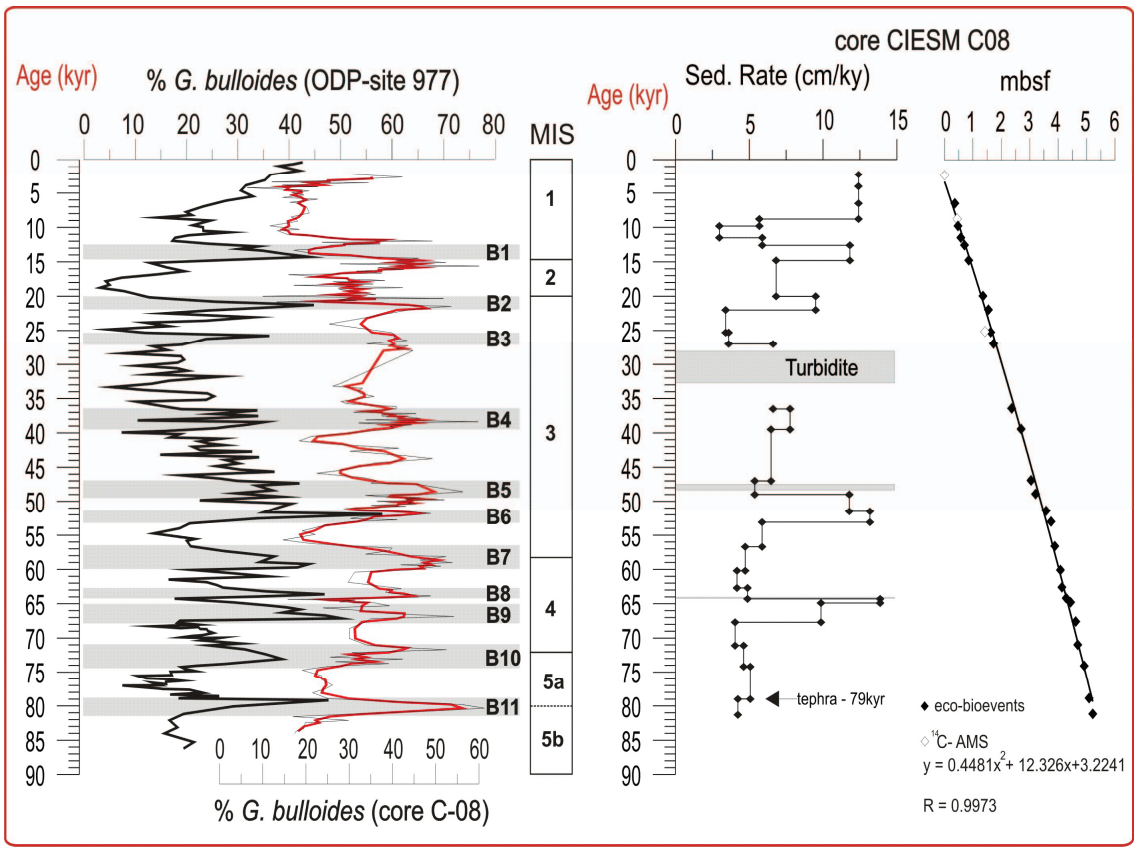

Fig. 6.4 From left to right: comparison in time domain between the distribution pattern of *G. bulloides* from ODP-Site 977 (Perez-Folgado et al., 2004) and the studied core CIESM C08 (the red curve represents a 3-points average). The grey bands and the labels B1 to B11 are from Perez-Folgado et al., (2004). Age-depth profile and sedimentation rates of core CIESM C08. The adopted tie-points by eco-bioevents and by ^{14}C–AMS data are shown respectively with black boxes and grey boxes.

The second step consisted of the comparison of colour reflectance record at 550 nm (%) of the core CIESM C08 with the record of the ODP-Site 964 (Fig. 6.5), drilled in the Ionian Sea at 3650 mbsl and astronomically calibrated (Lourens, 2004). Using the proposed age-depth profile (Fig. 6.4), the colour reflectance record of the studied core

was plotted against time by a cubic spline interpolation method. This comparison (Fig. 6.5) shows that the large-scale reflectance fluctuations in core CIESM C08 not only

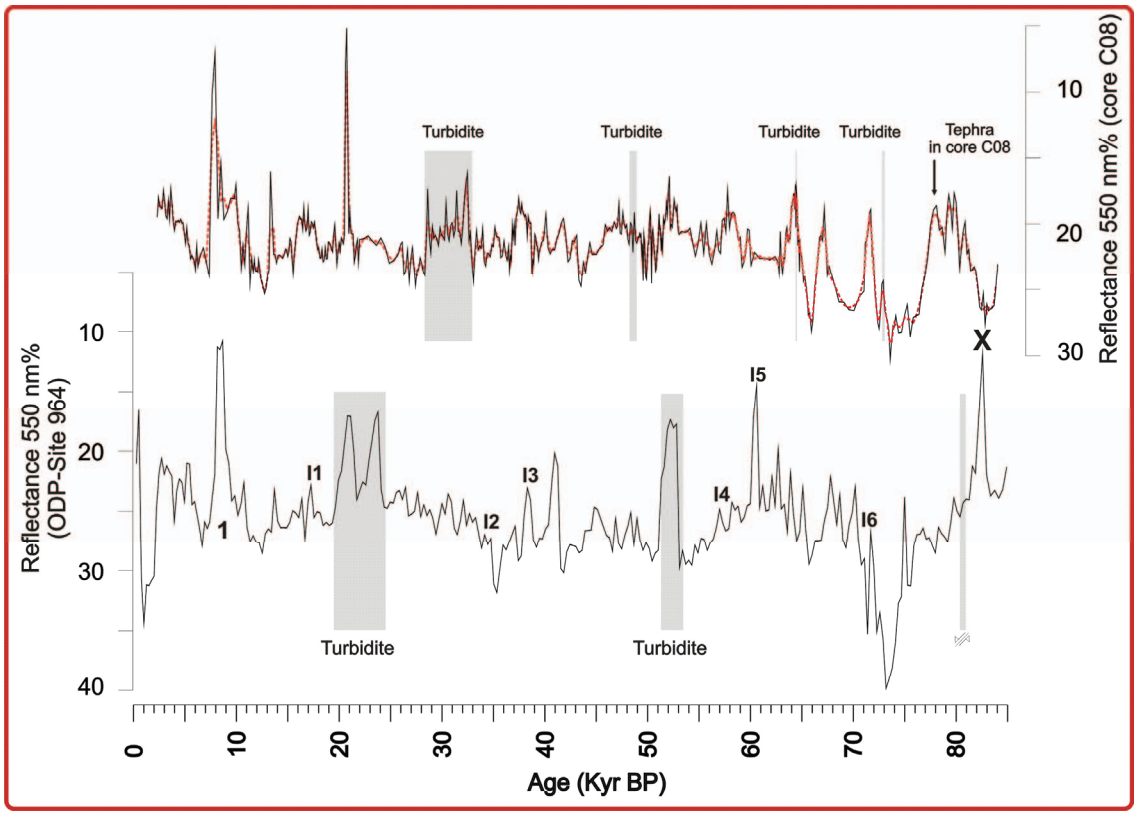

Fig. 6.5 Comparison in time domain of colour reflectance data of core CIESM C08 (black curve, with 3-points average, red dotted curve) with reflectance data after Lourens, (2004) for ODP-Site 964 (thin black curve) in the Ionian Sea. The numbers **I1-I6** indicate tephra layers in ODP-Site 964, and **1** and **X** indicate the position of the sapropel 1 and X, respectively.

have a similar pattern to those reported in the Ionian Sea record but also encompass absolute values in the same range (±10 nm). Lourens (2004) used the reflectance parameter to detect sapropel and tephra layers in the Ionian Sea (Mediterranean area), which in turn, are tuned to the insolation curve of Laskar et al. (2004). According to

Hilgen et al. (2003 and references therein), the Neogene marine successions (on land and in ODP-sites) in the Mediterranean area are often characterized by the cyclic recurrence of sapropels layers and sedimentary patterns, clearly forced by variation in astronomical parameters (Hilgen, 1991a, 1991b; Hilgen et al., 1999, 2003; Hilgen and Krijgsman, 1999; Lourens et al., 1996a, 1996b, 1998 and references therein). Therefore it is not surprising that the cyclic patterns in the colour reflectance records relative to two adjacent deep environmental Mediterranean areas are similar. There is also a strong similarity between the colour reflectance signature of the sapropel S1 equivalent, recorded in the studied core, with the sapropel S1 colour reflectance signature in the Ionian basin. Nevertheless, some of the minimum peaks of the ODP-Site 964 reflectance record, related to the occurrence of tephra layers, are not present in the studied core. This is probably due to the different spatial distribution of the tephra layers in the Mediterranean. On the whole, the good visual correlation obtained between the two records supports the validity of the age model based on the identified eco-bioevents and ^{14}C-AMS calibrations.

The third control step consisted in the comparison of the cronology *G. ruber* distribution with the δ^{18}O NGRIP ice core record. The ecological features of *G. ruber* associated with warm and oligotrophic surface waters has been established in several oceanographic settings (Hemleben et al., 1989; Pujol and Vergnaud-Grazzini, 1995; Watkins et al., 1996; Zaric et al., 2005). Moreover, several authors (Sprovieri, 1991; Sanvoisin et al., 1993; Sprovieri et al., 2003; 2006) have confirmed the utility of relative abundance fluctuations of *G. ruber* as recorders of climatic variability and as for age model proxies. The *G. ruber* and δ^{18}O NGRIP ice core records exhibit a remarkable agreement, with the identification of the Heinrich events (H1-H6) and of the Younger Dryas (YD) in the studied record, which further support the reliability of our tuning (Fig. 6.6).

The observed strong link between $\delta^{18}O$ of Greenland ice cores, a proxy for Greenland air temperature, and the thermal character of surface water masses of Mediterranean area has been previously established in several papers and is usually explained by

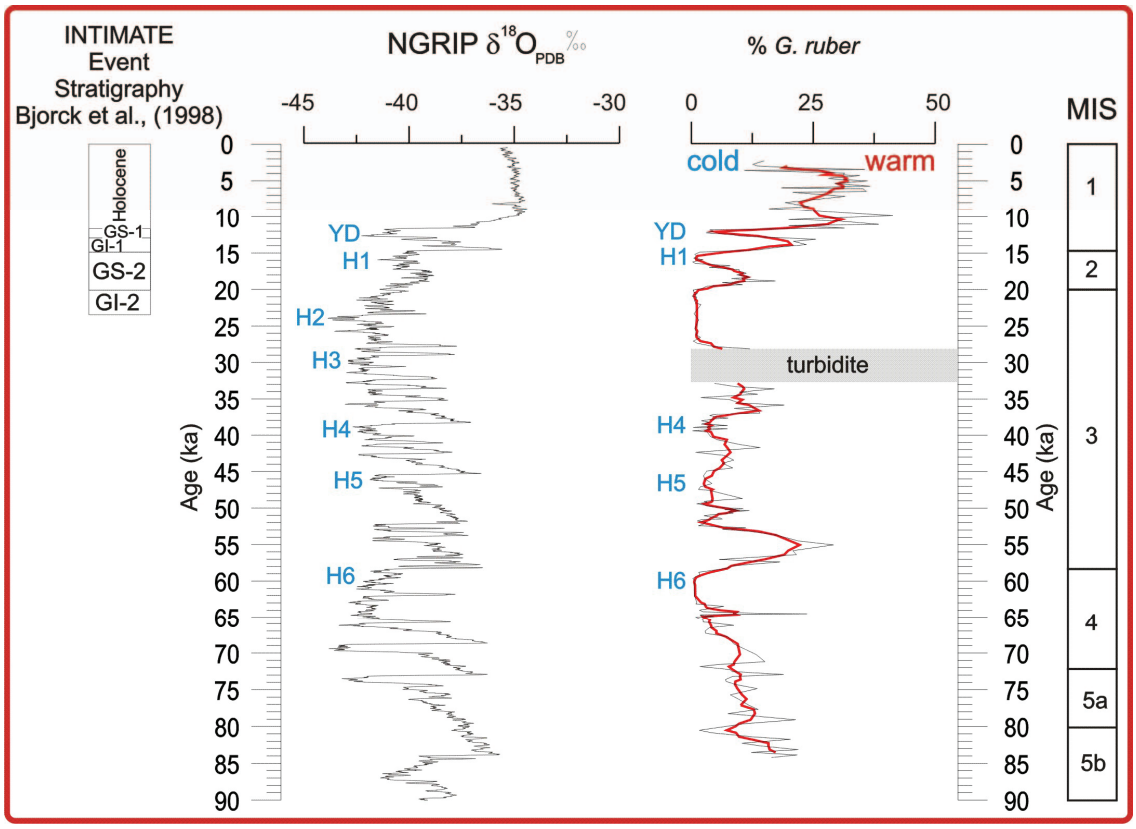

Fig. 6.6 Distribution pattern of *G. ruber* (thin black line) with 3-points average (red line) of core CIESM C08 plotted versus $\delta^{18}O$ NGRIP (NGRIP members, 2004) record, with 7-points average, in time domain. Labels **H1** to **H6** indicate the position of Heinrich events and the label **YD** the position of the Younger Dryas.

teleconnective phenomena (Rohling et al., 1998; Cacho et al., 1999, 2000; Sbaffi et al., 2004; Combourieu Nebout et al., 2002; Moreno et al., 2002; Rohling et al., 2002).

The proposed age model also was adopted to plot paleomagnetic data against time (Fig. 6.7). We note that the time interval spanned by the core encompasses three known geomagnetic excursions (the Mono Lake, dated at 33±1 kyr; the Laschamp, dated at 41±1 kyr, and the Norwegian-Greenland Sea, dated at 61±2 kyr; see Lund et al., 2006). Nevertheless in the paleomagnetic record of CIESM C08 core there is no clear marked oscillation that can be ascribed to any of such excursions. The lack of the paleomagnetic evidence for geomagnetic excursions in this record may be due to a relatively low sedimentation rate (cfr. 5.1, Fig. 6.4), which may have resulted in a prolonged time interval for the lock-in of the natural remanence of the sediments (Roberts and Winklhofer, 2004; Sagnotti et al., 2005), as well as the response functions of the SQUID sensors in the magnetometer (i.e. Oda and Shibuya, 1996; Guyodo et al., 2002). Despite the suggested smoothing of the paleomagnetic signal, the well-defined paleomagnetic data of core CIESM-08 provide an original source of information to improve the confidence of geomagnetic paleosecular variation reconstructions in the Mediterranean for the last 83 kyr.

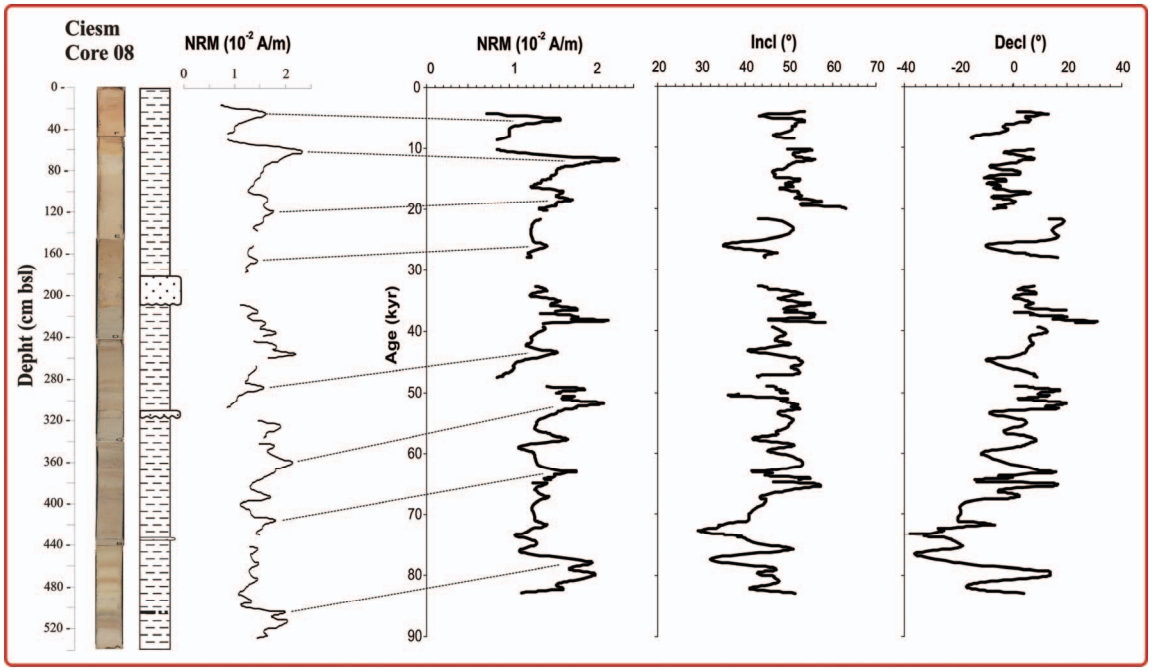

Fig. 6.7 Downcore plot of paleomagnetic data. The NRM intensity plotted versus stratigraphic depth is shown beside to the main paleomagnetic data (NRM, inclination and declination of the characteristic remanent magnetization) plotted versus age, according to the independently derived age model discussed in this study.

6.5.3 Ages and provenance of turbidite events

The size population of grains, the grain fabric, the high content in bioclasts (gastropod, bivalve and echinoderm debris) and the features of the surfaces bounding T1, T2 and T3 turbidites lead us to infer a distant source of transported material, since it seems to have been remobilized from areas of high productivity. Both the slope of the median Ridge, and the southern Cornaglia slope can be ruled out as possible source areas for this sand-rich bioclastic turbidites, since thei are too deep, respectively 1300 and 1000 m b.s.l.. Sartucya 6 diving survey (Mascle et al., 2001a) showed that the base of the southern slope of the median Ridge (2270-1940 m b.s.l.) is draped with mud, shaped by current bed-forms, while the upper slope (1990-1640 m b.s.l.) is characterized by conglomerates and sandstone layers outcropping from the mud, then volcanic rocks. The lithology to the southern Cornaglia slope was described during the Sarcya 2 submersible diving (Mascle et al., 2001a), by the occurrence of pelagic mud at 2500-2250 m b.s.l., and cemented coarse material in correspondence on the steep slopes (2250-2060 m b.s.l.). Although several canyons are noted along the southern Cornaglia slope (Brocard, 2001), they enter the Sentinelle Valley seaward to the core site and thus they possibly feed the deepest parts of the basin. Thus, we must infer that the Bizerte Canyon acted as the main conduit to transport the bioclastic sand from high productivity areas on the Tunisian plateau (Fig. 6.1); inferring transport of more than 50 km before sedimenting. As highlighted by many authors over the years (Walker, 1967; Normark et al., 1984; Reading and Richards, 1994) gentle gradient slopes or pre-existing slope conduits can drive very efficient density currents (Damuth and Flood, 1984; Richards et al., 1998) able to cover long distances quickly and to “segregate the original grain

populations into distinct and relatively well-sorted facies types with distances" (Mutti et al., 1999). The beds occurring in C08 core, in particular T1 and T2, could correspond to the facies tract F7 in Mutti et al. (1999), composed predominantly of medium to fine grained well-sorted sand. In fact in this model, which associates the horizontal grain-size partition of the deposit with the different degrees of flow efficiency, the F7 facies tract consists of medium to fine sand overlying a mm-thick traction carpet that accounts for the development of an erosion surface at the base. This model may explain why T1 and T2 turbidites lack parallel and ripple lamination and pelitic divisions.

The turbidite layers in CIESM core C08 are confined in the lower 4 m of the core and their thicknesses increase upward, peaking at T1 (Fig. 6.2) and pointing to a general regressive trend. Through the age model scheme of CIESM C08 core here proposed, it is possible to date T layers, respectively, at 28 kyr cal. BP (T1), 48 kyr cal. BP (T2) and 63 kyr cal. BP (T3) (Fig. 6.5), thus during the MIS 4 and MIS 3. The emplacement of T1 event bed caused the removal of an undefined thickness of hemipelagic mud correspondent to a time span of about 4 kyr (Fig. 6.4).

Plotting their inferred age on sea-level curve relative to the last 100 kyr (Waelbroeck et al., 2002; Imbrie et al., 1984), T2 and T3 turbidite event beds appear to correlate with two relative sea-level low stands, and T1 with regressing sea level that led to the maximum low stand at ~20 kyr BP (Fig. 6.8). This observation seems in agreement with the most accepted stratigraphic models of deep-sea deposition (Normark et al., 1998). Thus, the part of the basin fan intercepted by the CIESM core C08 was actively and fed with bioclastic sand deposition during the relative sea-level minimum and increased its transport efficiency following the sea level lowering. Nevertheless the CIESM core C08 does not record any further event of sand deposition during the MIS 2 sea-level low stand. A rapid starvation in detritus supply occurred in this area beginning at 28 kyr and the middle fan fossilized below a drape of hemipelagic mud. It is reasonable to suppose that during this phase, this sector of the fan acted mainly as bypass area. Thus, any

possible sand flow would have been deposited basinward, possibly moving through the channel showed in fig. 6.1(B).

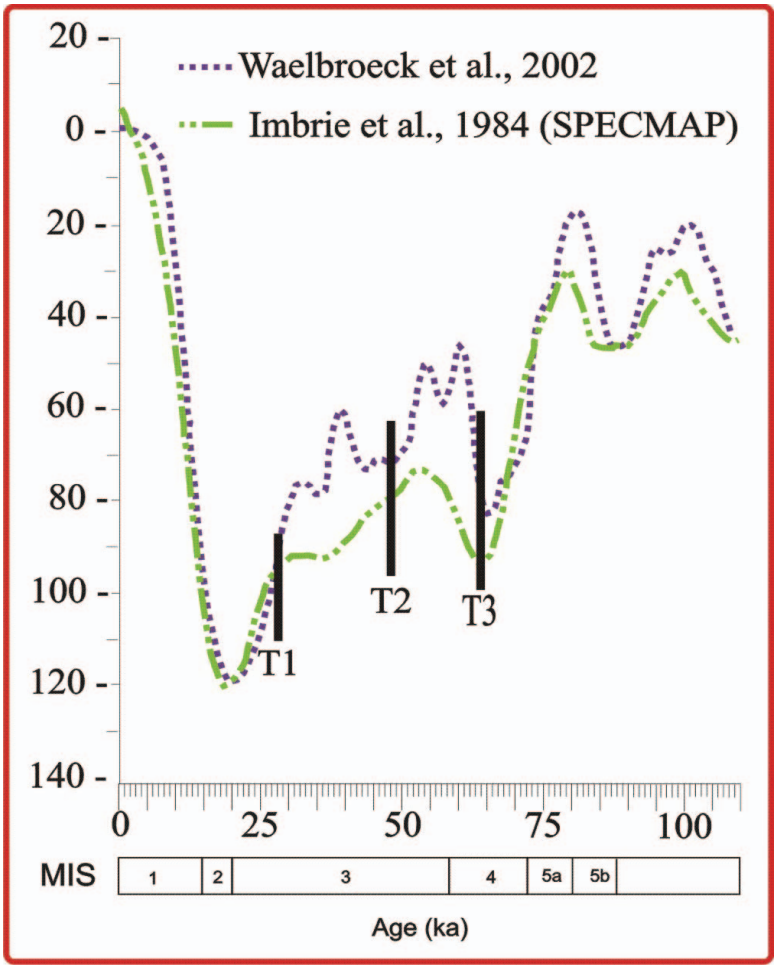

Fig. 6.8 The inferred age of turbitite sand beds is plotted relative to the sea level variations over the past 100 kyr (from Antonioli et al., 2004, modified). T2 and T3 turbidites occur during two relative low-stand phases of the MIS 4 and 3, while the T1 turbidite falls during the last sea-level regression of MIS 3.

6.6 CONCLUSION

The multidisciplinary study of core C08, recovered from the deep sector of the Sardinia Channel, based on planktonic foraminiferal assemblages, petrophysical (MS, Grape density, 550 nm% reflectance) and paleomagnetic (NRM Intensity, ChRM Inclination, ChRM Declination) data, provides an integrated stratigraphic reference record for the Western Mediterranean Sea that spans back for about 83 kyr. The most important eco-bioevents widely used for large-scale correlation in the Western Mediterranean area provide a detailed correlation with the eco-stratigraphic reconstruction proposed by Perez-Folgado et al. (2003, 2004) for the Alboran Sea.

In particular, the relative abundance of selected climate-sensitive planktonic foraminiferal species have led us to identify several eco-bioevents in *G. bulloides* (B3-B11 eco-bioevents), *G. inflata* left coiled (I3-I5 eco-bioevents), *T. quinqueloba* (Q4-Q9 eco-bioevents) and *N. pachyderma* right coiled (P5-P7 eco-bioevents). According to Perez-Folgado et al. (2003, 2004), the documented short-term oscillations in the planktonic foraminiferal fauna are clearly associated with the stadial/interstadial excursions over the last 80 kyr, allowing the identification in core C08 of the S1, YD, GI-1 and GS-2 climatic events in the last 23 kyr. Furthermore, the comparison between the $\delta^{18}O$ NGRIP ice core record and *G. ruber* distribution in core C08 suggests the presence, in the studied record, of the Heinrich events (H1- H6) and of the Younger Dryas (YD).

The eco-bioevents chronology combined with ^{14}C–AMS data were used to define a detailed age model that was compared by means of reflectance parameters to the astronomically tuned age model proposed for the Ionian Sea ODP-Site 964 (Lourens 2004). The similarity between the two reflectance records plotted vs time, validates the age model of the studied record, especially in the time intervals between 2-25 kyr and 60-83 kyr. This methodology, if confirmed with further study, could prove a powerful

tool for reliably correlating marine records between comparable deep-sea environment settings.

The sector of the Sentinelle Valley intercepted by the CIESM core C08 has been sporadically fed by sand turbidite flows, likely driven along the Bizerte Canyon from the northern sector of the Tunisian Plateau, during relative sea-level minimum and sea-level regression during MIS 4 and 3. This sector of the basin was reached by three sand deposition events of increasing thickness between 64 and 28 kyr cal. BP. After about 28 kyr this part of the fan was deactivated and fossilized beneath a carpet of hemipelagic mud at a sedimentation rate of about 7 cm/kyr.

The combined logging of sedimentological, petrophysical and paleomagnetic data of core CIESM C08, integrated with the eco-biozone stratigraphy, could provide an important source of information to improve the confidence of correlations in the Mediterranean over the last 83 kyr.

In this framework, future efforts will be focused on the comparison of the ChRM directions obtained for the core with the other available European geomagnetic paleosecular variation records, as well as on the reconstruction of a relative geomagnetic paleointensity curve, to establish a Mediterranean paleomagnetic reference record to be used as an original dating tool for coeval sequences of this region.

ACKNOWLEDGEMENTS

The authors gratefully acknowledge Lucas J. Lourens of the University of Utrecht for original reflectance data of Ionian cores and Carmine Lubritto of CIRCE Radiocarbon Laboratory, (Caserta, Italy) for ^{14}C–AMS dates. Sincere thanks are also due to Laura Giuliano, who involved some of us in CIESM SUB2 cruise. Captain Vincenzo Lubrano di Lavadera and the crew of R/V Urania, who sailed despite a very rough sea, are kindly acknowledged. Two anonymous reviewers and Patricia Scalfani are sincerely thanked for the comments and the English revision to the manuscript.

REFERENCES

Andersen, K. K., Svensson, A., Johnsen S. J., Rasmussen, S. O., Bigler, M., Rothlisberger, R., Ruth U., Siggaard-Andersen, M. L., Steffensen J. P., Dahl-Jensen, D., Vinther, B. M., Clausen, H. B., 2006. The Greenland ice core chronology 2005, 15-42 ka. Part 1: Constructing the time scale. Quaternary Science Reviews 25, 3246–3257.

Antonioli, F., Bard, E., Potter, E. K., Silenzi S., Improta, S., 2004. 215-ka history of sea-level oscillations from marine and continental layers in Argentarola Cave speleothems (Italy). Global and Planetary Change 43, 1-2, 57-78

Arason, P., Levi, S., 1990. Models of inclination shallowing during sediment compaction. Journal of Geophysical Research 95, 4481–4499.

Ariztegui, D., Asioli, A., Lowe, J. J., Trincardi, F., Vigliotti, L., Tamburini, F., Chondrogianni, C., Accorsi, C.A., Bandini Mazzanti, M., Mercuri, A. M., Van der Kaars, S., McKenzie, J. A., Oldfield, F., 2000. Palaeoclimate and the formation of sapropel S1: inferences from Late Quaternary lacustrine and marine sequences in the central Mediterranean region. Palaeogeography, Palaeoclimatology, Palaeoecology, 158, 215-240.

Asioli, A., Trincardi, F., Lowe, J. J., Ariztegui, D., Langone, L., Oldfield, F., 2001. Sub-millennial scale climatic oscillations in the central Adriatic during the Lateglacial. Paleoceanographic implications. Quarternary Science Review 20, 1201-1221.

Asioli, A., Trincardi, F., Lowe, J. J., Oldfield, F., 1999. Short-term climate changes during the last Glacial-Holocene transition: comparison between Mediterranean and North Atlantic records. Journal of Quaternary Science 4, 3732-3781.

Beaudouin, C., Dennielou, B., Melki, T., Guichard, F., Kallel, N., Berné, S., Huchon, A., 2004. The Late-Quaternary climatic signal recorded in a deep-sea turbiditic levee (Rhône Neofan, Gulf of Lions, NW Mediterranean): palynological constraints. Sedimentary Geology 172(1-2), 85-97.

Bouma, A. H., 1962. Sedimentology of some Flysch Deposits, a Graphic Approach to Facies Interpretation. Elsevier Co., 168 pp., Amsterdam.

Brocard, G., 2001. Le canal de Sardaigne au Néogène: analyse morphologique et structurale. Apports de la bathymétrie multifaisceaux et des plongées Sarcya et Sartucya. In Mascle, G., and Tricart, P. (eds.), Le Canal de Sardaigne: les plongées Cyana. Geologie Alpine, Mém. H.S. vol. 34, 115-166.

Bryden, H. L., Kinder, T**.** H., 1991. Steady two-layer exchange through the Strait of Gibraltar. Deep-Sea Research 38(1), S445-S463.

Buccheri, G., Capretto G., Di Donato, V., Esposito P., Ferruzza G., Pescatore T. S., Russo Ermolli E., Senatore M. R., Sprovieri M., Bertoldo M., Carella D., Madonia G. 2002. A high resolution record of the last deglaciation in the southern Tyrrhenian Sea: environmental and climatic evolution. Marine Geology 186, 447-470.

Cacho, I., Grimalt, J. O., Pelejero, C., Canals, M., Sierro, F. J., Flores J. A., Shackleton, N. 1999. Dansgaard–Oeschger and Heinrich event imprints in Alboran Sea paleotemperatures, Paleoceanography 14, 6, 698–705.

Cacho, I., Grimalt, J. O., Sierro, F. J, Shackleton N. J., Canals, M., 2000. Evidence for enhanced Mediterranean thermohaline circulation during rapid climate coolings, Earth and Planetary Science Letters 183, 417–429.

Cacho, I., Grimalt, J. O., Canals, M., Sbaffi, L., Shackleton, N. J., Schönfeld, J., Zahn, R., 2001. Variability of the western Mediterranean Sea surface temperature during the last 25,000 years and its connection with the Northern Hemisphere climatic changes. Paleoceanography 16, 40-52.

Capotondi, L., Borsetti, A. M., Morigi, C., 1999. Foraminiferal eco-biozones, a high resolution proxy for the late Quaternari biochronology in the central mediterranean. Marine Geology 153, 253-274.

Casford, J. S. L., Rohling, E. J., Abu-Zied, R., Cooke, S., Fontanier, C., Leng, M., Lykousis, V., 2002. Circulation changes and nutrient concentrations in the late

Quaternary Aegean Sea: A nonsteady state concept for sapropel formation. Paleoceanography 17, 1-11.

Combourieu Nebout, N., Turon, J. L., Zahn, R., Capotondi, L., Londeix, L., Pahnke, K., 2002. Enhanced aridity and atmospheric high-pressure stability over the western Mediterranean during the North Atlantic cold events of the past 50 kyr. Geology 30, 863–866.

Curry, W. B., Shackleton, N. J., Richter, C., Bralower, T. J., 1995. Shipboard Scientific Party. Proceedings of the Ocean Drilling Program, Initial Reports, 154, College Station, TX, Ocean Drilling Program, 1111 pp..

Damuth, J. E., Flood, R. D., 1984. Morphology, sedimentation processes, and growth pattern of the Amazon Deep-Sea fan. Geo-Marine Letters 3, (2-4),109-117

Dansgaard, W., Johnsen, S. J., Clausen, H. B., Dahl-Jensen, D., Gunderstrup, N. S., Hammer, C. V., Hvidberg, C. S., Steffensen, J. P., Sveinbjornsdottin, A. E., Jouzel J., Bard, G., 1993. Evidence for general instability of past climate from a 250 kyr ice-core record. Nature 364**,** 218–220.

Deamer, G. A., Kodama, K. P., 1990. Compaction-induced inclination shallowing in synthetic and natural clayrich sediments. Journal of Geophysical Research 95, 4511-4529.

Ducassou, E., Capotondi, L., Murat, A., Bernasconi, S., Mulder, T., Gonthier, E., Migeon, S., Duprat, J., Giraudeau, J., Mascle, J., 2007. Multiproxy Late Quaternary stratigraphy of the Nile deep-sea turbidite system-towards a chronology of deep-sea terrigeneous systems. Sedimentary Geology, 200,(1-2), 1-13.

Emeis, K. C., Emeis, H. Schulz, U,. Struck, M., Rossignol-Strick, H., Erlenkeuser, M. W., Howell, D., Kroon, A., Mackensen, S., Ishizuka, T., Oba, T., Sakamoto, I., Koizumi., 2003. Paleoceanography, 18, 1-18.

Geraga M., Tsaila-Monopolis S., Ioakim C., Papatheodorou G., Ferentinos G., 2005. Short-term climate changes in the southern Aegean Sea over the last 48,000 years. Palaeogeography, Palaeoclimatology, Palaeoecology 220, 311-332

GRIP members, 1993. Greenland Ice-Core Project (GRIP) members, Climate instability during the last interglacial period recorded in the GRIP ice core. Nature 364, 203–207.

Guyodo, Y., Channell, J. E. T., Thomas Ray, G., 2002. Deconvolution of u-channel paleomagnetic data near geomagnetic reversals and short events. Geophysical Research Letters 29(17), 1845.

Hemleben, C., Spindler, M., Anderson, O. R., 1989. Modern Planktonic Foraminifera. Springer, New York (pp. 1–363).

Heinrich, H., 1988. Origin and consequences of cyclic ice rafting in the Northeast Atlantic Ocean during the past 130,000 years. Quaternary Research 29**,** 142–152.

Hilgen, F. J., 1991*a*. Astronomical calibration of Gauss to Matuyama sapropels in the Mediterranean and implication for the geomagnetic polarity timescale. Earth Planetary Science Letters 104, 226-244.

Hilgen, F. J., 1991*b.* Extension of the astronomically calibrated (polarity) timescale to the Miocene-Pliocene boundary. Earth Planetary Science Letters 107, 349{368.

Hilgen, F. J., Abdul Aziz, H., Krijgsman, W., Langereis, C. G., Lourens, L. J., Meulenkamp, J. E., Raffi, I., Steenbrink, J., Turco, E., van Vugt, N., Wijbrans, J. R., Zachariasse, W. J., 1999. Present status of the astronomical (polarity) time-scale for the Mediterranean Late Neogene. Phil. Trans. R. Soc. Lond. A, The Royal Society, 357, 1931-1947.

Hilgen, F. J., Abdul Aziz, H., Krijgsman,W., Raffi, I., Turco, E., 2003. Integrated stratigraphy and astronomical tuning of the Serravallian and lower Tortonian at Monte dei Corvi (Middle-Upper Miocene, northern Italy). Palaeogeography, Palaeoclimatology, Palaeoecology 199, 229–264.

Hilgen, F. J., Krijgsman, W., 1999. Cyclostratigraphy and astrochronology of the Tripoli diatomite Formation (pre-evaporite Messinian Sicily, Italy). Terra Nova 11, 16–22.

Imbrie, J., Hays, J. D., Martinson, D. G., McIntyre, A., Mix, A. C., Morley, J. J., Pisias, N. G., Prell, W. L., Shackleton, N. J., 1984. The orbital theory of Pleistocene climate: support from a revised chronology of the marine δ18O record. In: Berger, A.L., et al., (Ed.), Milankovitch and Climate. Part 1, Reidel, 269–305,.

Iorio, M., Sagnotti, L., Angelino, A., Budillon, F., D'Argenio, B., Dinare`s-Turell, J., Macrì, P., Marsella, E., 2004. High-resolution petrophysical and palaeomagnetic study of late-Holocene shelf sediments, Salerno Gulf, Tyrrhenian Sea. The Holocene 14, 3, 426–435.

Jorissen, F. J., Asioli, A., Borsetti, A. M., de Visser, L., Hilgen, F. J., Rohiling, E. J., van der Borg, K., Vergnaud-Grazzini, C., Zachariasse, W. J., 1993. Late Quaternary central Mediterranean biochronology. Marine Micropaleontology 21, 169-189.

Kenyon, N. H., Klaucke, I., Millington, J., Ivanov, M. K., 2002. Sandy submarine canyon-mouth lobes on the western margin of Corsica and Sardinia, Mediterranean Sea. Marine Geology, 184, 69-84.

Kirschvink, J. L., 1980. The least-square line and plane and the analysis of paleomagnetic data. Geophysical Journal of the Royal Astronomical Society 62, 699-718.

Laskar, M., Gastineau, F., Joutel, B., Levrard, P, ,Robutel, 2004. A new astronomical solution for the long term evolution of the insolation quantities of Mars. Lunar and Planetary Science XXXV, 1-2.

Lourens, L. J., 2004. Revised tuning of Ocean Drilling Program Site 964 and KC01B (Mediterranean) and implication for the $\delta^{18}O$, tephra, calcareous nannofossil, and geomagnetic reversal chronologies of the past 1.1 Myr. Paleocenography 19, 3010.

Lourens, L. J., Hilgen, F. J., Zachariasse, W. J., Van Hoof, A. A. M., Antonarakou, A., Vergnaud-Grazzini, C., 1996*a.* Evaluation of the Plio-Pleistocene astronomical time scale. Paleoceanography 11, 391-413.

Lourens, L. J., Hilgen, F. J., Raffi I., Vergnaud-Grazzini, C., 1996*b.* Early Pleistocene chronology of the Vrica section (Calabria, Italy). Paleoceanography 11, 797-812.

Lourens, L. J., Hilgen, F. J., Raffi, I. 1998. Base of large Gephyrocapsa and astronomical calibration of Early Pleistocene sapropels in site 967 and hole 969D: solving the chronology problem of the Vrica section (Calabria, Italy). In Proc. ODP, Sci. Results (ed. A. H. F. Robertson, K.-C. Emeis, C. Richter & A. Camerlinghi), vol. 160, 191-197.

Lund, S., Stoner, J. S., Channell, J. E. T., Acton, G., 2006. A summary of Brunhes paleomagnetic field variability recorded in Ocean Drilling Program cores. Physics of the Earth and Planetary Interiors 156, 194–204.

Mascle, G., Tricart, P., Bouillin,J. P., Compagnoni, R., Depardon, S., Mascle, J., Pecher, A., Peis, D., Rekhiss, F., Rolfo, F., Torelli, L., 2001a. Données de campagne des plongées Cyana Sarcya-Sartucya. In Mascle, G., and Tricart, P. (eds.), Le Canal de Sardaigne: les plungées Cyana. Geologie Alpine, Mém. H.S., 34, 7-113.

Mascle, G. H., Tricart, P., Torelli, L., Bouillin, J. P., Rolfo, F., Lapierre, H., Monié P., Depardon, S., Mascle J., Peis D., 2001b. Evolution of the Sardinia Channel (Western Mediterranean): new constraints from a diving survey on Cornacya seamount off SE Sardinia. Marine Geology**,** 179 (3-4), 179-201.

Mascle, G. H., Tricart, P., Torelli, L., Bouillin, J. P., Compagnoni, R., Depardon, S., Mascle, J., Pecher, A., Peis, D., Rekhiss, F., Rolfo, F., Bellon, H., Brocard, G., Lapierre, H., Monié, P., Poupeau, G., 2004. Structure of the Sardinia Channel: crustal thinning and tardi-orogenic extension in the Apenninic-Maghrebian orogen; results of the Cyana submersible survey (SARCYA and SARTUCYA) in the Western Mediterranean. Bull. Soc. Geol.. Fr., 175 (6), 607-627.

Millot, C., 1987. Circulation in the western Mediterranean Sea. Oceanology Acta 10, 143–149.

Moreno, A., Cacho, I., Canals, M., Prins, M.A., Sanchez-Goni, M. F., Grimalt, J. O., Weltje, G. J., 2002. Saharan dust transport and highlatitude glacial climatic variability: the Alboran Sea record. Quaternary Research 58, 318–328.

Mutti, E., Tinterri, R., Remacha, E., Mavilla, N., Angella, and Fava, L., 1999. An Introduction to the Analysis of Ancient Turbidite Basins From an Outcrop Perspective. American Association Petroleum Geologists, Continuing Education Course Note Series 39, Tulsa, Oklahoma.

NGRIP Members, 2004. High-resolution record of Northern Hemisphere climate extending into the last interglacial period. Nature, 431, 147–151.

Narcisi, B., Vezzoli, L., 1999. Quaternary stratigraphy of distal tephra layers in the Mediterranean – an overview. Global Planetary Change 21, 31-50.

Normark,W. R., Barnes, N. E., Coumes, F., 1984. Rhone deep-sea fan: a review. Geo-Marine Letteres, 3 (2-4), 155-160.

Normark, W. R., Piper, D. J. W., Hiscott, R. N., 1998. Sea level control on the textural characteristics and depositional architecture of the Hueneme and associated fan systems, Santa Monica Basin, California. Sedimentology 26, 749-774.

Oda, H., Shibuya, H., 1996. Deconvolution of long-core paleomagnetic data of Ocean Drilling Program by Akaike's Bayesian information criterion minimization. Journal of Geophysical Research 101, 2815-2834.

Palike, H., Frazier, J., Zachos, J. C., 2006. Extended orbitally forced palaeoclimatic records from the equatorial Atlantic Ceara Rise. Quaternary Science Reviews 25, 3138–3149.

Pérez-Folgado, M., Sierro, F. J., Flores, J. A., Cacho, I., Grimalt, J. O., Zahn, R., Shackleton, N. 2003. Western Mediterranean planktonic foraminifera events and millennial climatic variability during the last 70 kyr. Marine Micropaleontology, 48, 1-2, 49-70.

Perez-Folgado, M., Sierro, F. J., Flores, J. A., Grimalt, J. O., Zahn, R., 2004. Paleoclimatic variations in foraminifer assemblages from the Alboran Sea (Western

Mediterranean) during the last 150 ka in ODP Site 977. Marine Geology 212, 113–131.

Peterson, L.C., Haug, G. H., Hughen, K. A., Rohl, U., 2000. Rapid changes in the hydrologic cycle of the tropical Atlantic during the Last Glacial. Science, 290, 1947-1951.

Pinardi, N., Masetti, E., 2000. Variability of the large scale general circulation of the Mediterranean Sea from observations and modelling: a review. Palaeogeography, Palaeoclimatology, Palaeoecology 158,153–173.

Principato, M. S., Giunta, S., Corselli, C., Negri, A., 2003. Late Pleistocene–Holocene planktonic assemblages in three box-cores from the Mediterranean ridge area (west–southwest of Crete): palaeoecological and palaeoceanographic reconstruction of sapropel S1 interval. Palaeogeography, Palaeoclimatology, Palaeoecology 190, 61–77.

Prins, M. A., Postma, G., Cleveringa, J., Cramp, A., Kenyon, N. H., 2000. Controls on terrigenous supply to the Arabian Sea durin the Late Quaternary: the Indus Fan. Marine Geology, 169, 327-349.

Pujol, C., Vergnaud-Grazzini, C., 1995. Distribution patterns of live planktonic foraminifers as related to regional hydrography and productive system of the Mediterranean Sea. Marine Micropaleontology 25, 187–217.

Reading, H. G., Richards, M. T., 1994. The classification of deep-water siliciclastic depositional systems by grain size and feeder system. American Association Petroleum Geologists Bulletin, 78, 792-822.

Richards, M., Bowman, M., Reading, H., 1998. Submarine-fan systems I: Characterization and stratigraphic prediction. Marine and Petroleum Geology, 15, 7, 671-689.

Roberts, A. P., Winklhofer, M., 2004. Why are geomagnetic excursions not always recorded in sediments? Constraints from post-depositional remanent magnetization lock-in modelling. Earth and Planetary Science Letters 227(3-4), 345-359.

Rohling, E. J., Cane, T. R., Cooke, S., Sprovieri, M., Boulabassi, I., Emeis, K. C., Schiebel, R., Kroon, D., Jorissen, F. J., Lorre A., Kemp, A. E. S., 2002. African monsoon variability during the previous interglacial maximum, Earth and Planetary Science Letters 202, 61-75.

Rohling, E. J., Hayes, A., Kroon, D., De Rijk, S., Zachariasse, W. J., Eisma, D., 1998. Abrupt cold spells in the NW Mediterranean. Paleoceanography 13, 316-322.

Rohling, E. J., Mayewski P. A., Challenor P., 2003. On the timing and mechanism of millennial-scale climate variability during the last glacial cycle. Climate Dynamics 20, 257–267.

Sagnotti, L., Budillon, F., Dinarès-Turell, J., Iorio, M., Macrì, P., 2005. Evidence for a variable paleomagnetic lock-in depth in the Holocene sequence from the Salerno Gulf (Italy): implications for "high-resolution" paleomagnetic dating. Geochemistry, Geophysics, and Geosystems 6(11), 1-11.

Sangiorgi, F., Dinelli, E., Maffioli, P., Capotondi, L., Giunta, S., Morigi, C., Principato, M. S., Negri, A., Emeis K. C., Corselli, C., 2006. Geochemical and micropaleontological characterisation of a Mediterranean sapropel S5: a case study from core BAN89GC09 (south of Crete). Palaeogeography, Palaeoclimatology, Palaeoecology 235, 192–207.

Sanvoisin, R., D'Onofrio, S., Lucchi, R., Violanti, D., Castradori, D., 1993. 1Ma Paleoclimatic record from the Eastern Mediterranean- Marflux Project: the first results of micropaleontological and sedimentological investigation of a long piston core from the Calabrian Ridge. Il Quaternario 6, 169–188.

Sartori, R., Carrara, G., Torelli, L. and Zitellini, N., 2001. Neogene evolution of the southwestern Tyrrhenian Sea (Sardinia Basin and western Bathyal plain). Marine Geology, 1-4, 175, 47-66.

Sbaffi, L., Wezel, F. C., Curzi, G., Zoppi, U., 2004. Millennial- to centennial-scale palaeoclimatic variations during Termination I and the Holocene in the central Mediterranean Sea. Global and Planetary Change 40, 201–217.

Sprovieri, R., 1991. Plio-Pleistocene paleoclimatic evolution at ODP Leg 107 Site 653 (Tyrrhenian Sea, Western Mediterranean). Memorie della Societa` Geologica Italiana 44, 135–144.

Sprovieri, R., Di Stefano, E., Incarbona, A., Gargano, M. E., 2003. A high-resolution of the last deglaciation in the Sicily Channel based on foraminiferal and calcareous nannofossil quantitative distribution. Palaeogeography, Palaeoclimatology, Palaeoecology 202, 119-142.

Sprovieri, R., Di Stefano, E., Incarbona, A., Oppo D. W., 2006. Suborbital climate variability during Marine Isotopic Stage 5 in the central Mediterranean basin: evidence from calcareous plankton record. Quaternary Science Reviews 25 , 2332–2342.

Stuiver, M., Reimer, P. J., 1993. Extended ^{14}C data base and revised CALIB 3.0 ^{14}C Age calibration program. Radiocarbon 35(1), 215-230.

Tan, X., Kodama, K. P., Lin, H., Fang, D., Sun, D., Li, Y., 2003. Palaeomagnetism and magnetic anisotropy of Cretaceous red beds from the Tarim basin, northwest China: evidence for a rock magnetic cause of anomalously shallow palaeomagnetic inclinations from central Asia, Journal of Geophysical Research 108(B2), 2107.

Tan, X., Kodama, K. P., 2003. An analytical solution for correcting palaeomagnetic inclination error. Geophysical Journal International 152 (1), 228–236.

Tauxe, L., Kent, D. V., 1984. Properties of a detrital remanence carried by hematite from study of modern river deposits and laboratory redeposition experiments. Geophysical Journal of the Royal Astronomical Society 77, 543–561.

Tauxe, L., Kent, D. V., 2004. A simplified statistical model for the geomagnetic field and the detection of shallow bias in paleomagnetic inclinations: was the ancient magnetic field dipolar? In: Channell, J.E.T., et al. (Eds.), Timescales of the Paleomagnetic field. Geophysical Monograph vol. 145, 101-116.

Terrasi, F., Rogalla, D., De Cesare, N., D'Onofrio, A., Lubritto, C., Marzaioli, F., Passariello, I., Rubino, M., Sabbarese C., Casa G., Palmieri A., Gialanella L.,

Imbriani G., Roca V., Romano M., Sundquist, M., Loger R., 2007. A new AMS facility in Caserta/Italy. AMS 10 Conferences, Radiocarbon. (In press).

Walker, M. J. C., Bjòrck, S., Lowe, J. J., Cwynar, L.C., Johnsen, S., Knudsen, K. L., Wohlfarth, B., 1999. Isotopic 'events' in the GRIP ice core: a stratotype for the late Pleistocene. Quaternary Science Reviews, 18, 1143–1150.

Walker, R. G., 1992. Turbidites and submarine fans. In Walker R.G. and James N.P. (eds.), Facies Model Response to Sea-level Change. Geological Association of Canada, Ontario, 239-263.

Walker, R. G., 1967. Turbidite sedimentary structures and their relationship to proximal and distal depositional environments. Journal of Sedimentary Petrology, 37 (1), 25-37.

Waelbroeck, C., Labeyrie, L., Michel, E., Duplessy, J. C., Lambeck, K., McManus, J. F., Balbon, E., Labracherie, M., 2002. Sea-level and deep water temperature changes derived from benthic foraminifera isotopic records. Quaternary Science Reviews 21, 295– 305.

Watkins, J. M., Mix, A. C., Wilson, J., 1996. Living planktic foraminifera: tracers of circulation and productivity regimes in the central equatorial Pacific. Deep-Sea Research II 43, 1257–1282.

Wolf-Welling, T. C. W., Cowan, E. A., Daniels, J., Eyles, N., Maldonado, A., Pudsey, C.J., 2001. Diffuse spectral reflectance data from rise Sites 1095, 1096, 1101 and Palmer Deep Sites 1098 and 1099 (Leg 178, Western Antarctic Peninsula). In: Barker, P.F., Camerlenghi, A., Acton, G.D., Ramsay, A.T.S. (Eds.), Proceeding Ocean Drilling Program, Scientific Results, vol. 178, 1-22.

Zaric, S., Donner, B., Fischer, G., Mulitza, S., Wefer, G., 2005. Sensitivity of planktic foraminifera to sea surface temperature and export production as derived from sediment trap data. Marine Micropaleontology 55, 75–105.

Chapter 7

THESIS CONCLUSIONS

CONCLUSIONS

The strong relationships between Mediterranean Sea and continental environments, dominated by different climatic processes, allows a detailed analysis of climate variations at global scale. The high sedimentation rates recorded during the late Quaternary make this area strategic to study past climate by means of high-resolution analysis of marine sediments.

High-resolution analysis of continuous and well-preserved sedimentary Holocene records collected from key areas of the Mediterranean Basin (Aegean Sea, Southern Tyrrhenian Sea, Sicily Channel and Alborean Sea) (Rohling et al., 2002; Cacho et al., 1999, 2001; Sprovieri et al. 2003; Incarbona et al. 2008) documented the principal climate events and oscillations of the Northern Hemisphere, identified in the Greenland GRIP and GISP ice cores.

Firstly, Cacho et al. (1999, 2000) and Rohling et al. (1998) have suggested, on the basis of high-resolution multi-proxy analysis of marine sedimentary records, that the millennial scale Dansgaard/Oesheger and Heinrich events reduce polar outbreaks intensity and directly control the winds and precipitation systems on the Northern Mediterranean basin. Following this approach, a detailed chronology for the Tyrrhenian cores based on the integration of ^{14}C-AMS radiocarbon data, ^{210}Pb and ^{137}Cs radionuclides and tephrostratigraphic studies, combined with an high-resolution calcareous plankton events, allowed me to obtain a detailed Event Stratigraphy for the Eastern Tyrrhenian region during the last 80 kyr from continental shelf and deep marine records.

In particular, the new data proposed in this PhD thesis allowed to identify and calibrated the eco-biozones and the main climatic events for the last 80 kyr.

The two studied areas (deep sector of Sardinia Channel and the continental shelf of Salerno Gulf) provided different marine records with different sedimentation rates and consequently covering different time intervals. The gravity core C08 recovered in the

Sardinia Channel at 2370 m below sea level, spans the last 80 kyr with a mean sedimentation rate of 7cm/kyr. The composite core [C90-1m _C90_C836] recovered in the continental shelf of Salerno Gulf at ~100 m, spans the last 10 kyr with a sedimentation rate variable from 20cm/100yr for the last 2 millennia to 0.75cm/100yr back to 10 kyr. So that, if the deep marine record from core C08 allowed the possibility to clearly recognise pre-Holocene events, the shallow water marine record from composite core [C90-1m_C90_C836] experienced the secular climatic variation which represent the main tools for Holocene correlation.

The integrated study of core C08 provided a detailed chronostratigraphic framework for the last 80 kyr. This framework provided the identification of the most important eco-bioevents widely used for large scale correlation in the Western Mediterranean area. In particular, 10 eco-biozones have been identified spanning MIS1 to MIS5a. Furthermore, detailed study of associations of planktonic foraminifera has allowed the identification of 30 faunal events, defined by abrupt changes in the abundances of *Neogloboquadrina pachyderma* r.c., *Globorotalia scitula*, *Globigerina bulloides*, *Turborotalita quinqueloba* and *Globorotalia inflata* l.c..

The recognised eco-biozones and planktonic faunal events rendered possible to establish a direct comparison between the Tyrrhenian marine records proposing a eco-biostratigraphic transect from west to east of the Western Mediterranean basin during the last 80 kyr.

In core C08, 10 eco-biozone have been identified and labelled from 1F to 10F according to the eco-biostratigraphic scheme proposed by Sprovieri et al. (2003). In terms of Event Stratigraphy, in core C08 (Sardinia Channel), the sapropel S1 equivalent, the Younger Dryas (YD), the Greenland isotope interstadial 1 (GI-1) and the Greenland isotope stadial 2 (GS-2) have been recognised. Furthermore, the comparison between the $\delta^{18}O$ N-GRIP ice core record with *G. ruber* (that, usually thrive in the warm waters) oscillation suggests the presence in the studied record of the Heinrich events (H1 to H6).

In the composite succession, recovered in the continental shelf of Salerno Gulf (Eastern Tyrrhenian sea), four eco-biozones labelled from 1F to 4F have been identified and accurately dated. In particular, the eco-biozone 4F spans from 9.8 kyr to 5.8 kyr, the eco-biozone 3F spans from 5.8 kyr to 3.9 kyr, the eco-biozone 2F spans from 3.9 kyr to 2.7 kyr and finally the eco-biozone 1F spans from 2.7 kyr to present day. Furthermore, the last eco-biozone 1F has been subdivided in two sub-eco-biozones 1Fa and 1Fb which boundary is placed at 1270 AD.

In terms of climatic variability, it was possible to recognised and dated the sapropel S1 equivalent, the Medieval warm period (MWP), the rapid climatic change (RCC) associated to the MWP/LIA transition and the Little Ice Age (LIA) events.

Concerning the sapropel S1 equivalent, identified in the shallow water core of Salerno Gulf, as well as in the deep core C08 (Sardinia Channel), is clearly detect through calcareous plankton signatures. This planktonic faunal signature allowed the identification, the two warm phases (S1a and S1b) interrupted by a cold one S1i (interruption of the sapropel deposition). The interruption of the sapropel deposition is centred at a calibrated age of about 8.2 kyr BP (Rohling & Palike 2005). In detail, two distinct peaks in *G. ruber* oscillations show the occurrence of S1a and S1b phases separated by an interval (S1i) of decreased abundances of *G. ruber* and drastic increase of *N. pachyderma* and *T. quinqueloba*. In terms of calcareous nannofossils, this humid phase is marked by an increase in abundance of *F. profunda*. Furthermore, the interruption phase S1i is marked by a drastic peak in *B. bigelowii* and by a decrease in abundance of *F. profunda*. These data validate those obtained by Sprovieri et al. (2003) in ODP-Site 963 (Sicily Channel), confirming the good correlation of this event between different sub-basins of the Western Mediterranean.

The successive important climatic event recorded, in the shallow water core of Salerno Gulf, between 2.25 kyrBP and 3.625 kyrBP (spanning from Bronze to Golden age) suggested the occurrence of a distinct humid phase well comparable with that associated to the sapropel S1 equivalent event. The calcareous plankton signature of this second

humid phase presents two warm phases (A and B) separated by a cold one (Ai) as well as in humid phase associate to sapropel S1 equivalent deposition, supporting the hypothesis that during that time the climate (and/or the solar forcing) has to be the same of the early Holocene humid phase (Sapropel S1).

The other two important climatic events, on which there are no universally accepted and precise definitions for the duration are the Medieval Warm Period (MWP) and Little Ice Age (LIA).

The MWP was generally characterized by temperatures that were slightly higher than present-day conditions. Tentatively, this warm interval may coincide with time interval spanning from ~560 AD to ~1300 AD, where is clearly evident a dominance of warm carnivore species *G. ruber*, *G. siphoniphera* and *Orbulina* spp.. Within this long interval two distinct warm water taxa oscillations are present, where the uppermost can be really associated to the historically warmest part of the MWP (~900-1300AD).

The subsequently MWP-LIA transition, here dated at 1480 AD, which represents a global-scale rapid climate change (RCC) event, is strongly marked by a progressive turnover between carnivore species and herbivore-opportunistic ones.

The LIA, here dated between 1500 AD and 1905 AD, is clearly marked by a strong increase in abundance of *T. quinqueloba*. During this time interval the Maunder event is here centred at ~1700 AD. This cold event is characterised by the definitive decrease in abundance of warm water taxa and by the further increase of herbivore-opportunistic species. At that time, in northern part of Italy, during 1708-09 AD is reported the occurrence of the coldest winter in Europe for the least half millennium during which the Venice Lagoon was freeze (Luterbacher et al., 2006).

Finally, the uppermost climatic event which experienced the Mediterranean area is represented by the onset of modern warm condition. Our data do not show a clear relationship with the modern global warming. Contrarily, they suggest a clear human impact on the marine environmental ecosystem associated to the building dam on Sele River (Salerno Gulf) at 1934 AD.

REFERENCES

Alessio, M., Bella, F., Improta, S., Belluomini, G., Calderoni, G., Cortesi, C., Turi, B., 1976. University of Rome carbon-14 dates XIV. Radiocarbon 18, 321–349.

Broecker, W. S., 2001. Was the Medieval Warm Period Global?. Science Vol. 291. no. 5508, pp. 1497 – 1499 DOI: 10.1126/science.291.5508.1497.

Cacho, I., Grimalt, J. O., Canals, M., Sbaffi, L., Shackleton, N. J.,Schònfeld, J.,Zahn, R., 2001. Variability of the western Mediterranean Sea surface temperature during the last 25,000 years and its connection with the Northern Hemisphere climatic changes. Paleoceanography 16,40-52.

Cacho, I., Grimalt, J. O., Sierro, F. J., Shackleton, N. J. and Canals, M., 2000. Evidence for enhanced Mediterranean thermohaline circulation during rapid climatic coolings, Earth Planet. Sci. Lett., 183, 417– 429.

Cacho, I., Grimalt, J. O., Pelejero, C., Canals, M., Sierro, F. J., Flores, J. A. and Shackleton, N. J., 1999. Dansgaard-Oeschger and Heinrich event imprints in the Alboran Sea paleotemperatures. Paleoceanography 14, 698– 705.

Crowley, T. J., & Lowery, T. S., 2000. How warm was the Medieval Warm period? A comment on man-made versus natural climate change. Ambio, 39, 51.

Geraga M., Tsaila-Monopolis S., Ioakim C., Papatheodorou G., Ferentinos G., 2005. Short-term climate changes in the southern Aegean Sea over the last 48,000 years. Palaeogeography, Palaeoclimatology, Palaeoecology 220, 311– 332.

Hughes, M. and Diaz, H., 1994. Was there a “Medieval Warm Period”, and if so, where and when?, Clim. Change, 26, 109–142.

Incarbona, A., Di Stefano, E., Patti, B., Pelosi, N., Bonomo, S., Mazzola, S., Sprovieri, R., Tranchida, G., Zgozi, S. and Bonanno, A., 2008. Holocene millennial-scale productivity variations in the Sicily Channel (Mediterranean Sea). Paleoceanography, 23, PA3204, doi:10.1029/2007PA001581.

Luterbacher, J., Xoplaki, E., Casty, C., Wanner, H., Pauling, A., Kùttel, M., Rutishauser, T., Brònnimann, S., Fischer, E., Fleitmann, D., Gonzàlez-Rouco, F. J., Garcìa-Herrera, R., Barriendos, M., Rodrigo, F., Gonzalez-Hidalgo, J. C., Saz, M. A., Gimeno, L., Ribera, P., Brunet, M., Paeth, H., Rimbu, N., Felis, T., Jacobeit, J., Dù nkeloh, A., Zorita, E., Guiot, J., Tùrkes, M., Alcoforado, M. J., Trigo, R., Wheeler, D., Tett, S., Mann, M. E., Touchan, R., Shindell, D. T., Silenzi, S., Montagna, P., D.,Camuffo, Mariotti, A., Nanni, T., Brunetti, M., Maugeri, M., Zerefos, C., De Zolt, S., Lionello, P., Nunes, M. F.,Rath, V., Beltrami, H., Garnier, E. and Le Roy Ladurie, E., 2006. Mediterranean Climate Variability. Chapter1: Mediterranean Climate Variability Over the Last Centuries: A Review Elsevier Oxford pp. 27–143.

Pérez-Folgado, M., Sierro, F. J., Flores, J. A., Grimalt, J .O., Zahn, R., 2004. Paleoclimatic variations in foraminifer assemblages from the Alboran Sea (Western Mediterranean) during the last 150 ka in ODP Site 977. Marine Geology 212, 113–131.

Pérez-Folgado, M., Sierro, F. J., Flores, J. A., Cacho, I., Grimalt, J. O., Zahn, R., Shackleton, N. 2003. Western Mediterranean planktonic foraminifera events and millennial climatic variability during the last 70 kyr. Marine Micropaleontology, 48, 1-2, 49-70.

Rohling, E. J. and Pälike, H., 2005. Centennial-scale climate cooling with a sudden cold event around 8,200 years ago, Nature, 434, 975-979.

Rohling, E. J., Cane, T. R., Cooke, S., Sprovieri, M., Boulabassi, I., Emeis, K. C., Schiebel, R., Kroon, D., Jorissen, F. J., Lorre A. and Kemp, A. E. S., 2002. African monsoon variability during the previous interglacial maximum, Earth and Planetary Science Letters 202, 61–75.

Rohling, E. J., Fenton, M., Jorissen, F. J., Bertrand, P., Ganssen, G., and Caulet, J. P., 1998. Magnitudes of sea-level lowstands of the past 500,000 years. Nature*, 394*, 162-165.

Sbaffi, L., Wezel, F. C., Curzi, G., Zoppi, U., 2004. Millennial- to centennial-scale palaeoclimatic variations during Termination I and the Holocene in the central Mediterranean Sea. Global and Planetary Change 40, 201–217.

Sprovieri R., Di Stefano E., Incarbona A., Gargano M. E., 2003. A high-resolution of the last deglaciation in the Sicily Channel based on foraminiferal and calcareous nannofossil quantitative distribution. Palaeogeography, Palaeoclimatology, Palaeoecology 202, 119-142.

RIASSUNTO

RIASSUNTO

L'acquisizione di serie storiche, finalizzata ad una più profonda comprensione del sistema climatico terrestre e ad una più adeguata previsione della sua evoluzione futura, rappresenta attualmente uno dei compiti prioritari della comunità scientifica. In questo quadro, lo studio di serie temporali rappresenta ad oggi l'unico strumento di analisi delle dinamiche del sistema climatico terrestre in condizioni differenti da quelle attuali, ed è insostituibile per testare la validità dei modelli previsionali a medio e lungo termine.

Inoltre, la determinazione degli effetti dell'impatto antropico sull'evoluzione ambientale del nostro pianeta non può prescindere da una chiara comprensione delle modalità naturali con cui il clima terrestre risponde al complesso insieme di forzanti esterne (variazioni della costante solare, cicli di Milankovitch, interazioni con il sistema oceanico, etc).

Negli ultimi anni, un numeroso gruppo di ricercatori ha focalizzato la propria attenzione sullo studio dell'evoluzione climatica del tardo-Quaternario in sedimenti prelevati nell'area mediterranea, considerata un ottimo laboratorio naturale per lo studio delle dinamiche di evoluzione del clima a scala globale (e.g., Emeis et al., 1996; Cacho et al., 1999, 2000, 2001; Asioli et al., 2001; Rohling et al., 2002; Perez-Folgado et al., 2003; Sprovieri et al. 2003; Mayewski et al., 2004; Sbaffi et al., 2004; Massch et al., 2005; Incarbona et al. 2008; Piva et al., 2008; Di Donato et al., 2008).

In questo quadro internazionale la scelta di una tematica scientifica di importanza strategica quale lo studio degli "*Eventi a Foraminiferi planctonici e variazioni climatiche registrate in sedimenti del Tirreno meridionale durante gli ultimi 80 ka*.", risiede nella possibilità di studiare con estremo dettaglio, in un bacino semi chiuso come quello del Mediterraneo, le principali variazioni climatiche riconosciute a scala globale. Inoltre la possibilità di studiare record marini con elevati tassi di sedimentazione offre potenzialmente la possibilità di riconoscere l'effetto dell'uomo sul sistema marino

costiero. Proprio questo ultimo passaggio ha permesso di inserire questo Dottorato di Ricerca all'interno del progetto finanziato FISR "VECTOR" finalizzato alla definizione della Vulnerabilità delle Coste e degli ecosistemi marini italiani ai cambiamenti climatici e loro ruolo nei cicli del carbonio mediterraneo.

In relazione agli eventi a foraminiferi planctonici, è evidente che attualmente, non esiste uno schema eco-biotratigrafico completo ed accettato all'unanimità, il quale possa portare ad una facile correlazione fra i settori differenti del Mar Mediterraneo. Inoltre, per l'intervallo stratigrafico di fine Pleistocene-Olocene, il concetto di Biostratigrafia classico non può essere utilizzato, in quanto gli eventi biostratigrafici di FAD (first appearance datum) e LAD (last appearance datum), utili per suddividere questo piccolo intervallo temporale, non sono presenti nel record planctonico calcareo.

Per risolvere il problema, negli ultimi anni, alcuni autori (e.g. Capotondi et al., 1999; Asioli et al., 2001; Sprovieri et al., 2003; Sbaffi et al., 2004), hanno proposto, per il Mediterraneo, l'istituzione di una serie di eco-biozone basate sulle fluttuazioni relative nell'abbondanza dei foraminiferi planctonici. Allo stesso tempo, esistono lavori (Sbaffi et al., 2001; Giunta et al., 2003; Principato et al., 2003; Sprovieri et al., 2003) che riportano una sequenza di eco-biozone anche per quanto riguarda le fluttuazioni relative alle associazioni a nannofossili calcarei.

Da questo punto di vista, il principale scopo di questa tesi di Dottorato, è aumentare le conoscenze, di verificare la validità, e se necessario, proporre modifiche sugli schemi eco-biostratigrafici proposti per il bacino del Mediterraneo occidentale, e di calibrare attraverso metodi radiometrici i limiti di queste eco-biozone.

Inoltre, attraverso un approccio multidisciplinare (foraminiferi planctonici e bentonici, nannofossili calcarei, livelli vulcanici, datazioni radiometriche) questa tesi di Dottorato mira a comprendere le modalità di riconoscimento delle principali variazioni climatiche registrate nel Mediterraneo, negli ultimi 80 ka, in termini di eventi a foraminiferi planctonici.

Si è scelto di focalizzare l'attenzione su questo arco temporale, in quanto, ad oggi risulta chiaro, che negli ultimi 100 ka, l'Emisfero Settentrionale è stato soggetto a rapidi cambiamenti climatici, globalmente distribuiti, e drammatici in termini di magnitudo e tempo, i quali hanno condizionato la distribuzione globale dei foraminiferi planctonici. Infatti, dati sulle associazioni dei foraminiferi planctonici, fossili e viventi, hanno messo in luce una variabilità stagionale e geografica nella loro distribuzione. Questa variabilità può essere associata a parametri differenti, quali: temperatura, sostanze nutrienti, propensione ad una determinata tipologia di alimento, modellazione idrografica, etc.. Ampliare le informazioni relative alla distribuzione delle comunità planctoniche, e non solo, (con risoluzioni sempre più elevate), in funzione di questi parametri, sono alla base del significato biostratigrafico e biocronologico di un ambiente, e quindi, possono fornire un utile contributo alla conoscenza, alla variabilità, alla cronologia ed alla correlazione a scala regionale dei cambiamenti ambientali riconosciuti in una determinata area di studio.

In questo ambito, si è scelto di concentrare lo studio sul settore meridionale del Mar Tirreno, per i suoi caratteristici elevati tassi di sedimentazione (che permettono studi ad alta risoluzione) e per la presenza, nelle sequenze sedimentarie di questo settore, di livelli di "tephra" che possono essere utilizzati per definire una corretta cronologia dei sedimenti carotati.

In particolare, in collaborazione con ricercatori di diversi enti di ricerca (CNR e INGV) e dell'Università, è stato condotto uno studio integrato di record marini del Mar Tirreno meridionale utilizzando le seguenti metodiche:

1. foraminiferi platonici;
2. foraminiferi bentonici;
3. nannofossili calcarei;
4. tefrostratigrafia;
5. datazioni ^{14}C-AMS;
6. datazioni con radionucleidi ^{137}Cs e ^{210}Pb;

7. proprietà petrofisiche e variazioni paleomagnetiche.

Insieme alla loro differente posizione geografica, i siti scelti per questo studio offrono la possibilità di recuperare ed analizzare sequenze sedimentarie continue ed indisturbate e di acquisire ottimi archivi paleoclimatici, su cui effettuare studi eco-biostratigrafici e di Event Stratigraphy ad alta risoluzione.

In particolare, sono state studiate le seguenti sequenze sedimentarie marine:

1. la carota C90-1m, è stata prelevata nel Golfo di Salerno (40°35.750'N; 14°42.414'E), alla profondità di 103 m. Il prelievo della carota è stato effettuato con l'ausilio del carotiere SW104 (brevettato dall'IAMSR-CNR Bologna), che preserva intatta l'interfaccia acqua-sedimento. Lo studio multidisciplinare effettuato, ha indicato che questo record copre l'intervallo temporale degli ultimi 500 anni.
2. le carote C90 e C836, prelevate nel Golfo di Salerno. In particolare, la carota C90 (40°35.76' N; 14°42.38'E) è stata prelevata ad una profondità di 103 m., mentre la carota C836 (40°35.98'N; 14°40.47'E), alla profondità di 110 m. Dagli studi effettuati, si è riscontrato che le carote C90-1m, C90 e C836 sono perfettamente correlabili sia tramite le fluttuazioni di abbondanza dei foraminiferi planctonici sia tramite le proprietà petrofisiche che attraverso studi tefrostratigrafici. Il record della carota composita C90-1m_C90_C836 copre l'intervallo temporale degli ultimi 10.000 anni.
3. la carota C08, è stata prelevata nel canale di Sardegna (38°38.5364'N, 10°21.5576'E), durante la campagna oceanografica CIESM 2 (dicembre 2005), alla profondità di 2370 m. Lo studio multidisciplinare svolto su questa carota ha indicato che i relativi sedimenti coprono l'intervallo temporale compreso tra 2.000 e 80.000 anni.

SINOSSI

SINOSSI

Durante gli ultimi 100.000 anni, l'area Mediterranea è stata soggetta a drastici e/o graduali cambiamenti, diversi per magnitudo e tempo, che risultano rilevabili in paleo-archivi marini sia di ambiente di Piattaforma, sia di ambiente Pelagico.

La ricerca presentata è focalizzata su paleo-archivi del Mar Tirreno, che rappresenta l'area marina meno studiata dell'intero Mediterraneo. Da questo punto di vista, è importante ricordare che il mar Tirreno rappresenta un area chiave del Mediterraneo, dove l'Acqua Atlantica Modificata (MAW), che proviene dallo Stretto di Gibilterra (Bryden and Kinder, 1991), diverge dividendosi in due flussi. In particolare, una parte entra nel Mediterraneo Orientale, mentre l'altra parte fluisce, attraverso il Canale di Sardegna, nel Mar Tirreno lungo la costa settentrionale della Sicilia (Millot, 1987), formando una circolazione ciclonica secondaria.

Per questo motivo, la parte meridionale del Mar Tirreno, rappresenta un interessante area per studi paleoceanografici ad alta risoluzione. Di conseguenza, studiare archivi marini di questa regione, che presentano diversi tassi di sedimentazione, offre un'opportunità unica, per identificare, attraverso un approccio multidisciplinare, i principali eventi a cui l'area Tirrenica è stata soggetta, provando, inoltre, ad identificare, gli eventi regionalmente riconosciuti.

La Tesi di Dottorato proposta, include studi dettagliati, affrontati con differenti tipologie di approccio, effettuati su sequenze sedimentarie riferibili agli ultimi 80.000 anni. In dettaglio, sono stati analizzati tre differenti siti marini, che corrispondono agli ultimi 500 anni, al periodo Olocenico e agli ultimi 80.000 anni.

Insieme alla loro differente posizione geografica, questi siti offrono la possibilità di recuperare sequenze sedimentarie continue ed indisturbate, le quali permettono di acquisire paleo-archivi climatici utilizzabili per studi sugli Eventi Stratigrafici ad alta risoluzione.

In particolare, questa ricerca è basata sulle fluttuazioni nell'abbondanza dei foraminiferi planctonici (per tutti gli intervalli studiati), associati ai nannofossili calcarei (per l'Olocene) e foraminiferi bentonici (per gli ultimi 500 anni).

In questo senso, e' importante notare che, i capitoli 4, 5 e 6 di questa Tesi di Dottorato rappresentano singoli lavori, che sono stati pubblicati (capitolo 6), oppure che saranno pubblicati su riviste scientifiche specializzate (capitoli 4 e 5). Inoltre, l'interdisciplinalità della Tesi, ha coinvolto, attraverso collaborazioni scientifiche, ricercatori di differenti Istituzioni.

Di seguito sono riportate le Istituzioni coinvolte:

- Istituto per l'Ambiente Marino Costiero **(IAMC) – CNR** di Napoli
- Istituto Nazionale di Geofisica e Vulcanologia **(INGV)** di Pisa
- Istituto Nazionale di Geofisica e Vulcanologia **(INGV)** di Roma
- Dipartimento di Scienze della Terra – **Università degli Studi "Federico II"** di Napoli
- Dipartimento di Scienze Ambientali, **Seconda Università** di Napoli
- Istituto Scienze Marine (Sezione di Geologia Marina), **ISMAR – CNR** di Bologna.

Questa Tesi di Dottorato è supportata finanziariamente dal progetto VULCOST (il cui Responsabile scientifico è il Prof. Bruno D'Argenio). Questo progetto rappresenta la Linea2 del progetto italiano VECTOR.

Chapter 4

In questo capitolo, è presentato uno studio ad alta risoluzione, basato su un approccio multidisciplinare (foraminiferi planctonici e bentonici, Tefrostratigrafia), effettuato su sedimenti marini di piattaforma (profondità di circa 100 m) carotati sul margine Orientale del Mar Tirreno (Golfo di Salerno).

In particolare, questo studio, ha permesso l'identificazione dei più importanti eventi climatici riconosciuti negli ultimi 520 anni. La datazione radiometrica, ottenuta

attraverso l'analisi dell'attività del ^{137}Cs ed del ^{210}Pb, ha permesso la calibrazione del record studiato e quindi la costruzione di un profilo età-profondità che suggerisce un tasso di sedimentazione medio di 0.20 cm/anno per gli ultimi 520 anni.

In termini di distribuzione quantitativa di foraminiferi bentonici e planctonici, durante questo intervallo temporale, sono stati identificati tre eco-intervalli.

I margini di questi di questi eco-intervalli risultano quasi coincidenti, suggerendo una risposta simile alla variabilità del clima.

In termini fauna bentonica, il record studiato sembra arricchito di quelle specie che dominano in condizioni eutrofiche. In termini di fauna planctonica, nella fase successiva all'evento di minima attività solare definito Maunder, si registra un forte cambio tra specie carnivore ed erbivore-opportuniste, ed un possibile innalzamento del livello nella colonna d'acqua, di produttività del fitoplancton, come indicato dall'aumento di abbondanza della specie *Globigerina bulloides* nel secolo scorso.

Questo cambio di associazione, nella fase successiva all'evento Maunder, potrebbe essere relazionato ad una variazione della disponibilità di nutrienti nella colonna d'acqua. Inoltre, il forte aumento nell'abbondanza della specie *Globigerinoides quadrilobatus,* durante gli intervalli caldi, riflette le attuali condizioni oligotrofiche delle acque del Mediterraneo.

Per concludere, i dati acquisiti suggeriscono un possibile effetto antropico sull'ecosistema marino, associato alla costruzione della diga sul fiume di Sele (1934), che ha possibilmente cambiato l'apporto di materiale grossolano e di conseguenza di nutrienti trasportati a mare.

Questa ipotesi, sembra essere supportata, dal forte e progressivo aumento nell'abbondanza della specie *G. bulloides*, dall'improvviso aumento nell'abbondanza della specie bentonica *B. aculeate,* e dal prominente aumento dei foraminiferi bentonici e planctonici (come numero degli esemplari per grammo di sedimento asciutto) successivamente al 1934 AD.

Chapter 5

In questo capitolo è presentato uno studio, ad alta risoluzione, sugli Eventi Stratigrafici degli ultimi 10.000 anni, effettuato su un record marino di piattaforma continentale carotato sul margine Orientale del Mar Tirreno.

In particolare, la cronologia dettagliata, della carota composita studiata, basata sull'integrazione di varie discipline e metodologie, tra cui: datazioni al radiocarbonio ^{14}C-AMS, datazioni con metodo radiometrico basato sull'attività del ^{210}Pb e del ^{137}Cs e l'analisi tefrostratigrafica di livelli di tefra riconosciuti nel record studiato, ha permesso di identificare quattro eco-biozone. Dalla base alla sommità, del record composito, sono state identificate la eco-biozona definita 4F (9.8-5.8 ka BP), la eco-biozona 3F (5.8-3.9 ka BP), la ecobiozona 2F (3.9-2.7 ka BP), ed infine la eco-biozona 1F (2.7 ka BP to present). E' importante notare che l'eco-biozona 1F è stata suddivisa in 1Fa ed 1Fb con margine datato a 1270 AD.

In relazione agli eventi climatici, sono state riconosciute due fasi umide, di cui la prima riconosciuta nella prima metà dell'Olocene. Allo stesso tempo, nella fase finale dell'Olocene, sono stati riconosciuti il Periodo Medioevale Caldo (MWP) , la Piccola Era Glaciale (LIA) e il riscaldamento moderno.

In particolare, dalla base al sommità del record studiato sono stati registrati i seguenti eventi climatici:

La ben conosciuta fase umida all'inizio dell'Olocene, associata alla deposizione, nell'area Mediterranea, del Sapropel S1, è registrata tra 9.8 ka BP e 6.3 ka BP.

Nel Mar Tirreno, la marcatura litologica (strati di colore scuro, laminati ed arricchiti di materiale organico) del sapropel S1 non è presente, quindi l'identificazione di questo evento climatico è associata alla marcatura del plancton calcareo.

In particolare, due distinti picchi nella distribuzione quantitativa della specie planctonica *G. ruber*, sono associati alle fasi di deposizione S1a e S1b. Queste due fasi sono separate da un intervallo definito S1i (interruzione della deposizione del Sapropel

S1), in cui si ha un decremento nell'abbondanza del *G. ruber* ed un drastico aumento nell'abbondanza delle specie *N. pachiderma* e *T. quinqueloba*. Inoltre, la concomitanza di un picco distinto nell'abbondanza della specie di nannofossile calacareo *Brarudosphaera bigelowii*, supporta il riconoscimento di questo periodo di interruzione del Sapropel (S1i).

Questa marcatura del plankton calcareo è registrata chiaramente, in alcune parti del bacino Mediterraneo, con piccole differenze per la posizione di *B. bigelowii,* aumentata maggiormente, nel mar Ionio.

La successiva importante fase umida registrata tra 3.625 ka BP and 2.25 ka BP, è ben documentata dalla marcatura planctonica calcarea. E' importante notare che questa fase umida presenta la stessa marcatura planctonica calcarea della precedente fase umida associata alla deposizione del Sapropel equivalente, con la sola eccezione che durante questo intervallo temporale (3.625 - 2.25 ka BP), *G. quadrilobatus* (specie tipica di zone di dwelling nel Mediterraneo e più prolifica alla fine dell'estate), presenta un distinto acme nella sua distribuzione (>30%). Questo dato, potrebbe supportare l'ipotesi che durante questo intervallo temporale, il clima era simile a quello della fase umida (Sapropel S1) registrata all'inizio dell'Olocene.

I dati, riguardanti il plancton calcareo, per gli ultimi 2000 anni rappresentano il primo "dataset", ad alta risoluzione, disponibile nell'area Mediterranea. Per questo motivo, questi dati non possono essere correlati con altri di diverse aree del bacino Mediterraneo.

In dettaglio, durante gli ultimi 2000 anni, i due più importanti eventi climatici riconosciuti, ma non universalmente accettati, in termini di precisa definizione della loro durata, sono il Periodo Medioevale Caldo (MWP), e la Piccola Era Glaciale (LIA).

Il Periodo Medioevale Caldo (MWP), in genere caratterizzato, da temperature lievemente più alte rispetto alle condizioni attuali, non mostra, nell'associazione dei foraminiferi planctonici, distinte variazione.

In particolare, questo intervallo caldo potrebbe coincidere con l'intervallo temporale compreso tra ~560 AD e ~1300 AD, il quale risulta caratterizzato, fondamentalmente, da specie planctoniche carnivore. All'interno di questo intervallo temporale si distinguono due distinte oscillazioni di specie ecologicamente associate ad acque calde. La parte superiore di quest'intervallo temporale può essere certamente associata alla storica parte più calda del Periodo Medioevale Caldo (~900-1300 AD), testimoniata nel record studiato, da un forte picco di abbondanza della specie *G. ruber*.

La successiva fase di transizione tra Periodo Medioevale Caldo (MWP) e Piccola Era Glaciale (LIA),datata 1480 AD, rappresenta un evento di rapido cambiamento climatico (RCC). Questa transizione è marcata da un progressivo scambio tra specie carnivore e specie erbivore-opportuniste .

L'inizio della Piccola Era Glaciale (LIA), è contraddistinto da un'associazione a foraminiferi planctonici controllata, essenzialmente, da un forte aumento nell'abbondanza della specie *T. quinqueloba*. Nel presente studio la Piccola Era Glaciale inizia a ~1500 AD e finisce, all'incirca nel 1905 AD. In questo intervallo temporale, l'evento freddo definito Maunder risulta centrato a ~1700 AD.

Nel record studiato, l'evento freddo Maunder, è caratterizzato da un definitivo decremento nell'abbondanza delle specie di acque calde e da un relativo aumento di specie erbivore-opportuniste.

E' importante notare che durante il 1708-09 AD, gli archivi storici, riportano l'occorrenza in Europa, dell' inverno più freddo degli ultimi 500 anni. Nel Nord dell'Italia, durante questo inverno, la Laguna di Venezia gelò.

Infine, successivamente al 1900 AD, l'ultimo evento climatico registrato nell'area Mediterranea è rappresentato dall'inizio delle calde condizioni attuali.

I dati sull'associazione a foraminiferi planctonici mostrano bassi valori nell'abbondanza della specie *G. ruber* ed un progressivo aumento (dal 1934 AD) nella distribuzione della specie *G. bulloides* associata ad un leggero aumento (dal 1934 AD) nell'abbondanza della specie *G. quadrilobatus*.

Apparentemente, questi dati sembrano non riflettere il moderno riscaldamento globale. Al contrario, essi suggeriscono un chiaro impatto antropico sull'ecosistema marino, associato alla costruzione, nel 1934 AD, della Diga sul fiume Sele (Golfo di Salerno).

Chapter 6

L'analisi quantitativa dei foraminiferi planctonici, accoppiata a misure petrofisiche e paleomagnetiche, e la calibrazione attraverso la datazione al radiocarbonio ^{14}C-AMS, effettuata su una carota di sedimenti marini, prelevata nel Canale di Sardegna (Mediterraneo Occidentale) durante la campagna oceanografica Ciesm sub2, ha fornito un record stratigrafico calibrato in tempo per gli ultimi 80.000 anni.

Cambiamenti significativi nella distribuzione quantitativa dei foraminiferi planctonici hanno permesso l'identificazione di alcuni eco-bioeventi accuratamente marcati dai margini delle 10 eco-biozone intensamente riconosciute in paleo-archivi marini del Mediterraneo Occidentale ed utilizzate per correlazioni su grande scala.

Inoltre, sedici eco-bioeventi codificati sono stati correlati con dati relativi alla distribuzione dei foraminiferi planctonici nel Mare di Alboran, ciò ha permesso il riconoscimento di quattro eventi climatici a scala globale (Sapropel S1, Younger Dryas, Greenland Isotope Interstadial 1/GI1, Greenland Isotope Stadial 2/GS2), per gli ultimi 23 ka. Allo stesso tempo, la comparazione tra i dati isotopici δ^{18}O della carota di ghiaccio N-GRIP, con i dati di distribuzione della specie planctonica *G. ruber* (che, solitamente prospera in acque calde) nella carota C08, suggeriscono la presenza, nel record studiato, degli eventi di Heinrich (H1 to H6) e dello Younger Dryas (YD/GS1).

L'identificazione degli eco-bioeventi, insieme alla calibrazione con ^{14}C AMS, ed alla comparazione dei dati di Riflettanza (550 nm%) del record studiato con l'age-model calibrato su base astronomica dei record (ODP-Site 964 and of cores KC01 and KC01B) nel Mar Ionio, hanno permesso la definizione di un accurato profilo età-profondità compreso tra 83 e 2 ka cal. BP., con un tasso medio di sedimentazione pari a circa

7cm/ka. Sulla base di questo profilo, tre eventi di torbida sono stati cronologicamente calibrati nelle fasi di MIS4 e MIS3, insieme ad un distinto livello di tefra presente alla base della carota, datato 75.5 ka.

FIGURE CAPTIONS

CAPITOLO 1

Fig. 1.1 Global temperature oscillations (warm-cold) at different time scales (from 300 million to 1000 years), with indication of data sources. The dates on the right diagram correspond to the top and bottom of the Little Ice Age (LIA) (by Ruddiman, 2001).

Fig. 1.2 Climatic events chronology scheme for the last 100 kyr. The framework of the scheme show different time scales resolution. *Left*: climatic events recognised from 1 kyr to present (***Med/Oort Minimum*** (AD 1060-1090), the ***Medieval Warm Period*** (MWP) (AD 1100-1250), ***Wolf Minimum*** (AD 1280–1340), ***Sporer Minimum*** (AD 1420–1540), the ***Maunder Minimum*** (AD 1645–1710), ***Dalton Minimum*** (AD 1790-1830), ***Damon Minimum*** (AD 1880-1900) that occur in the ***Little Ice Age*** (LIA, AD 1450–1900), ***modern warming*** **(**AD 1900-present)). *Center*: climatic events recognised from 10 kyr to 1 kyr BP (***Sapropel S1 deposition*** in the Eastern Mediterranean Sea (9.8-6.5 kyr BP), ***9.4 Kyr event (Bond event 6), 8.2 Kyr event (Bond event 5) 5.9 Kyr cold event/Early Neolithic (Bond event 4), 5.5 Kyr cold event/Early-Middle Neolithic, Neolithic/Copper age warm period (5.2 – 4.5 Kyr B.P.), 4.5 Kyr cold event/end of Middle Neolithic (Bond event 3), 3.8 Kyr cold event/beginning of Bronze age, Bronze age (3.5 – 3 Kyr B.P.), 3 – 2.8 Kyr cold event/Late of Bronze age (Bond event 2), Homeric/Iron Age cold Epoch (2.8 – 2.6 Kyr B.P.), Greek (2.3 – 2.1 Kyr B.P.), Roman warm Period (1.9 – 1.5 Kyr B.P.) with (RomanI, RomanII, Roman III), 1.5 Kyr cold event/Migration Period of the late Iron Age (Bond event 1), 1.2 Kyr event/Roman IV, 1.1 Kyr Viking period of the late Iron age***). *Right*: climatic events recognised from 100 kyr to 10 kyr BP (***The Dansgaard/Oeschger events*** (or Bond cycle, **22** interstadial events, or Dansgaard/Oeschger interstadial between 100 and 15 kyr B.P.), ***Sapropel*** "***S3"*** deposition in the Eastern Mediterranean Sea (84 kyr BP), ***Heinrich Events***

(labeled H6-H1 between 60 and 15 kyr B.P.), ***Sapropel "S2?"*** (whose existence is controversial) deposition in the Eastern Mediterranean (53 kyr BP), ***Younger Dryas*** (GS-1) 12,900 to 11,500 years B.P.). The references for all the climatic events chronology is also reported.

Fig. 1.3 Timing of Heinrich events and Dansgaard-Oeschger events (Interstadial) (Bond, 1992, 1993; NGRIP members, 2004; Hemming, 2004) inferred from geochemical records ($\delta^{18}O$ signal) of ice core NGRIP.of

Fig. 1.4 Comparison between the GRIP event stratigraphy (Walker et al., 1999; INTIMATE group) for the Last Glacial-Interglacial Transition (*left side*) and the classic Lateglacial stratigraphy of NW Europe (Mangerud et al., 1974).

Fig. 1.5 a) Venice Lagoon freezing (Camuffo, 1997). b)Winter Landscape (Pieter Bruegel the Elder).

Fig. 1.6 Mediterranean Sea map.

Fig. 1.7 Mediterranean Sea map, with location of the main volcanic sources.

Fig. 1.8 Northern Hemisphere summer atmospheric circulation. Main winds are indicated as black arrows. ITCZ = intertropical convergence zone; H and L = areas of high and low sea level pressure, respectively. Main air masses reaching the eastern Mediterranean in winter as grey arrows. AC and PC = Arctic continental and Polar air masses, respectively (Reichart, 1997 and Rohling et al., 2008a; Marino, 2008).

Fig. 1.9 West - East cross-section showing water mass circulation in the Mediterranean Sea during winter (after Wüst, 1961). Isolines indicate salinity values and arrows indicate the direction of water circulation in the Mediterranean Sea (Rohling et al., 2008a).

Fig. 1.10 Water mass circulation in the Mediterranean Sea (**a**) The schematic of major basin current and gyres systems. **0** Ligurian-Provencal current; **1** Lion Gyre; **2** Thyrrenian cyclonic circulation; **3** Algerian current; ; **4** Rhodes Gyre; **5** Western Cretan Gyre; **6** Western Ionian Gyre; **7**Anticyclone in the Gulf of Syrte; **8**

Shikmona and Mers a-Matruh gyres system; **9** Cilican and asia Minor current; **10** Southern Adriatic gyre; **11** Western Adriatic Coastal current. Ligur. - Prov. crt. = Ligurian-Provencal current; Adr. crt. = Adriatic current; Mid Med. Jet = Mid Mediterranean Jet. (**b**) ***LIW*** dispersal pathways. (**c**) Sites of deep water overturning. **WMDW** (western Mediterranean Deep Waters); ***ADW*** (Adriatic Deep Waters); ***AeDW*** (Aegean Deep Waters). (slightly modified after Pinardi and Masetti, 2000 and Marino, 2008).

Fig. 1.11 **Image 1.** *Globigerinoides ruber* (x 200). Apertural view. **Image 2.** *Globigerinoides ruber* (x 200). Spiral view. **Image 3.** *Globigerinoides sacculifer*, without sac (x 150). Apertural view. **Image 4.** *Globigerinoides sacculifer*, with a sac (x 100). Apertural view. **Image 5.** *Globigerinella siphonifera* (x 100). **Image 6.** *Globoturborotalita rubescens* (x200). Apertural view. **Image 7.** *Globoturborotalita tenella* (x 200). Apertural view. **Image 8.** *Globoturborotalita tenella* (x 200). Spiral view. **Image 9.** *Orbulina universa* (x 150). **Image 10.** *Globigerina bulloides* (x 200). Apertural view. **Image 11.** *Globigerina bulloides* (x 200) Spiral view. **Image 12.** *Globigerinita glutinata* (x 350). Apertural view. **Image 13.** *Globigerinita glutinata* (x 350). Spiral view. **Image 14.** *Globorotalia inflata* (x 150). Apertural view. **Image 15.** *Globorotalia inflata* (x 150). Spiral view. **Image 16.** *Globorotalia scitula* (x 100). Spiral view and apertural view. **Image 17.** *Globorotalia truncatulinoides* (right-coiling) (x 200). Spiral view. **Image 18.** *Globorotalia truncatulinoides* (right-coiling) (x 100). Apertural view. **Image 19.** *Globorotalia truncatulinoides* (left-coiling) (x 150). Spiral view. **Image 20.** *Globorotalia truncatulinoides* (left-coiling) (x 150). Apertural view. **Image 21.** *Neogloboquadrina pachyderma* (right-coiling) (x 200). Apertural view. **Image 22.** *Neogloboquadrina pachyderma* (left-coiling) (x 200). Apertural and spiral view. **Image 23.** *Turborotalita quinqueloba* (x 200). Apertural and spiral view. (Images by Hayes, 1999).

CAPITOLO 2

CAPITOLO 3

CAPITOLO 4

Fig. 4.1 Location map of the studied core (**C90-1m**) and of other very close cores (C836 and C90).

Fig. 4.2 Lithology, Reflectance and Magnetic Susceptibility of the studied core (**C90-1m**).

Fig. 4.3 The ^{210}**Pb** and ^{137}**Cs** activity–depth profiles in core **C90-1m** with the age-depth profile for the first 40 cmbsf.

Fig. 4.4 Magnetic Susceptibility, Reflectance, Age-depth profile for the core **C90-1m**, with the position of the tie points. The numbers in black colour on the right side are the radiometric tie-points.

Fig. 4.5 The chemical compositions of the pumice fragments of investigated tephra layer have been classified according to Total Alkali - Silica plot (TAS - Le Bas et al., 1986).

Fig. 4.6 Correlation of recognized tephra layer with very close gravity cores **C90** and **C836** (Fig. 1). The correlation is based on lithology and magnetic susceptibility data. Radiocarbon calibrated age (^{14}C-AMS on the top of the tephra **V0**) by Insinga et al., (2008). Magnetic susceptibility profile for cores **C90** and **C836** are from Iorio et al., (2004). Magnetic susceptibility profile of the core **C90-1m,** is from this work.

Fig. 4.7 Distribution of selected species of planktonic and benthic foraminifera of the studied core **C90-1m,** with the position of the recognised eco-intervals. Correlation between the planktonic and benthic foraminifera species (as number of specimens per gram of dry sediment) with tree-ring Δ^{14}C (Stuiver et al., 1998), Total Solar Irradiance (TSI) (Bard et al., 2000) and sun spot data (Usoskin et al., 2002). The blue band correspond to the time of the solar activity minima, for the last 550 years. In particular, the ***Sporer Minimum*** (AD 1420–1540), the ***Maunder Minimum*** (AD 1645–1715), ***Dalton Minimum*** (AD 1790-

1830), ***Damon Minimum*** (AD 1880-1900) that occur in the ***Little Ice Age*** (LIA, AD 1450–1900) (Stuiver and Kra, 1986; Stuvier et al., 1997, 1998; Bard et al., 2000; Desprat et al., 2003; Luterbacher et al., 2006; Usoskin et al., 2003, 2007).

Table 4.1 Major (wt %) element composition of the tephra.

CAPITOLO 5

Fig. 5.1 Location map of the studied cores.

Fig. 5.2 Pictures of cores C90 and C836.

Fig. 5.3 Correlation of the three studied cores with the constructed composite core. **V0-V6** are labelled all the recognised tephra layers. Magnetic susceptibility for cores **C90** and **C836** are from Iorio et al., (2004). Magnetic susceptibility from core **C90-1m** is from this work.

Fig. 5.4 Correlation of the studied cores based on the distribution patterns of selected planktonic foraminifera (*Turborotalita quinqueloba*, *Globigerinoides quadrilobatus* and *Globorotalia truncatulinoides* left coiled). The thickness of tephra associated to 79 AD volcanic event has been excluded in the construction of the composite core.

Fig. 5.5 Quantitative distribution of planktonic foraminifera with the position of the recognised eco-biozones. **V0-V6** are labelled all the tephra layers. The yellow band represent the bioclastic layer.

Fig. 5.6 Quantitative distribution of calcareous nannofossils with the position of the recognised eco-biozones. **V0-V6** are labelled all the tephra layers. The yellow band represent the bioclastic layer. For *F. Profunda, Siracosphaera spp and G.*

Oceanica, the reference scales (% of the taxon), below the yellow layer (yellow band) is different from that reported for the upper interval (above yellow band).

Fig. 5.7 The chemical compositions of the pumice fragments of investigated tephra layers have been classified according to Total Alkali - Silica plot (TAS - Le Bas et al., 1986).

Fig. 5.8 The ^{210}**Pb** and ^{137}**Cs** activity–depth profiles in core **C90-1m** with the age-depth profile for the first 40 cmcd.

Fig. 5.9 Age-depth profile for the composite core with the position of all the tie points. The numbers in black colour close to composite core are the radiometric tie-points, while the red numbers represent the age of volcanic events after the tephrostratigraphic study. Red curve is a third order polynomial used to interpolated the tie-points. Yellow diamonds are the AMS ^{14}C radiocarbon data, the black diamonds are the ^{210}Pb tie-points, the pink diamonds are the mid-point of sapropel S1 equivalent (astronomically data at 8.5 kyr, Lourens 2004) and the base of sapropel S1 equivalent (dated at 9.8 kyr, Casford et al., 2002, 2007).

Fig. 5.10 Quantitative distribution patterns of selected planktonic foraminifer and calcareous nannofossils species, superimposed to 3 point-moving average, plotted vs depth (cmcd) used for Event Stratigraphy. The black arrows and numbers close to composite core are the radiometric tie-points while the red numbers represent the age of volcanic events after the tephrostratigraphic study (tephra layers labelled from **V0** to **V6**). The blue and orange bands represent the cold (blue) and warm (orange) climatic events according to the solar variability proxy Δ^{14}C, measured in tree rings (Stuiver te al., 1998). The Bond cycles are following Bond et al. (2001).

Tab. 5.1 Position in cm and labels of the recognised tephra layers.

Tab. 5.2 Major (wt%) element composition of the tephra V0, V3, V4, V5 and V6.

Tab. 5.3 ^{14}C-AMS radiocarbon data available for the composite core.

Tab. 5.4 List of the tie-points used for constructing the age depth model.

CAPITOLO 6

Fig. 6.1 A) Location map of CIESM Core C08. Bathymetry from The General Bathymetric Chart of the Oceans (GEBCO, 1997); B) bathymetric detail of core site, close to a channel South-North oriented (green arrow).

Fig. 6.2 The core CIESM 08: photography, lithologic log, petrophysical properties curves (magnetic susceptibility, Grape density, reflectance 550 nm %), paleomagnetic measurements curves (Normalized intensity, ChRM inclination, ChRM declination, MAD) plotted against depth (cm below sea floor). In the paleomagnetic curves each dot represents a single measurement taken at 1-cm spacing. NRM: natural remanent magnetization; ChRM: characteristic remanent magnetization determined by principal component analysis on the demagnetization data; MAD: maximum angular deviation. The piston core was not azimuthally oriented, but a fiducial mark ensured the reciprocal orientation of each section from which u-channels were collected. The declination of each u-channel was rotated to bring the average value at 0°.

Fig. 6.3 Relative abundance of selected planktonic foraminifera from core C08 plotted vs depth (mbsf). Eco-biozones 1 to 10 are pointed out, according to the Ecozonal scheme of Sprovieri et al. (2003) slightly modified. Grey bands show the selected eco-bioevents proposed by Perez-Folgado et al. (2003, 2004). Event Stratigraphy according to GRIP scheme. MIS and age scale according to Perez-Folgado et al. (2003, 2004). Associated to *G. ruber* curve, two grey bands interbedded with the black one correspond to the position of sapropel 1 equivalent with the two interval S1a and S1b. The two banded areas indicate the position of the turbidite layers.

Fig. 6.4 From left to right: comparison in time domain between the distribution pattern of G. bulloides from ODP-Site 977 (Perez-Folgado et al., 2004) and the studied core CIESM C08 (the red curve represents a 3-points average). The grey bands

and the labels B1 to B11 are from Perez-Folgado et al., (2004). Age-Depth profile and Sedimentation Rate of core CIESM C08. The adopted tie-points by eco-bioevents and by 14C – AMS data are shown respectively with black boxes and grey boxes.

Fig. 6.5 Comparison in time domain of colour reflectance data of core CIESM C08 (black curve, with 3 points average, red dotted curve) with reflectance data after Lourens, (2004) for ODP-Site 964 (thin black curve) in the Ionian Sea. The numbers I1-I6 indicate tephra layers in ODP-Site 964 and the code 1 and X indicate the position of the sapropel 1 and X, respectively.

Fig. 6.6 Distribution pattern of G. ruber (thin black line) with 3 points average (red line) of core CIESM C08 plotted versus δ18O NGRIP (NGRIP members, 2004) record, with 7 points average, in time domain. Labels H1 to H6 indicate the position of Heinrich events and the label YD the position of the Younger Dryas.

Fig. 6.7 Downcore plots of paleomagnetic data. The NRM intensity plotted versus stratigraphic depth is shown aside to the main paleomagnetic data (NRM, inclination and declination of the characteristic remanent magnetization) plotted versus age, accordingly to the independently derived age model discussed in this study.

Fig. 6.8 The inferred age of turbitite sand beds is plotted on curves of sea level variations over the last 100 kyr (from Antonioli et al., 2004, modified). T2 and T3 turbidites occur during two relative lowstand phases of the MIS 4 and MIS 3, while the T1 turbidite falls during the last dropping phase of sea level of MIS 3.

Tab. 6.1 Tie-points used for age-depth profile of core C08. The *Globigerina bulloides* eco-bioevents B3 to B11 are coded according to Perez-Folgado et al. (2003, 2004).

ACKNOWLEDGEMENTS

I want to express my deeper gratefulness to the people that have helped me in the realization of this PhD Thesis, they have believed in me, and they have given to me, the possibility to grow personally and scientifically.

In particular, I would like to thank my Tutor Prof. Bruno D'Argenio, who showed an interest in this PhD Thesis right away and who saw its potential. I am grateful for more than three years of his scientific and financial support.

I would like to thank my Tutor Prof. Vittoria Ferreri (per aver acettato di essere la relatrice della mia tesi), for her interest in the work during these years.

I would like to thank Fabrizio Lirer for having trust in me, for the idea behind this interesting project, for providing unpublished data, for careful reading of the thesis as a co-examinier and his interest in the work during these years, I'll never forget this!!!!

I would like to thank Luciana Ferraro, for her interest in the work during these years, for assuring me in every bad moment of this PhD Thesis.

I would like to thank Mario Sprovieri, for his scientific support and his incomparable enthusiasm for the Research.

I would like, with great esteem, to thank the Dr. Ennio Marsella, for the logistic and financial support to my research, I thank you very much!

I would like to thank all the my I.A.M.C.-colleagues of the geochemical group (Michele, Serena, Lidia, Daniela, Paola, Marianna, Maria Luisa, Stefania), of the boys room (Salvatore, Simone, Stefano, Claudio, Antonello), and of the map-making's room (Sara, Grabiella e Marco), in these years they have shared with me, the joys and the pains of the world of the Research.

Moreover, I would like to thank all the others colleagues and people of the Institutions who provided a helping hand, especially: Francesca Budillon, Renato Tonielli, Antimo Angelino, Marina Iorio, Donatella Insinga, Lucilla Capotondi, Luca Bellucci, Sonia Albertazzi, Silvia Giuliani, Mauro Frignani, Paola Petrosino, Carmine Lubritto, Nicola Pelosi, Lucia Toro, Rosaria De Martino, Patricia Sclafani… I feel I forgot somebody here, but to remember all people it's not easy, I am very sorry for this!!

I thank all my family (specially: my parents, Salvatore, Grazia, Giusi, Fabio, Monica and Antimo), my blood's brothers Pasquale and Umberto, Francesco, Ilaria, my acquired family (Michele, Silvana, Livia, Dario, Jacopo), Torunn, for all kinds of support you can think of.

Infine, voglio ringraziare tutte le donne del Mondo, ed in particolare una, a cui devo quello che sono oggi ed a cui voglio dire:

STELLA, YOU ARE MY PRINCESS. YOURS MATTO!!

I would to dedicate this work to my parents (I LOVE YOU!!!!).

Desidero dedicare questo lavoro ai miei genitori Tommaso e Rosa, consciamente ed inconsciamente costretti a condividere con me, in questi anni, tutti i miei stati d'animo!!!